Heteroaryl carbene complexes: synthesis, reactivity and redox behaviour

by

Belinda van der Westhuizen

Submitted in partial fulfillment of the requirements for the degree

PHILOSOPHIAE DOCTOR

Chemistry

In the Faculty of Natural and Agricultural Sciences

Department of Chemistry

University of Pretoria

November 2013

I declare that the thesis, which I hereby submit for the degree *Philosophiae Doctor* (Chemistry) at the University of Pretoria, is my own work and has not previously been submitted by me for a degree at this or any other tertiary institution.

_____ 5 February 2014

Belinda van der Westhuizen **Date**

I declare that the thesis, which I hereby submit for the degree *Philosophiae Doctor* (Chemistry) at the University of Pretoria, is my own work and has not previously been submitted by me for a degree at this or any other tertiary institution.

_____ _____

Belinda van der Westhuizen **Date**

Summary

A series of Fischer mono- and biscarbene complexes of the type [ML_n{C=(XR)R'}] was synthesized and characterized. The redox behavior of the complexes was studied by different techniques, including cyclic voltammetry, spectroelectrochemistry, ESR and computational methods. Different transition metals (M) and carbene substituents (XR, R') were employed to compare both the effect of the central metal atom as well as the carbene substituent.

Thienyl, furyl and ferrocenyl chromium(0) mono- and biscarbene complexes with ethoxy and amino substituents were electrochemically studied in CH_2Cl_2. Results were mutually consistent with computational data showing that the carbene double bond of all complexes is reduced pseudo reversibly to an anion radical, $^{-}$Cr-C$^{\bullet}$. The Cr centers are oxidized in two successive one electron transfer steps to Cr(II) via the Cr(I) intermediate. For all ferrocenyl carbene complexes the Fe(II) is oxidized after the first oxidation of Cr. It was found that with respect to the aryl substituents the donating effect decreases from Fc>Fu>Th. Stabilization from the XR substituent, where XR = NHR, also resulted in lower redox potentials compared to their OEt analogues.

The inclusion of ferrocene in the carbene substituent was done, as its redox activity and increased donating effect are well known. Mono- and biscarbene complexes with ethoxy and amino substituents of both chromium and tungsten were electrochemically studied. Again experimental data were supported by computational studies. Similar to the ethoxy chromium complexes, reduction of the W=C fragment to $^{-}$W-C$^{\bullet}$ was observed. However oxidation of the Fc group occurred first before the electrochemically irreversible oxidation process for W(0) involving a three electron-mediated process as seen in chronocoulometric analyses. The tungsten oxidation was restricted to a $W^{0/II}$, consistent with computational studies, by the use of the electrolyte [$N^{n}Bu_4$][$B(C_6F_5)_4$]. The short-lived W(II) species were calculated to be stabilized by agostic CH···W interactions, similar to the chromium analogues. To extend linkers between the metal-carbene termini and investigate metal-metal interaction, biferrocenyl and 2,5-thienylbiferrocenyl tungsten(0) mono-and biscarbene complexes were synthesized and studied by spectroelectrochemistry. A metal-metal charge transfer transition

between the tungsten carbonyl increment and the biferrocenyl / 2,5-thienylbiferrocenyl unit was confirmed by infrared spectroelectrochemical studies. The electronic interaction in the corresponding cationic species can be described as weakly coupled class II systems according to Robin and Day.

The cymantrenyl moiety, $Mn(\eta^5\text{-}C_5H_4)(CO)_3$, provides an interesting alternative to ferrocene as an organometallic molecular tag, however the instability of the radical cation impairs its use. Improved stability of the cation, monitored by electrochemical measurements, was accomplished by substituting a carbonyl with a ferrocenyl Fischer carbene ligand resulting in Mn(I) oxidation occuring at lower potentials than ferrocenyl oxidation. These uncommon Fischer carbene complexes is the first organometallic *multi*-tags reported. The mono cationic species, $[CpMn(CO)_2\{=C(OEt)Fc\}][PF_6]$, could be isolated and characterized with ESR analysis.

Finally, transmetallation from the tungsten(0) Fischer carbene complexes yielded examples of rare acyclic alkoxy- and aminocarbene complexes of gold(I). Single x-ray structures for all complexes could be obtained including the novel ferrocenophane dinuclear biscarbene Au(I) complex. All structures display unsupported aurophilic interactions, while the bridging biscarbene shows a semi-supported Au-Au interaction. In the case of the furanyl/thienyl methoxy monocarbene complexes, extended Au-Au interactions result in oligomeric structures. Although this study is of a fundamental nature, it is imperative for the understanding and design of gold compounds with specific applications.

Acknowledgements

I would like to express my sincere gratitude to the following people and institutions:

Dr. Daniela Bezuidenhout for her guidance, support and motivation to successfully finish this study. Also for being, not only a great supervisor, but also a dear friend.

Prof Heinrich Lang for the opportunity to visit his lab at the Technische Universitat Chemnitz, Germany. As well as the friends I made in there who gave me the motivation for the last stretch.

Mr Eric Palmer for recording of the NMR spectra.

All the collaborators as indicated: it was all together a very educational, professional and lovely journey to work with all of you. I have learned a lot! To say the least.

My colleagues Nina van Jaarsveld, Mia Ackermann, Elize Smit, Ian Strydom, George Kleinhans and Prof Simon Lotz for their encouragement and camaraderie.

My family for their understanding and support. Especially my parents whom I have seen very little during my time of writing. Without your love, I would never have made it this far.

Also a special thanks to my sister, Adel van der Westhuizen, and very dear friend, Lewis Tolley. You have supported me round the clock with lots of tea and love. You will never know how much it meant to me.

My dancing teacher, Gerrie de Beer. Thank you for your patience and understanding.

All my love,

Belinda

Publications: published, accepted and submitted

This thesis is based on the following manucripts:

Published papers

D. I. Bezuidenhout, B. van der Westhuizen, A. J. Rosenthal, D. C. Liles, I. Fernández, *Dalton Trans.*, **2014**, *43*, 389-401. DOI:10.1039/C3DT52961D

B. van der Westhuizen, P. J. Swarts, I. Strydom, D. C. Liles, I. Fernández, J. C. Swarts, D. I. Bezuidenhout, *Dalton Trans.,* **2013**, *42*, 5367-5378. DOI: 10.1039/c3dt32913e.

B. van der Westhuizen, P. J. Swarts, L. M. van Jaarsveld, D. C. Liles, U. Siegert, J. C. Swarts, I. Fernández, D. I. Bezuidenhout, *Inorg. Chem.*, **2013**, *52*, 6674-6684. DOI: 10.1021/ic4007422.

B. van der Westhuizen, J. M. Speck, M. Korb, J. Friedrich, D. I. Bezuidenhout, H. Lang, *Inorg. Chem.*, **2013**, *52(24)*, 14255-14263. DOI:10.1021/ic402202w.

D. I. Bezuidenhout, I. Fernández, B. van der Westhuizen, P. J. Swarts, J. C. Swarts, *Organometallics*, **2013**, *32(24)*, 7334-7344. DOI:10.1021/om400865m.

Accepted papers

Daniela I. Bezuidenhout,[a*] Belinda van der Westhuizen,[a] Pieter J. Swarts,[b] Teshica Chatturgoon,[c] Orde Q. Munro,[c*] Israel Fernández[d*] and Jannie C. Swarts[b*] , *Chem. Eur. J.*, 2014, DOI: 10.1002/chem.201304711.

Papers submitted and in revision

D. I. Bezuidenhout, B. van der Westhuizen, I. Strydom, P. J. Swarts, J. C. Swarts, I. Fernández, *J. Organomet. Chem.*, **2013**.

Submitted papers

B. van der Westhuizen, J. M. Speck, M. Korb, J. Friedrich, D. I. Bezuidenhout, H. Lang *Organometallics*, **2013**.

Table of contents

List of compounds

CHAPTER 2

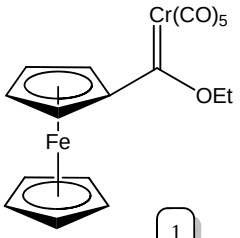

1

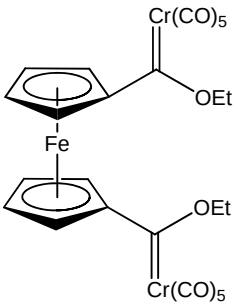

2

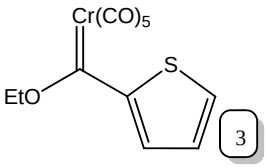

3

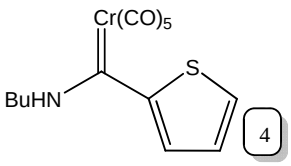

4

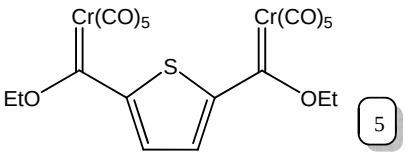

5

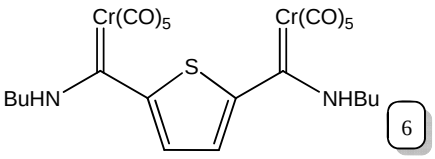

6

CHAPTER 3

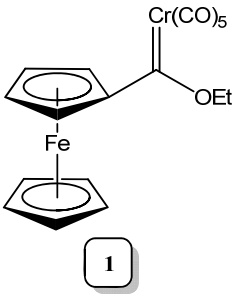

1

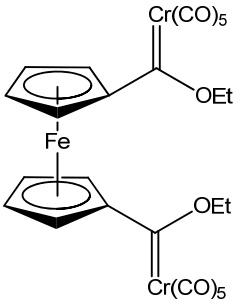

2

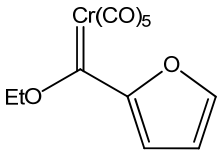

3a

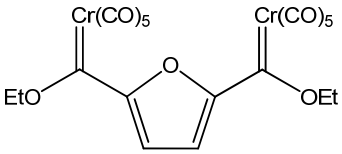

4a

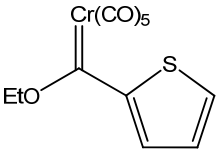

3b

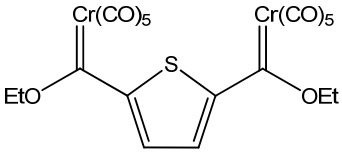

4b

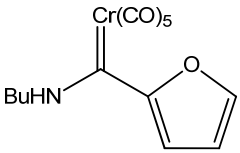

5a

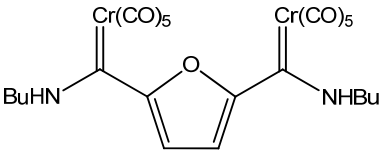

6a

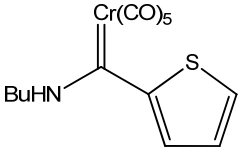

5b

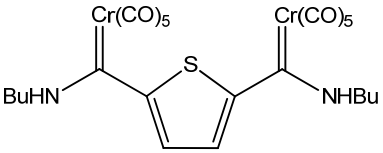

6b

CHAPTER 4

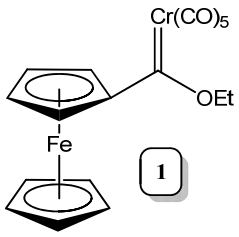

1

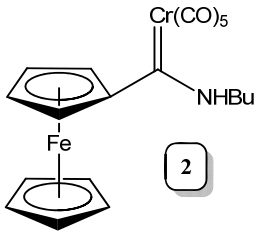

2

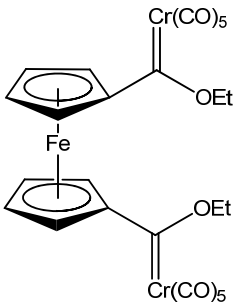

3

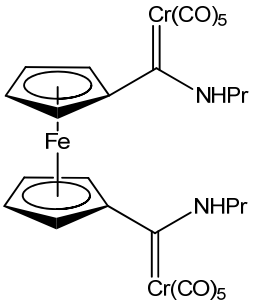

4

CHAPTER 5

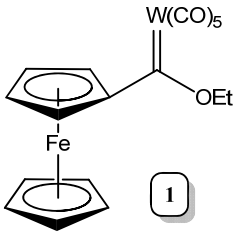

1

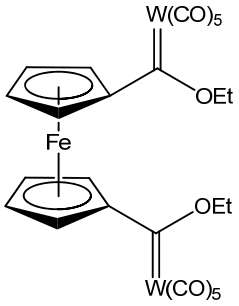

2

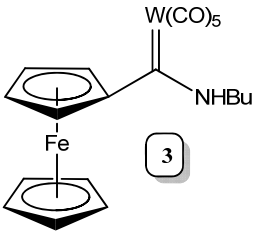

3

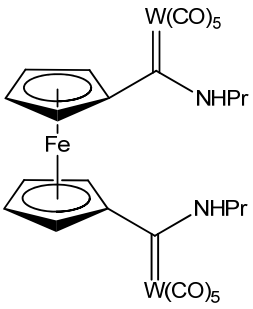

4

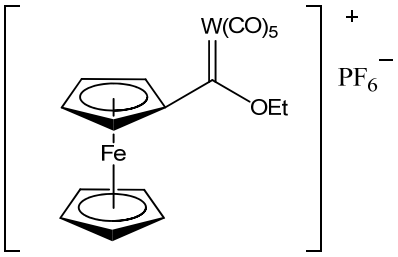

1+

CHAPTER 6

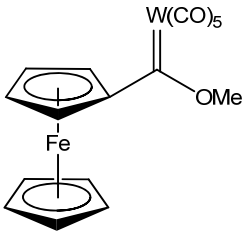

1

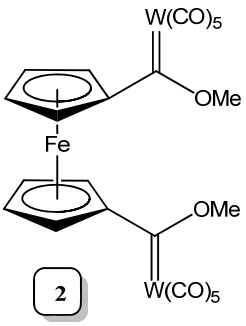

2

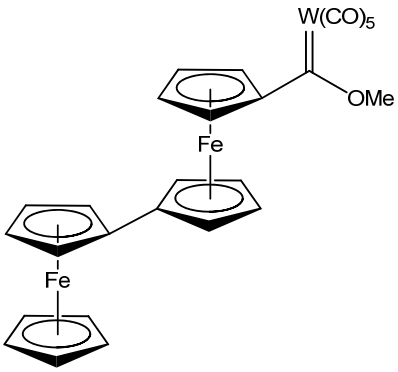

3

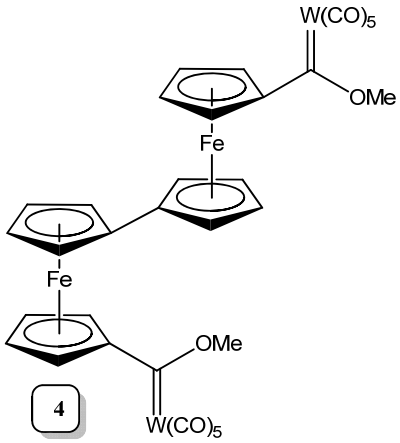

4

CHAPTER 7

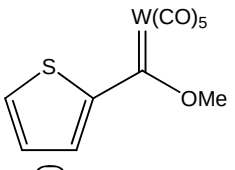

1

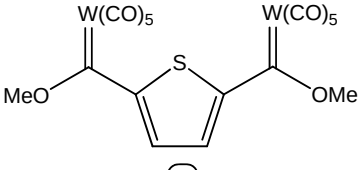

2

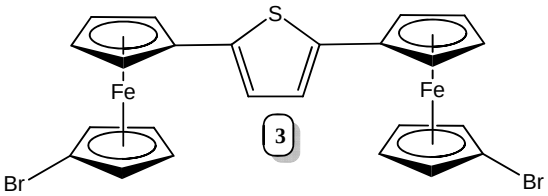

3

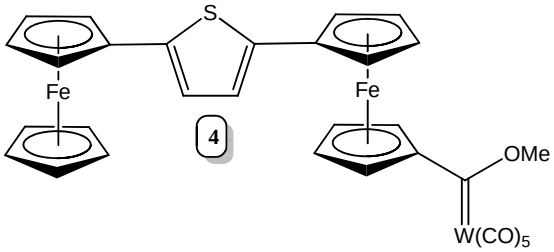

4

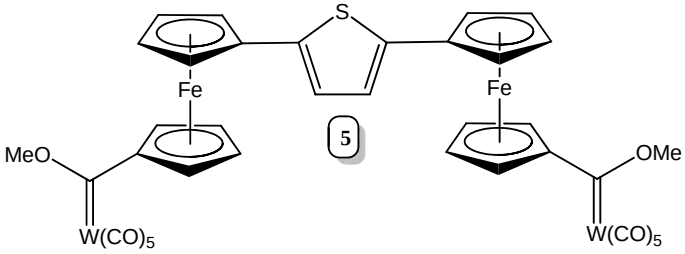

5

CHAPTER 8

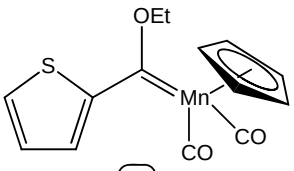

1a

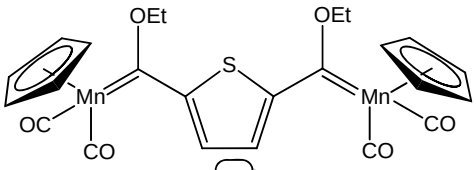

1b

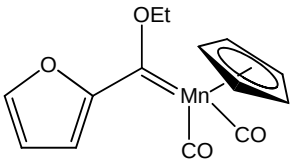

2a

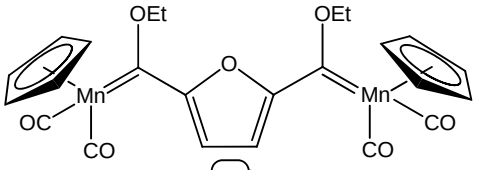

2b

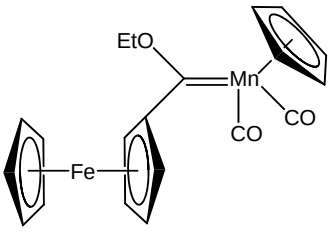

3a

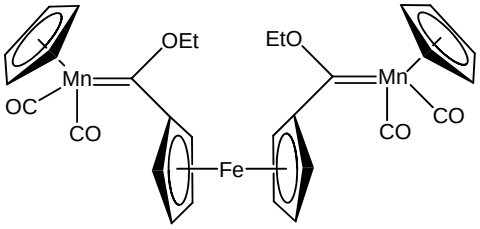

3b

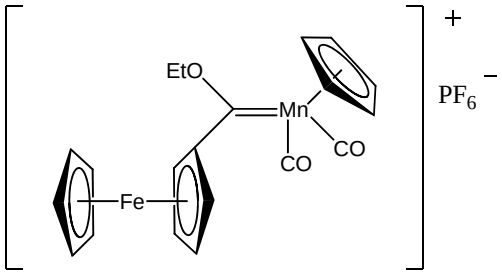

[3a][PF_6]

CHAPTER 9

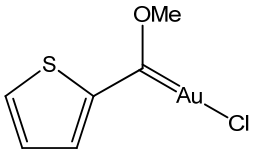

1

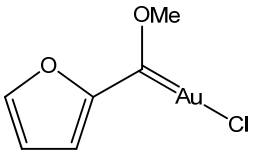

2

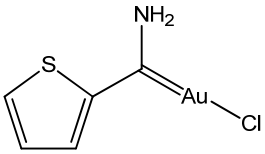

3

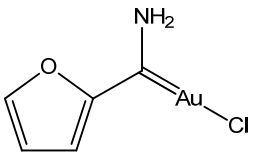

4

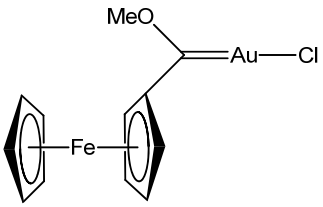

5

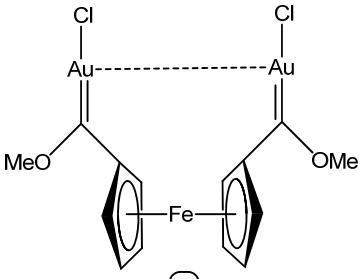

6

CHAPTER 1

Introduction

1.1 BACKGROUND

Since the first Fischer carbene complex of the type [$(CO)_5$M=C(XR)R'] was synthesized by Fischer and Maasböl in 1964,[1] these complexes have received much attention in terms of synthesis and application. The metal carbon double bond in this type of carbene complexes allows for a carbene carbon centre with unique electrophilic properties. Consequently, applications of Fischer carbene complexes have evolved around the reactivity of the M=C bond or the carbene bonded heteroatom. As such, Fischer carbenes (both as active and auxiliary ligands) have found application in organic synthesis and catalysis.[2] The Dötz benzannulation is an example of CO substitution[3a] which is essential for most subsequent conversions and Aumann reaction procedure is an example of α-deprotonation and consequences thereof.[3b]

The roles of the carbene carbon substituents have been well-studied by means of computational tools.[4] The heteroatom (X) has been investigated in terms of its donor/acceptor properties, steric and electronic effects in stabilizing the singlet carbene carbon.[4] Alternatively, the aryl substituents (R') can be incorporated into the π-delocalized network surrounding the carbene carbon and can also act as either electron withdrawing or donating (Fig. 1.1).[5]

These modulable properties of Fischer carbenes paves the way for the design of complexes to target specific applications. It is therefore important to investigate new and innovative methods to study these properties.

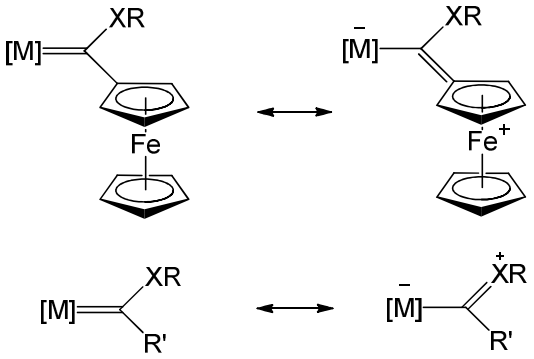

Figure 1.1 Stabilization of the carbene carbon by the carbene substituents (ferrocenyl serves as an example of an aryl group = R'; heteroatom = X; alkyl group = R)

1.2 ELECTROCHEMISTRY OF GROUP VI TRANSITION METAL FISCHER CARBENE COMPLEXES

Electrochemistry is a neglected but very useful tool for investigating different carbene substituent effects, if the central transition metal moiety is a redox-active centre[6] In a series of complexes $[M(CO)_5=C(XR)R']$ with different R, X and R' groups, the ease of oxidation of the redox-active centre can be established and even quantified by relating the formal reduction potential, $E^{o'}$, of the redox centre with the Gordy scale group electronegativity, χ_R, of R' groups in the complex.[7]

1.2.1 Fischer carbene complexes: group VI carbene metal as only redox centre

Electrochemical studies of Fischer carbene complexes (Figure 1.2) are scarce and available reports were concentrated mainly on their reduction. Molecular orbital (MO) calculations showed that the LUMO is localized on the carbene ligand[6b] and that the first reduction resulted in a carbene radical. Thus, the reduction centre was found on the carbene moiety and included the $C_{carbene}$-N bond in the case of amino carbene complexes.[8] Recent studies on chromium(0) and tungsten(0) carbene complexes showed that reduction of the carbene does not depend on the nature of the central metal, but rather on the carbene ligand substituents.[9] On the other hand the first oxidation of these complexes was localized on the central metal atom and oxidation potentials were dependent on the nature of the ligands coordinated to the metal: decrease in oxidation potential was observed when a strong π-accepting (eg. CO

ligand) was replaced with a mild π-accepting ligand (eg. C=C ligand).[7] The oxidation potential related to the first oxidation of Cr(0) to Cr(I) was found at significantly lower potentials compared to the potential of W(0) to W(I). However, the second oxidation was found to be independent of the type of metal as the potentials were found to be almost the same.[6a,c,10] The first oxidation products seemed stable for the chromium derivatives, but not for the tungsten ones and this feature might be better understood when looking at the respective electronic structure of the two metals (Cr = [Ar] $3d^5$ $4s^1$ and W = [Xe] $4f^{14}$ $5d^4$ $6s^2$). The peak current densities for tungsten were double compared to that of chromium, which might indicate that the first oxidation of tungsten was directly followed by the second and this would also explain the irreversible nature of this process. In the case of chromium a reversible one electron oxidation process was mostly observed. In general if the alkoxy substituent was replaced with an amino group, the first oxidation was facilitated and reduction potentials occured at more negative values.[11] Tungsten and molybdenum showed greater tendency for seven-coordination compared to chromium and consequently any cation formed would be more reactive toward nucleophilic attack.[12]

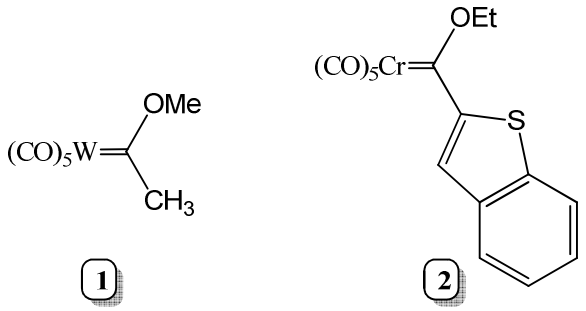

Figure 1.2 Examples of mono-metallic Fischer carbene complexes: **1**[10e] and **2**[13]

1.2.2 Fischer carbene complexes: bi- to multi-metal complexes containing a group 6 metal.

Transition metal moieties used in the design of these complexes are not limited to the carbene metal fragment alone. Additional transition metal (TM) centra can be incorporated through carbene substituents containing such a centre, for example ferrocene (Fc) as an aryl (R') substituent bonded directly to the carbene carbon or titanocene chloride (R = $TiCp_2Cl$) bonded to the carbene heteroatom (X).[14] Using a ferrocenyl group as a redox-active label or tag in complexes may be beneficial for a number of reasons. The electron-donating

characteristics of the ferrocenyl group,[15] the electron-withdrawing properties of the oxidized ferrocenium species[16] and the electrochemical reversible nature of the Fc/Fc^{+} couple[17] are but some of the reasons why ferrocene derivatives are applied in molecular sensors,[18] energy transfer processes[19] and cancer therapy.[20] Ferrocenyl carbene complexes of group 6 transition metals have been studied for the electronic effects of the ferrocenyl substituent on the carbene ligand as part of an investigation into the properties of carbonyl carbene groups.[21] Ferrocene provides the same degree of stability to adjacent electron deficient centra compared to amino substituents.[22] The redox behavior of metal carbene complexes are greatly influenced when additional metal centra are introduced.[23]

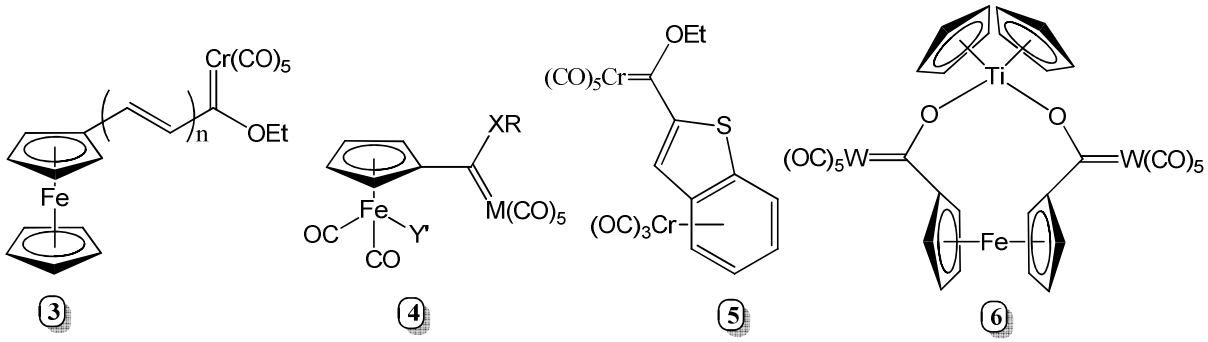

Figure 1.3 Examples of multi-metal carbene complexes: **3**[24], **4**[25], **5**[16] and **6**[17]

If a linker, for example a polyene, was used to separate a ferrocenyl fragment from a metal carbonyl carbene complex, redox potentials decreased with increase in length of the linker. This might indicate some electronic transfer between the terminal moieties (Fig. 1.3, **3**).[27]

The oxidation potential of the Fe^{+2}/Fe^{+3} in half sandwich complexes of iron ($CpFe(CO)_2Y'$) (Fig. 1.3, **4**) was found in the range of 0.68-0.75V and varied with different Y' substituents.[26] When an alkoxy Fischer carbene substituent was added on the ring, this potential decreased by approximately 0.1V and even more so when the alkoxy group was substituted with an amino group.[27] No oxidation potential was observed for the chromium moiety. This was also the case when two $CpFe(CO)_2$ fragments were linked together by a C-3 alkane chain having chromium Fischer carbene substituents on the rings. Although the oxidation potential of the complex was significantly lower, only one oxidation process was observed regardless of the four redox metals available in the complex.

Chromium Fischer carbene complexes with metal containing substituents on the carbene carbon (Fig. 1.3, **5** and **6**) showed oxidation processes for each redox centre in the complexes except for the titanocene chloride moiety.[16] The oxidation potential for the $Cr(CO)_5$ in the studied series of complexes decreased with increasing donating ability of the R and R' substituents. The oxidation potential of the ferrocenyl couple Fe^{+2}/Fe^{+3} observed did not vary significantly with varying substituents. A relative consistent potential was also observed for $Cr(CO)_3$ fragment for these chromium carbene complexes.

Caution should be exercised when assigning redox processes in these multi-metal carbene complexes as it becomes increasingly difficult with increasing number of redox centra. One should also consider the fact that the metal centra involved are not restricted to localized behavior as the HOMO of such complexes might not only be located on a specific redox centre, for eg. ferrocene.[28] Significant differences for a single process can be observed by using different electrolytes, electrodes, solvent window, temperature, time, etc. (as mentioned in the above example of $Cr(CO)_6$) and results should at least be supported by molecular orbital analysis or DFT calculations.

1.2.3 Application: Electron Transfer

Electron transfer (ET) in Fischer carbene complexes has, to date, received little attention. This might be attributed to current developing methods to study ET in organometallic complexes. One method employed to study ET in a series of carbene complexes was ESI-MS. The series of complexes consisted of donating (Fc) and acceptor ($Co(CO)_6$) moieties as well as conjugated biscarbenes.[29] Signs of ET was observed in complexes where a ferrocenyl substituent was linked with a $M(CO)_5$ fragment *via* a π-system (Fig. 1.3, **3**). However, the conjugated biscarbenes acted as two separate monocarbenes while the last example containing a $Co(CO)_6$ moiety prevented any ET due to its electron sink character.

Another, more recent, method employed in studying electron transfer in organometallic complexes is spectroelectrochemistry. For these studies, the complexes usually contain a well-studied organometallic tag, such as ferrocene.[7,19,30] After a reversible oxidation process is observed during cyclic voltammetry of a specific complex, the complex can be studied by *in situ* UV/vis-near-IR spectroscopy. Spectroelectrochemical studies are carried out by a

stepwise increase of the potential which allows the *in situ* generation of mixed-valent species of the complex. The increase and decrease of absorption bands are monitored. These include ligand to metal charge transfer (LMCT), intervalent charge transfer (IVCT) and ligand field (LF) transitions.[31] Electronic communication is confirmed with the presence of an IVCT absorption and electrostatic communication is confirmed with the absence thereof.[30] Electron transfer studies employing spectroelectrochemistry have never been used to study Fischer carbenes.[14,32] However, investigation of targeted ferrocenyl compounds has recently been reported. In a study regarding diferrocenylthiophenes it was found that the mono oxidized species of 2,5-diferrocenylthiophene had the greatest interaction.[20b]

Electrochemistry in combination with spectroelectrochemistry is a much more comprehensive technique to study metal-metal communication in multi-metal complexes and UV-vis-NIR investigations are efficient in establishing charge transfer transitions between the separated metal entities.[20b,33]

1.3 ELECTROCHEMISTRY AND ORGANOMETALLIC MUTI-TAGS

As mentioned in the above section, a ferrocenyl moiety is a well-studied molecular label, but is not the only label available in organometallic electrochemistry. The electron withdrawing and IR-active carbonyl groups of a cymantrenyl moiety, $Mn(\eta^5\text{-}C_5H_4)(CO)_3$,[34] provides and interesting and different alternative. Application in the reduction process of this half-sandwich transition metal compound was found in cymantrenyl-labeled bovine serum albumin for immunoassays.[35] Application of its anodic chemistry is currently lacking but actively investigated. It has been found that the $[MnCp(CO)_3]^{0/+1}$ was at least partially reversible.[36] Recently, $MnCp(CO)_3$ has been covalently linked to an electrode through an ethynyl linkage and studied.[37] After removal of one electron in the presence of $P(OMe)_3$, the irreversible cymantrene wave disappeared and was replaced by two reversible waves attributed to the mono- and disubstituted phosphine derivatives. The drawback in the use of this fragment as an organometallic tag can be attributed to its instability of the radical cation compared to the ferrocenium ion. Stabilizing this species by, for example, substituting a

highly π-accepting ligand (CO) with a less π-accepting ligand (phosphine), it becomes a more attractive molecular label or organometallic tag.[38]

Examples of Fischer carbene complexes employing $CpMn(CO)_3$ as the metal carbonyl reagent are not as common as group 6 Fischer carbenes, and only alkoxy derivatives are known.[32a,39] In addition, the electrochemical behavior of these types of group 7 Fischer carbenes have not been reported yet.

1.4 GOING FOR GOLD

The first gold carbene complexes were reported in the early 1970's by F. Bonati and G. Minghetti.[40] Since then, new methods for these complexes have been developed and preparation focused on specific applications, such as catalysis.

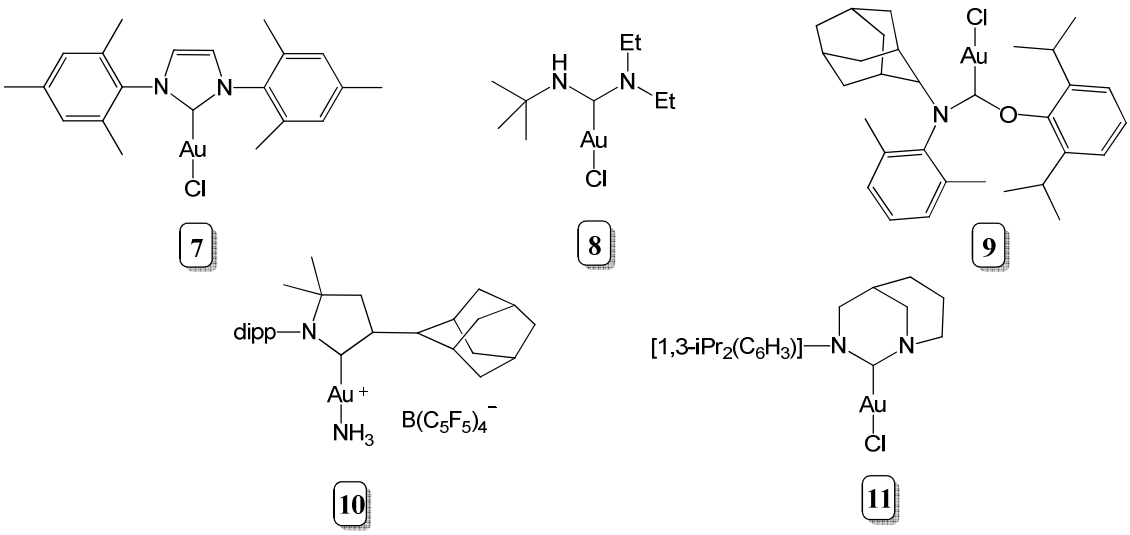

Figure 1.4 Examples of different types of gold(I) catalysts

Figure 1.4 illustrates some recent examples of different gold(I) carbenes complexes used in catalysis. Their use, reactivity and exceptional properties are summarized as follows:

- Compound **7** represents the well-studied N-heterocyclic carbene (NHC) gold(I) complexes used in a variety of organic transformations, hydroamination, cycloisomerizations, etc.[41] In a recent study by Urbano *et al.* catalytic studies in

activation of alkynes, allenes and alkenes were performed.[42] It was found that the NHC-Au(III)Br_3 complex was more effective as a pre-catalyst in contrast to the NHC-Au(I)Cl compound.

- The second type of catalyst represented by complex **8** is referred to as acyclic diamino carbene (ADC) gold (I) complexes. These proved to be just as effective (or even more so) in 1,6-enyne cyclizations as its NHC analogue.[43] Both the NHC and ADC gold(I) type catalysts were more efficient than their phosphine analogues. In some cases dinuclear NHC complexes of gold(I) have proven to be better catalysts than their mono-nuclear analogues. A study by Wang *et al.* found an enantiomeric excess of up to 91% during the asymmetric transformation of propargyl esters versus the 0-7% obtained with the mono-nuclear analogues. [44]
- The very sterically demanding acyclic aminooxycarbene (AAOC), **9**, showed high efficiency in the intramolecular hydroaminiation of different alkenyl ureas.[45] The reaction rates found proved even beter than the rates found for acyclic diaminocarbene (ADC) Au(I) catalysts.
- Cyclic alkyl amino carbene (CAAC) complexes of gold (I) (eg. **10**) were employed in hydroamination of alkynes and allenes with ammonia.[46] Some drawbacks were that elevated temperatures were needed and during catalysis and that the complex underwent a dismutation into the catalytic inactive biscarbene Au(I) complex. Electrochemical interest is found in these complexes due to its ability to stabilize electron-rich gold(0) centres.[47] A reversible one electron reduction was observed for the specific CAAC biscarbene complexes of gold(I) to gold(0). Surprisingly, when cathodic chemistry was performed on the mono-carbene complex, the dimer, a dinuclear biscarbene of gold(0), was isolated!
- Development in the CAAC complexes resulted in the anti-Bredt N-heterocyclic carbene gold(I) complex, **11**.[48] It resembled a CAAC more than an NHC complex due to its strong σ-donor and π-acceptor properties. The advantages above CAACs are that it allows for room temperature hydroamination of terminal alkynes with hydrazine and also, no formation of the inactive biscarbene complex was observed.

Examples of Fischer carbene complexes of gold are very limited[49] and electrochemistry hereof are currently non-existent. As stated by Raubenheimer in a 2012 review,[50] the possibility of employing acyclic Fischer carbene complexes hold promise for catalytic applications. However, examples of more fundamental studies on the synthesis and structure of Fischer carbene complexes are still required to characterize their properties, eg. known relativistic effects such as Au-Au interactions,[51] and their reactivity and catalytic activity in for example hydroamination reactions.

1.5 AIM OF THIS STUDY

- Electrochemical investigation and molecular orbital analysis of simple Fischer carbenes of the group VI transition metals will be employed to characterize the substituent effect in these complexes (Chapter 2-5).
- One or two redox-active ferrocenyl substituents will be incorporated in Fischer carbene complexes followed by electrochemical and spectroelectrochemical studies to investigate metal-metal interactions between the metal carbonyl and ferrocenyl moieties (Chapter 6-7).
- Synthesis and isolation of chemically oxidized species will be attempted.
- Above mentioned synthesis and investigation methods will be applied to cymantrenyl carbene complexes to design organometallic multi-tags (Chapter 8).
- Synthesis of (hetero)aryl gold(I) Fischer carbene complexes by transmetallation will be performed with the aim to investigate the Au^{I}/Au^{III} species electrochemically (Chapter 9).

1.6 ORGANIZATION OF THESIS

This thesis is written and put together in the format of publications. Some results, although relevant to each other, were published in more than one publication, illustrating the different outcomes as it became clearer to the authors. Subsequent chapters were presented in terms of different compounds and techniques used (see 1.5).

1.7 REFERENCES

[1] E. O. Fischer, A. Maasböl, *Angew. Chem. Int. Ed. Engl.,* **1964**, *3*, 580.

[2] J. W. Herndon, *Coord. Chem. Rev.*, **2013**, *257 (21-22)*, 2899.

[3] (a) K. H. Dötz, *Angew. Chem., Int. Ed. Engl.*, **1975**, *14*, 644; (b) R. Aumann, H. Heinen, *Chem. Ber.*, **1987**, *120*, 537.

[4] (a) J. Poater, M. Cases, X. Fradera, M. Duran, M. Sola, *Chem. Phys.,* **2003**, *294*, 129; (b) A. Krapp, G. Frenking, *J. Am. Chem. Soc.*, **2008**, *130*, 16646; (c) A. Krapp, K. K. Pandey, G. Frenking, *J. Am. Chem. Soc.*, **2007**, *129*, 7596; (d) M. Casey, G. Frenking, M. Duran, M. Sola, *Organometallics*, **2002**, *21*, 4182; (e) G. Frenking, M. Sola, S. F. Vyboishchikov, *J. Organomet. Chem.*, **2005**, *690*, 6178; (f) M. L. Lage, I. Fernandez, M. J. Mancheno, M. A. Sierra, *Inorg. Chem.*, **2008**, *47*, 5253; (g) D. M. Andrade, M. E. Z. Michoff, I. Fernandez, A.M. Granados, M. A. Sierra, *Organometallics*, **2007**, *26*, 5854.

[5] (a) O. S. Mills, A. D. J. Redhouse, *Chem. Soc. A*, **1968**, 642-647; (b) E. O. Fischer, *Angew. Chem.*, **1974**, *86*, 651-663.

[6] (a) M. K. Lloyd, J. A. McCleverty, D. G. Orchard, J. A. Connor, M. B. Hall, I. H. Hillier, E. M. Jones, G. K. McEwen, *J. Chem. Soc., Dalton Trans.*, **1973**, 1743; (b) C. P. Casey, L. D. Albin, M. C. Saeman, D. H. Evans, *J. Organomet. Chem.*, **1978**, *155*, C37; (c) A. Limberg, M. A. N. D. A. Lemos, A. J. L. Pombeiro, S. Maiorana, A. Papagni, E. Licandro, *Portugaliae Electrochim. Acta*, **1995**, *13*, 319; (c) A. J. L. Pombeiro, *New J. Chem.*, **1997**, *21*, 649.

[7] (a) H. J. Gericke, A. J. Muller, J. C. Swarts, *Inorg. Chem.*, **2012**, *51*, 1552; (b) A. Auger, A. J. Muller, J. C. Swarts, *Dalton Trans*. **2007**, 3623.

[8] I. Hoskovcova, R. Zverinoca, J. Rohacova, D. Dvoa, T. Tobrman, S. Zalis, J. Ludvik, *Electrochim. Acta*, **2011**, *56*, 6853.

[9] I. Hoskovcova, J. Rohacova, L. Meca, T. Tobrmand, D. Dvorak, J. Ludvik, *Electrochim. Acta*, **2005**, *50*, 4911.

[10] (a) G. Facchin, M. Mozzon, R. A. Michelin, M. T. A. Ribeiro, A. J. L. Pombeiro, *J. Chem. Soc., Dalton Trans.*, **1992**, *19*, 2827; (b) I. R. Farrell, F. Harrtl, S. Zalis, M. Wanner, W. Kaim, A. Vlvek, Jr., *Inorg. Chim. Acta*, **2000**, *318*, 143; (c) C. Baldoli, P. Cerea, L. Falciola, C. Giannini, E. Licandro, S. Maiorana, P. Mussini, D. Perdicchia, *J. Organomet. Chem.* **2005**, *690*, 5777.

[11] I. Hoskovcova, J. Rohacova, D. Dvorak, T. Tobrman, S. Zalis, R. Zverinova, J. Ludvik, *Electrochim. Acta,* **2011**, *55*, 8341.

[12] C. J. Pickett, D. Pletcher, *J. Chem. Soc., Dalton Trans.*, **1975**, 881.

[13] D. I. Bezuidenhout, W. Barnard, B. van der Westhuizen, E. van der Watt, D. C. Liles, *Dalton Trans.*, **2011**, *40*, 6711.

[14] Bezuidenhout, D. I., van der Watt, E., Liles, D. C., Landman, M., Lotz, S., *Organometallics*, **2008**, *27*, 2447.

[15] (a) W. C. Du Plessis, W. L. Davis, S. J. Cronje, J. C. Swarts, *Inorg. Chim. Acta*, **2001**, *314*, 97; (b) S. Otto, A. Roodt, J. J. C. Erasmus, J. C. Swarts, *Polyhedron*, **1998**, *17*, 2447.

[16] A. Hildebrandt, T. Rüffer, E. Erasmus, J.C. Swarts, H. Lang, *Organometallics*, **2010**, *29*, 4900.

[17] (a) N. G. Connelly, W. E. Geiger, *Chem. Rev.*, **1996**, *96*, 877; (b) J. M. Speck, R. Claus, A. Hildebrandt, T. Rüffer, E. Erasmus, L. van As, J. C. Swarts, H. Lang, *Organometallics*, **2012**, *31*, 6373; (c) U. Pfaff, A. Hildebrandt, D. Schaarschmidt, T. Hahn, S. Liebing, J. Kortus, H. Lang, *Organometallics*, **2012**, *31*, 6761.

[18] A. R. Pike, L. C. Ryder, B. R. Horrocks, W. Clegg, B. A. Connolly, A. Houlton, *Chem. Eur. J.*, **2005**, *11*, 344.

[19] F. Spanig, C. Kolvacs, F. Hauke, K. Ohlubo, F. Fukuzumi, D. Guldi, A. Hirsch, *J. Am. Chem. Soc.*, **2009**, *131*, 8180.

[20] (a) C. E. J. van Rensburg, E. Kreft, J. C. Swarts, S. R. Dalrymple, D. M. Macdonald, M. W. Cooke, M. A. S. Aquino, *Anticancer Res.*, **2002**, *22*, 889; (b) J. C. Swarts, T. G. Vosloo, S. J. Cronje, W. C. Du Plessis, C. E. J. van Rensburg, E. Kreft, J. E. van Lier, *Anticancer Res.*, **2008**, *28*, 2781; (c) R. F. Shago, J. C. Swarts, E. Kreft, C. E. J. van Rensburg, *Anticancer Res.*, **2007**, *27*, 3431; (d) I. Ott, K. Kowalski, R. Gust, J. Maurer, P. Mücke, R. F. Winter, *Bioorg. Med. Chem. Lett.*, **2010**, *20*, 866; (e) A. Gross, N. Hüsken, J. Schur, L. Raszeja, I. Ott, N. Metzler-Nolte, *Bioconjug. Chem.*, **2012**, *23*, 1764; (f) J. T. Chantson, M. V. V. Falzacappa, S. Crovella, N. Metzler-Nolte, *J. Organomet. Chem.*, **2005**, *690*, 4564; (g) M. Maschke, M. Lieb, N. Metzler-Nolte, *Eur. J. Inorg. Chem.*, **2012**, 5953.

[21] J. A. Connor, E. M. Jones, J. P. Lloyd, *J. Organomet. Chem.*, **1970**, *24*, C20.

[22] B. Bildstein, *J. Organomet. Chem.*, **2001**, *28*, 617.

[23] M. A. Sierra, M. Gomez-Gallego, R. Martinez-Alvarez, *Chem. Eur. J.*, **2007**, *13*, 736.

[24] K. N. Jayaprakash, P. C. Ray, I. Matsuoka, M. M. Bhadbhade, V. G. Puranik, P. K. Das, H. Nishihara, A. Sarkar, *Organometallics*, **1999**, *18*, 3851.

[25] M. Swarz, M. Vollmann, R. Wartchow, H. Butenschön, *J. Organomet. Chem. Chem.*, **2005**, *690*, 2263.

[26] U. Behrendt, R. M. Pfeifer, R. Wartchow, H. Butenschön, *New J. Chem.*, **1999**, *23*, 891.

[27] M. Swarz, R. Wartchow, H. Butenschön, *J. Organomet. Chem. Chem.*, **2005**, *690*, 6217.

[28] A. J. L. Pombeiro, *J. Organomet. Chem.,* **2005**, *690*, 6021.

[29] R. Martinez-Alvarez, M. Gomez-Gallego, I Fernandez, M. J. Mancheno, M. A. Sierra, *Organometallics*, **2004**, *23*, 4647.

[30] (a) A. Hildebrandt, D. Schaarschmidt, H. Lang, *Organometallics*, **2011**, *30*, 556; (b) A. Hildebrandt, D. Schaarschmidt, L. van As, J. C. Swarts, H. Lang, *Inorg. Chim. Acta*, **2011**, *374*, 122; (c) A. Hildebrandt, U. Pfaff, H. Lang, *Rev. Inorg. Chem.*, **2011**, *31*, 111; (d) A. Hildebrandt, D. Schaarschmidt, R. Claus, H. Lang, *Inorg. Chem.*, **2011**, *50*, 10623; (e) A. Hildebrandt, H. Lang, *Dalton Trans.*, **2011**, *40*, 11831; (f) K. Kaleta, A. Hildebrandt, F. Strehler, P. Arndt, H. Jiao, A. Spannenberg, H. Lang, U. Rosenthal, *Angew. Chem., Int. Ed.*, **2011**, *50*, 11248; (g) J. M. Speck, D. Schaarschmidt, H. Lang, *Organometallics*, **2012**, *31*, 1975.

[31] (a) Y. S. Sohn, D. N. Hendrickson, H. B. Gray, *J. Am. Chem. Soc.*, **1971**, *93*, 3603; (b) D. E. M. Duggan, D. N. Hendrickson, *Inorg. Chem.*, **1975**, *14*, 955; (c) P. Zanello, G. Opromolla, F. Fabrizi de Biani, A. Ceccanti, G. Giorgi, *Inorg. Chim. Acta*, **1997**, *255*, 47; (d) Y. Zhu, M. O. Wolf, *Chem. Mater.*, **1999**, *11*, 2995; (e) Y. Zhu, M. O. Wolf, *J. Am. Chem. Soc.*, **2000**, *122*, 10121; (f) M. Lohan, P. Ecorchard, T. Rüffer, F. Justaud, C. Lapinte, H. Lang, *Organometallics*, **2009**, *28*, 1878; (g) F. Paul, L. Toupet, J.-Y. Thépot, K. Costuas, J.-F. Halet, C. Lapinte, *Organometallics,* **2005**, *24*, 5464; (h) C. G. Atwood, W. E. Geiger, *J. Am. Chem. Soc.*, **1994**, *116*, 10849.

[32] (a) D. I. Bezuidenhout, S. Lotz, M. Landman, D. C. Liles, *Inorg. Chem.*, **2011**, *50*, 1521; (b) H. Helten, M. Beckman, G. Schnakenburg, R. Streubel, *Eur. J. Inorg. Chem.*, **2010**, *16*, 2337; (c) E. Fischer, V. N. Postnov, F. R. Kreissl, *J. Organomet. Chem.,* **1982**, *23*, C73.

[33] A. Hildebrandt, H. Lang, *Dalton Trans.*, **2011**, *40*, 11831.

[34] (a) S. D. Lepore, A. Khoram, D. C. Bromfield, P. Cohn, V. Jairaj, M. A. Silvestri, *J. Org. Chem.*, **2005**, *70*, 7443; (b) Z. Zhang, S. D. Lepore, *Tetrahedron Lett.*, **2002**, *43*, 7357; (c) H. Grade´n, N. Kann, *Curr. Org. Chem*., **2005**, *9*, 733; (d) L. M. Dorozhkin, V. A. Nefedov, A. G. Sabelnikov, V. G. Sevastjanov, *Sens. Actuators*, **2004**, *B99*, 568; (e) M. Salmain, A. Vessieres, S. Top, G. Jaouen, I. S. Butler, *J. Raman Spectrosc.*, **1995**, *26*, 31; (f) Z. Wang, B. A. Roe, K. M. Nicholas, R. L. White, *J. Am. Chem. Soc.*, **1993**, *115*, 4399; (g) M. Salmain, A. Vessieres, G. Jaouen, I. S. Butler, *Anal. Chem.*, **1991**, *63*, 2323; (h) I. Avastre, J. Besancon, P. Brossier, C. Moise, *Appl. Organomet. Chem.*, **1990**, *4*, 9; (i) P. Hublau, C. Sergheraert, L. Ballester, M. Dautrevaux, *Eur. J. Med. Chem.,* **1983**, *18*, 131;

[35] (a) M. Hromadova, M. Salmain, N. Fischer-Durand, L. Pospisil, G. Jaouen, *Langmuir*, **2006**, *22*, 506; (b) M. Hromadova, M. Salmain, R. Sokolova, L. Pospisil, G. Jaouen, *J. Organomet. Chem.*, **2003**, *668*, 17.

[36] D. R. Laws, D. Chong, K. Nash, A. L. Rheingold, W. E. Geiger, *J. Am. Chem. Soc.*, **2008**, *130*, 9859.

[37] M. V. Sheridan, K. Lam, W. E. Geiger, *J. Am. Chem. Soc.*, **2013**, *135*, 2939.

[38] C. G. Atwood, W. E. Geiger, T. E. Bitterwolf, *J. Electroanal. Chem.*, **1995**, *397*, 279.

[39] (a) M. Landman, W. Barnard, P. H. van Rooyen, D. C. Liles, *J. Mol. Struct.*, **2012**, *1021*, 76; (b) D. I. Bezuidenhout, S. Lots, M. Landman, D. C. Liles, *Inorg. Chem.*, **2011**, *50(4)*, 1521; (c) Y. M. Terblans, M. Roos, L. Lotz, *J. Organomet. Chem.*, **1998**, *566(1-2)*, 133; (d) E. O. Fischer, V. N. Postnov, F. R. Kreissl, *J. Organomet. Chem.*, **1982**, *231(4)*, C73.

[40] (a) F. Bonati, G. Minghetti, *Synthetic and reactivity in inorganic and metal-organic chemistry*, 1971, 1(4), 299; (b) G. Minghetti, F. Bonati, *J. Organomet. Chem.*, **1973**, *54*, C62.

[41] N. Marion, S. P. Nolan, *Chem. Soc. Rev.*, **2008**, *37*, 1776.

[42] J. Urbano, A. J. Hormigo, P. de Frement, S. P. Nolan, M. M. Diaz-Requejo, P. J. Perez, *Chem. Commun.*, **2008**, *6*, 759.

[43] (a) A. S. K. Hashmi, T. Hengst, C. Lothschutz, F. Rominger, *Adv. Synth. Catal.*, **2010**, *352*, 1315; (b) C. Bartolome, Z. Ramiro, D. Garcia-Cuadrado P. Perez-Galan, M. Raducan, C. Bour, A. M. Echavarren, P. Espinet, *Organometallics*, **2010**, *29*, 951; (c) C.

Bartolome, D. Garcia-Cuadradok, Z. Ramiro, P. Espinet, *Organometallics*, **2010**, *29*, 3589.

[44] Y-M. Wang, C. N. Kuzniewski, V. Rauniyar, C. Hoong, F. D. Toste, *J. Am. Chem. Soc.*, **2011**, *133*, 12972.

[45] H. Seo, D. R. Snead, K. A. Abboud, S. Hong, *Organometallics*, **2011**, *30*, 5725.

[46] V. Lavallo, G. D. Frey, B. Donnadieu, M. Soleilhavoup, G. Bertrand, *Angew. Chem. Int. Ed.*, **2008**, *47*, 5224.

[47] D. S. Weinberger, M. Melaimi, C. E. Moore, A. L. Rheingold, G. Frenkin, P. Jarabek, G. Bertrand, *Angew. Chem. Int. Ed.*, **2013**, *52*, 8964.

[48] M. J. Lopez-Gomez, D. Mrtin, G. Bertrand, *Chem. Commun.*, **2013**, *49*, 4483.

[49] C. E. Strasser, S. Cronje, H. G. Rubenheimer, *New J. Chem.*, **2010**, *34*, 458.

[50] H. G. Raubenheimer, *LitNet Akademies*, **2012**, *9*, 23.

[51] D. J. Gorin, D. Toste, *Nature*, **2007**, *446*, 395.

CHAPTER 2

Electrochemical illumination of thienyl and ferrocenyl chromium(0) Fischer carbene complexes

This chapter was published in Dalton Transactions. The format reflects the style set by the journal.

B. van der Westhuizen,[a] P. J. Swarts,[b] I. Strydom,[a] D. C. Liles,[a] I. Fernández,[c] J. C. Swarts,[*b] D. I. Bezuidenhout,[*a] *Dalton Trans.*, **2013**, *42*, 5367-5378. DOI: 10.1039/c3dt32913e.

Author contributors

Synthetic work: B. van der Westhuizen, I. Strydom

Cyclic voltammetry and data analysis: B. van der Westhuizen, D. I. Bezuidenhout, P. J. Swarts, J. C. Swarts

Computational work: I. Fernández

Crystallography: D. C. Liles

Article written, submitted and response to reviewers: B. van der Westhuizen, D. I. Bezuidenhout, J. C. Swarts, I. Fernández.

[a] *Chemistry Department, University of Pretoria, Private Bag X20, Hatfield, 0028, South Africa. Fax: +27-(0)12-420-4687; Tel: +27-(0)12- 420-2626; E-mail: daniela.bezuidenhout@up.ac.za*
[b] *Chemistry Department, University of the Free State, PO Box 339, Bloemfontein 9300, South Africa. Fax:+27-(0)51-444-6384; Tel: +27-(0)51-401-2781; E-mail: swartsjc@ufs.ac.za*
[c] *Departamento de Química Orgánica I, Facultad de Química, Universidad Complutense,28040-Madrid,Spain.*

Supporting Information: The Cartesian coordinates and energies for the optimized compounds 1, 3, and 4 and the corresponding radical cations (**Appendix 1, CD**). CCDC 913650 for complex 3. For electronic supplementary information and crystallographic data in CIF or other electronic format see DOI: 10.1039/c3dt32913e.

ABSTRACT

A series of ferrocenyl and thienyl mono- and biscarbene chromium(0) complexes **1** - **6** were synthesised. The complexes were characterised both spectroscopically and electrochemically, and the single crystal X-ray structure of **3** was determined. Electrochemical measurements in CH_2Cl_2 revealed that the carbene double bon of 1-6 is reduced to an anion radical, $^{-}$Cr-C$^{\bullet}$ at formal reduction potentials <-1.7 V *vs*. FcH/FcH^{+}. A computational study on **1**,**3** and **4** (B3LYP/def2-SVP level) is consistent with electrochemical results in showing that electrochemically generated chromium(I) species may be further electrochemically irreversibly oxidised to chromium(II) at E_{pa} > 0.95 V. The reactivity towards follow-up chemical reactions of the anodically produced Cr(II) species is much higher than the reactivity of the cathodically produced radical anions as the latter was still observably reoxidised to the parent Cr=C species at fast scan rates. The ferrocenyl group is oxidised electrochemically reversibly to ferrocenium at larger potentials than the electrochemically reversible ocidation of the Cr(0) centre to Cr(I). That all redox centres in **1**-**6** are involved in one electron transfer steps was confirmed by comparing the ferrocenyl voltammetric wave with those of the other redox centres in linear sweep voltammetric experiments. The ferrocenyl group was electrochemically shown to stabilize the Cr=C centre almost as much as the NHBu, and much more than the ethoxy and thienyl groups.

2.1 INTRODUCTION

The applications of Fischer carbene complexes of the type [ML_n{C=(XR)R′}] as active or auxiliary ligands in organic synthesis and catalysis evolve around the reactivity of the metal-carbon double bond or the carbene-bonded heteroatom X.[1] Alternatively, modification of conjugated carbene substituents R′ allows for tailored organic synthesis (Fig. 2.1).

Theoretical calculations have focused on the donor/acceptor nature of the heteroatom X on the carbene substituent,[2] or on the steric and electronic effects of the heteroatom on the carbene ligand.[3] Only a few studies on the use of electrochemistry as an elucidative tool for the abovementioned properties have been reported.[4] In general, electrochemical properties of electro-active compounds, A-R, can be utilised to establish the relative ease by which a redox-active centre, A, may be oxidised (or reduced) in a series of differently R-substituted

compounds.[5] The electron-donating or electron-withdrawing properties of different R-groups in a series of compounds may be quantified by relating the formal reduction potential, $E^{o'}$, of a redox centre in the compounds with the Gordy scale group electronegativity, χ_R, of R groups of the molecules.[6] Recently, a renewal of interest in the redox behaviour of Group VI Fischer carbene complexes has been seen.[7] This is a result of their promising application as, for example, electrochemical probes.[8]

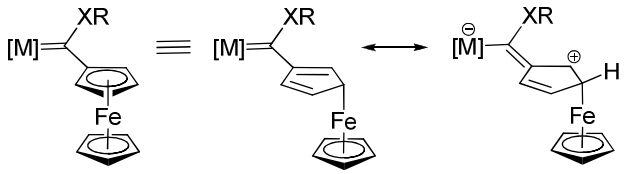

Fig. 2.1 Two of the many canonical forms that explains the stabilisation of carbenes by a ferrocenyl group.

In this paper, we report the synthesis, characterisation and results of an electrochemical investigation of 2-thienyl (Th) ethoxy- and two new aminocarbene complexes, as well as the corresponding 2,5-thiendiyl (Th′) biscarbene complexes of chromium(0).[9] The choice of planar, aromatic and electron-rich thiophene as a carbene substituent was based on its ability to be incorporated into the π-delocalised network surrounding the carbene carbon atom, acting as an electron donating substituent for the electrophilic carbene carbon.

In addition, the chromium ferrocenyl (Fc) ethoxycarbene complex $[Cr(CO)_5\{C(OEt)Fc\}]$ (**1**)[10] and the analogous biscarbene complex with bridging 1,1′-ferrocendiyl (Fc′) $[(CO)_5Cr\{C(OEt)(Fc')C(OEt)\}Cr(CO)_5]$ (**2**)[11] were also studied to verify the number of electrons that was transferred in each redox observed. Ferrocene-containing complexes are studied due to the well characterised electrochemical reversible one-electron transfer behaviour of the ferrocenyl group,[12] the ease by which it can be derivatised,[13] and its strong electron-donating properties[14] that may provide significant stabilisation of adjacent electron deficient centres.[15]

2.2 EXPERIMENTAL

General

All operations were carried out under an inert atmosphere of nitrogen or argon gas using standard Schlenk techniques. Solvents were dried by refluxing on sodium metal (hexane, thf and diethylether) or over phosphorous pentoxide (CH_2Cl_2) and then distilled under nitrogen prior to use. Chemicals were used without further purification unless stated otherwise. Triethyloxonium tetrafluoroborate (Et_3OBF_4) was synthesized according to literature procedures.[16] Purification with column chromatography was done using silica gel 60 (0.0063 – 0.200mm) as stationary phase. A Bruker AVANCE 500 spectrometer was used for NMR recordings. ^{1}H NMR spectra were recorded at 500.139 MHz and ^{13}C NMR spectra at 125.75 MHz. The signal of the solvent was used as reference: ^{1}H $CDCl_3$ at 7.24ppm and ^{13}C $CDCl_3$ at 77.00ppm. . IR spectra were recorded on a Perkin-Elmer Spectrum RXI FT-IR spectrophotometer in hexane as solvent. Only the vibration bands in the carbonyl-stretching region (*ca.* 1600-2200 cm^{-1}) were recorded.

Synthesis of carbene complexes 1 - 6

Ethoxycarbene complexes **1**,[17] **2**,[11] **3**,[18] and **5**[19] were prepared (Scheme 2.1) according to published procedures; spectroscopic characterisation data are as follows:

*[Cr(CO)$_5${C(OEt)Fc}] (**1**)*

Yield 79%, dark red crystals, NMR ($CDCl_3$) ^{1}H: 4.99 (q, *J*=7.1Hz, 2H, C**H**$_2$), 4.93 (br, 2H, Fc-H$_\alpha$), 4.71 (br, 2H, Fc-H$_ß$), 4.16 (s, 5H, Fc-Cp), 1.55 (t, *J*=7.1Hz, 3H, C**H**$_3$); ^{13}C : 329.7 (C$_{carbene}$), 223.0 (CO$_{trans}$), 217.3 (CO$_{cis}$), 93.6 (Fc-C$_{ipso}$), 75.5(O**C**H$_2$), 74.5 (Fc-C$_\alpha$), 72.3 (Fc-C$_ß$), 70.6 (Fc-Cp), 15.5 (**C**H$_3$). IR ν(CO) (hexane): 2056 m (A″$_1$), 1977 vw (B), 1949 s (A′$_1$), 1938 vs (E).

*[(CO)$_5$Cr{C(OEt)(Fc′)C(OEt)}Cr(CO)$_5$] (**2**)*

Yield (68%), red-black solid, NMR ($CDCl_3$) ^{1}H: 5.07 (q, *J*=7.1Hz, 4H, C**H**$_2$), 5.00 (dd, *J*=2.3, 1.9Hz, 4H, Fc′-H$_{\alpha,\alpha'}$), 4.73 (dd, *J*=2.3, 1.9Hz, 4H, Fc′-H$_{\beta,\beta'}$), 1.63 (t, *J*=7.0, 6H, C**H**$_3$); ^{13}C: 306.2 (C$_{carbene}$), 223.6(CO$_{trans}$), 217.1 (CO$_{cis}$), 99.2 (Fc′-C$_{ipso}$), 76.2 (Fc′-C$_{\alpha,\alpha'}$), 72.7 (Fc′-C$_{\beta,\beta'}$) 77.4 (**C**H$_2$), 15.5 (**C**H$_3$). IR ν(CO) (hexane): 2054 m (A″$_1$), 1979 sh (B), 1938 vs (A′$_1$ overlap E).

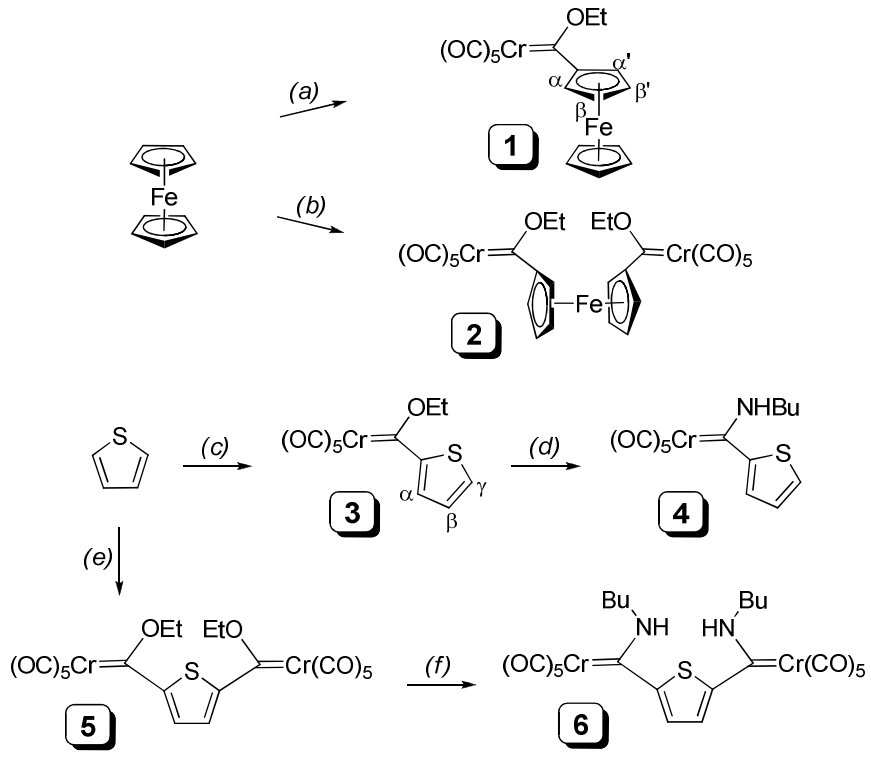

Scheme 2.1 Reagents and conditions: (a) (i) 1eq ^{t}BuLi, thf, -78°C; (ii) 1eq [$Cr(CO)_6$], thf, -50°C; (iii) 1.3eq Et_3OBF_4, CH_2Cl_2, -30°C; (b) (i) 2.2eq ^{n}BuLi, TMEDA, hexane, 60°C; (ii) 2eq [$Cr(CO)_6$], thf, -50°C; (iii) 2.5eq Et_3OBF_4, CH_2Cl_2, -30°C; (c) (i) 1eq ^{n}BuLi, thf, -78°C; (ii) 1eq [$Cr(CO)_6$], thf, -50°C; (iii) 1.3eq Et_3OBF_4, CH_2Cl_2, -30°C; (d) 1.1eq NH_2Bu, Et_2O, rt; (e) (i) 2.2eq ^{n}BuLi, thf, -78°C; (ii) 2eq [$Cr(CO)_6$], thf, -50°C; (iii) 2.5eq Et_3OBF_4, CH_2Cl_2, -30°C; (f)) 2.2eq NH_2Bu, Et_2O, rt.

*[$Cr(CO)_5${C(OEt)Th}] (**3**)*

Yield (83%), red solid, NMR ($CDCl_3$) ^{1}H: 8.24 (dd, *J*=4.1, 0.7Hz, 1H, Th-H_α), 7.68 (dd, *J*=5.0, 0.7Hz, 1H, Th-H_γ), 7.20 (dd, *J*=5.0, 4.1Hz, 1H, Th-H_β), 5.17 (q, *J*=7.0, 2H, C**H**$_2$), 1.69 (t, *J*=7.0, 3H, C**H**$_3$); ^{13}C: 316.4 ($C_{carbene}$), 223.2(CO_{trans}), 217.0 (CO_{cis}), 155.4 (Th-C_{ipso}), 141.1 (Th-C_α), 134.8 (Th-C_γ), 129.0 (Th-C_β) 76.0 (**C**H_2), 15.2 (**C**H_3). IR ν(CO) (hexane): 2058 m (A″$_1$), 1983 vw (B), 1957 s (A′$_1$), 1946 vs (E).

*[(CO)$_5$Cr{C(OEt)(Th′)C(OEt)}Cr(CO)$_5$] (**5**)*

Yield 75%, purple crystals, NMR ($CDCl_3$) ^{1}H: 8.06 (s, 2H, Th-H$_{\alpha,\alpha'}$), 5.21 (q, 2H, *J*=7.2, C**H**$_2$), 1.69 (t, 3H, *J*=7.1, C**H**$_3$); ^{13}C: 321.9 (C$_{carbene}$), 223.7(CO$_{trans}$), 216.5 (CO$_{cis}$), 157.7 (Th′-C$_{ipso}$), 137.1 (Th′-C$_{\alpha,\alpha'}$), 77.4 (**C**H$_2$), 15.2 (**C**H$_3$). IR ν(CO) (hexane): 2054 m (A″$_1$), 1987 vw (B), 1964 s (A′$_1$), 1953 vs (E).

*Synthesis of [Cr(CO)$_5${C(NHBu)Th}] (**4**)*

Complex **3** (2 mmol, 0.66g) was dissolved in ether and *n*-butylamine (2.2 mmol, 0.22 mL) was added at room temperature. A rapid colour change from red to yellow was observed. Volatiles were removed by reduced pressure and column chromatography was performed using a 1:1 hexane/CH_2Cl_2 eluent mixture. A duplication of the NMR data sets (^{1}H and ^{13}C) indicates the formation of *syn*- and *anti*-isomers, in a ratio of 1:1.3, respectively. Yield 0.63g (88%), yellow crystals Yield 0.63g (88%) yellow crystals. For *syn*-isomer: NMR ($CDCl_3$) ^{1}H: 8.85 (s, 1H, NH), 7.44 (d, *J* = 5.0Hz, 1H, Th-H$_\alpha$), 7.04 (d, *J* = 3.0 Hz, 1H, Th-H$_\gamma$), 6.80 (d, *J* = 3.0Hz, 1H, Th-H$_\beta$), 3.48 (dt, *J* = 5.0, 4.9Hz, 2H, NC**H**$_2$), 1.67 (m, 2H, C**H**$_2$CH$_2$), 1.38 (m, 2H, CH$_2$C**H**$_2$), 0.92 (t, *J* = 7.4Hz, 3H, C**H**$_3$); For *anti*-isomer: NMR ($CDCl_3$) ^{1}H: 8.54 (s, 1H, NH), 7.44 (d, *J* = 5.0Hz, 1H, Th-H$_\alpha$), 7.36 (d, *J* = 3.4 Hz, 1H, Th-H$_\gamma$), 7.08 (dd, *J* =3.4, 3.0Hz, 1H, Th-H$_\beta$), 4.09 (dt, *J* = 5.1, 5.0Hz, 2H, NC**H**$_2$), 1.81 (m, 2H, C**H**$_2$CH$_2$), 1.54 (m, 2H, CH$_2$C**H**$_2$), 1.02 (t, *J* = 7.3Hz, 3H, C**H**$_3$); For *syn*-isomer; ^{13}C: 271.9(C$_{carbene}$), 222.9(CO$_{trans}$), 217.1(CO$_{cis}$), 148.8(C$_{ipso}$), 137.3(Th-C$_\alpha$), 127.2(Th-C$_\gamma$) , 122.5(Th-C$_\beta$), 51.3(N**C**H$_2$), 31.6(**C**H$_2$CH$_2$), 19.6(CH$_2$**C**H$_2$), 13.5(**C**H$_3$). For *anti*-isomer; ^{13}C: 260.9(C$_{carbene}$), 223.1(CO$_{trans}$), 217.4(CO$_{cis}$), 155.6(C$_{ipso}$) , 138.5(Th-C$_\alpha$), 128.3(Th-C$_\gamma$) , 126.7(Th-C$_\beta$), 53.3(N**C**H$_2$), 31.8(**C**H$_2$CH$_2$), 20.00(CH$_2$**C**H$_2$), 13.7(**C**H$_3$). IR ν(CO) (hexane): 2056 m (A″$_1$), 1977 vw (B), 1918 s (A′$_1$), 1942, 1934 vs (E). Anal. calc. for $CrC_{14}H_{13}NO_5S$: C, 46.79; H, 3.65. Found: C, 47.47; H, 3.87.

*Synthesis of [(CO)$_5$Cr{C(NHBu)(Th′)C(NHBu)}] (**6**)*

Complex **5** (2 mmol, 1.16 g) was dissolved in ether and *n*-butylamine (4.2 mmol, 0.42 mL) was added at room temperature. The colour changed from purple to deep yellow and volatiles removed under reduced pressure. Column chromatography was performed using a 1:1 hexane/CH_2Cl_2 solvent mixture. Yield 0.95g (75%), dark yellow crystals. A mixture of 3 isomers was obtained, which could not be separated. Significant overlap of the resonances in the

^{1}H NMR spectrum was observed, and the data reported were integrated over the collective region for each chemical shift. The ^{13}C NMR shifts were assigned from 2D NMR experiments and relative intensities, and the *syn,syn*-, *anti,anti*- and *syn,anti*-isomers could be distinguished. NMR ($CDCl_3$) ^{1}H: 8.80, 8.64, 8.50, 8.35 (s, 2H, N**H**), 7.87, 7.84, 7.70, 7.69 (2H, Th-$H_{\alpha,\alpha'}$, 4.13-3.79, 3.58-3.34 (m, 4H, N**C**$\mathbf{H_2}$), 1.82-1.55 (m, 4H, **C**$\mathbf{H_2}$$CH_2$), 1.40-1.22 (m, 4H, CH_2**C**$\mathbf{H_2}$), 0.95-0.84 (m, 6H, **C**$\mathbf{H_3}$);). For *syn,syn*-isomer; ^{13}C: 268.8 ($C_{carbene}$), 223.2(CO_{trans}), 217.5(CO_{cis}), 155.2(C_{ipso}), 133.2(Th′-$C_{\alpha,\alpha'}$), 53.1(N**C**H_2), 31.6(**C**$H_2$$CH_2$), 22.7($CH_2$**C**$H_2$), 14.1(**C**$H_3$). For *anti,anti*-isomer; ^{13}C: 258.1 ($C_{carbene}$), 223.0(CO_{trans}), 217.5(CO_{cis}), 153.5(C_{ipso}), 137.8(Th′-$C_{\alpha,\alpha'}$), 51.3(N**C**H_2), 33.3(**C**$H_2$$CH_2$), 22.1($CH_2$**C**$H_2$), 13.7(**C**$H_3$ For *syn,anti*-isomer; ^{13}C: 261.3, 261.0($C_{carbene}$), 222.7, 222.5(CO_{trans}), 217.2, 217.2(CO_{cis}), 160.4, 160.4(C_{ipso}), 137.2, 137.1(Th′-$C_{\alpha,\alpha'}$), 53.4, 53.3(N**C**H_2), 34.7, 33.6(**C**$H_2$$CH_2$), 22.2, 22.1($CH_2$**C**$H_2$), 13.8, 13.7(**C**$H_3$). IR ν(CO) (hexane): 2054 m (A''_1), 1975 w (B), 1918 s (A'_1), 1935 vs (E). Anal. calc. for $Cr_2C_{24}H_{22}N_2O_{10}S$: C, 45.42; H, 3.50. Found: C, 45.57; H, 3.45.

Crystal structure determination

The crystal data collection and refinement details for complex **3** are summarized in Table 2.3, and the Ortep/PovRay (Fig. 2.2).[20] The X-ray crystal structure analysis was performed using data collected at 23°C on a Bruker kappa duo diffractometer with a PROTON CMOS detector and APEX2 control software[21] using QUAZAR-multilayer-optics-monochromated, Mo-Kα radiation by means of a combination of ϕ and ω scans. Data reduction was performed using SAINT[21] and the intensities were corrected for absorption using SADABS.[21] The structures were solved by direct methods using SHELXTS[22] and refined by full-matrix least squares using SHELXTL[22] and SHELXL-97.[22] In the structure refinements all hydrogen atoms were added in calculated positions and treated as riding on the atom to which they are attached. All non-hydrogen atoms were refined with anisotropic displacement parameters, all isotropic displacement parameters for hydrogen atoms were calculated as $X \times U_{eq}$ of the atom to which they are attached, X = 1.5 for the methyl hydrogens and 1.2 for all other hydrogens.

Table 2.1 Crystal, data collection and refinement data for complex **3**

Identification code	BvdWCrThOEt
Chemical formula	$C_{12}H_8CrO_6S$
Formula weight	332.25
Temperature	296(2) K
Wavelength	0.71073 Å
Crystal size	0.118 x 0.177 x 0.179 mm
Crystal habit	dark orange hexagonal-prism
Crystal system	Monoclinic
Space group	$P2_1/m$
Unit cell dimensions	a = 9.5803(6) Å α = 90°
	b = 7.6532(5) Å β = 98.737(3)°
	c = 9.6551(6) Å γ = 90°
Volume	699.70(8) Å^3
Z	4
Density (calculated)	1.577 g/cm^3
Absorption coefficient	0.986 mm^{-1}
F(000)	336
Theta range for data collection	2.13 to 26.13°
Index ranges	$-11 \le h \le 11$, $-9 \le k \le 9$, $-11 \le l \le 11$
Reflections collected	20399
Independent reflections	1497 [R_{int} = 0.0433]
Completeness to θ = 26.13°	99.8%
Absorption correction	multi-scan
T_{min}, T_{max}	0.677, 0.745
Structure solution technique	direct methods
Structure solution program	*SHELXS*-97
Refinement method	Full-matrix least-squares on F^2
Refinement program	*SHELXL*-97
Function minimized	$\Sigma\, w(F_o^2 - F_c^2)^2$
Data / restraints / parameters	1497 / 0 / 122
Goodness-of-fit on F^2	1.199
Δ/σ_{max}	0.000
Final R indices all data	R_1 = 0.0861, wR_2 = 0.2371
1330 data; $I > 2\sigma(I)$	R_1 = 0.0787, wR_2 = 0.2325
Weighting scheme	$w = 1/[\sigma^2(F_o^2)+(0.0878P)^2+3.5878P]$
	where $P = (F_o^2+2F_c^2)/3$
Largest diff. peak and hole	0.850 and -0.570 eÅ^{-3}
R.M.S. deviation from mean	0.122 eÅ^{-3}

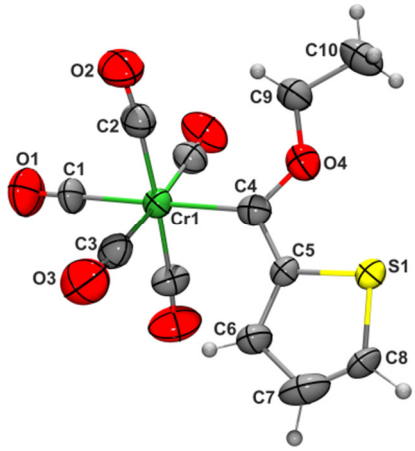

Fig. 2.2 An Ortep/PovRay[20] drawing of the structure of 3 showing the atom numbering scheme. Only the major orientation of the thienyl-ethoxy-carbene ligand is shown. ADPs are shown at the 50% probability level.

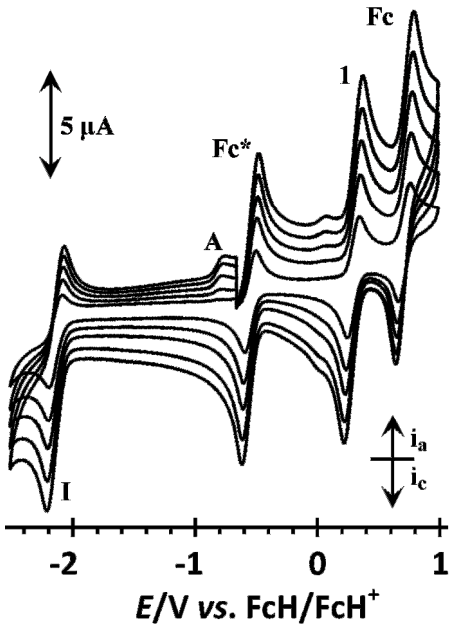

Fig. 2.3 Cyclic voltammograms of **1** in CH_2Cl_2/0.1 mol dm^{-3} [N(^{n}Bu)$_4$][PF_6] on a glassy carbon-working electrode at scan rates of 100 (smallest currents), 200, 300, 400 and 500 mV/s. Decamethylferrocene, Fc*, was used as internal standard. Peak A is ascribed to a new species that is generated during Cr=C reduction (peak 1) because if scans are initiated at -1 V, peak A is absent during the initial cycle.

Electrochemistry

Cyclic voltammograms (CV's), square wave voltammograms (SW's) and linear sweep voltammograms (LSV's) were recorded on a Princeton Applied Research PARSTAT 2273 voltammograph running PowerSuite (Version 2.58). All experiments were performed in a dry three-electrode cell. A platinum wire was used as auxiliary electrode while a glassy carbon working electrode (surface area 3.14 mm^2) was utilized after polishing on a Buhler polishing mat first with 1 micron and then with ¼ micron diamond paste. A silver wire was used as pseudo internal reference under an argon atmosphere inside an M Braun Lab Master SP glovebox filled with high purity argon (H_2O and O_2 < 5 ppm). All electrode potentials are reported using the potential of the ferrocene/ferrocenium redox couple [FcH/FcH^+] ($FcH = (\eta^5\text{-}C_5H_5)_2Fe$, $E^{o'}$ = 0.00 V) as reference.[23] However, decamethyl ferrocene, Fc*, was used as internal standard to prevent signal overlap with ferrocenyl of **1** and **2**. Decamethylferrocene has a potential of -550 mV versus free ferrocene with ΔE = 72 mV and i_{pc}/i_{pa} = 1 under the conditions employed.[24] Analyte solutions (0.5 mmol dm^{-3}) were prepared in dry CH_2Cl_2 in the presence of 0.1 mol dm^{-3} [($^nBu_4$)N][PF_6]. Analyses were performed at 20 °C. Data were exported to a spread sheet program for manipulation and diagram preparation (Fig. 2.3-2.5).

Computational details

Geometry optimizations without symmetry constraints were carried out using the Gaussian09 suite of programs.[25] Electron correlation was partially taken into account using the hybrid functional denoted as B3LYP[26] (and uB3LYP for radical cations) in combination with double-ζ quality plus polarization def-SVP[27] basis set for all atoms (this level is denoted B3LYP/def2-SVP). Calculation of the vibrational frequencies[28] at the optimized geometries showed that the compounds are minima on the potential energy surface.

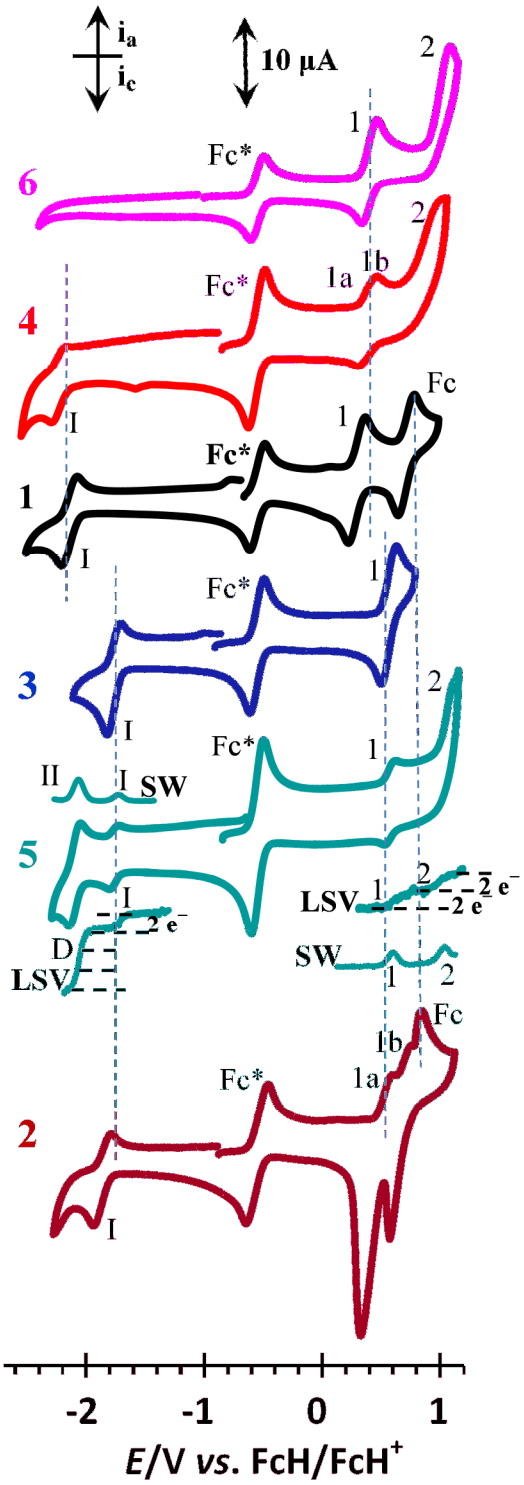

Fig. 2.4 Cyclic voltammograms of 0.5 mmol dm^{-3} solutions of **1–6** in CH_2Cl_2/0.1 mol dm^{-3} $[N(^nBu)_4][PF_6]$ on a glassy carbon-working electrode at a scan rate of 400 mV/s. Decamethylferrocene, Fc*, was used as internal standard. For **5** ([**5**] = 0.25 mmol dm^{-3} for better clarity) linear sweep (LSV, 2 mV/s; currents are enhanced 5 times for clarity) and square wave voltammograms (SW, 20 Hz; currents are enhanced 2 times) are also shown.

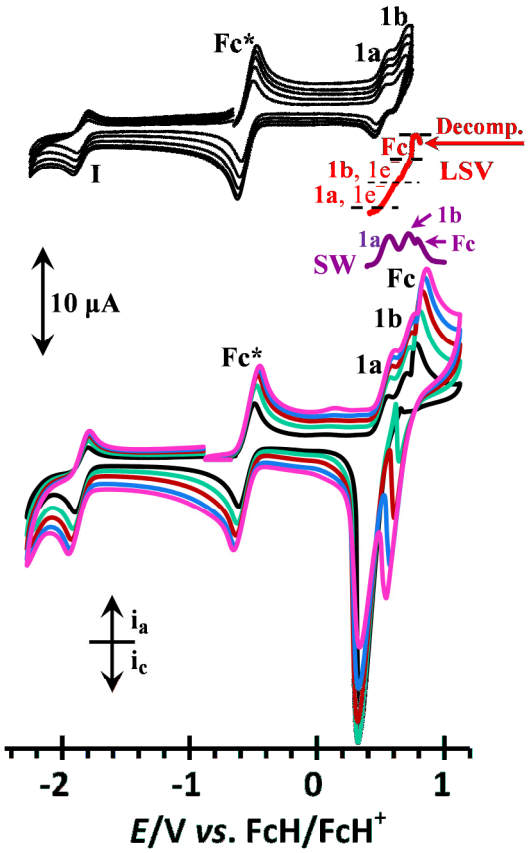

Fig. 2.5 Bottom: Cyclic voltammograms of **2** in CH_2Cl_2/0.1 mol dm^{-3} $[N(^nBu)_4][PF_6]$ on a glassy carbon-working electrode at scan rates of 100 (smallest currents), 200, 300, 400 and 500 mV/s. Decamethylferrocene, Fc*, was used as internal standard. Resolved waves 1a and 1b are associated with the oxidation of the two Cr(0) species. Top: When the reversal anodic potential is chosen to be sufficiently small to eliminate wave Fc, electrode deposition as indicated by the large cathodic currents in the bottom CV's were not observed. LSV measurements showed waves 1a, 1b and Fc are involved in the same number (one) of electrons being transferred.

2.3 RESULTS AND DISCUSSION

Synthesis

Four ethoxycarbene complexes, **1** - **3**, and **5**, as well as two new aminocarbene complexes **4** and **6** were synthesised according to Scheme 1. The classical Fischer carbene route using Group VI metal carbonyls was employed for the preparation of the ethoxycarbene complexes **1**, **2**, **3** and **5**: attack of a lithiated substrate on a carbonyl ligand of $[Cr(CO)_6]$ forms the metal acylate, which, after alkylation with an oxonium salt, yields the corresponding ethoxycarbene complexes. Synthesis of aminocarbene complexes **4** and **6** were achieved by aminolysis[29] of complexes **3** and **5**, to liberate the new aminocarbene complexes **4** and **6** in 88 and 75% respectively. Compounds were purified by column chromatography to give the products as dark red (ethoxy derivatives) or yellow solids.

All neat compounds were stable in the absence of oxygen and could be stored for months in the cold under argon. Electrochemical evidence indicated that in CH_3CN or CH_2Cl_2 solutions, they decomposed to an observable extent within ca. 30 minutes. This is slow enough to allow spectroscopic and electrochemical measurements.

Single crystal X-ray structure for 3

The molecular structure of 3 has crystallographic mirror symmetry with the thienyl-ethoxy-carbene ligand, the Cr atom and the carbonyl *trans* to the carbene all lying in the mirror plane. The carbene ligand is disordered with the two orientations in a ratio of 0.526(8) : 0.474(8), each rotated by 180º from the other about the Cr—$C_{carbene}$ bond. The Cr—$C_{carbene}$ and $C_{carbene}$—O bond distances of 2.077(9) and 1.333(11) Å respectively are comparable to the ranges of Cr—$C_{carbene}$ bond distances, 2.05(1) – 2.081(4) Å and $C_{carbene}$—O bond distances, 1.317(5) – 1.33(1) Å for a number of chromium-ethoxy-carbene-sububstituted thienyl structures reported previously.[11,30]

Spectroscopy

Electronic effects of the carbene substituents can be followed in solution by both NMR and IR spectroscopy. Since H_α (see atom numbering in Scheme 2.1) is the position closest to the site of coordination of the carbene carbon atom, the chemical shift of this proton is influenced most and is a sensitive probe for electronic ring substituent involvement. Significant downfield shifts of H_α were observed in the ^{1}H NMR spectra for **1** – **6** (see Table 2.1), compared to free ferrocene (4.19 ppm) and thiophene (7.20 ppm). This is consistent with the electron-withdrawing effect of the metal carbonyl fragment bonded to the carbene ligand, comparable, for example, to an ester functionality,[31] as well as the π-delocalization of the (hetero)aryl rings towards stabilizing the electrophilic carbene carbon atom (Fig. 2.1). Less ring-involvement of the thienyl substituent is seen for both aminocarbene complexes **4** and **6**, as reflected by the higher field H_α resonances. For **4** and **6**, a duplication of all the resonances is also observed in both the ^{1}H and ^{13}C spectra. This duplication is due to the formation of two different isomers of **4**, rotamers **A** (*anti*-configuration) and **C** (*syn*-configuration) (Scheme 2.2) with restricted rotation around the $C_{carbene}$-N bond.[32] For **6**, up to three different isomers could be distinguished via NMR spectroscopy. These were ascribed to three different biscarbene complex isomers; in one case, a *syn,syn*-configuration for both carbene ligands, (*syn,syn*-isomer, Experimental section), another where both carbene ligands have *anti*-configuration (*anti,anti*-isomer, Experimental section), and finally, the biscarbene complex featuring one carbene ligand with *syn*-, the other ligand with *anti*-configuration (*syn,anti-i*somer, Experimental section). The *syn,anti*-isomer displays two sets of signals for all observed signals, corresponding to the presence of two different carbene ligands within the molecule. Increased electron donation from the nitrogen lone pair towards the carbene carbon atom results in a $C_{carbene}$-N bond order greater than one. The bonding situation is best described as an intermediate between the zwitterionic isomers **A**, **C** and the neutral carbene **B**. The carbene carbon resonances obtained from the ^{13}C NMR spectra reflect this marked contribution from the carbene heteroatom substituent, -OEt vs –NHBu. In the case of **4** and **6**, upfield shifts for the carbene carbon atom (271.9, 260.9ppm for **4**, and 268.8, 261.3, 261.0 and 258.1, respectively, for the three isomers of **6**), compared to **3** and **5** (316.4 and 321.9ppm, respectively).

Table 2.2 Selected ^{1}H and ^{13}C NMR resonance data and IR ν(CO) stretching frequencies for **1** – **6**.

Complex	H_α δ ^{1}H (ppm)	$C_{carbene}$ δ ^{13}C, (ppm)	A_1'' ν(CO), (cm^{-1})	A_1' ν(CO), (cm^{-1})
1	4.93	329.7	2056	1949
2	5.00	306.2	2054	1938 (overlap E)
3	8.24	316.4	2058	1957
4	7.44, 7.44	271.9, 260.9	2056	1917
5	8.06	321.9	2054	1964
6	7.87, 7.84, 7.70, 7.69	268.8, 261.3, 261.0, 258.1	2054	1918

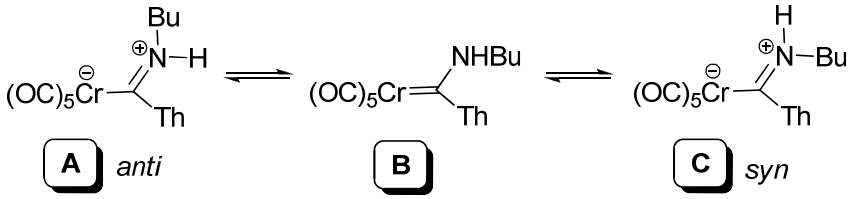

Scheme 2.2 Stabilisation of aminocarbene complex **B** by formation of the mesomeric zwitter ionic species **A** and **C**, see text.

The infrared spectra of all complexes clearly displayed the expected band pattern associated with the carbonyl stretches of a $[Cr(CO)_5L]$ system,[33] and no duplication of carbonyl frequencies was observed for the *syn*- and *anti*-isomers of **4** and **6**, as the carbonyls are fairly insensitive to changes of substituents of ligands.[28] In the case of **3**, the IR spectrum measured shows the lifting of the degeneracy of the E-band that appears as two separate signals. In **2**, overlapping of the signals associated with the A'_1 and the E-modes occur. The A''_1 mode defines the symmetric stretch of the CO ligands in the equatorial plane, and is mostly unaffected by the π-acceptor ability of the ligand L; stretching frequencies vary between 2054 – 2058 cm^{-1} (see Table 2.1). The A'_1 mode in the pseudo-C_{4v} local symmetry represents the mode with the greatest

contribution to the stretching of the C-O bond *trans* to L, and is most affected by changes in the electronic environment caused by the carbene ligand.[29] For aminocarbene complexes **4** and **6**, nitrogen lone pair stabilisation causes a marked decrease in chromium π-backbonding towards the carbene ligand. This is demonstrated by the occurrence of the A'_1-band at lower wavenumbers (Table 2.1), at frequencies lower than even the E-band.

Electrochemistry and molecular orbital analyses

Cyclic voltammetry (CV), linear sweep voltammetry (LSV), and Osteryoung square-wave voltammetry (SW) were conducted on **1** – **6** in dry, oxygen-free CH_2Cl_2 utilizing 0.1 mol dm^{-3} $[N(^nBu)_4][PF_6]$ as supporting electrolyte. Data for cyclic voltammetry experiments are summarized in Table 2.2, CV's are shown in Fig. 2.3-2.5.

Four redox processes are identifiable. These are (a) the reduction of the carbene double bond; peaks for this process are labelled I throughout in Fig.'s 2.3 – 2.5, (b) oxidation of the Cr(0) centre to Cr(I) is observed at peak 1, (c) oxidation of the ferrocenyl group in **1** and **2** (peak Fc), and (d) oxidation of electrochemically generated Cr(I) centre to Cr(II). The latter redox process is labelled as peak 2 in Table 2.2 and Fig. 2.4. Molecular orbital calculations (see below) proved peak 2 is associated with the $Cr^{I/II}$ couple and not with oxidation of the :OEt or :NHBu groups. Central to this electrochemical study is the ferrocenyl oxidation of **1** and **2** (Fig. 2.3-2.5). The ferrocenyl group is well established as a moiety that undergoes electrochemical and chemical reversible one electron oxidation. Electrochemical and chemical reversible redox process are characterised by $\Delta E = E_{pa} - E_{pc} = 59$ mV and $i_{pc}/i_{pa} = 1$.[34] For **1**, the ferrocenyl-based redox process is observed at 0.700 V vs. the free FcH/FcH^+ couple and exhibits $\Delta E = 89$ mV and $i_{pc}/i_{pa} = 1$ (Table 2.2). The observed $E^{o'}$=0.700 V is a large shift to positive potentials from 0 V, and illustrates the electrophilic nature of the chromium carbene system.[10] It is important to note that peak 1 in the CV of **1** at $E^{o'}$=0.289 V is not associated with the ferrocenyl couple, but rather with Cr(0) oxidation to Cr(I); this will be discussed below. The ferrocenyl wave of **2** is observed at $E^{o'}$ = 730 mV, but this redox process leads to adsorption and decomposition, Fig. 2.4 and 2.5, implying E_{pc} and current ratios are not reliable. However the LSV applicable to the oxidation of the ferrocenyl group and the two Cr(0) centres (waves 1a, 1b and Fc, Fig. 2.5) were still consistent with three separate 1-electron transfer processes.

Table 2.3 Cyclic voltammetry data of 0.5 mmol dm^{-3} solutions of **1** – **6** in CH_2Cl_2 containing 0.1 mol dm^{-3} $[N(nBu)_4][PF_6]$ as supporting electrolyte at a scan rate of 100 mV s^{-1} and 20 °C. Potentials are relative to the FcH/FcH^+ couple.

Complex	Peak no.	$E^{o'}$/V, ΔE/mV	$i_{pa}/\mu A$, i_{pc}/i_{pa}
1	I(=)	-2.148, 111	3.20 [b], 0.41
	1($Cr^{0/I}$)	0.289, 102	3.48, 0.89
	(Fc)	0.700, 89	3.29, 0.85
	2($Cr^{I/II}$)	- [a] , - [a]	- [a] , - [a]
2	I(=)	-1.845, 104	3.81 [b], 0.39
	1a($Cr^{0/I}$)	0.499, 83	3.71, 0.73
	1b($Cr^{0/I}$)	0.650, 80	3.51, 0.23
	(Fc)	0.730, 97	3.78, < 0.1
	2($Cr^{I/II}$)	- [a] , - [a]	- [a] , - [a]
3	I(=)	-1.762, 98	3.71 [b], 0.43
	1($Cr^{0/I}$)	0.565, 85	3.98, 0.88
	2($Cr^{I/II}$)	- [a] , - [a]	- [a] , - [a]
4	I(=)	-2.232, 132	3.21 [b], 0.11
	1a($Cr^{0/I}$)	0.258,	1.83, 0.80
	1b($Cr^{0/I}$)	242	1.75, - [c]
	2($Cr^{I/II}$)	0.435[c], - [c]	7.02, - [c]
		0.951[c], - [c]	
5	D(=)	-2.091, 88	1.89 [b], 0.59
	I(=)	-1.845, 232	0.68[b], 0.78
	1($Cr^{0/I}$)	0.576, 68	0.81, 0.81
	2($Cr^{I/II}$)	1.098[d], - [d]	2.50[d], - [d]
6	I(=)	- [a] , - [a]	- [a] , - [a]
	1($Cr^{0/I}$)	0.399, 138	4.81, 0.69
	2($Cr^{I/II}$)	1.150[d], - [d]	7.42[d], - [d]

[a] no peak detected within the potential window of the solvent; [b] i_{pc} and i_{pa}/i_{pc} values to maintain the current ratio convention of $i_{forward\ scan}/i_{reverse\ scan}$; [c] Estimated E_{pa}; resolution not good enough to estimate E_{pc}; [d] E_{pa} value, no E_{pc} detected.

Having confirmed the one-electron transfer nature of the ferrocenyl group in **1**, all the other redox processes in **1–6** can now be interpreted in terms of the number of electrons that is transferred during their redox cycles. Alkene reduction occurs at far negative potentials and in aprotic solvents results in the generation of a radical anion of considerable instability during a one-electron transfer process.[35] Follow-up chemical reactions destroy this electrochemically generated species quickly. Unconjugated alkenes often are reduced at such negative potentials that they cannot be studied in convenient electrochemical solvents; for them reduction often takes place at potentials outside the solvent potential window.[31] Conjugated alkenes are reduced at slightly larger potentials; reduction in aprotic media may be observed in the vicinity of -2 V vs. FcH/FcH^+.[31] The carbene double bond, Cr=C, of the present series of compounds benefits from the presence of the electron-donating thienyl or ferrocenyl group which allows for conjugation (Fig. 2.1). Reduction of the Cr=C double bond in **1** – **5** was observed at potentials less than −1.76 V vs FcH/FcH^+ (Table 2.2, wave I). That the Cr=C double bond reduction represents a one-electron reduction follows from comparing the i_{pc} value of peak I of **1** (Table 2.2 and Fig. 2.3) with the i_{pa} value of the ferrocenyl, i.e. wave Fc. Since they are striving to the same value (ca. 3.34 μA), and since the ferrocenyl couple represents a one-electron transfer process, wave I must also represent a one-electron reduction process to initially generate $^{-}$Cr-C$^{\bullet}$, not only in **1**, but also in the other carbene complexes of this study. This assignment is possible because it is known that the LUMO is mainly carbene-ligand based,[17] and single electron transfer reactions followed by ESI-MS have also indicated the formation of such $^{-}$Cr-C$^{\bullet}$ species.[36] Since the orbitals associated with carbenes are delocalized over metal, carbon, and heteroatom, one can envisage the $^{-}$Cr-C$^{\bullet}$ species as being stabilised by distributing charge and radical all over the ligand system.

Cr=C reduction is electrochemically quasi reversible because ΔE for this process is substantially larger than 59 mV (Table 2.2). It is also only partially chemically reversible because the i_{pa}/i_{pc} current ratios for **1–5** (Table 2.2) deviate more than 40% from unity. This low current ratio is consistent with the high reactivity that is associated with carbon radicals, here $^{-}$Cr-C$^{\bullet}$, as described before.[31] The ferrocenyl group stabilized the Cr=C bond much more towards reduction than the thienyl group as the Cr=C bond of **1** was reduced at a potential 386 mV more negative than the carbene double bond of **3.** Strikingly, stabilisation towards reduction of the

Cr=C bond with a ferrocenyl group is almost as effective as stabilisation with an amine because the peak I $E^{o'}$ value of **4** is only 84 mV more negative than that of **1**, but 470 mV more negative than that of **3** (Table 2.2).

The biscarbene complexes **2** and **5** exhibited Cr=C reduction at potentials 303 mV more positive than **1**. This move towards higher potentials is consistent with the extended conjugation paths present in the bis-compounds.[31] The CV of the biscarbene complex **5** exhibits two reduction waves labelled I and D (Fig. 2.4). The first, wave I, is assigned to the simultaneous reduction of both the Cr=C bonds as the LSV (Fig. 2.4) shows it involves transfer of two electrons, one for each double bond. For reference purposes at this stage it is sufficient to observe peak 1 also represents 2x1e^- transfer processes, 1 e^- for each of the Cr(0) processes. The second reduction wave, wave D, is attributed to electrode processes of decomposition products[31] of **5** because the LSV shows that six electrons in total is associated with this redox process. Complex **2** was too unstable for LSV measurement because of decomposition on LSV timescale at large negative potentials. However, the i_{pc} value of wave I for **2** , if one allows for limited decomposition of the Cr=C double bond, and compares it with the i_{pa} values of waves 1a, 1b and Fc, is consistent with two overlapping one-electron Cr=C reductions. The biscarbene **6** showed no Cr=C reductions (Table 2.2) within the usable potential window of CH_2Cl_2. This is expected since one NHBu group shifted peak I of **4** at -2.232 V to potentials 470 mV more negative compared to peak I of **3**. This is already almost at the limit of the potential window that CH_2Cl_2 allows. Since **6** possesses two NHBu groups, an additional shift to more negative potentials is expected which would result in wave I not being detectable in the workable potential window of CH_2Cl_2.

Oxidation of the Cr(0) centre itself is associated with peak 1 in Fig. 2.3 – 2.5 and Table 2.2. Once again, by comparing peak currents of wave 1 and wave Fc for **1** it is clear that Cr(0) oxidation involves a one-electron transfer process to generate Cr(I). To decide whether Cr(0) or ferrocenyl oxidation takes place first, from an electrochemical point of view, comparison of the position of wave 1 in **1** with those of amino carbenes **4** and **6**, Fig. 2.3, is appropriate. It is clear that Cr oxidation waves are in all three cases in the same potential range. The ferrocenyl group is therefor expected to be associated with the wave at larger potentials, that is wave Fc for **1**. This conclusion is mutually consistent with the result obtained by molecular orbital calculations. Density functional theory (DFT) calculations at the B3LYP/def2-SVP[37] level show that the HOMO of complexes **1**, **3** and **4** is mainly located at the chromium(0) atom (Fig. 2.6),[2d,38] thus

confirming that the first oxidation process in all complexes can be attributed to the Cr(0) to Cr(I) oxidation. Interestingly, the energy order of the HOMO's (**3** = -5.96 eV > **1** = -5.84 eV > **4** = -5.70 eV, see Fig. 2.6) agrees with the trend the measured wave 1 electrochemical potentials suggests in that a more stabilized HOMO results in a more difficult oxidation process (**3**, $E^{o'}$=0.565 V > **1**, $E^{o'}$=0.289 V > **4**, $E^{o'}$=0.258 V, see Table 2.2).

Electrochemical evidence also imply that Cr(0) oxidation occurs before ferrocenyl oxidation in the biscarbene complex **2**. Fig. 2.4, bottom, shows the CV's of **2** where oxidation peaks 1a, 1b and Fc are all three observed. Importantly, each of these waves represents a one-electron transfer process as highlighted by the LSV (Fig. 5). After the third oxidation though (i.e. after wave Fc), the complex decomposes on LSV time scale. In contrast, on CV time scale, the observed larger-than-expected peak cathodic currents are consistent with electrode deposition of the oxidised substrate. That electrode deposition takes place after the third (ferrocenyl) oxidation to generate $\mathbf{2}^{3+}$ was confirmed by repeating CV experiments utilising a reversal potential small enough to exclude wave Fc. This resulted in waves 1a and 1b having the normal CV shape. Waves 1a and 1b are associated with two consecutive and partially resolved one-electron Cr(0) oxidations because they are both observed at potentials smaller than the ferrococenyl oxidation of **1**, Table 2.2. This excludes the possibility of either of these waves to be associated with the oxidation of the ferrocenyl group. After both Cr(0) centres have been oxidised to liberate a more electron-deficient and therefore more electron-withdrawing species, $\mathbf{2}^{2+}$, than the mother compound **2**, the oxidation of the ferrocenyl group of **2** is observed at a larger potential (30 mV larger) than that of **1**. Because the ferrocenyl group is oxidised in a one-electron transfer step, it follows that the Cr(0) centres are also oxidised in a one-electron transfer step as confirmed by LSV measurements. That wave 1 could be resolved into two components 1a and 1b is not unusual. Different formal reduction potentials for symmetrical complexes in which mixed-valent redox-active intermediates are generated (here, for example $\mathbf{2}^{+}$ and $\mathbf{2}^{2+}$ respectively) are well known in systems that allow through-bond electronic communication between these molecular fragments.[39] Since a similar split of wave 1 into two components was not observed for the thiophene biscarbene derivative **5**, it is concluded that the ferrocenyl group is more effective in allowing through-bond electronic communication between molecular fragments than a thienyl group.

Chromium oxidation in the ethoxy derivatives **1**- **3** and **5** are, like ferrocenyl oxidation,

electrochemical and chemical reversible on CV time scale as ΔE deviated within acceptable limits from the theoretical value of 59 mV and because peak current ratios for these compounds approached unity, Table 2.2.

The aminobutyl derivatives **4** and **6** exhibit electrochemically irreversible Cr(0) oxidations by virtue of ΔE values exceeding 130 mV under our conditions. Chemical reversibility as identified by peak current ratios approaching 1 is achieved when the reversal anodic potential is small enough to exclude wave 2. The CV of amino carbene **4** hinted that the Cr(0) oxidation peak, peak 1, may also split into two very poorly resolved components, 1a and 1b (Fig. 2.4). This may be indicative of the presence of two Cr(0) species of sufficient stability and long enough existence time to allow detection on CV timescale. Aminocarbene complexes have high stability due to the existence of the zwitterionic stabilised form as shown in Scheme 2.2. CV peak 1a is consistent with forms A and C and peak 1b with form B. Although it was possible to distinguish between A and C spectroscopically, it is unlikely that electrochemical techniques can distinguish between forms A and C of Scheme 2.2. Electrochemical observation of two components of a slow equilibrium is not unknown. A similar situation arose with metallocene-containg β-diketones, where the kinetics between keto and enol forms was slow enough to allow detection of both equilibrium components, and to determine the rate of keto to enol conversion and vice versa.[40] No evidence of peak 1 splitting into two components could be observed for the biscarbene **6** implying peaks 1a and 1b in this case may simply be so close to each other that they are unresolved.[41]

The last electrochemical process that was observed (peak 2 in Fig. 2.3 and 2.4 and Table 2.2) in **1** – **6** is the oxidation of the electrochemically generated Cr(I) centre to generate a Cr(II) species (Scheme 2.3). This electrochemical process is not assigned to oxidation of the : OEt group of **1** - **3** and **5** or the :NHBu group of **4** and **6** because DFT calculations showed the spin densities of the electrochemically generated radical cations formed during the oxidation of Cr(0) are situated on the newly formed Cr(I) centre and not the hetero atoms (Fig. 2.6). Cr(I) oxidation of the monocarbenes **1** and **3** fell outside the potential window of the solvent, CH_2Cl_2, but wave 2 in the CV of the bis-complex **5** is consistent with two Cr(I) centres being irreversibly oxidised (Fig. 2.4) at ca. 1.1 V. The LSV suggests that the number of electrons that are transferred at this wave is the same as for wave 1, that is two electrons. In contrast, the CV itself (Fig. 2.4, Table 2.2) show $i_{pa,\ wave\ 2}$ to be almost double that of $i_{pa,\ wave\ 1}$. However, wave 2 is so close to the edge of

the potential window of the solvent, that the observed peak anodic current for wave 2 of **5** may well include the beginning of solvent degradation.

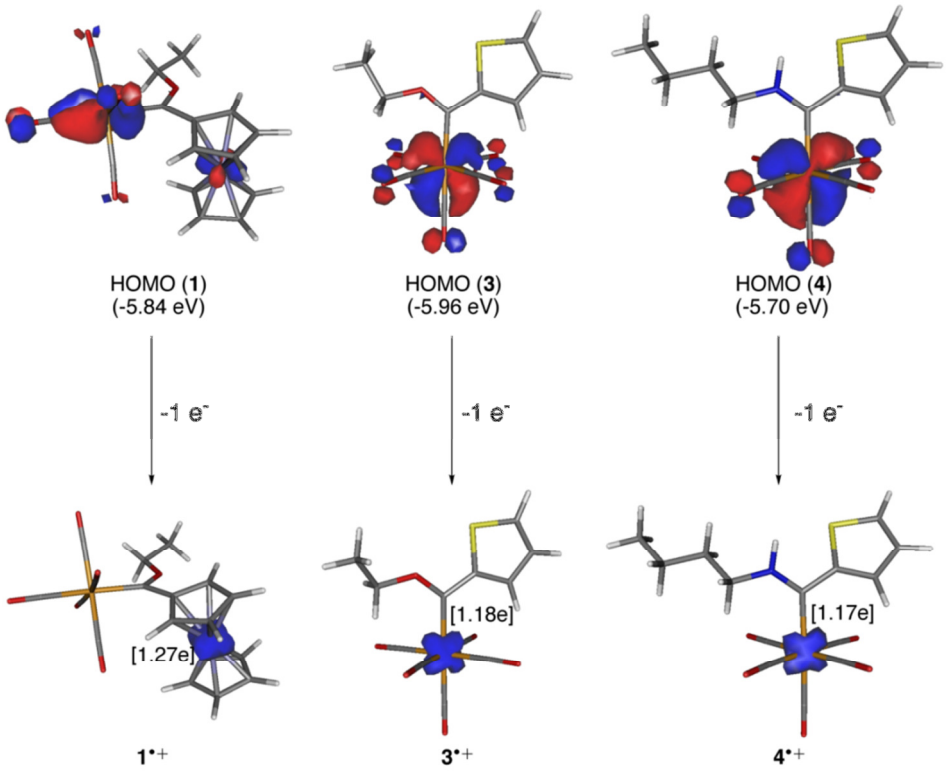

Fig. 2.6 Computed HOMO's of complexes **1**, **3** and **4** (top) and spin densities of the corresponding radical cations (bottom). Numbers in brackets indicate the computed Mulliken-spin densities. All data have been computed at the B3LYP/def2-SVP level.

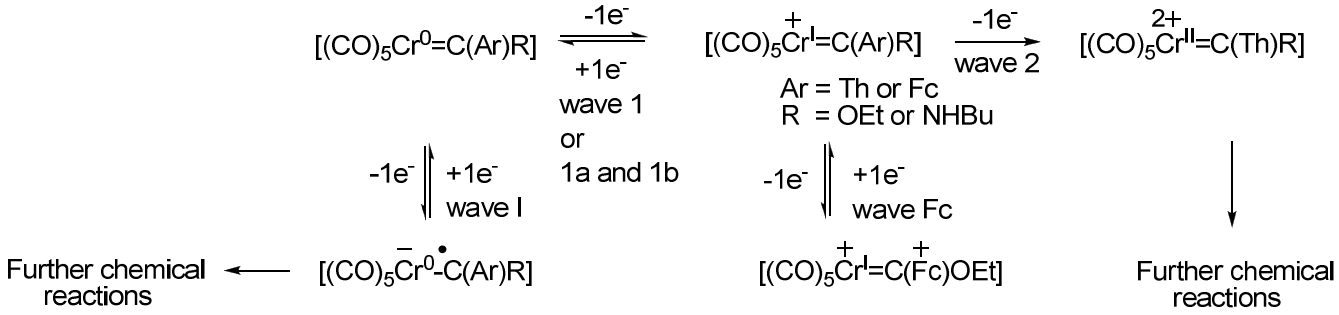

Scheme 2.3 Electrochemical reactions associated with **1**, **3** and **4**. The radical anions and Cr(II)-containing cations that are generated during the final electrochemical reduction or oxidation step undergoes further chemical reactions. The biscarbene complexes undergo the same reaction sequences except that a second radical anion and Cr(II)-containing cation also forms at potentials close to the edges of the solvent, dichloromethane. Two Cr(0) oxidations was also observed in the biscarbene compounds.

The aminocarbene complexes **4** and **6** also exhibit wave 2 (Fig. 2.4), showing Cr(I) oxidation is irreversible, and occurring at slightly lower potentials than in the ethoxycarbene complexes (Table 2.2). The irreversible nature of these oxidations illustrates the high reactivity of the Cr(II) species that form during the oxidation. They chemically react to form new species on time scales faster than that of cyclic voltammetry. This contrasts the lower reactivity of the radical anions, $^{-}$Cr-C$^{\bullet}$, which did not react chemically fast enough to escape detection of electrochemical reoxidation to the mother Cr=C species at fast scan rates (wave I, Fig 2.4).

Fig. 2.6 gathers the computed spin density of the neutral complexes **1**, **3** and **4** as well as the spin density of the corresponding radical cations formed by one-electron oxidation of these complexes to generate **1**$^{\bullet+}$, **3**$^{\bullet+}$ and **4**$^{\bullet+}$. Whereas the unpaired electron is located on the chromium atom in complexes **1**, **3** and **4** as well as on **3**$^{\bullet+}$ and **4**$^{\bullet+}$, it is located on the iron atom in the ferrocenyl-substituted radical cation **1**$^{\bullet+}$. This suggests that the oxidation associated with peak 2 in the CV's of Fig. 2.4 can be assigned to the oxidation of Cr(I) to Cr(II) in compounds **3** and **4**, while the oxidation associated with wave Fc of complex **1** (Fig. 2.3) should be a ferrocenyl-based process.

2.4 CONCLUSION

The novel mono- and bisaminocarbene complexes **4** and **6** were prepared by aminolysis of the ethoxy(thienyl) chromium(0) precursors **3** and **5**. Ferrocenyl mono- and bisethoxychromium(0) carbene complexes **1** and **2** were also synthesised and characterised spectroscopically. An electrochemical investigation of these complexes in CH_2Cl_2 showed the carbene double bond, Cr=C, of **1 – 6** are reduced to an anion radical, $^{-}$Cr-C$^{\bullet}$, at large negative potentials. Electrochemical measurements and DFT calculations were mutually consistent in showing Cr(0) oxidation to Cr(I) occurs before ferrocenyl oxidation, and that the electrochemically generated Cr(I) centre can undergo a second irreversible oxidation to generate Cr(II) at large positive potentials. No oxidation of the hetero atoms in the OEt or NHBu groups could be detected. Cr(II) oxidation for **1** and **3** as well as Cr=C reduction for **6** fell outside the solvent potential window.

The reactivity towards follow-up chemical reactions of the anodically produced Cr(II) centres is much higher than the reactivity of the cathodically produced radical anions as the latter was still

observably reoxidised to the parent Cr=C species at fast scan rates. The former showed no indication of any reductive regeneration, even at fast scan rates. The ferrocenyl group is oxidised electrochemically reversible to ferrocenium at larger potentials than the electrochemically reversible oxidation of the Cr(0) centre to Cr(I). All redox active groups in **1** – **6** were involved in one-electron transfer steps. The ferrocenyl group was electrochemically shown to stabilise the Cr=C centre almost as much as the NHBu, and much more than the ethoxy and thienyl groups. Poorly resolved peak splitting of the Cr(0) oxidation of **4** into components a and b is consistent with the parent aminocarbene being in slow equilibrium with the zwitter ionic species $[(OC)_5Cr^{-}–C=(N^{+}BuH)Th]$. An electrochemical scheme is proposed to account for all observed electrochemical steps.

2.5 ACKNOWLEDGEMENTS

This work is supported by the National Research Foundation, (DIB, Grant number 76226; JCS, Grant number 81829).

2.6 REFERENCES

1 See annual reviews by: J.W. Herndon, *Coord. Chem. Rev.,* 2002 – 2012.

2 *(a)* J. Poater, M. Cases, X. Fradera, M. Duran and M. Sola, *Chem. Phys.* 2003, **294**, 129; *(b)* A. Krapp and G. Frenking, *J. Am. Chem. Soc.,* 2008, **130**, 16646; *(c)* A. Krapp, K.K. Pandey and G. Frenking, *J. Am. Chem. Soc.* 2007, **129**, 7596; *(d)* M. Cases, G. Frenking, M. Duran and M. Sola, *Organometallics,* 2002, **21**, 4182; *(e)* G. Frenking, M. Sola and S.F. Vyboishchikov, *J. Organomet. Chem.,* 2005, **690**, 6178; *(f)* M.L. Lage, I. Fernandez, M.J. Mancheno and M.A. Sierra, *Inorg. Chem.,* 2008, **47**, 5253.

3 D.M. Andrade, M.E.Z. Michoff, I. Fernandez, A.M. Granados and M.A. Sierra, *Organometallics,* 2007, **26**, 5854.

4 *(a)* M.K. Lloyd, J.A. McCleverty, D.G. Orchard, J.A. Connor, M.B. Hall, I.H. Hillier, E.M. Jones and G.K. McEwen, *J. Chem. Soc., Dalton Trans.,* 1973, 1743; *(b)* C.P. Casey, L.D. Albin, M.C. Saeman and D.H. Evans, *J. Organomet. Chem.,* 1978, **155**, C37; *(c)* A. Limberg, M.A.N.D.A. Lemos, A.J.L. Pombeiro, S. Maiorana, A. Papagni and E.

Licandro, *Portugaliae Electrochim. Acta,* 1995, **13**, 319; *(c)* A.J.L. Pombeiro, *New J. Chem.,* 1997, **21**, 649.

5 *(a)* T. Kuwana, D.E. Bublitz, and G. Hoh, *J. Am. Chem. Soc.* 1960, **82**, 5811; *(b)*T. Ogata, K. Oikawa, T. Fujisawa, S. Motoyama, T. Izumi, A. Kasahara,. And N. Tanaka, *Bull. Chem. Soc. Jpn*, 1981, **54**, 3723; *c)* K.-F. Chin and K.-Y. Wong and C.-M. Che, *J. Chem. Soc. Dalton Trans.* 1993, 197.

6 *(a)* H.J. Gericke, A.J. Muller and J.C. Swarts, *Inorg. Chem.*, 2012, **51**, 1552; *(b)* A. Auger, A.J. Muller and J.C. Swarts, *Dalton Trans.* 2007, 3623.

7 *(a)* For a recent review, see: D. I. Bezuidenhout, S. Lotz, D.C. Liles and B. van der Westhuizen, *Coord. Chem. Rev.,* 2012, **256**, 479; *(b)* I. Hoskovcova, R. Zverinova, J. Rohacova, D. Dvorak, T. Tobrman, S. Zalis and J. Ludvik, *Electrochim. Acta,* 2011, **56**, 6853; *(c)* I. Hoskovcova, J. Rohacova, D. Dvorak, T. Tobrman, S. Zalis, R. Zverinova and J. Ludvik, *Electrochim. Acta,* 2010, **55**, 8341; *(d)* A.J.L. Pombeiro, *J. Organomet. Chem.*, 2005, **690**, 6021; *(e)* I. Hoskovcova, J. Rohacova, L. Meca, T. Tobrman, D. Dvorak and J. Ludvik, *Electrochim. Acta,* 2005, **50**, 4911; *(f)* H.G. Raubenheimer, A. du Toit, M. du Toit, J. An, L. van Niekerk, S. Cronje, C. Esterhuysen and A.M. Crouch, *Dalton Trans.,* 2004, 1173.

8 C. Baldoli, P. Cerea, L. Falciola, C. Giannini, F. Licandro, S. Maiorana, P. Mussini and D. Perdiccia, *J. Organomet. Chem.,* 2005, **690**, 5777.

9 While writing this publication, the authors became aware of an independent but simultaneously conducted electrochemical study of related but different chromium carbene complexes, see R. Metelkova, T. Tobrman, H. Kvapilova, I. Hoskovcova and J. Ludvik, *Electrochim. Acta*, 2012, **82**, 470.

10 J.A. Connor, E.M. Jones and J.P. Lloyd, *J. Organomet. Chem*., 1970, **24**, C20.

11 D.I. Bezuidenhout, E. van der Watt, D.C. Liles, M. Landman and S. Lotz, *Organometallics,* 2008, **27**, 2447.

12 *(a)* A. Hildebrandt, T. Rüffer, E. Erasmus, J.C. Swarts and H. Lang, *Organometallics*, 2010, **29**, 4900; *(b)* V. Chandrasekhar and R. Thirumoorthi, *Organometallics* 2007, **26**, 5415; *(c)* S. Ogawa, H. Muroaka, K. Kikuta, F. Saito, R. Sato, *J. Organomet. Chem.* 2007, **692**, 60.

13 *(a)*W.L. Davis, R.F. Shago, E.H.G. Langner and J.C. Swarts, *Polyhedron*, 2005, **24**, 1611 *(b)* P.J. Swarts, M. Immelman, G.J. Lamprecht, S.E. Greyling and J.C. Swarts, *S. Afr. J. Chem.* **1997**, *50*, 208; *(c)* S. Campidelli, L. Perez, J. Rodrigues-Lopez, J. Barbera, F. Langa, and R. Deschenaux, *Tetrahedron*, 2006, **62**, 2115.

14 J. Conradie and J.C. Swarts, *Organometallics*, 2009, **28**, 1018.

15 *(a)* B. Bildstein, *J. Organomet. Chem*., 2001, **617–618**, 28; *(b)* E.W. Neuse and D.S. Trifan, *J. Am. Chem. Soc.* 1963, **85**, 1952.

16 H. Meerwin, *Org. Synth.*, 1966, **46**, 113.

17 D.I. Bezuidenhout, W. Barnard, B. van der Westhuizen, E. van der Watt and D.C. Liles, *Dalton Trans.*, 2011, **40**, 6711.

18 J.A. Connor and J.P. Lloyd, *J. Chem. Soc., Dalton Trans*., 1972, **14**, 1470.

19 Y.M. Terblans, H.M. Roos and S. Lotz*, J. Organomet. Chem*., 1998, **566**, 133.

20 *(a)* L.J. Faruggia, *J. Appl. Crystallogr.*, 1997, **30**, 565, *(b)* C.J. Cason, *POV-RAY for Windows;* Persistence of Vision, 2004.

21 *APEX2 (including SAINT and SADABS)*; Bruker AXS Inc., Madison, WI, 2012.

22 G.M. Sheldrick, *Acta Crystallogr., Sect A: Found. Crystallogr*., 2008, **A64**, 112.

23 *(a)* G. Gritzner and J Kuta, *J. Pure Appl. Chem.*, 1984, **56**, 461; *(b)* R.R. Gagne, C.A. Koval and G.C. Lisensky, *Inorg. Chem.*, 1980, **19**, 2855.

24 Leading references describing the electrochemical activity and behaviour of ferrocene and decamethylferrocene in a multitude of organic solvents are *(a)* I. Noviandri, K.N. Brown, D.S. Fleming, P.T. Gulyas, P.A. Lay, A.F. Masters and L. Phillips, *J. Phys. Chem. B*, 1999, **103**, 6713; *(b)* N.G. Connelly, W.E. Geiger, *Chem. Rev.*, 1996, **96**, 877; *(c)* J. Ruiz, D. Astruc, C.R. Acad. Sci. (Paris), Ser. IIc 1998, **1**, 21; *(d)* R.J. Aranzaes, M.C. Daniel and D. Astruc, *Can. J. Chem.*, 2006, **84,** 288.

25 Gaussian 09, Revision B.1, M. J. Frisch, G. W. Trucks, H. B. Schlegel, G. E. Scuseria, M. A. Robb, J. R. Cheeseman, G. Scalmani, V. Barone, B. Mennucci, G. A. Petersson, H. Nakatsuji, M. Caricato, X. Li, H. P. Hratchian, A. F. Izmaylov, J. Bloino, G. Zheng, J. L. Sonnenberg, M. Hada, M. Ehara, K. Toyota, R. Fukuda, J. Hasegawa, M. Ishida, T. Nakajima, Y. Honda, O. Kitao, H. Nakai, T. Vreven, J. A. Montgomery, Jr., J. E. Peralta, F. Ogliaro, M. Bearpark, J. J. Heyd, E. Brothers, K. N. Kudin, V. N. Staroverov, R. Kobayashi, J. Normand, K. Raghavachari, A. Rendell, J. C. Burant, S. S. Iyengar, J.

Tomasi, M. Cossi, N. Rega, J. M. Millam, M. Klene, J. E. Knox, J. B. Cross, V. Bakken, C. Adamo, J. Jaramillo, R. Gomperts, R. E. Stratmann, O. Yazyev, A. J. Austin, R. Cammi, C. Pomelli, J. W. Ochterski, R. L. Martin, K. Morokuma, V. G. Zakrzewski, G. A. Voth, P. Salvador, J. J. Dannenberg, S. Dapprich, A. D. Daniels, Ö. Farkas, J. B. Foresman, J. V. Ortiz, J. Cioslowski, and D. J. Fox, Gaussian, Inc., Wallingford CT, 2009.

26 (a) A. D. Becke, *J. Chem. Phys*. **1993**, *98*, 5648. (b) Lee, C.; Yang, W.; Parr, R. G. *Phys. Rev. B* **1998**, *37*, 785.

27 F. Weigend, R. Ahlrichs, *Phys. Chem. Chem. Phys*. **2005**, *7*, 3297.

28 J. W. McIver, A. K. Komornicki, *J. Am. Chem. Soc*. **1972**, *94*, 2625.

29 *(a)* D.I. Bezuidenhout, D.C. Liles, P.H. van Rooyen and S. Lotz, *J. Organomet. Chem.,* 2007, **692**, 774; *(b)* U. Klabunde and E.O. Fischer, *J. Am. Chem. Soc*., 1967, **89**, 7141.

30 *(a)* M. Landman, H. Görls, S. Lotz, *J. Organomet. Chem*., 2001, **617**, 280, *(b)* M. Landman, H. Görls, S. Lotz, *Eur. J. Inorg. Chem*., 2001, 233, *(c)* M. Landman, J. Ramontja, M. van Staden, D.I. Bezuidenhout, P.H. van Rooyen, D.C. Liles, S. Lotz, *Inorg. Chim. Acta*, 2010, **363**, 705.

31 T.E. Pickett and C.J. Richards, *Tetrahedron Lett.,* 1999, **40**, 5251.

32 *(a)* E.W. Post and K.L. Watters, *Inorg. Chim. Acta,* 1978, **26**, 29; *(b)* E. Moser and E.O. Fischer, *J. Organomet. Chem.*, 1968, **15**, 147.

33 *(a)* P.S. Braterman, *Metal Carbonyl Spectra*; Academic Press Inc.: London, 1975, p 68*; (b)* D. M. Adams, *Metal–Ligand and Related Vibrations*, Edward Arnold Publishers Ltd, London, 1967, p 98.

34 *(a)* H.J. Gericke, N.I. Barnard, E. Erasmus, J.C. Swarts, M.J. Cook and M.A.S. Aquino, *Inorg. Chim. Acta,* 2010, **363**, 2222; *(b)* D. H. Evans, K. M. O'Connell, R. A. Peterson and M. J. Kelly, *J. Chem. Educ.*, 1983, **60**, 290. *(c)* P.T. Kissinger and W.R. Heineman, *J. Chem. Educ.* 1983, **60**, 702. *(d)* J. J. Van Benshoten, L.Y. Lewis and W.R. Heineman, *J. Chem. Educ.*, 1983, **60**, 772. *(e)* G. A. Mobbott, *J. Chem. Educ.*, 1983, **60**, 697.

35 *(a)* A. J. Fry, *Synthetic Organic Electrochemistry*, 2nd ed., John Wiley and Sons, New York,1989, p 208, 232; *(b)* J Volke and F Liska, *Electrochemistry in Organic Synthesis*, Springer-Verlag, Berlin, 1994, p 90.

36 M. L. Lage, M. J. Mancheño, R. Martínez-Álvarez, M. Gómez-Gallego, I. Fernández and M. A. Sierra, *Organometallics* **2009**, *28*, 2762.

37 See Computational Details.

38 This result is not surprising as the HOMO of the group 6 Fischer carbene complexes is located in the transition metal in most cases. See, for instance: (a) I. Fernández, M. A. Sierra and F. P. Cossío, *J. Org. Chem.* **2006**, *71*, 6178; (b) I. Fernández, M. A. Sierra and F. P. Cossío, *J. Org. Chem.* **2008**, *73*, 2083; M. L. Lage, I. Fernández, M. J. Mancheño and M. A. Sierra, *Inorg. Chem.* **2008**, *47*, 5253; D. M. Andrada, A. M. Granados, M. Solà and I. Fernández, *Organometallics* **2011**, *30*, 466.

39 *(a)* C. Creutz and H. Taube, *J. Am. Chem. Soc.* 1969, **91**, 3988; *(b)* M.J. Cook, I. Chambrier, G. White, E. Fourie and J.C. Swarts, *Dalton Trans.* 2009, 1136; *(c)* N. Van Order, W.E. Geiger, T.E. Bitterwolf and A.L. Reingold, *J. Am. Chem. Soc.* 1987, **109**, 5680; (d) D.T Pierce, and W.E. Geiger, *Inorg. Chem.* 1994, **33**, 373; *(e)* E. Fourie, J.C. Swarts, I. Chambrier and M.J. Cook, *Dalton Trans*. 2009, 1145; *(f)* W.E. Geiger, N. Van Order, D.T. Pierce, T.E. Bitterwolf, A.L. Reingold and N.D. Chasteen, *Organometallics* 1991, **10**, 2403.

40 *(a)* K.C. Kemp, E. Fourie, J. Conradie and J.C. Swarts, *Organometallics*, 2008, **27**, 353; *(b)* W.C. Du Plessis, W.L. Davis, S.J. Cronje and J.C. Swarts, *Inorg. Chim. Acta*, 2001, **314**, 97.

41 The potentials of two closely-spaced redox events are very difficult to determine utilising voltammetric methods, see D.E. Richardson and H. Taube, *Inorg. Chem.*, 1981, **20**, 1287.

CHAPTER 3

Substituent Effects on the Electrochemical, Spectroscopic and Structural Properties of Fischer Mono- and Biscarbene Complexes of Chromium(0)

This chapter was published in Inorganic Chemistry. The format reflects the style set by the journal.

Belinda van der Westhuizen,[a] Pieter J. Swarts,[b] Louise M. van Jaarsveld,[a] David C. Liles,[a] Uwe Siegert,[b] Jannie C. Swarts,[b] Israel Fernández,[c] and Daniela I. Bezuidenhout[a], *Inorganic Chemistry,* **2013**, *52*, 6674-6684.

Author contributors

Synthetic work: Belinda van der Westhuizen, Louise M. van Jaarsveld

Cyclic voltammetry and data analysis: Pieter J. Swarts, Jannie C. Swarts, Uwe Siegert

Computational work: Israel Fernández

Chrystallography: David C. Liles

Article written, submitted and response to reviewers: Belinda van der Westhuizen, Daniela I. Bezuidenhout, Jannie C. Swarts, Israel Fernández.

[a] *Chemistry Department, University of Pretoria, Private Bag X20, Hatfield, 0028, South Africa. Fax: +27-(0)12-420-4687; Tel: +27-(0)12- 420-2626; E-mail: daniela.bezuidenhout@up.ac.za*
[b] *Chemistry Department, University of the Free State, PO Box 339, Bloemfontein 9300, South Africa. Fax:+27-(0)51-444-6384; Tel: +27-(0)51-401-2781; E-mail: swartsjc@ufs.ac.za*
[c] *Departamento de Química Orgánica I, Facultad de Química, Universidad Complutense,28040-Madrid,Spain.*

Supplementary Information: The Cartesian coordinates and energies for the optimised compounds **3a** and **4a** and the corresponding radical ions (**Appendix 2, CD**). X-ray crystallographic data on **4a** in CIF format. This material is available free of charge via the Internet at http://pubs.acs.org.

ABSTRACT

A series of ten ferrocenyl, furyl and thienyl mono- and biscarbene chromium(0) complexes were synthesized and characterized spectroscopically and electrochemically. The single crystal structure of the biscarbene complex [$(CO)_5Cr$=C(OEt)-Fu'- (OEt)C=$Cr(CO)_5$] (**4a**) was determined**:** $C_{20}H_{12}Cr_2O_{13}$; triclinic; *P*1; *a* = 6.2838(5), *b* = 12.6526(9), *c* = 29.1888(19) Å, α = 89.575(2), β = 88.030(2), γ = 87.423(2)°; *Z* = 4. Results from an electrochemical study in CH_2Cl_2 were mutually consistent with a computational study in showing that the carbene double bond of 1 - 6 is reduced to an anion radical, -Cr-C• at formal reduction potentials < -1.7 V vs. FcH/FcH+. The Cr centers are oxidized in two successive one electron transfer steps to Cr(II) via the Cr(I) intermediate. Only Cr(I) oxidation is electrochemically irreversible. Dicationic Cr(II) species formed upon two consecutive one-electron oxidation processes are characterized by a peculiar bonding situation as they are stabilized by genuine CH···Cr agostic interactions. With respect to aryl substituents, carbene redox processes occurred at the lowest potentials for ferrocene derivatives followed by furan complexes. Redox process in the thiophene derivatives occurred at the highest potentials. This result is mutually consistent with a ^{13}C NMR study that showed the Cr=C functionality of furyl complexes were more shielded than thienyl complexes. The NHBu carbene substituent resulted in carbene complexes showing redox processes at substantially lower redox potentials than carbenes having OEt substituents.

3.1 INTRODUCTION

The very first metal carbene complex of the type [$(OC)_5$M=C(XR)R'] (M = Group 6 transition metal) reported by Fischer et al. contained an aromatic phenyl substituent (R') on the carbene carbon atom.[1] The structural data published shortly thereafter illustrated the role of the heteroatom X lone-pair in stabilizing the singlet carbene carbon, in conjunction with the metal's synergic *d*(t_{2g})-*p* π-interaction with the carbene carbon atom.[2] This bonding situation has been extensively studied also by means of computational tools.[3] On the other hand, the aryl substituent, R', can be incorporated into the π-delocalized network surrounding the carbene

carbon and can act as either an electron withdrawing or electron donating substituent. The general structural motif of employing heteroaromatic compounds as conjugated spacer units in mono- and biscarbene complexes has long been of interest in our laboratories.[4] In the design of complexes specifically tailored for electronic transfer processes within the molecule, and their regioselective reactions, the incorporation of the carbene ligands renders communication possible from one terminal metal to the other metal fragment via the π-frame of the molecule (Figure 3.1).[5]

The use of electrochemistry as a tool for the illumination of such intramolecular electronic communication wherever a convenient redox-active moiety is present is well established.[6] We have recently reported an electrochemical investigation of thienyl mono- and biscarbene complexes of chromium(0).[7] We have shown that the Cr center of the carbene ligands undergoes electrochemical reversible one–electron oxidation to Cr(I) and thereafter it may be irreversibly oxidized in a one electron transfer process to Cr(II). The carbene formal double bond Cr=C may be reduced to $^{-}$Cr-C•. That each process represents a one electron transfer process was confirmed by comparing the intensity of each wave with the intensity of the ferrocenyl group of $[(OC)_5Cr=C(OEt)Fc]$, **1**, and $[(OC)_5Cr=C(OEt)\text{-}Fc'\text{-}(OEt)C=Cr(CO)_5]$, **2**, with linear sweep voltammetric (LSV) techniques and also by comparing i_{pc} and i_{pa} currents (c = cathodic and a = anodic, p = peak) in all cyclic voltammograms (CV's). The LSV studies were hampered by the lack of stability of the oxidized and reduced products, in that the compounds decomposed within 80 seconds of oxidation. On the cathodic (reducing) cycles, decomposition times were even faster. For this reason, i_{pc} and i_{pa} currents were used to interpret reversibility. Older studies of Fischer carbene complexes detail especially Cr(0) oxidation studies.[8] The revival in the interest of the electrochemical behavior of Fischer carbene complexes[9] can be attributed to the many applications of the redox activity of these complexes, including their use in organic synthesis and catalytic transformations,[10] and as electrochemical probes.[11]

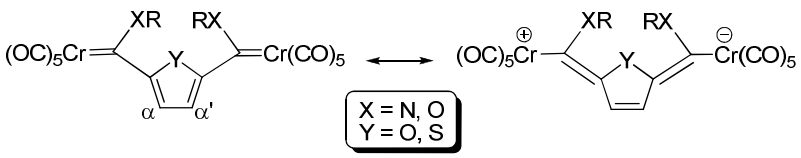

Figure 3.1 Stabilization of biscarbene complexes with heteroaryl spacer moieties.

The carbene substituents XR and R' control the electrophilicity of the complex,[12] although for the heteroaryl substituents R', stabilization of the carbene carbon atom occurs by both the conjugative release of electrons as well as specific $\pi \rightarrow p$ donation.[3(d),13] Modification of the steric and electronic nature of the carbene ligand can therefore be effected by both the heteroatom and the heteroaryl substituents. To enable us to establish especially electrochemical changes that are introduced by the heteroaryl substituent we report here the synthesis, characterization and electrochemical properties of 2-furyl (Fu) monocarbene and 2,5-furadiyl (Fu') complexes with both the known alkoxy- and the new amino-substituted carbene carbon atoms.[14] By comparing the results with those of the 2-thienyl (Th) and 2,5-thiendiyl (Th') biscarbene complexes of chromium(0) which we reported earlier this year,[7] we could establish a trend regarding the effects ring-heteroatom (O *vs* S), and carbene-heteroatom (O *vs* N), as well as the effect a second metal carbene moiety (mono- *vs* biscarbene ligands) has on the redox activity of this series of (hetero)aryl Fischer carbene complexes of chromium(0). The electrochemical results are supported by theoretical calculations which allow us to gain more insight into the nature of the species involved in the electrochemical processes. The single crystal X-Ray structure of the biscarbene furan-containing complex $[(CO)_5Cr=C(OEt)\text{-}Fu'\text{-}(OEt)C=Cr(CO)_5]$ (**4a**) is also described.

3.2 SYNTHESIS AND CHARACTERIZATION

The ethoxycarbene complexes were prepared by reaction of mono- or dilithiated (hetero)arene (ferrocene, furan or thiophene) with 1 or 2 eq. of $[Cr(CO)_6]$, followed by alkylation with 10% excess Et_3OBF_4[15] to yield the ethoxy monocarbene complexes **1**[16] and **3**[17], or biscarbene complexes **2**[18] and **4**,[4(e),(f)] respectively (see Scheme 3.1).

Scheme 3.1. Synthesis of chromium(0) heteroaryl mono- and biscarbene complexes

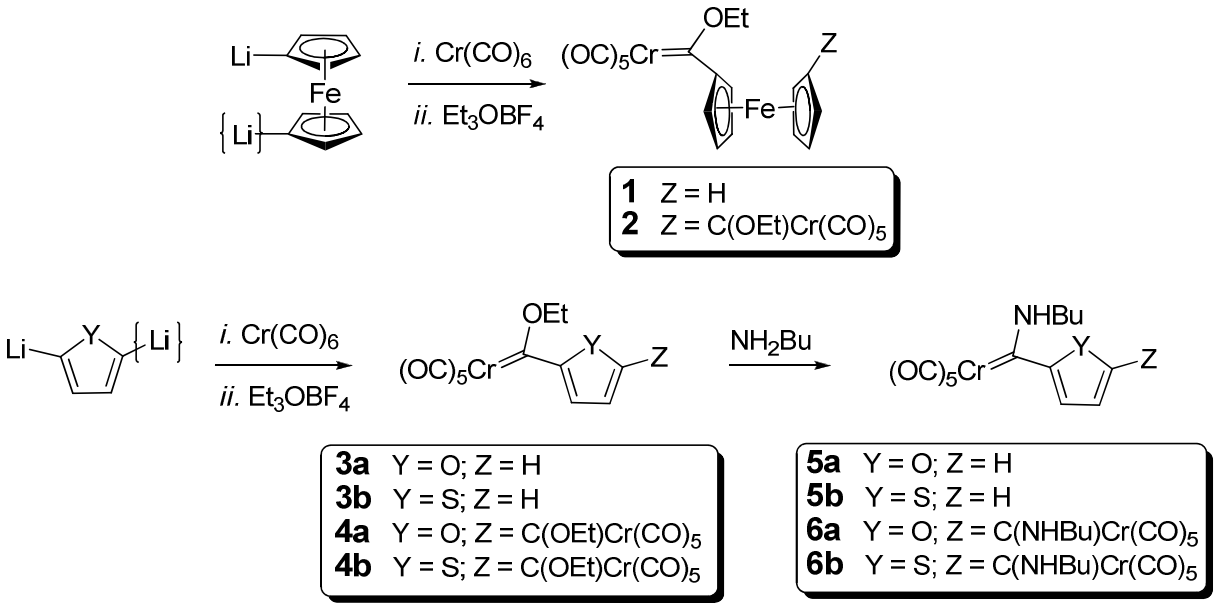

Aminolysis[19] of the ethoxycarbene complexes with n-butylamine was performed by addition of 2.2 mmol or 4.2 mmol NH_2Bu to a solution of **3** (2 mmol) or **4** (2 mmol), respectively, in 20 mL diethyl ether at room temperature. Stirring was maintained for 30 min, whereafter the solvent was removed under reduced pressure. Column chromatography with eluent hexane:CH_2Cl_2 (1:1) yielded the new furyl and thienyl aminocarbene products **5a**, **5b**[7] (monocarbene complexes), **6a** and **6b**[7] (biscarbene complexes), respectively (Scheme 3.1). For the monocarbene complex **5a**, NMR spectroscopy revealed the duplication of all resonances, due to the formation of both the *syn* and *anti*-isomers (see Figure 3.2),[20] in a ratio of approximately 1:1. Trace amounts of isomers were observed for biscarbene complex **6a**, but only one configuration could be isolated and characterized. All neat compounds were stable in the absence of oxygen and could be stored for months at -4°C under argon. Electrochemical evidence indicated that in CH_3CN or CH_2Cl_2 solutions, they decomposed to an observable extent within *ca*. 30 minutes at room temperature. This is slow enough to allow spectroscopic and electrochemical measurements.

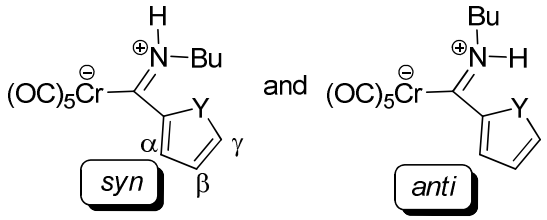

Figure 3.2. *Syn*- and *anti*-configuration of zwitterionic rotamers of aminocarbene complexes, with atom numbering system employed for NMR characterization.

Coordination of the metal-carbene moiety causes a deshielding of the α and β-protons in the ^{1}H NMR, effected by the partial positive charges afforded on these protons caused by π-resonance effects. However, unlike for the thienyl carbene complexes (**3b** – **6b**), H_{α} of the furyl carbene complexes (**3a** – **6a**) cannot be employed as a probe for electronic ring substituent involvement due to their upfield shift compared to H_{γ} (see Experimental Section). The atypical assignment of the furyl ring proton chemical shifts is based on assignments following predicted shifts for ester derivatives.[5(e),21] The resonances for the H_{γ} chemical shifts do reflect the decreased electron donation from the furyl rings for the aminocarbene complexes (**5a**, 7.67 and 7.44 ppm; **6a**, 7.13 ppm) compared to the ethoxy-analogues (**3a**, 7.82 ppm; **4a**, 7.22 ppm). The formation of both *syn*- and *anti*-rotamers across the restricted $C_{carbene}$ –N bond was observed by the duplication of all NMR signals of **5a** in a ratio of 1:0.95 (*syn:anti*) (see Figure 3.1).[22] For the biscarbene complex **6a**, although three possible isomers exist (*syn,syn*; *anti,anti* or *syn,anti*), only one isomer could be observed but could not be unambiguously assigned as either the *syn,syn*- or *anti,anti*- configuration. Significant upfield shifts of the carbene carbon ^{13}C NMR resonances of the aminocarbene complexes (**5a**, 243, 250 ppm; **6a**, 250 ppm) reflect the increased $C_{carbene}$-N bond order and resultant less electrophilic carbene carbon atoms compared to **3a** (311 ppm) and **4a** (313 ppm). This corresponds to the expected decrease in the *trans*-CO stretching frequency (A_1' band)[23] of **5a** and **6a** (1910, 1916 cm^{-1}, respectively) compared to that observed for **3a** and **4a** (1960, 1962 cm^{-1}, respectively).

Comparison of ring-heteroatom effect on the ^{13}C NMR shifts of the carbene carbon atom reveals that furyl-substituted aminocarbene ligands (**5a**, **6a**) are more shielded (243, 250 ppm,

respectively) than the thienyl-substituted complexes **5b** and **6b** (258 – 272 ppm). A smaller effect is observed when comparing thienyl ethoxycarbene ligands (**3b**, 316 ppm; **4b**, 322 ppm) with the furyl amino-analogues (**3a**, 311 ppm; **4a**, 313 ppm).

3.3 X-RAY STRUCTURAL STUDY

Complex **4a** crystallizes with two molecules in the asymmetric unit. Crystallographic data are given in Table 3.1. The molecular structure of molecule 1 is shown in Figure 3.3. The structures of both molecules are similar and are also similar to that of the methoxy-carbene analogue.[24] Selected geometric parameters (mainly about the carbene C atoms) are given in Table 3.2. A *trans* conformation of O_{alkoxy} and O_{furan} about the $C_{carbene}$–C_{furan} bond is electronically favored in alkoxy-furan-carbene complexes, however, in mono-furan biscarbene complexes a *trans* - *trans* conformation cannot be adopted as this would bring the two $Cr(CO)_5$ moieties too close to one another and thus a *cis* - *trans* conformation is adopted.

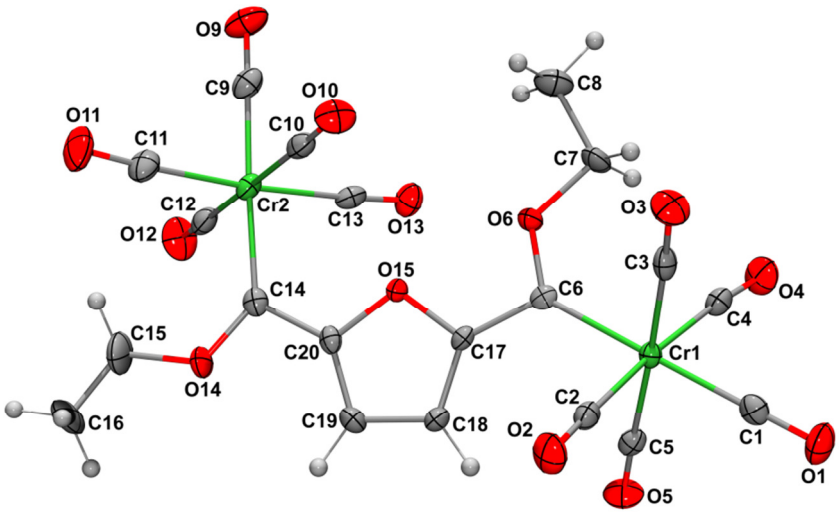

Figure 3.3 An Ortep/PovRay[25] drawing of the structure of molecule 1 of 4a showing the atom numbering scheme. For the atom numbering scheme of molecule 2, add 20 to each of the numbers shown. ADPs are shown at the 50% probability level.

Table 3.1 Crystallographic Data for 4a.

chemical formula: $C_{20}H_{12}Cr_2O_{13}$	formula weight: 564.30
a = 6.2838(5) Å	space group $P\bar{1}$ (No. 2)
b = 12.6526(9) Å	T = -123 °C
c = 29.1888(19) Å	λ = 0.71073 Å
α = 89.575(2)°	D_{calcd} = 1.168 g cm^{-3}.
β = 88.030(2)°	μ = 1.005 mm^{-1}
γ = 87.423(2)°	R = 0.0757 (all), 0.0478 (I > 2σI)
V = 2316.9(3) Å^3	R_w = 0.0858 (all), 0.0786 (I > 2σI)
Z = 4	

$R = \Sigma \mid |F_o| - |F_c| \mid / \Sigma |F_o|$ $\quad R_w = \{ \Sigma [w(F_o^2 - F_c^2)^2] / \Sigma [w(F_o^2)^2] \}^{1/2}$

$w=1/[\sigma^2(F_o^2)+(0.0292P)2+2.2628P]$ where $P=[\mathrm{Max}(F_o^2,0)+2F_c^2]/3$

Table 3.2 Selected geometric parameters for 4a. (Å,°)

Cr-$C_{carbonyl}$ [a]	1.889(3)	Cr-$C_{carbonyl}$ [b]	1.904(9)
Cr1-C6	2.036(3)	Cr21-C26	2.049(3)
Cr2-C14	2.035(3)	Cr22-C34	2.038(3)
C6-O6	1.325(3)	C26-O26	1.317(3)
C6-C17	1.460(4)	C26-C37	1.463(4)
C14-O14	1.330(4)	C34-O34	1.326(4)
C14-C20	1.461(4)	C34-C40	1.464(4)
Cr1-C6-O6	131.0(2)	Cr21-C26-O26	131.4(2)
Cr1-C6-C17	123.7(2)	Cr21-C26-C37	123.1(2)
O6-C6-C17	105.3(2)	O26-C26-C37	105.4(2)
Cr2-C14-O14	132.5(2)	Cr22-C34-O34	132.3(2)
Cr2-C14-C20	124.0(2)	Cr22-C34-C40	123.8(2)
O14-C14-C20	103.4(3)	O34-C34-C20	103.9(2)
O6-C6-C17-O15	-5.3(3)	O26-C26-C37-O35	-3.3(3)
O14-C14-C20-O15	-174.5(2)	O34-C34-C40-O35	-174.4(3)

[a] mean bond distance for carbonyls *trans* to a carbene. [b] mean bond distance for carbonyls *cis* to a carbene.

3.4 ELECTROCHEMISTRY

Cyclic voltammetry (CV), linear sweep voltammetry (LSV), and Osteryoung square-wave voltammetry (SW) were conducted on 0.5 mmol.dm^{-3} solutions of **1** – **6** in dry, oxygen-free CH_2Cl_2 utilizing 0.1 mol.dm^{-3} [N(*n*Bu)$_4$][PF_6] as supporting electrolyte. Data are summarized in

Table 3.3, CV's are shown in Figures 3.4 and 3.5 while Figure 3.6 summarizes potential shifts due to changes in aryl, OEt or NHBu carbene substituent.

Three carbene-based redox processes were observed. These are:

(a) the one-electron reduction of the carbene double bond; peaks for this process are labelled I throughout in Figures 3.4 and 4.5 and Table 3.3,

(b) oxidation of the Cr(0) centre to Cr(I) is associated with peak 1, and

(c) peaks labelled 2 are associated with the one-electron oxidation of the electrochemically generated Cr(I) centre to Cr(II).

One-electron oxidation of the ferrocenyl group in **1** and **2** (peak Fc in Table 3.3 and Figure 3.4), is observed after Cr(0) oxidation but before Cr(I) and have been thoroughly described in our previous report.[7] It should be noted that it is very difficult to separate redox events that take place at closely overlapping potentials by electrochemical techniques, as discussed in detail by Taube *et al.*[26]

Reduction in aprotic solvents of alkenes[27] in general and the carbene double bond, Cr=C, in particular[7] are known to occur at far negative applied potentials. During a one-electron transfer process a radical anion of considerable instability is generated; follow-up chemical reactions destroy this electrochemically generated species quickly.[7]

Electrochemical reversible one-electron transfer processes are characterized by ΔE_p = 59 mV and peak current ratios approaching 1.[28] All ethoxy mono- and biscarbene complexes $[(OC)_5Cr=C(OEt)Ar]$ and $[(OC)_5Cr=C(OEt)\text{-}Ar'\text{-}(OEt)C=Cr(CO_5)]$ **1**, **2** (Ar = Fc), **3a**, **4a** (Ar = Fu) and **3b** and **4b** (Ar = Th), exhibited pseudo electrochemical reversible one-electron reduction ($\Delta E_p = E_{pa} - E_{pc} > 88$ mV, $0.39 < i_{pa}/i_{pc} < 0.73$) of the Cr=C functionality to $^{-}$Cr-C• at $E^{o'} < -1.762$ V vs. FcH/FcH^{+}. The assignment of $^{-}$Cr-C• as reduction product is mutually consistent with the computational studies described below, and also with single electron transfer reactions followed by ESI-MS that indicated the formation of such species.[29] For the NHBu mono- $[(OC)_5Cr=C(NHBu)Ar]$ and biscarbene $[(OC)_5Cr=C(NHBu)\text{-}Ar'\text{-}(NHBu)C=Cr(CO)_5]$ complexes **5a**, **6a** (Ar = Fu), **5b** and **6b** (Ar = Th), only **5b** exhibited partial chemical reversibility during Cr=C reduction (i_{pa}/i_{pc} = 0.11, Table 3.3, Figure 3.5). The other complexes exhibited electrochemical and chemical irreversible behavior for this process with i_{pa}/i_{pc} = 0. Potentials were, however, independent of scan rate between 100 and 500 $mV.s^{-1}$ (Figure 3.6). We

conclude the reduced $^{-}$Cr-C• species of the NHBu derivatives are much more reactive than their OEt counter parts.

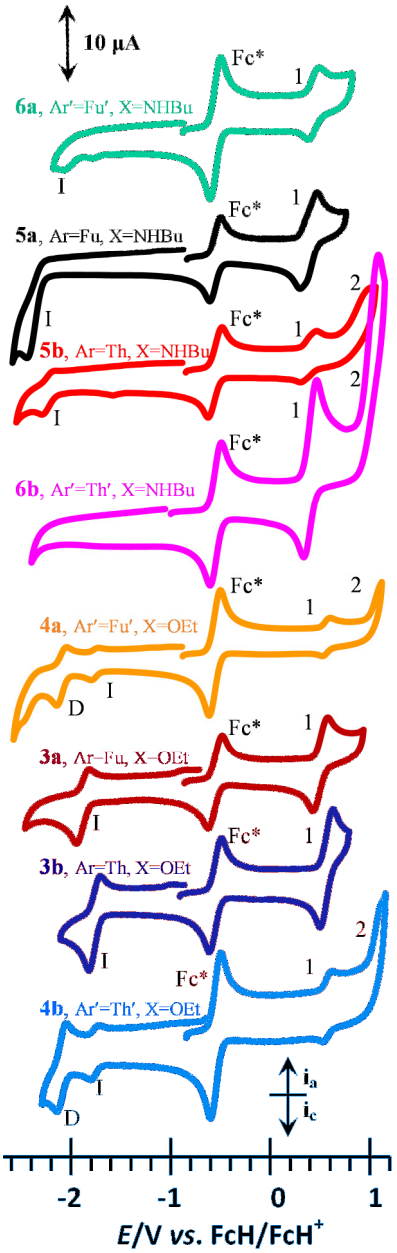

Figure 3.4 Cyclic voltammograms of 0.5 mmol.dm^{-3} solutions of monocarbenes **3a**, **3b**, **5a**, **5b**[$(OC)_5Cr$=C(Ar)X] and biscarbenes **4a**, **4b**, **6a** and **6b** [$(OC)_5Cr$=C(X)-Ar′-(X)C=$Cr(CO)_5$] in CH_2Cl_2/0.1 mol.dm^{-3} [N(*n*Bu)$_4$][PF_6] on a glassy carbon-working electrode at a scan rate of 400 mV/s. Decamethylferrocene, Fc*, was used as internal standard. For **4a**, **5b**, **6a** and **6b**, concentrations were 0.25 mmol.dm^{-3} for better clarity. Peaks labelled "D" represent decomposition processes of electrochemically generated $^{-}$Cr-C$^{\bullet}$ radical anions at the redox process labelled "I".

Table 3.3. Cyclic voltammetry data of 0.5 mmol.dm^{-3} solutions of the monocarbene [(OC)$_5$Cr=C(Ar)(X)] and biscarbene complexes [(OC)$_5$Cr=C(X)-Ar'-(X)C=Cr(CO)$_5$] in CH_2Cl_2, containing 0.1 mol.dm^{-3} [N(*n*Bu)$_4$][PF$_6$] as supporting electrolyte at a scan rate of 100 mV.s^{-1} and 20 ^{o}C. Potentials are relative to the FcH/FcH$^+$ couple.

Complex	Peak no.	$E^{o'}$/V, ΔE/mV	$i_{pa}/\mu A$, i_{pc}/i_{pa}
1	I(=)	-2.148, 111	3.20 [b],
Ar = Fc	1($Cr^{0/I}$)	0.289, 102	0.41
X = OEt	(Fc)	0.700, 89	3.48, 0.89
	2($Cr^{I/II}$)	- [a], - [a]	3.29, 0.85
			- [a], - [a]
2	I(=)	-1.845, 104	3.81 [b],
Ar′ = Fc′	1a($Cr^{0/I}$)	0.499, 83	0.39
X = OEt	1b($Cr^{0/I}$)	0.650, 80	3.71, 0.73
	(Fc)	0.730, 97	3.51, 0.23
	2($Cr^{I/II}$)	- [a], - [a]	3.78, < 0.1
			- [a], - [a]
3a	I(=)	-1.883, 120	3.54 [b],
Ar = Fu	1($Cr^{0/I}$)	0.498, 129	0.59
X = OEt	2($Cr^{I/II}$)	- [a], - [a]	3.75, 0.89
			- [a], - [a]
3b	I(=)	-1.762, 98	3.71 [b],
Ar = Th	1($Cr^{0/I}$)	0.565, 85	0.43
X = OEt	2($Cr^{I/II}$)	- [a], - [a]	3.98, 0.88
			- [a], - [a]
4a	D(=)[h]	-2.075, 110	3.31 [b],
Ar′	=I(=)	-1.772, 65	0.73
Fu′	1($Cr^{0/1}$)	0.565, 62	0.89[b],
X = OEt	1($Cr^{I/II}$)	1.100[d], - [d]	0.73
			1.21,
			0.74
			2.93[d], - [d]

4b	D(=)[h]	-2.091, 88	1.89 [b],
Ar′	=I(=)	-1.765, 232	0.59
Th′	1($Cr^{0/1}$)	0.576, 68	0.68[b],
X = OEt	1($Cr^{I/II}$)	1.098[d], -[d]	0.78
			0.81,
			0.81
			2.50[d], -[d]
5a	I(=)	-2.398[e], -[e]	3.26 [b], -
Ar = Fu	1a($Cr^{0/I}$)	0.340, 68	1.94, 0.91[f]
X	=1b($Cr^{0/I}$)	0.402, 98	2.86, 0.87[f]
NHBu	2($Cr^{I/II}$)	-[a], -[a]	-[a], -[a]
5b	I(=)	-2.232, 132	3.21 [b],
Ar = Th	1a($Cr^{0/I}$)	0.258, 242	0.11
X	=1b($Cr^{0/I}$)	0.435[c], -[c]	1.83, 0.80
NHBu	2($Cr^{I/II}$)	0.951[c], -[c]	1.75, -[c]
			7.02, -[c]
6a	I(=)[g]	-2.057 [e], -[e]	0.90 [b],
Ar′	=1($Cr^{0/I}$)	0.430, 90	-
Fu′	1($Cr^{I/II}$)	-[a], -[a]	1.43 ,
X	=		0.77
NHBu			-[a], -[a]
6b	I(=)	-[a], -[a]	-[a], -[a]
Ar′	=1($Cr^{0/I}$)	0.399, 138	4.81, 0.69
Th′	2($Cr^{I/II}$)	1.150[d], -[d]	7.42[d], -[d]
X	=		
NHBu			

(a) No peak detected within the solvent potential window; (b) i_{pc} and i_{pa}/i_{pc} values to maintain the current ratio convention of $i_{forward\ scan/ireverse\ scan}$; (c) Estimated E_{pa}; poor resolution disallowed estimates of E_{pc} or i_{pa}/i_{pc}; (d) E_{pa} value, no E_{pc} detected. (e) E_{pc} value, no E_{pa} detected. (f) Estimations only. (g) Prior to peak I, a small peak was detected at -1.778 V, i_{pc} = 0.33 µA. This current is so small that it is not regarded as part of the system. (h) Peaks labeled "D" represent decomposition processes of –Cr-C· radical anions that were generated at the redox process labelled "I".

Figure 3.7 shows the computed frontier molecular orbitals of **3a**.[30] The HOMO is located in a *d* atomic orbital of the chromium atom whereas the LUMO is mainly centered in the p_z atomic orbital of the carbene carbon atom. Therefore, it should be expected that the one-electron reduction process should lead to the radical anion **3a•-** whose unpaired electron remains mainly located on the p_z orbital of the carbene carbon atom. Indeed, the computed spin density on **3a•-** indicates a value of 0.60 e on the carbene carbon atom thus confirming the assignment of $^{-}$Cr-C• as reduction product. Similar LUMO's were observed for the rest of the mono- and biscarbene complexes.

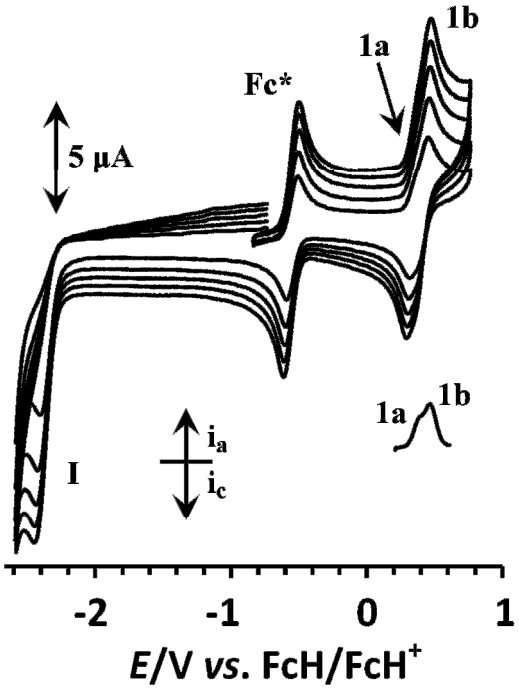

Figure 3.5 Cyclic voltammograms of **5a**, (0.5 mol.dm^{-3}, [$(OC)_5$Cr=C(NHBu)Fu]) in CH_2Cl_2/0.1 mol.dm^{-3} [N(*n*Bu)$_4$][PF_6] on a glassy carbon-working electrode at scan rates of 100 (smallest currents), 200, 300, 400 and 500 mV/s. Decamethylferrocene, Fc*, was used as internal standard. The $Cr^{0/1}$ couple at peak 1 splits into two components a and b, as highlighted by the SW at 20 Hz.

The carbene double bond, Cr=C, of the present series of compounds benefits from the presence of the electron-donating furyl, thienyl or ferrocenyl group which allows for conjugation (Figure

3.1). Conjugated substituents that have different electron donating capabilities are known to alter the redox potential of a redox active species: the more electron-donating a substituent is, the more the redox potential shifts to smaller values.[31] Non-conjugated substituents also influence the redox potentials of a redox active species but to a much lesser degree. It was found that if a substituent functionality is separated by an alkyl chain of more than four isolating (i.e. non-conjugated) carbon atoms from the redox active site, the redox active site is essentially not influenced by the substituent functionality.[32] The influence of three different conjugated aryl groups, ferrocenyl, furyl and thienyl, as well as OEt and NHBu functionalities on the potential of Cr=C reduction is highlighted in this study.

One-electron Cr=C reduction to $^{-}$Cr-C• for the ethoxy monocarbenes $[(OC)_5Cr=C(OEt)Ar]$ were observed at -2.148 V vs. FcH/FcH^+ for **1** (Ar = Fc), -1.883 for **3a** (Ar = Fu) and -1.762 V for **3b** (Ar = Th; $\Delta E^{o'} = E^{o'}_{Th,\mathbf{3b}} - E^{o'}_{Fu,\mathbf{3a}}$ = 121 mV; Figures 3.4 and 3.6, Table 3.3). These observed redox potentials show how aryl groups with different electron-donating capabilities influence $E^{o'}$. The strong electron-donating capability of the ferrocenyl group is known,[33] and from the above potentials it is evident that the observed electron-donating capability of the furyl group in the chromium-ethoxy carbenes is less than that of ferrocenyl, while thienyl is the weakest electron-donating aryl group in the present series of compounds. The observed electrochemical trend nicely correlates with the computed energy of the corresponding LUMO: -2.12 eV (Ar = Fc) > -2.52 eV (Ar = Fu) > -2.69 eV (Ar = Th) which shows that a less stabilized (i.e. less negative) LUMO is translated into a higher reduction potentials. In addition, this result supports the finding of the ^{13}C NMR study discussed above, showing that the Cr=C functionality of furyl complexes were more shielded than thienyl complexes.

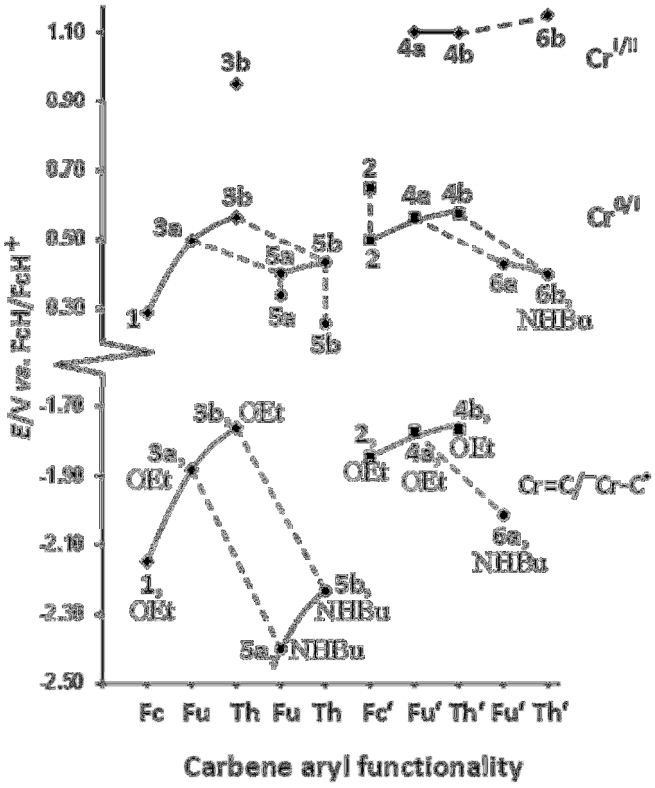

Figure 3.6 Redox potential changes for the Cr=C/¯Cr-C•, $Cr^{0/I}$ and $Cr^{I/II}$ couples as a function of aryl (Ar or Ar′ = Fc or Fc′, Fu or Fu′, Th or Th′), or X = OEt or NHBu substituents in monocarbenes $[(OC)_5Cr=C(X)Ar]$ **1**, **3a**, **3b**, **5a** and **5b** as well as the biscarbenes $[(OC)_5Cr=C(X)\text{-}Ar'\text{-}(X)C=Cr(CO)_5]$ **2**, **4a**, **4b**, **6a** and **6b**. Cr=C reduction for **6b** fell outside the solvent potential window, as did Cr(I) oxidation to Cr(II) for **1**, **3a**, **5a**, **5b** and **6a**. During Cr(0) oxidation of **5a**, **5b** and **2**, two poorly resolved redox processes were observed.

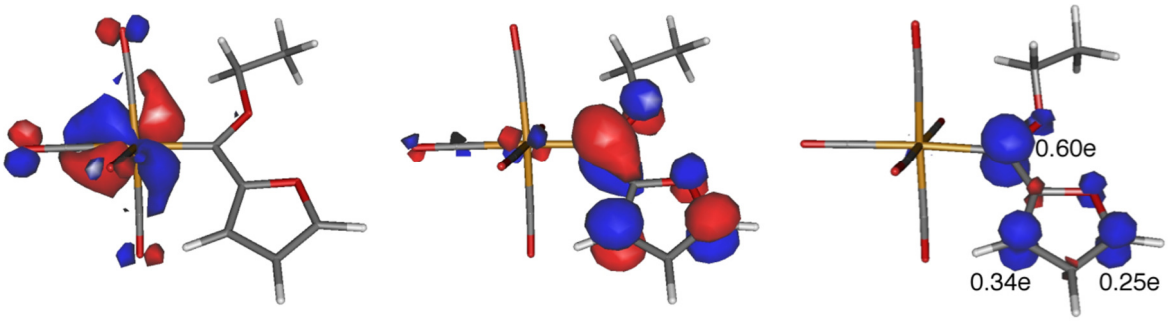

HOMO (3a) **LUMO (3a)** **3a·-**

Figure 3.7 Frontier Molecular Orbitals of **3a** and computed spin density on **3a**·⁻.

Upon changing the OEt substituent to NHBu to give [(OC)$_5$Cr=C(NHBu)Ar], the same trend was observed in that **5b** (Ar = Th) is also reduced at an E_{pc} 105 mV larger than **5a** (Ar = Fu). (There was no E_{pa} observed for **5a** implying $\Delta E^{o'}$ could not be calculated). Both the NHBu and OEt groups are directly bonded to the Cr=C centre and, like the aryl groups, also allow for conjugation (Figures 3.1 and 3.2). The NHBu group shifted the formal reduction potential of the Cr=C species with $\Delta E_{pc} = E_{pc,Fu\text{-}OEt,\mathbf{3a}} - E_{pc,Fu\text{-}NHBu,\mathbf{5a}} = -1823 - (-2398) = 575$ mV and $\Delta E^{o'} = E^{o'}_{Th\text{-}OEt,\mathbf{3b}} - E^{o'}_{Th\text{-}NHBu,\mathbf{5b}} = 470$ mV to more negative potentials than those observed for OEt derivatives, in agreement with the computed less negative LUMO energies (-2.16 and -2.20 eV for **5a** and **5b**, respectively). Clearly, from these large shifts to more negative potentials, the NHBu group is more successful in donating electrons to the Cr=C redox centre (Figure 3.2) than the OEt functionality, which agrees with the well-known higher donor-ability of nitrogen atoms compared to the more electronegative oxygen atoms.

The changes in Cr=C reduction potential as a function of Ar, OEt or NHBu for the biscarbenes was not as large, but in essence the same general directional changes in potentials were observed. The observed shifts in potentials as a function of aryl, OEt and NHBu functionalities are summarized in Figure 3.6. The only biscarbene Cr=C reduction that could not be interpreted within this context was **6b** since this redox process ($E_{pc} < -2.4$ V) fell outside the potential window of the solvent CH_2Cl_2.

Cr(0) oxidation to Cr(I) is observed in the potential range $0.289 < E^{o'} < 0.650$ V (Table 3.3). As shown in Figure 3.7, the HOMO of furyl complex **3a** is mainly located at the chromium(0)

atom.[34] Similar HOMO's were observed for the rest of the complexes. Thus, the first oxidation process in all complexes may be attributed to the one-electron oxidation of Cr(0) to Cr(I) which leads to a radical cation where the unpaired electron is located in the transition metal atom (see also Figure 3.8). For the biscarbene complexes **2**, **4** and **6** the oxidation of the two Cr(0) centers takes place at such closely overlapping potentials that, with the exception **2** (Table 3.3), they could not be resolved. Hence in the computational discussion of **4a** below, this oxidation was modeled as a process in which two electrons was transferred simultaneously. The $Cr^{0/1}$ redox couple has better ΔE_p values than Cr=C reduction with the ethoxy biscarbenes **4a** (Ar = Fu) and **4b** (Ar = Th) as well as the amino monocarbene **5a** showing $\Delta E_p < 69$ mV, but by and large this couple was also electrochemically pseudo reversible. Peak current ratios were better than 0.69 for almost all mono- and bis-Fu and Th complexes. The monomeric Fu and Th NHBu complexes **5a** and **5b** showed splitting of the $Cr^{0/1}$ couple into poorly resolved components a and b (Figures 3.5 and 3.6, Table 3.3), which is consistent with the rotamers shown in Figure 3.2. From NMR measurements, see above, the *syn* and *anti* zwitterionic rotamers are present in an approximate ratio of 1:1. The oxidation of one of the zwitterionic rotamers of **5a** and **5b** is associated with one of the two $Cr^{0/1}$ peaks, while the other $Cr^{0/1}$ peak may be associated with the other zwitterionic species shown in Figure 3.2.

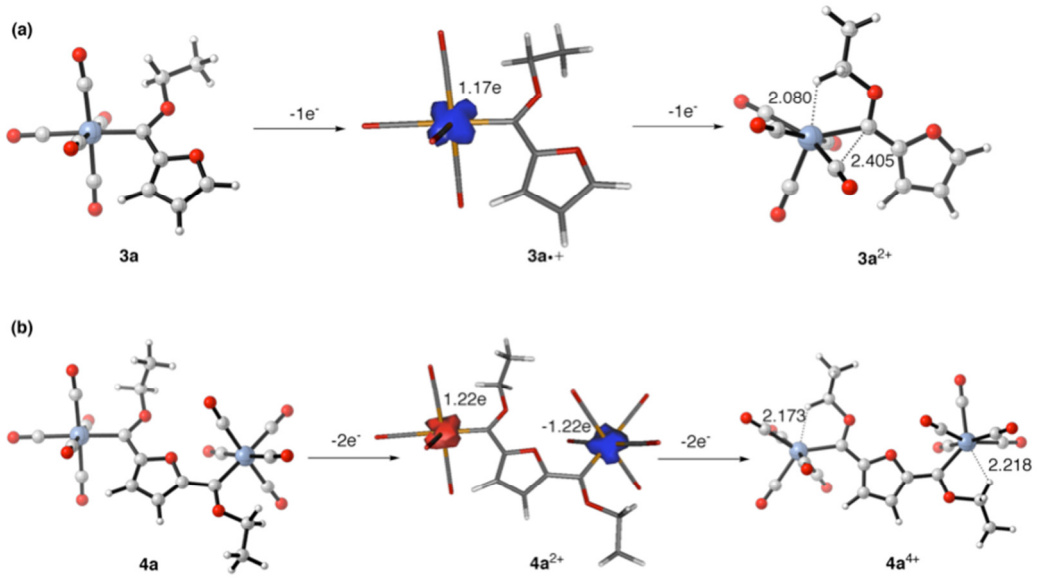

Figure 3.8 Species formed upon electrochemical oxidation processes of complexes **3a** (a) and **4a** (b). Bond lengths are given in angstroms.

As with reduction wave I, the potentials associated with Cr(0) oxidation of $[(OC)_5Cr=C(NHBu)Ar]$ for the Ar = Fc complex **1** (0.289 V) and the two NHBu complexes **5a** and **5b** were the lowest (Figure 3.6, Table 3.3). The ethoxy-furan carbene **3a** exhibited a Cr(0) oxidation potential 209 mV more positive than **1** (compared to the 265 mV more positive potential observed for Cr=C reduction) while the thienyl derivative is, as with Cr=C reduction, oxidized at the largest potential. $\Delta E^{o'} = E^{o'}_{Th,\mathbf{3b}} - E^{o'}_{Fu,\mathbf{3a}}$ was 67 mV for wave 1 while for Cr=C reduction the corresponding potential shift was 121 mV. The thienyl butylamino derivative **5b** also undergoes Cr(0) oxidation at a formal oxidation potential 33 mV more positive (wave 1b) than the furan derivative **5a**. Again, a clear correlation between the observed first oxidation potential and the computed HOMO energies can be found: -5.70 eV (**5b**) <-5.84 eV (**1**) < -5.94 (**3a**) < -5.96 eV (**3b**), thus showing that a more stabilized HOMO (i.e. more negative) is translated into a higher oxidation potential. In comparison to the OEt substituent, the NHBu functionality shifted the formal oxidation potential of the Cr(0) species with $\Delta E^{o'}_{Cr0/1} = E^{o'}_{Fu\text{-}OEt,\mathbf{3a}} - E^{o'}_{Fu\text{-}NHBu,\mathbf{5a}}$ = 96 mV and $\Delta E^{o'} = E^{o'}_{Th\text{-}OEt,\mathbf{3b}} - Eo'_{Th\text{-}NHBu,\mathbf{5b}}$ = 130 mV (utilising wave 1b for **5a** and **5b**) to more negative potentials (Table 3.3, Figure 3.6). Although this shift is less than that observed for Cr=C reduction, the shift was in the same direction and thus mutually consistent with the conclusion that the NHBu group are more successful in donating electrons to the Cr=C redox center than the OEt functionality.

Finally, at the positive edge of the potential window of CH_2Cl_2, we could observe a second, irreversible ($i_{pc} = 0$) oxidation process for **3b**, **4a**, **4b** and **6a**. For all other complexes this redox process fell outside the workable potential window of CH_2Cl_2. This second observed oxidation process at wave 2 (Figure 3.4) belongs to Cr(I) oxidation to Cr(II) because the unpaired electron in the corresponding radical cation is located in the metal atom (see Figure 3.8a). As the $Cr^{I/II}$ couple is electrochemical irreversible, and because the observed, quite similar, E_{pa} values (Figure 3.6) are so close to the edge of the solvent potential window, it was not possible to interpret any potential changes as a function of carbene substituents. The complete irreversibility of the $Cr^{I/II}$ couple with $i_{pc}/i_{pa} = 0$ (wave 2, Figure 3.4, Table 3.3) contrasts the Cr=C reduction (wave I) which exhibited in most cases nonzero i_{pa}/i_{pc} ratios. This highlights that the electrochemically generated Cr(II) species is much more reactive than the electrochemically generated ˙Cr-C• species, and destructs on a much faster timescale.

The latter result prompted us to analyze the nature of the dicationic species formed upon the second electrochemical oxidation process in detail. As is readily seen in Figure 3.8a, dicationic complex **3a**$^{2+}$ exhibits an unusual structure which is markedly different to the structures of **3a** and the radical cation **3a**$^{\bullet+}$. Indeed, a hydrogen atom of the ethoxy moiety is found close to the chromium atom (Cr···H distance of 2.080 Å), pointing to a possible C-H agostic interaction.

To gain more insight into the bonding situation of **3a**$^{2+}$, we also analyzed the C-H···Cr interaction with the help of the Atom in Molecules (AIM)[35] and Natural Bond Orbital (NBO)[36] methods. The laplacian distribution of **3a**$^{2+}$ in the Cr···H-C plane (Figure 3.9a) clearly reveals the occurrence of a bond critical point located at midpoint between the transition metal and the hydrogen atom, which is associated with a bond path running between the corresponding two atoms. This proves the existence of a direct interaction between both atoms. Moreover, the computed value of 0.035 e.Å^{-3} for the electron density at the bond critical point, is in the range expected for CH agostic interactions.[37] This is further supported by the NBO method which locates a stabilizing electronic donation from the doubly occupied σ(C-H) molecular orbital to the vacant *d* atomic orbital of the chromium (associated second-order perturbation energy of -36.7 kcal/mol, see Figure 3.9b). The presence of the vacant orbital is, of course, a direct consequence of the oxidation process which eliminates the two electrons present in the HOMO of **3a** (located in the chromium atom). The special bonding situation of **3a**$^{2+}$ seems to be general as a similar structure was found for the tetracationic species **4a**$^{4+}$ formed upon two consecutive two-electron oxidation processes from **4a** via the open-shell singlet species **4a**$^{2+}$ (see Figures 3.8b and 3.9c).

Finally, with respect to the furyl- and thienyl-containing butylamino monocarbene complexes **5a** and **5b**, Scheme 3.2 highlights the electrochemical pathway of the observed redox processes. The ethoxy monocarbene complexes undergo essentially the same processes while for the biscarbenes complexes a second $^{-}$Cr-C• radical anion, Cr(0) and Cr(I) oxidation at overlapping potentials with the first processes at waves I, **1** and **2** (Figure 3.4) also forms.

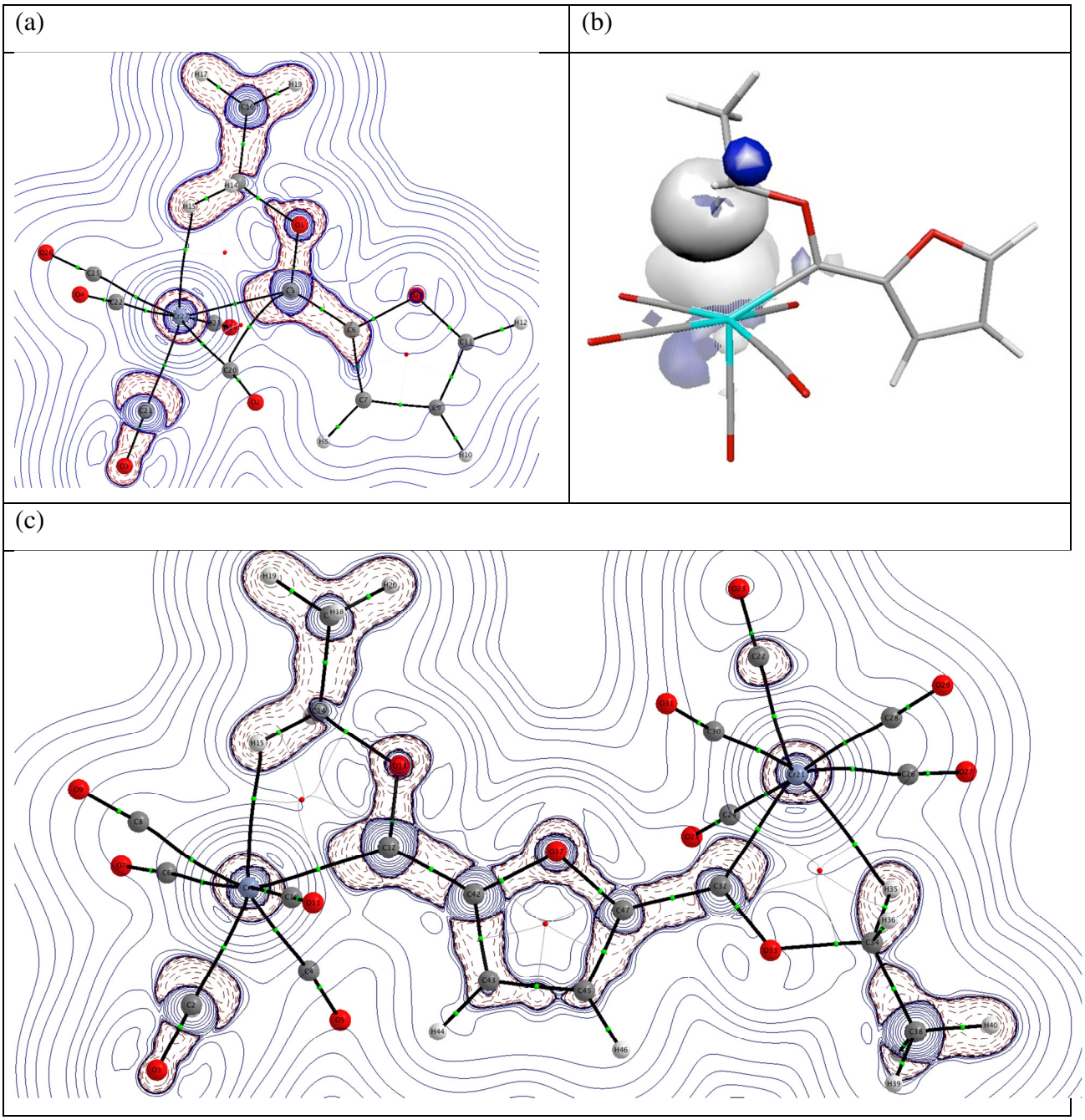

Figure 3.9 Contour line diagrams $\nabla^2\rho(r)$ for complexes **3a**$^{2+}$ (a) and **4a**$^{4+}$ (c) in the Cr−H−C plane. Solid lines indicate areas of charge concentration ($\nabla^2\rho(r) < 0$) while dashed lines show areas of charge depletion ($\nabla^2\rho(r) > 0$). The solid lines connecting the atomic nuclei are the bond paths while the small red spheres indicate the corresponding bond critical points. The solid lines separating the atomic basins indicate the zero-flux surfaces crossing the molecular plane. (b) NBO orbitals associated with the σ(C-H) → *d*(Cr) agostic interaction.

Scheme 3.2 Electrochemical reactions associated with 5a (Ar = Fu) and 5b (Ar= Th). Both the final reduction product possessing the $^{-}$Cr-C$^{\bullet}$ radical anion and the final oxidation product possessing the Cr(II) centre are highly reactive and undergo further chemical decomposition reactions.

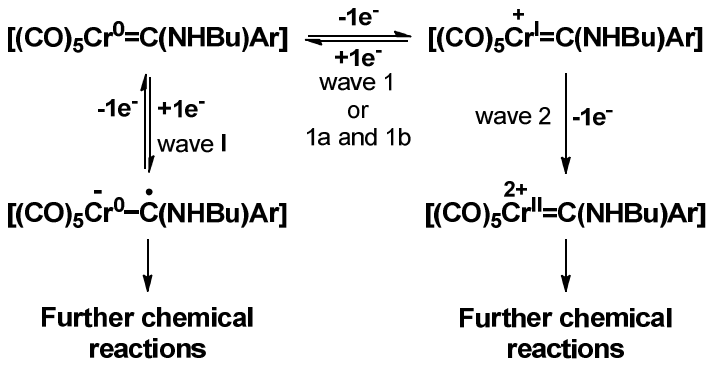

3.5 CONCLUSION

New furyl mono- and bis-butylaminocarbene chromium complexes [(CO)$_5$Cr=C(NHBu)Fu], **5a** and [(CO)$_5$Cr=C(NHBu)-Fu'-(NHBu)C=Cr(CO)$_5$], **6a**, were prepared from the ethoxy precursors. The formation of both *syn*- and *anti*-rotamers across the restricted C$_{carbene}$ –N bond was observed by the duplication of all ^{1}H NMR signals of **5a** in a ratio of 1:0.95 (*syn:anti*). Ferrocenyl and thienyl derivatives were also prepared, and the structure of **4a** [(CO)$_5$Cr=C(OEt)-Fu'-(OEt)C=Cr(CO)$_5$] was solved. From an electrochemical study it was found that the carbene functionality of all ferrocenyl substituted complexes were most electron-rich but that the Cr=C functionality of thienyl complexes were most electron-poor. This result is mutually consistent with a ^{13}C NMR study that showed the Cr=C functionality of furyl complexes were more shielded than thienyl complexes. Three carbene-based redox processes were observed: electrochemical pseudo reversible reduction of Cr=C to $^{-}$Cr-C• at far negative (< 1.7 V vs FcH/FcH^{+}) potentials, electrochemical pseudo reversible oxidation of Cr(0) to Cr(I) at 0.29-0.65 V and irreversible oxidation of Cr(I) to Cr(II) at the positive edge of the solvent (CH_2Cl_2) potential window. The ferrocenyl group is oxidized at potentials between that of the Cr$^{0/I}$ and Cr$^{I/II}$ couple. These redox assignments were mutually consistent with the computational data obtained at the DFT level, which suggest a peculiar bonding situation in the species formed upon the second oxidation process (i.e. stabilized by CH···Cr agostic interactions). Poorly resolved

peak splitting of the Cr(0) oxidation of the zwitterionic species $[(OC)_5Cr^{-}—C=(N^{+}BuH)Ar]$, Ar = Fu or Th into a and b components is consistent with the presence of *syn*- and *anti*-rotamers across the restricted $C_{carbene}$-N bond.

3.6 EXPERIMENTAL

General considerations. All operations were carried out under an inert atmosphere of nitrogen or argon gas using standard Schlenk techniques. Solvents were dried by refluxing on sodium metal (hexane, thf and diethylether) or over phosphorous pentoxide (CH_2Cl_2) and then distilled under nitrogen prior to use. Chemicals were used without further purification unless stated otherwise. Triethyloxonium tetrafluoroborate (Et_3OBF_4) was synthesized according to literature procedures.[15] Purification with column chromatography was done using silica gel 60 (0.0063 – 0.200mm) as stationary phase. A Bruker AVANCE 500 spectrometer was used for NMR recordings. ^{1}H NMR spectra were recorded at 500.139 MHz and ^{13}C NMR spectra at 125.75 MHz. The signal of the solvent was used as reference: ^{1}H $CDCl_3$ at 7.24 ppm and ^{13}C $CDCl_3$ at 77.00 ppm. Solution IR spectra were recorded on a Perkin-Elmer Spectrum RXI FT-IR spectrophotometer using hexane as solvent. Only the vibration bands in the carbonyl-stretching region (ca. 1600 – 2200 cm^{-1}) were recorded. Melting points were not recorded due to decomposition during heating.

Synthesis of carbene complexes 1- 4. The carbene complexes **1**,[16] **2**,[18] **3**,[17] **4a**,[4(e)] **4b**,[4(f)] **5b**[7] and **6b**[7] were prepared according to known literature procedures. Spectroscopic data for **1**, **2**, **3b**, **4b, 5b** and **6b** have been reported in our previous study.[7]

$[Cr(CO)_5\{C(OEt)Fu\}]$ ***3a***[17]

^{1}H NMR ($CDCl_3$, δ/ppm): 7.82 (dd, J=1.6, 0.8 Hz, 1H, Fu-H_γ), 6.96 (dd, J=3.6, 0.8 Hz, 1H, Fu-H_α), 6.56 (dd, J= 3.6, 1.6 Hz, 1H, Fu-H_β), 5.13 (q, J=7.0 Hz, 2H, OCH_2), 1.63 (t, J=7.0 Hz, 3H, CH_3); ^{13}C NMR ($CDCl_3$, δ/ppm) : 311 ($C_{carbene}$), 224 (CO_{trans}), 217 (CO_{cis}), 164 (Fu-C_{ipso}), 150 (Fu-C_γ), 113 (Fu-C_β), 112 (Fu-C_α), 76 (OCH_2), 15 (CH_3). IR (hexane, ν(CO)/cm^{-1}): 2061 s (A''_1), 1990 w (B), 1960 s (A'_1), 1946 vs (E).

[(CO)5Cr{C(OEt)(Fu')C(OEt)}Cr(CO)5] ***4a***[4(e)]

^{1}H NMR ($CDCl_3$, δ/ppm): 7.22 (s, 2H, Fu'-$H_{\alpha,\alpha'}$), 5.22 (q, 4H, J=7.0 Hz, OCH_2), 1.72 (t, 6H, J=7.1 Hz, CH_3); 13C NMR ($CDCl_3$, δ/ppm): 313 ($C_{carbene}$), 224 (CO_{trans}), 216 (CO_{cis}), 162 (Fu'-C_{ipso}), 119 (Fu'-$C_{\alpha,\alpha'}$), 77 (OCH_2), 15 (CH_3). IR (hexane, ν(CO)/cm^{-1}): 2054 s (A''_1), 1995 w (B), 1962 s (A'_1), 1955 vs (E).

Synthesis of new furyl aminocarbene complexes 5a and 6a.

$[Cr(CO)_5${C(NHBu)Fu}] ***5a***

3a (2 mmol, 0.69 g) was dissolved in ether and *n*-butylamine (2.2 mmol, 0.22 mL) was added at room temperature (rt). A rapid color change from red to yellow was observed. Volatiles were removed by reduced pressure and purification was done using column chromatography with a 1:1 hexane/CH_2Cl_2 solvent mixture. Two isomers formed and although it could not be separated by column chromoatography, two sets of NMR data could be distinguished. Yield 0.55g (85%) yellow crystals.

Syn-isomer: ^{1}H NMR ($CDCl_3$, δ/ppm) 9.22 (br, 1H, NH), 7.44 (d, J=1.7 Hz, 1H, Fu-H_γ), 7.09 (d, J=3.6 Hz, 1H, Fu-H_α), 6.57 (dd, 3.5, 1.9 Hz, 1H, Fu-H_β), 4.06 (td, 7.2, 6.0 Hz, 2H, NCH_2), 1.80 (m, 2H, CH_2CH_2), 1.50 (m, 2H, CH_2CH_2), 0.98 (t, 7.4 Hz, 3H, CH_3); ^{13}C NMR ($CDCl_3$, δ/ppm): 243 ($C_{carbene}$) , 223 (CO_{trans}), 218 (CO_{cis}), 157 (Fu-C_{ipso}), 144 (Fu-C_γ), 122 (Fu-C_α), 114 (Fu-C_β), 53 (NCH_2), 32 (CH_2CH_2), 20 (CH_2CH_2), 14 (CH_3).

Anti-isomer: 8.28 (br, 1H, NH), 7.67 (d, J=1.4 Hz, 1H, Fu-H_γ), 7.44 (d, J=3.7 Hz, 1H, Fu-H_α), 6.59 (dd, 3.6, 1.7 Hz, 1H, Fu-H_β), 3.70 (td, 7.1, 5.6 Hz, 2H, NCH_2), 1.76(m, 2H, CH_2CH_2), 1.45 (m, 2H, CH_2CH_2), 1.01 (t, 7.4 Hz, 3H, CH_3). ^{13}C NMR ($CDCl_3$, δ/ppm): 250 ($C_{carbene}$), 223 (CO_{trans}), 218 (CO_{cis}), 156 (Fu-C_{ipso}), 146 (Fu-C_γ), 125 (Fu-C_α), 113 (Fu-C_β), 53 (NCH_2), 32 (CH_2CH_2), 20 (CH_2CH_2), 14 (CH_3). IR (hexane, ν(CO)/ cm^{-1}) 2055 m (A_1''), 1971 vw (B), 1910 m (A_1'), 1935 vs (E).

$[(CO)_5Cr\{C(NHBu)(Fu')C(NHBu)\}Cr(CO)_5]$ ***6a***

4a (2 mmol, 1.24 g) was dissolved in ether and n-butylamine (4.2 mmol, 0.42 mL) was added at rt. The colour changed from purple to deep yellow and volatiles were removed under reduced pressure. Yield 0.98g (75%) orange crystals.

Syn,syn-isomer: ^{1}H NMR ($CDCl_3$, δ/ppm): 9.12 (br, 1H, NH), 7.13 (s, 2H, Fu'-$H_{\alpha,\alpha'}$), 4.12 (dd, J = 7.1, 6.7 Hz, 4H, NCH_2), 1.88-1.76 (m, 4H, CH_2CH_2), 1.59-1.48 (m, 4H, CH_2CH_2), 0.91 (t, J = 7.3 Hz, 6H, CH_3); ^{13}C NMR ($CDCl_3$, δ/ppm): 250 ($C_{carbene}$) 223 (CO_{trans}), 218 (CO_{cis}), 159(C_{ipso}) , 118 (Fu'-$C_{\alpha,\alpha'}$), 52 (NCH_2), 31 (CH_2CH_2), 20 (CH_2CH_2), 14 (CH_3). IR (hexane, ν(CO) / cm^{-1}): 2053 m (A_1''), 1975 vw (B), 1916 m ($A_{1'}$), 1936 vs (E).

Crystal structure determination

Data for a dark-purple needle crystal (0.018 x 0.020 x 0.376 mm) of **4a** were collected at 150 K on a Bruker D8 Venture kappa geometry diffractometer, with duo Iμs sources, a Photon 100 CMOS detector and APEX II[38] control software using Quazar multi-layer optics monochromated, Mo-*K*α radiation by means of a combination of ϕ and ω scans. Data reduction was performed using SAINT+[38] and the intensities were corrected for absorption using SADABS.[38] The structure was solved by intrinsic phasing using SHELXTS[39] and refined by full-matrix least squares using SHELXTL[39] and SHELXL-2012.[39] In the structure refinement all hydrogen atoms were added in calculated positions and treated as riding on the atom to which they are attached. All non-hydrogen atoms were refined with anisotropic displacement parameters, all isotropic displacement parameters for hydrogen atoms were calculated as $X \times U_{eq}$ of the atom to which they are attached, X = 1.5 for the methyl hydrogens and 1.2 for all other hydrogens. One methyl group in each molecule (C16, C36) is disordered and two sites were refined for each (in both cases with a refined sof ratio of 0.61 : 0.39). The major site for C16 (C16A) is shown in Figure 3.3.

Electrochemical studies

Cyclic voltammograms (CV's), square wave voltammograms (SW's) and linear sweep voltammograms (LSV's) were recorded on a Princeton Applied Research PARSTAT 2273

voltammograph running PowerSuite (Version 2.58) utilizing a standard three-electrode cell in a M Braun Lab Master SP glovebox filled with high purity argon (H_2O and O_2 < 5 ppm). A platinum wire auxiliary electrode, a silver wire pseudo internal reference and a glassy carbon working electrode (surface area 3.14 mm^2) was utilized after polishing on a Buhler polishing mat first with 1 micron and then with ¼ micron diamond paste. All electrode potentials are reported versus the ferrocene/ferrocenium redox couple (FcH/FcH^+, $FcH = Fe(\eta^5\text{-}C_5H_5)_2$, $E^{o\prime} = 0.00$ V) as reference.[40] However, decamethylferrocene, Fc*, was used as internal standard to prevent signal overlap with the ferrocenyl of **1** and **2**. Decamethylferrocene has a potential of -550 mV versus free ferrocene with ΔE = 72 mV and i_{pc}/i_{pa} = 1 under the conditions employed.[41] Analyte solutions (0.5 $mmol.dm^{-3}$) were prepared in dry CH_2Cl_2 in the presence of 0.1 $mol.dm^{-3}$ $[(n\text{Bu}_4)N][PF_6]$. Analyses were performed at 20 ^oC. Data were exported to a spread sheet program for manipulation and diagram preparation.

Computational studies

Geometry optimizations without symmetry constraints were carried out using the Gaussian09 suite of programs[42] at the B3LYP (uB3LYP for open-shell species)[43] using the double-ζ plus polarization def2-SVP[44] basis set for all atoms. This protocol is denoted B3LYP/def2-SVP. Zero point vibrational energy (ZPVE) corrections have been computed at the same level and have not been corrected. All species were characterized by frequency calculations, and have a positive defined Hessian matrix indicating that they are minima on the potential energy surface. Donor-acceptor interactions were computed using the natural bond orbital (NBO) method.[34] The energies associated with these two-electron interactions have been computed according to the following equation:

$$\Delta E^{(2)}_{\phi\phi^*} = -n_\phi \frac{\left\langle \phi^* \left| \hat{F} \right| \phi \right\rangle^2}{\varepsilon_{\phi^*} - \varepsilon_\phi}$$

where F is the DFT equivalent of the Fock operator and ϕ and ϕ^* are two filled and unfilled Natural Bond Orbitals having ε_ϕ and ε_{ϕ^*} energies, respectively; n_ϕ stands for the occupation number of the filled orbital.

The AIM[33] results described in this work correspond to calculations performed at the B3LYP/def2-SVP level on the optimized geometries. The topology of the electron density was studied using the AIMAll program package.[45]

3.7 ACKNOWLEDGMENT

This work is supported by the National Research Foundation, South Africa (D.I.B., Grant number 76226; J.C.S., Grant number 81829), and the Spanish MICINN and CAM (I.F., Grants CTQ2010-20714-CO2-01/BQU, Consolider-Ingenio 2010, CSD2007-00006, S2009/PPQ-1634).

3.8 REFERENCES

(1) Fischer, E. O.; Maasböl, A. *Angew. Chem.,* **1964**, *3b*, 645.

(2) *(a)* Mills, O. S.; Redhouse, A. D. *J. Chem. Soc. A,* **1968**, 642-647; *(b)* Fischer, E. O. *Angew. Chem.,* **1974**, *86*, 651-663.

(3) Representative examples: *(a)* Cases, M.; Frenking, G.; Duran, M.; Solà, M. *Organometallics,* **2002**, *21*, 4182-4191; (b) Poater, J.; Cases, M.; Fradera, X.; Duran, M.; Solà, M. *Chem. Phys.* **2003**, *294*, 129-139; (c) Frenking, G.; Solà, M.; Vyboishchikov, S. F. *J. Organomet. Chem.* **2005**, *690*, 6178-6204; (d) Lage, M. L.; Fernández, I.; Mancheño, M. J.; Sierra, M. A. *Inorg. Chem.* **2008**, *47*, 5253-5258; (*e*) Valyaev, D. A.; Brousses, R.; Lugan, N.; Fernández, I.; Sierra, M. A. *Chem. Eur. J.* **2011**, *17*, 6602-6605; (*f*) Lugan, N.; Fernández, I.; Brousses, R.; Valyaev, D. A.; Lavigne, G.; Ustynyukd, N. A. *Dalton Trans.* **2013**, *42*, 898-901.

(4) *(a)* For a recent review, see: Bezuidenhout, D. I.; Lotz, S.; Liles, D. C.; van der Westhuizen, B. *Coord. Chem. Rev.,* **2012**, *256*, 479-524; *(b)* Lotz, S.; van Jaarsveld, N. A.; Liles, D. C.; Crause, C.; Gorls, H.; Terblans, Y. M. *Organometallics,* **2012**, *31*, 5371-5383; *(c)* Bezuidenhout, D. I.; Lotz, S.; Landman, M.; Liles, D. C. *Inorg. Chem.,* **2011**, *50*, 1521-1533; *(d)* Bezuidenhout, D. I.; Barnard, W.; van der Westhuizen, B.; van der Watt, E.; Liles, D. C. *Dalton Trans.,* **2011**, *40*, 6711-6727; *(e)* Crause, C.; Gorls, H.; Lotz, S. *Dalton Trans.,* **2005**, 1649-1657; *(f)* Terblans, Y. M.; Roos, H. M.; Lotz, S. *J. Organomet. Chem.,* **1998**, *566*, 133-142.

(5) *(a)* Lotz, S.; Crause, C.; Olivier, A.J.; Liles, D.C.; Gorls, H.; Landman, M.; Bezuidenhout, D. I. *Dalton Trans.,* **2009**, 697-710; *(b)* Landman, M.; Ramontja, J.; van Staden, M.;

Bezuidenhout, D. I.; van Rooyen, P.H.; Liles, D. C.; Lotz, S. *Inorg. Chim. Acta,* **2010**, *363*, 705-717; (c) Chu, G. M.; Fernández, I.; Sierra, M. A. *Chem. Eur. J*. **2013**, doi: 10.1002/chem.201204512.

(6) *(a)* Auger, A.; Muller, A. J.; Swarts, J. C. *Dalton Trans.* **2007**, 3623-3633; *(b)* Cook, M. J.; Chambrier, I.; White, G.; Fourie, E.; Swarts, J.C. *Dalton Trans.* **2009**, 1136-1144; *(c)* Conradie, J.; Cameron, T. S.; Aquino, M. A. S.; Lamprecht, G. J.; Swarts, J. C. *Inorg. Chim. Acta*, **2005**, *358*, 2530-2542.

(7) Van der Westhuizen, B.; Swarts, P. J.; Strydom, I.; Liles, D. C.; Fernández, I.; Swarts, J. C.; Bezuidenhout, D. I.; *Dalton Trans.,* **2013**, *42,* 5367-5378.

(8) *(a)* Pombeiro, A. J. L. *New J. Chem.,* **1997**, *21*, 649-660; *(b)* Casey, C. P.; Albin, L. D.; Saeman, M. C.; Evans, D. H. *J. Organomet. Chem.,* **1978**, *155*, C37-C40; *(c)* Limberg, A.; Lemos, M. A. N. D. A.; Pombeiro, A. J. L.; Maiorana, S.; Papagni, A.; Licandro, E. *Portugaliae Electrochim. Acta,* **1995**, *13*, 319; *(c)* Lloyd, M. K.; McCleverty, J. A.; Orchard, D. G.; Connor, J. A.; Hall, M. B.; Hillier, I. H.; Jones, E. M.; McEwen, G. K. *J. Chem. Soc., Dalton Trans.,* **1973**, 1743-1747.

(9)(*a*) Fernández, I.; Mancheño, M. J.; Gómez-Gallego, M.; Sierra, M. A. *Org. Lett*. **2003**, *5*, 1237-1240; (b) Martínez-Álvarez, R.; Gómez-Gallego, M.; Fernández, I.; Mancheño, M. J.; Sierra, M. A. *Organometallics* **2004**, *23*, 4647-4654; (c) Wulff, W. D.; Korthals, K. A.; Martínez-Álvarez, R.; Gómez-Gallego, M.; Fernández, I.; Sierra, M. A. *J. Org. Chem.* **2005**, *70*, 5269-5277; (d) López-Alberca, M. P.; Mancheño, M. J.; Fernández, I.; Gómez-Gallego, M.; Sierra, M. A.; Hemmert, C.; Gornitzka, K. H. *Eur. J. Inorg. Chem.* **2011**, 842-849.

(10) Selected recent reviews on the chemistry and applications of Fischer carbenes: (a) Wu, Y. –T.; Kurahashi, T.; de Meijere, A. *J. Organomet. Chem.* **2005**, *690*, 5900-5911; (b) Gómez-Gallego, M.; Mancheño, M. J.; Sierra, M. A. *Acc. Chem. Res*. **2005**, *38*, 44-53; (c) Sierra, M. A.; Gómez-Gallego, M.; Martínez-Ávarez, R. *Chem.–Eur. J*. **2007**, *13*, 736-744; (d) Sierra, M. A.; Fernández, I.; Cossío, F. P. *Chem. Commun*. **2008**, 4671-4682; (e) Dötz, K. H.; Stendel, J. *Chem. Rev*. **2009**, *109*, 3227-3274; (f) Herndon, J. W. *Coord. Chem. Rev*. **2010**, *254*, 103-194; (g) Fernández-Rodríguez, M. A.; García-García, P.; Aguilar, E. *Chem. Comm*. **2010**, *46*, 7670-7687; (h) Fernández, I.; Cossío, F. P.; Sierra, M. A. *Acc. Chem. Res.* **2011**, *44*, 479-490.

(11) (a) Baldoli, C.; Cerea, P.; Falciola, L.; Giannini, C.; Licandro, F.; Maiorana, S.; Mussini, P.; Perdiccia, D.; *J. Organomet. Chem*., **2005**, *690*, 5777-5787; (b) Hoskovcova, I.; Zverinova,

R.; Rohacova, J.; Dvorak, D.; Tobrman, T.; Zalis, S.; Ludvik, *J. Electrochim. Acta*, **2011**, *56*, 6853-6859; (c) Hoskovcova, I.; Rohacova, J.; Dvorak, D.; Tobrman, T.; Zalis, S.; Zverinova, R.; Ludvik, *J. Electrochim. Acta*, **2010**, *55*, 8341-8351; (d) Pombeiro, A. J. L.; *J. Organomet. Chem.*, **2005**, *690*, 6021-6040; (e) Hoskovcova, I.; Rohacova, J.; Meca, L.; Tobrman, T.; Dvorak, D.; Ludvik, *J. Electrochim. Acta*, **2005**, *50*, 4911-4915; (f) Raubenheimer, H. G.; du Toit, A.; du Toit, M.; An, J.; van Niekerk, L.; Cronje, S.; Esterhuysen, C.; Crouch, A. M. *Dalton Trans*., **2004**, 1173-1180.

(12) *(a)* Bernasconi, C. F.; Ali, M.; Lu, F. *J. Am. Chem. Soc.,* **2000**, *122*, 1352-1359; *(b)* Dötz, K. H. *Angew. Chem., Int. Ed. Engl.,* **1975**, *14*, 644-645.

(13) *(a)* Connor, J. A.; Jones, E. M.; Randall, E. W.; Rosenburg, E. *J. Chem. Soc., Dalton Trans.,* **1972**, *22*, 2419; *(b)* Connor, J.A.; Jones, E.M. *J. Chem. Soc. A,* **1971**, *12*, 1974-1979.

(14) While writing this publication, the authors became aware of an independent but simultaneously conducted electrochemical study of related but different chromium carbene complexes, see Metelkova, R.; Tobrman, T.; Kvapilova, H.; Hoskovcova, I.; Ludvik, J. *Electrochim. Acta*, **2012**, *82*, 470-477.

(15) Meerwein, H.; *Org. Synth.*, **1966**, *46*, 113-115.

(16) Lopez-Cortez, J.G.; de la Cruz, L. F. C.; Ortega-Alfaro, M. C.; Toscano, R.A.; Alvarez-Toledano, C.; Rudler, H. *J. Organomet. Chem.,* **2005**, *690*, 2229-2237.

(17) *(a)* Aoki, S.; Fujimura, T.; Nakamura, E. *J. Am. Chem. Soc.,* **1992**, *114*, 2985; *(b)* Connor, J. A.; Lloyd, J. P. *J. Chem. Soc., Dalton Trans.,* **1972**, 1470-1476.

(18) *(a)* Bezuidenhout, D. I.; van der Watt, E.; Liles, D. C.; Landman, M.; Lotz, S. *Organometallics,* **2008**, *27*, 2447-2456; *(b)* Connor, J. A.; Jones, E. M.; Lloyd, J. P. *J. Organomet. Chem.,* **1970**, *24*, C20-C22.

(19) *(a)* Bezuidenhout, D. I.; Liles, D. C.; van Rooyen, P. H.; Lotz, S. *J. Organomet. Chem.,* **2007**, *692*, 774-783; *(b)* Klabunde, U.; Fischer, E. O. *J. Am. Chem. Soc*., **1967**, *89*, 7141-7142.

(20) For a definition of *syn/anti* conformers, see: (a) Fernández, I.; Cossío, F. P.; Arrieta, A.; Lecea, B.; Mancheño, M. J.; Sierra, M. A. *Organometallics* **2004**, *23*, 1065-1071; (b) Andrada, D. M.; Zoloff Michoff, M. E.; Fernández, I.; Granados, A. M.; Sierra, M. A. *Organometallics* **2007**, *26*, 5854-5858. See also references 3(e) and 3(f).

(21) Pretch, E.; Seibl, J.; Clerc, T.; Simon, W. *Tables for Spectral Data for Structure Determination of Organic Compounds,* 2nd Ed., Springer-Verlag, Berlin/Heidelberg, **1989**.

(22) *(a)* Post, E. W.; Watters, K. L. *Inorg. Chim. Acta*, **1978**, *26*, 29-36; *(b)* Moser, E.; Fischer, E. O. *J. Organomet. Chem.*, **1968**, *15*, 147-155.

(23) *(a)* Braterman, P.S. *Metal Carbonyl Spectra*; Academic Press Inc.: London, **1975**, p 68; *(b)* Adams, D. M. *Metal–Ligand and Related Vibrations*, Edward Arnold Publishers Ltd, London, **1967**, p 98.

(24) Liles, D. C.; Lotz, S. *Acta Cryst*., **2006**, E62, m331–m334.

(25) (a) Faruggia, L. J. *J. Appl. Crystallogr*., 1997, 30, 565; (b) Cason, C. J. POV-RAY for Windows, Persistence of Vision, 2004.

(26) Richardson, D.E.; Taube, H. *Inorg. Chem.,* **1981**, *20*, 1278-1285.

(27) *(a)* Fry, A. J. *Synthetic Organic Electrochemistry*, 2nd ed., John Wiley and Sons, New York, **1989**, p 208, 232; *(b)* Volke, J.; Liska, F. *Electrochemistry in Organic Synthesis*, Springer-Verlag, Berlin, **1994**, p 90.

(28) *(a)* Gericke, H. J.; Barnard, N. I.; Erasmus, E.; Swarts, J. C.; Cook, M. J.; Aquino, M. A. S. *Inorg. Chim. Acta,* **2010**, *363*, 2222-2232; *(b)* Evans, D. H.; O'Connell, K. M.; Peterson R. A.; Kelly, M. J. *J. Chem. Educ.*, **1983**, *60*, 290; *(c)* Kissinger, P.T.; Heineman, W. R. *J. Chem. Educ.* **1983**, *60*, 702. *(d)* Van Benshoten, J. J.; Lewis, L.Y.; Heineman, W. R. *J. Chem. Educ.*, **1983**, *60*, 772; *(e)* Mobbott, G. A. *J. Chem. Educ.*, **1983**, *60*, 697.

(29) Lage, M. L.; Mancheño, M. J.; Martínez-Álvarez, R.; Gómez-Gallego, M.; Fernández, I.; Sierra, M. A. *Organometallics*, **2009**, *28*, 2762-2772.

(30) See computational details.

(31) *(a)* Kemp, K. C.; Fourie, E.; Conradie, J.; Swarts, J. C. *Organometallics*, **2008**, *27*, 353; *(b)* Conradie, J.; Swarts, J. C. *Dalton Trans*. **2011**, *40*, 5844-5851.

(32) Siegert, U.; Muller, T. J.; Swarts, J. C. *Polyhedron*, **2013**, *51*, 41-45.

(33) *(a)* Conradie, J.; Swarts, J. C. *Eur. J. Inorg. Chem.*, **2011**, 2439-2449; *(b)* Conradie, J.; Swarts, J. C. *Organometallics*, **2009**, *28*, 1018-1026; *(c)* Connelly, N. G.; Geiger, W. E. *Chem. Rev*. **1996**, *96*, 877-910.

(34) This result is not surprising as the HOMO of the group 6 Fischer carbene complexes is located on the transition metal in most cases. See, for instance: (a) Fernández, I.; Sierra, M. A.; Cossío, F. P. *J. Org. Chem.* **2006**, *71*, 6178-6184; (b) Fernández, I.; Sierra, M. A.; Cossío, F. P. *J. Org. Chem*. **2008**, *73*, 2083-2089; (c) Andrada, D. M.; Granados, A. M.; Solà, M.; Fernández, I. *Organometallics* **2011**, *30*, 466-476.

(35) Bader, R. F. W. *Atoms in Molecules. A Quantum Theory*; Oxford University Press: Oxford, U.K., 1990.

(36) (a) Foster, J. P.; Weinhold, F. *J. Am. Chem. Soc*. **1980**, *102*, 7211-7218. (b) Reed, A. E.; Curtiss, L. A.; Weinhold, F. *Chem. Rev*. **1988**, *88*, 899-926.

(37) Lein, M. *Coord. Chem. Rev*. **2009**, *253*, 625-634.

(38) APEX2 (including SAINT and SADABS); Bruker AXS Inc., Madison, WI, 2013

(39) Sheldrick, G. M.. Acta Cryst. **2008** A64, 112-122.

(40) *(a)* Gritzner, G.; Kuta, J.; *Pure Appl. Chem.*, **1984**, *56*, 461-466; *(b)* Gagne, R. R.; Koval, C. A.; Lisensky, G. C. *Inorg. Chem.*, **1980**, *19*, 2855-2857.

(41) Leading references describing the electrochemical activity and behaviour of ferrocene and decamethylferrocene in a multitude of organic solvents are *(a)* Noviandri, I.; Brown, K. N.; Fleming, D. S.; Gulyas, P. T.; Lay, P. A.; Masters A. F.; Phillips, L. *J. Phys. Chem. B*, **1999**, *103*, 6713-6722; *(b)* Connelly, N. G.; Geiger, W. E. *Chem. Rev.*, **1996**, *96*, 877-910; *(c)* Ruiz, J.; Astruc, D. *C.R. Acad. Sci. (Paris), Ser. IIc* **1998**, *1*, 21; *(d)* Aranzaes, R. J.; Daniel, M. C.; Astruc, D. *Can. J. Chem.*, **2006**, *84***,** 288-299; *(e)* Fourie, E.; Swarts, J. C.; Chambrier, I.; Cook, M. J. *Dalton Trans*. **2009**, 1145-1154.

(42) Gaussian 09, Revision B.1, Frisch, M. J.; Trucks, G. W.; Schlegel, H. B.; Scuseria, G. E.; Robb, M. A.; Cheeseman, J. R.; Scalmani, G.; Barone, V.; Mennucci, B.; Petersson, G. A.; Nakatsuji, H.; Caricato, M.; Li, X.; Hratchian, H. P.; Izmaylov, A. F.; Bloino, J.; Zheng, G.; Sonnenberg, J. L.; Hada, M.; Ehara, M.; Toyota, K.; Fukuda, R.; Hasegawa, J.; Ishida, M.; Nakajima, T.; Honda, Y.; Kitao, O.; Nakai, H.; Vreven, T.; Montgomery, Jr., J. A.; Peralta, J. E.; Ogliaro, F.; Bearpark, M.; Heyd, J. J.; Brothers, E.; Kudin, K. N.; Staroverov, V. N.; Kobayashi, R.; Normand, J.; Raghavachari, K.; Rendell, A.; Burant, J. C.; Iyengar, S. S.; Tomasi, J.; Cossi, M.; Rega, N.; Millam, N. J.; Klene, M.; Knox, J. E.; Cross, J. B.; Bakken, V.; Adamo, C.; Jaramillo, J.; Gomperts, R.; Stratmann, R. E.; Yazyev, O.; Austin, A. J.; Cammi, R.; Pomelli, C.; Ochterski, J. W.; Martin, R. L.; Morokuma, K.; Zakrzewski, V. G.; Voth, G. A.; Salvador, P.; Dannenberg, J. J.; Dapprich, S.; Daniels, A. D.; Farkas, Ö.; Foresman, J. B.; Ortiz, J. V.; Cioslowski, J.; Fox, D. J. Gaussian, Inc., Wallingford CT, 2009.

(43) (a) Becke, A. D. *J. Chem. Phys*. **1993**, *98*, 5648-. (b) Lee, C.; Yang, W.; Parr, R. G. *Phys. Rev. B* **1988**, *37*, 785-789.

(44) Weigend, F.; Ahlrichs, R. *Phys. Chem. Chem. Phys*. **2005**, *7*, 3297-3305.

(45) Keith, T. A. AIMAll, 2010, http://tkgristmill.com

CHAPTER 4

Synthesis and electrochemical investigation of ferrocenyl aminocarbene chromium(0) complexes.

This chapter was submitted to the Journal of Organometallic Chemistry. The format reflects the style set by the journal.

Daniela I. Bezuidenhout,[a] Belinda van der Westhuizen,[a] I. Strydom,[a] Pieter J. Swarts,[b] Jannie C. Swarts,[b] Israel Fernández,[c] *Journal of Organometallic Chemistry,* **2013.**

Author contributors

Synthetic work: Belinda van der Westhuizen, Ian Strydom

Cyclic voltammetry and data analysis: Pieter J. Swarts, Jannie C. Swarts

Computational work: Israel Fernández

Article written, submitted and response to reviewers: B. van der Westhuizen, D. I. Bezuidenhout, J. C. Swarts, I. Fernández.

[a] *Chemistry Department, University of Pretoria, Private Bag X20, Hatfield, 0028, South Africa. Fax: +27-(0)12-420-4687; Tel: +27-(0)12- 420-2626; E-mail: daniela.bezuidenhout@up.ac.za*
[b] *Chemistry Department, University of the Free State, PO Box 339, Bloemfontein 9300, South Africa. Fax:+27-(0)51-444-6384; Tel: +27-(0)51-401-2781; E-mail: swartsjc@ufs.ac.za*

[c] *Departamento de Química Orgánica I, Facultad de Química, Universidad Complutense,28040-Madrid,Spain.*

Supplementary information: The LSV and CV of complex **2**, (**Appendix 3a**) and Cartesian coordinates and energies of all the stationary species discussed in the text are included. (**Appendix 3b, CD**)

ABSTRACT

The series [Fc-(R)C=Cr(CO)$_5$], **1** (R = OEt) and **2** (R = NHBu) as well as [(OC)$_5$Cr=C(R)-Fc'-(R)C=Cr(CO)$_5$], **3** (R = OEt) and **4** (R = NHPr) of mono- and biscarbene chromium(0) complexes with Fc = Fe^{II}(C$_5$H$_5$)(C$_5$H$_4$) for monosubstituted derivatives and Fc′ = Fe^{II}(C$_5$H$_4$)$_2$ for disubstituted derivatives were synthesized and characterized spectroscopically, electrochemically and computationally. Electrochemical studies on the biscarbene complexes **3** and **4** provided evidence for electronic interaction between different redox sites, including the Cr-centers. The Cr$^{0/I}$ couples are electrochemically reversible with the difference in formal oxidation potentials between the "a" and "b" components being $\Delta E^{o'} = E^{o'}_{Cr(0)\ oxd\ 1b} - E^{o'}_{Cr(0)\ oxd\ 1a}$ = 151 and 105 mV in 3 and 4 respectively. Computational and electrochemical results were mutually consistent in showing unambiguously that the Cr(0) centre is oxidised before the ferrocenyl group in the carbene complexes **2**, **3** and **4**. Electrochemical experiments on the monoethoxy carbene **1** were also consistent with this redox sequence of events, but surprisingly, our calculations suggest that for **1**, the ferrocenyl group is oxidised *before* Cr(0) oxidation. The ethoxycarbenes **1** and **3** also showed a carbene double bond reduction to an anion radical, $^{-}$Cr=C$^{\bullet}$, while **4** was the only derivative to show irreversible Cr(I) oxidation to Cr(II) within the potential window of the solvent.

4.1 INTRODUCTION

The development of bi- and polymetallic complexes with σ,σ-attachments to transition metal fragments and containing a π-conjugated bridge has attracted considerable attention in recent years. Applied to Fischer carbene complexes, their potential use to obtain bi- or trimetallic polyenes that show metal-metal interactions are especially attractive [1]. Such systems may have interesting optical and electrochemical properties [2]. Fischer carbene complexes have also been extensively studied as catalysts [3], as reactants to facilitate many organic transformations [4], or as electrochemical probes [5]. Thermal [3,6] and photochemical transformations [7] have also been investigated.

Incorporation of the redox-active ferrocenyl group in complexes may be beneficial for a number of reasons. The electron-donating [8] characteristics of the ferrocenyl group, the electron-withdrawing properties of the oxidized ferrocenium species [9], the high thermal stability of both the oxidized and reduced states, and the electrochemical reversible nature of the Fc/Fc^{+} couple [10] are but some of the reasons why ferrocene derivatives have been studied as molecular sensors [11] and in energy transfer processes [12]. Considering reaction rates, as a part of a ligand system it will enhance oxidative addition reactions [13] but retard substitution processes [14]. Ferrocene derivatives are also used as high burning rate catalysts in rocket propellants [15] and as catalyst in various chemical reactions [16]. A particularly interesting application of ferrocene derivatives, which are strongly dependent on fine tuning of the ferrocenyl oxidation potential with suitable substituents, lies in the field of cancer therapy [17]. Differences in drug activity, catalyst specificity and reaction rates in the above sited applications are frequently the result of electronic interactions between the ferrocenyl group and functional groups in the substrate.

Recent reports suggest that any two non-conjugated metal carbene moieties in homo- and heterobimetallic biscarbene complexes behave as two independent monocarbene entities with separate, localized redox centres [18]. From our recently published results related to an electrochemical and theoretical investigation of 2,5-thiendiyl (Th′) and 2,5-furadiyl (Fu′) bis-heteroaryl carbene chromium(0) complexes [19,20], it is known that no significant electronic interaction exists between the two Cr(0) centers of $[(CO)_5Cr\{C(OEt)(Ar')C(OEt)\}Cr(CO)_5]$ with Ar′ = Th′ or Fu′. Because of this, the computational study of the recently published Cr(0) oxidation to Cr(I) of 2,5-thiendiyl- [19] and 2,5-furadiyl-biscarbene complexes [20] treated these redox processes as a two-electron transfer process that comprises of two simultaneously occurring but independent one-electron transfer steps, one for each Cr(0) center. However, for $[(CO)_5Cr\{C(OEt)(Fc')C(OEt)\}Cr(CO)_5]$, where the 2,5-thiendiyl or 2,5-furadiyl linking aryl unit between the two Cr carbene functionalities was replaced by a ferrocen-1,1′-diyl functionality, we *did* observe electrochemical evidence that some interaction may exist between the two Cr(0) centers [19], which needs further investigation. We herewith report the synthesis of the two new aminocarbene complexes $[Cr(CO)_5\{C(NHBu)Fc\}]$, **2**, and $[(CO)_5Cr\{C(NHPr)(Fc')C(NHPr)\}Cr(CO)_5]$, **4**, from the previously reported ethoxy complexes

$[Cr(CO)_5\{C(OEt)Fc\}]$, **1** [21], and $[(CO)_5Cr\{C(OEt)(Fc')C(OEt)\}Cr(CO)_5]$, **3** [22]. Results from an electrochemical study on **1 – 4**, and new insights from a computational study to elucidate the species generated in each redox process, are also presented.

4.2 RESULTS AND DISCUSSION

*Synthesis and spectroscopic characterization of complexes **1 - 4***

The Fischer reaction between ferrocenyllithium [23] and $[Cr(CO)_6]$ and subsequent alkylation with Et_3OBF_4 [24] yielded the known complex **1** $[Cr(CO)_5\{C(OEt)Fc\}]$, for which the crystal structure has been previously reported [18,25]. 1,1'-Dilithiated ferrocene [26] was reacted according to literature procedures with two equivalents of metal carbonyl. The resulting metal bisacylate is then quenched with oxonium salt, to yield the known bridging ferrocenyl biscarbene complex **3**, $[(CO)_5Cr\{C(OEt)(Fc')C(OEt)\}Cr(CO)_5]$ [22]. Considering the ease of dilithiation of ferrocene, it is surprising that so few Fischer biscarbene complexes containing a bridging ferrocen-1,1'-diyl (Fc') spacer have been reported, and the first crystal structure of this complex was only reported in 2008 [22(a)].

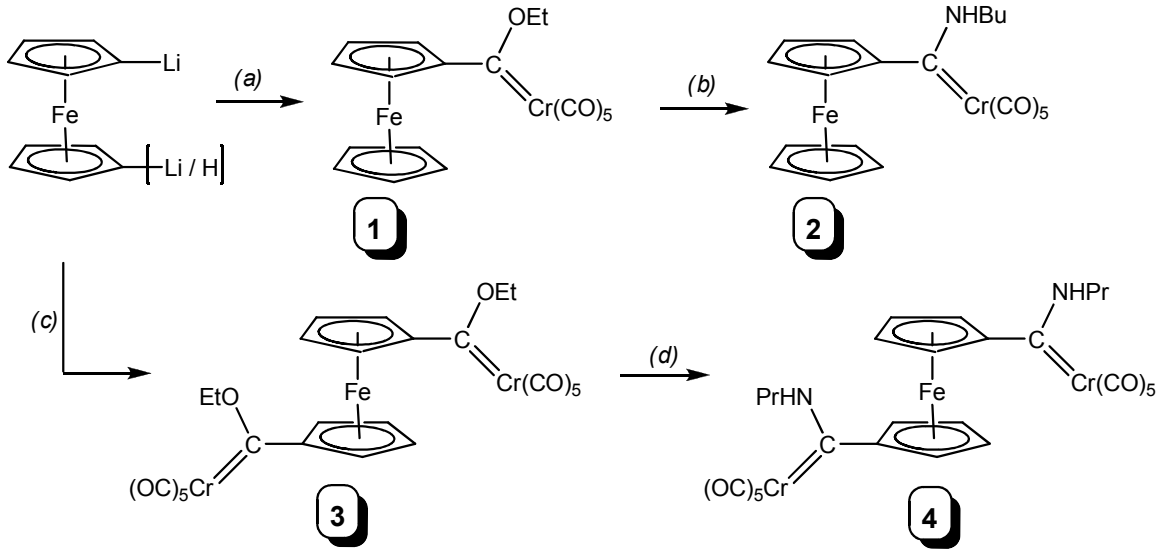

Scheme 4.1 Synthesis of ferrocenyl mono- and biscarbene complexes. Reagents and conditions: (a) (i) 1eq $[Cr(CO)_6]$, thf, -50°C; (ii) 1.3eq Et_3OBF_4, CH_2Cl_2, -30°C; (b) 1eq NH_2Bu, Et_2O, rt; (c) (i) 2eq $[Cr(CO)_6]$, thf, -50°C; (ii) 2.5eq Et_3OBF_4, CH_2Cl_2, -30°C; (d) 2eq NH_2Pr, Et_2O, rt.

Aminolysis [27] of the ethoxycarbene complexes **1** and **3** was achieved by reaction with either *n*-butylamine or *n*-propylamine to yield the new complexes $[Cr(CO)_5\{C(NHBu)Fc\}]$ (**2**) and $[(CO)_5Cr\{C(NHPr)(Fc')C(NHPr)\}Cr(CO)_5]$ (**4**), see Scheme 4.1. The shorter-chain *n*-propylamino substituent, rather than *n*-butylamino, was employed for the biscarbene complex in an attempt to improve the crystallinity of the complex.

Notably, only the *syn* isomer was observed for both the mono- and bisaminocarbene complexes **2** and **4**, and contrasts the mixture of *syn*- and *anti*-isomers around the $C_{carbene}$-N bond that was found for 2,5-thiendiyl and 2,5-furadiyl aminocarbene complexes [19,20]. The lack of formation of *anti*-configurational isomers for **3** and **4** can presumably be ascribed to the steric bulk of the ferrocenyl carbene substituent. Stabilization of ferrocene-containing carbenes is achieved in both the σ (through inductive effects) and the π (through π-resonance effects) modes of the bridging ligand [28]. Additionally, aminocarbenes are further stabilized by imine formation. Fig. 4.1 demonstrates both stabilization modes.

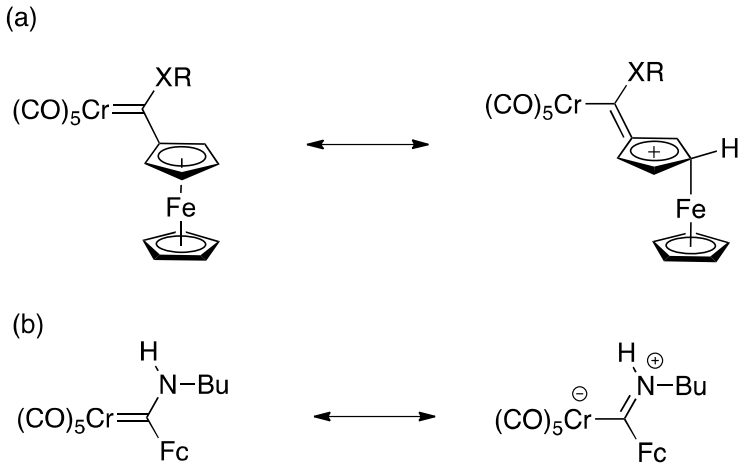

Fig. 4.1 Stabilization modes of the Fischer chromium(0) carbene complexes **1** and/or **2** (XR = OEt or NHBu) due to the (a) ferrocenyl and (b) amino substituents. For **2**, only the *syn* rotamer is observed.

In all cases, spectroscopic characterization gave the expected upfield shift of the carbene carbon atom in the ^{13}C NMR spectra for the aminocarbene ligand compared to the corresponding ethoxycarbene ligand, see Table 4.1. This is in accordance with increased heteroatom stabilization from the nitrogen carbene substituent (Fig. 4.1(b)). The IR spectra of the carbonyl

frequencies also demonstrate decreased π-backbonding required from the central metal atom for the aminocarbene complexes, as seen by the lower frequencies of the A'_1 mode carbonyl vibration (Table 4.1) [27,29]. The most significant observable, however, was the diminished electronic ring substituent involvement of the Fc-Cp bound to the $C_{carbene}$ atom. Usually, a marked downfield shift of H_α of the ring is observed, consistent with the electron-withdrawing effect of the metal carbonyl fragment and the π-delocalization of the aryl carbene substituent towards stabilizing the electrophilic carbene carbon atom [22,30]. In the case of the aminocarbene complexes **2** and **4**, the observed H_α ^{1}H NMR resonance was consistently shifted upfield from the corresponding ethoxycarbene **1** and **3** H_α shifts (Table 4.1), but also found to be much closer in value to the H_β chemical resonances; even overlapping in the case of **4** ($\delta(H_{\alpha,\beta})$ = 4.42 ppm). This evidences considerably less ring-involvement required for the aminocarbene complexes.

Table 4.1 Selected ^{1}H and ^{13}C NMR data and IR ν(CO) stretching frequencies for **1** – **4**.

Complex	H_α δ ^{1}H (ppm)	H_β δ ^{1}H (ppm)	$C_{carbene}$ δ ^{13}C (ppm)	A'_1 ν(CO) (cm^{-1})
1 [21]	4.93	4.71	329.7	1949
2	4.42	4.17	270.6	1931 (overlap E)
3 [22]	5.00	4.73	306.7	1938 (overlap E)
4	4.42	4.42	270.6	1925 (overlap E)

Electrochemistry and computational analyses

Cyclic voltammetry (CV), linear sweep voltammetry (LSV), and Osteryoung square-wave voltammetry (SW) were conducted on 0.5 mmol dm^{-3} solutions of **1** – **4** in dry, oxygen-free CH_2Cl_2 utilizing 0.1 mol dm^{-3} $[N(nBu)_4][PF_6]$ as supporting electrolyte. Electrochemical data are summarized in Table 4.2, CV's are shown in Fig.'s 4.4 and 4.5.

Four redox processes were observed. The first of these is associated with wave I in Fig. 4.4 and Table 4.2 and is ascribed to the one-electron reduction of the carbene double bond to $^-$Cr-C• [31], as the LUMO (i.e. the orbital accepting the additional electron) is mainly located on the p_z

atomic orbital of the carbene carbon atom (see Fig. 4.2) [32]. Only the ethoxy derivatives **1** and **3** showed this redox process at formal reduction potentials $E^{o'} = (E_{pa} + E_{pc})/2 < -1.8$ V (Fig. 4.4). The electrochemistry of **1** and **3** were described in an earlier communication [19] and we refrain from further commenting here on Cr=C reduction. That the new aminocarbene analogues **2** and **4** do not exhibit this redox process within the solvent potential window of CH_2Cl_2, but furyl (Fu) and thienyl (Th) derivatives do [20], bears testimony to the stronger electron-donating power of the ferrocenyl group compared to Fu and Th. Also, the amino-groups of **2** and **4** are much more electron-donating than OEt, which results in the stabilizing imine resonance form shown in Fig. 4.1(b). As a consequence of such donation, the electronic occupation of the "empty" p_z atomic orbital of the carbene carbon atom is significantly higher in complexes **2** and **4** compared to **1** and **3**. This makes the reduction process far more difficult and therefore, the Cr=C reduction potentials appear at more negative values than the lowest potential the solvent, CH_2Cl_2, can accommodate.

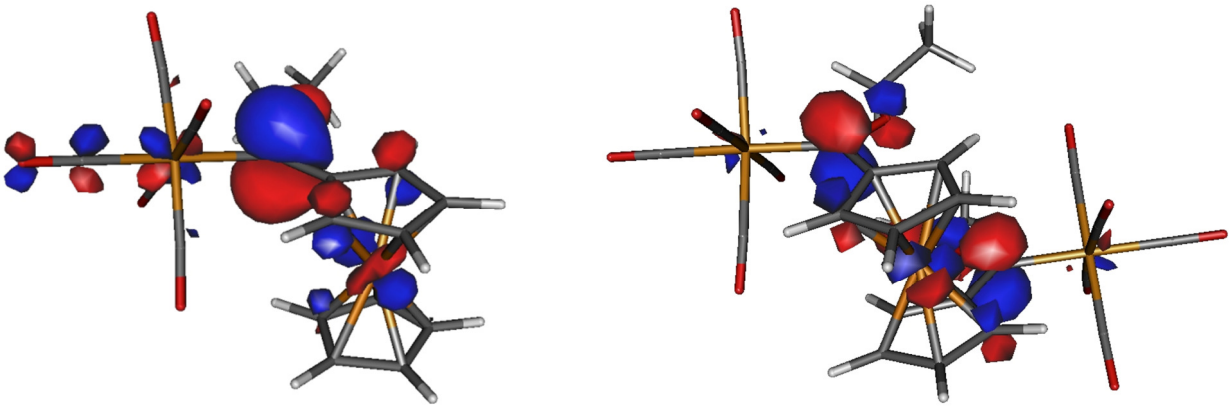

LUMO (1) **LUMO (3)**

Fig. 4.2 Computed LUMO of complexes **1** and **3** (isosurface value of 0.045 au).

In our recent report [19,20] on the second redox process (wave 1) for **3** we described electrochemical evidence that is consistent with both Cr(0) centers being oxidized *before* the ferrocenyl group. We concluded that the monoethoxycarbenederivative **1** should behave analogously to **3** and suggested that in **1**, Cr(0) is also oxidized before the ferrocenyl centre. This

conclusion was thought reasonable because this assignment meant that Cr(0) oxidation in **1** and **3** differed with only 210 mV and the ferrocenyl waves were only 30 mV apart, see Table 4.2. Our present computational study showed that this original assignment on the sequence of redox events for the biscarbene **3** was correct, see Fig 4.3. However, from the computational study described below, DFT calculations at the B3LYP/def2-SVP level indicate that complex **1** is electrochemically oxidized to the radical cation $\mathbf{1}^{\bullet+}$ because of ferrocenyl oxidation, not Cr(0) oxidation (see Fig. 4.3, top). The computed spin density of this species indicates that the unpaired electron is located at the iron atom (1.27e). Differently, for biscarbene complex **3**, the spin density of the corresponding radical cation $\mathbf{3}^{\bullet+}$ is not located at the iron atom but at one of the chromium centers (1.17e, Fig. 4.3, bottom). Thus, the oxidation process associated with wave 1 in the biscarbene complex **3** involves Cr(0) oxidation to Cr(I) rather than ferrocenyl oxidation as in its monocarbene counterpart, complex **1**. It is clear that for **1**, DFT calculations cast a different perspective than the results obtained from the experimental electrochemistry. In an attempt to validate the B3LYP calculations on carbene complex **1** by using different functionals (at the BP86/def2-SVP and OLYP/def2-SVP levels), the computed spin density was found to be located *ca.* 70 % on the Fe(III) center. To judge whether this unexpected sequence of oxidative redox events might be endorsed by the electrochemistry, one has to reassign the electrochemical observed redox event 1, as an Fe(II) oxidation process and a Cr(0) oxidation to the wave labeled Fc. Such a reassignment would imply that the Fe(II) oxidation processes of **1** and **3** occur at potentials 441 mV apart (rather the the 30 mV if the reassignment is not made). In addition, the Cr(0) oxidations of **1**and **3** would then be 201 mV apart rather than 210 mV as in the original assignment. Although this large difference in ferrocenyl oxidation potential is not impossible, it is very unlikely. We conclude that the computed sequence of redox processes for **1** is not compatible with the electrochemical experimental result.

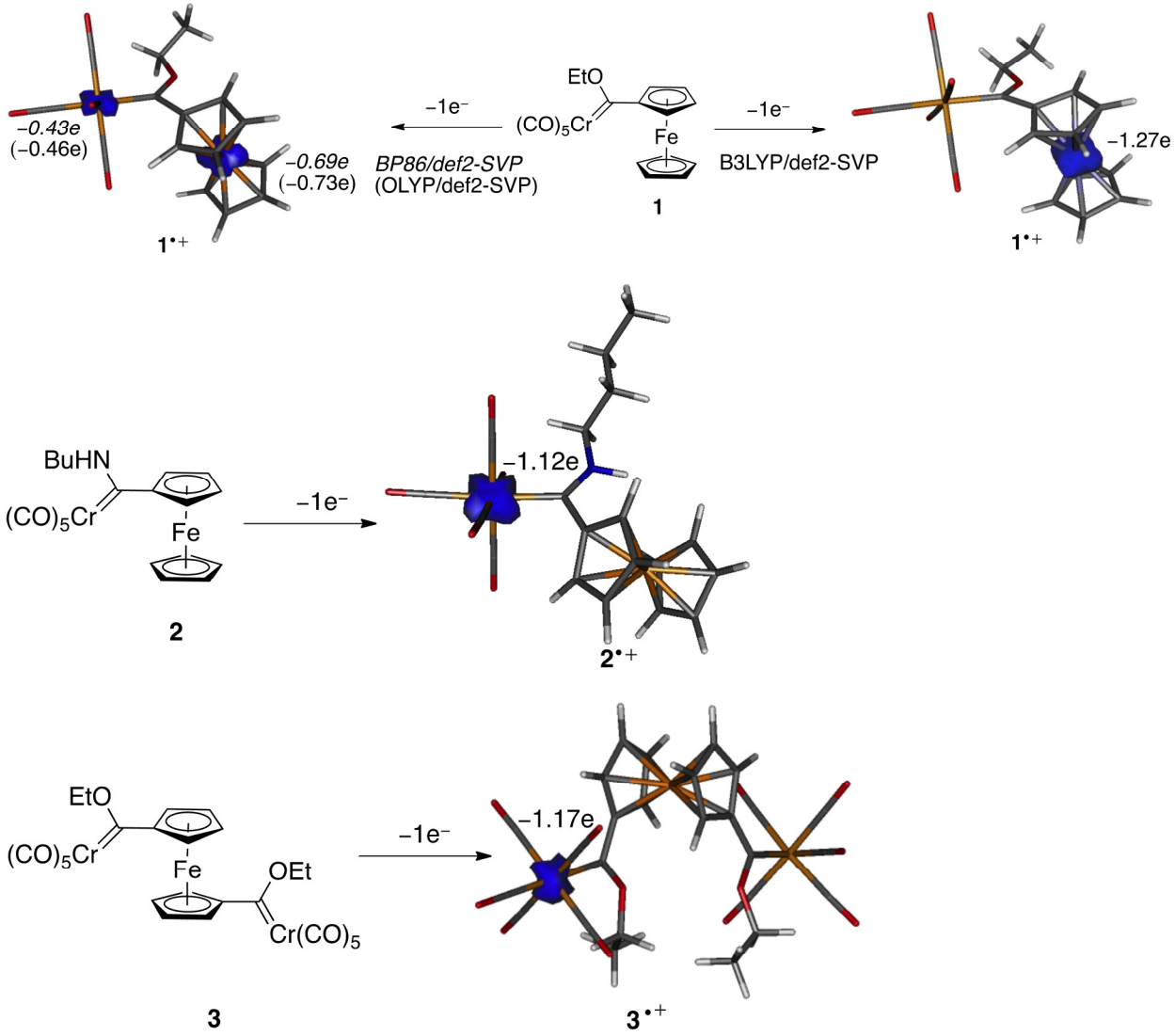

Fig. 4.3 First one-electron oxidation processes of complexes **1**, **2** and **3**.

In a further attempt to rationalize the unexpected computed sequence of redox events for **1**, we also computed the first oxidation process for the aminocarbene and biscarbene derivatives **2** and **3**. Our calculations indicate that the corresponding radical cations $\mathbf{2}^{\bullet+}$ and $\mathbf{3}^{\bullet+}$ that formed upon 1-electron oxidation of complexes **2** and 3 respectively, exhibit a spin density mainly located on the chromium atom (see Fig. 4.3). This result shows that the presence of an amino-group directly attached to the carbene carbon atom does not modify the *computed* order of oxidation events of **2** compared to **3**, nor did it contradict the *electrochemically* determined order of events for **1** – **4**; the oxidation order was still such that the ferrocenyl center is oxidized *after* the Cr(0) moiety. An

additional computational study on **4** (see further below, Fig. 4.7) confirmed that for this complex, Cr(0) oxidation is also preceding Fe(II) oxidation. In the absence of any supportive evidence why **1** should exhibit a different sequence of oxidation events than **2** – **4**, we conclude that, while note should be taken of the computational result of this complex, compound **1** probably also undergoes first a Cr(0) oxidation to Cr(1) followed by ferrocenyl oxidation. The reasons why the computed results for **1** do not fit this trend are at this stage not clearly understood but they might be the result of the delocalization of the unpaired electron within the ferrocenyl fragment.

To quantify the influence of the NHBu group on the oxidative redox processes of the monocarbene **2**, it is noted that **2** exhibits the Cr(0) electrochemical reversible oxidation process at 0.196 V vs. FcH/FcH^+ (Table 4.2). This potential is 93 mV lower than for **1**, and again reflects the stronger electron-donating power of NHBu compared to the OEt group. The Cr(0) centre of the NHBu-ferrocenyl complex **2** is oxidized at potentials 144 and 239 mV smaller than those observed for the recently reported furyl and thienyl NHBu monocarbene complexes. These different potentials as well as those observed for wave I above are indicative of electronic interactions between redox-active fragments within the molecules.

A further key observation in favor of such interactions is associated with the splitting of the $Cr^{0/I}$ couple into two definite "a" and "b" components, one for each of the two Cr(0) centers of the biscarbene complexes **3** and **4** (Fig. 4.4, middle two CV's and Fig. 4.5). This is consistent with some electronic interaction, which may be electrostatic and/or otherwise, between the two separate Cr(0) centers. The separation between Cr(0) formal oxidation potentials for waves 1a and 1b of **3** and **4** are $\Delta E^{o'} = E^{o'}_{Cr(0)\ oxd\ 1b} - E^{o'}_{Cr(0)\ oxd\ 1a} =$ 151 and 105 mV, respectively. In contrast, when the Fc′-linking functionality is changed to a 2,5-thiendiyl or 2,5-furadiyl functionality, no similar peak splitting for wave 1 was observed [19,20]. Different formal reduction potentials, $E^{o'}$, for symmetrical complexes in which mixed-valent intermediates are generated (for **3** and **4** this refers to complexes where the Cr(0) center of one of the two carbene functionalities was oxidized to a Cr(I) center but not the other) are well known [33,34] in systems that allow electron delocalization or where electrostatic interactions are possible. It is important to recognize, though, that the electrode potentials of closely-spaced redox events are notoriously difficult to assess using CV methods. Richardson and Taube discussed this in detail [35].

Table 4.2. Cyclic voltammetry data of 0.5 mmol.dm^{-3} solution of $[(OC)_5Cr{=}C(Fc)X]$ and $[(OC)_5Cr{=}C(X)\text{-}Fc'\text{-}(X)C{=}Cr(CO)_5]$ complexes in CH_2Cl_2 containing 0.1 mol.dm^{-3} $[N(^nBu)_4][PF_6]$ as supporting electrolyte at a scan rate of 100 mV s^{-1} and 20 °C. Potentials are relative to the FcH/FcH^+ couple.

Complex	Peak lable	$E^{o'}$/V, ΔE/mV	$i_{pa}/\mu A$, i_{pc}/i_{pa}
1	I(=)	-2.148, 111	3.20 [b], 0.41
X = OEt	1($Cr^{0/I}$)	0.289, 102	3.48, 0.89
	(Fc)	0.700, 89	3.29, 0.85
	2($Cr^{I/II}$)	- [a] , - [a]	- [a] , - [a]
2	I(=)	- [a] , - [a]	- [a] , - [a]
X = NHBu	1($Cr^{0/I}$)	0.196, 78	3.04, 1.00
	(Fc)	0.539, 78	2.78, 0.98
	2($Cr^{I/II}$)	- [a] , - [a]	- [a] , - [a]
3	I(=)	-1.845, 104	3.81 [b], 0.39
X = OEt	1a($Cr^{0/I}$)	0.499, 83	3.71, 0.73
	1b($Cr^{0/I}$)	0.650, 80	3.51, 0.23
	(Fc)	0.730, 97	3.78, < 0.1
	2($Cr^{I/II}$)	- [a] , - [a]	- [a] , - [a]
4	I(=)	- [a] , - [a]	- [a] , - [a]
X = NHPr	1a($Cr^{0/I}$)	0.341 [c], 76	3.79, 0.83 [c]
	1b($Cr^{0/I}$)	0.446 [c], 78	3.71, 0.63 [c]
	(Fc)	0.700, 88	3.52, 0.67 [c]
	2($Cr^{I/II}$)	0.977 [d], -	6.66, -

(a) No peak detected within the solvent potential window; (b) i_{pc} and i_{pa}/i_{pc} values to maintain the current ratio convention of $i_{forward\ scan}/i_{reverse\ scan}$. (c) inaccurate values due to poor resolution, especially in the cathodic sweep; (d) E_{pa} value, no E_{pc} or i_{pc} detected.

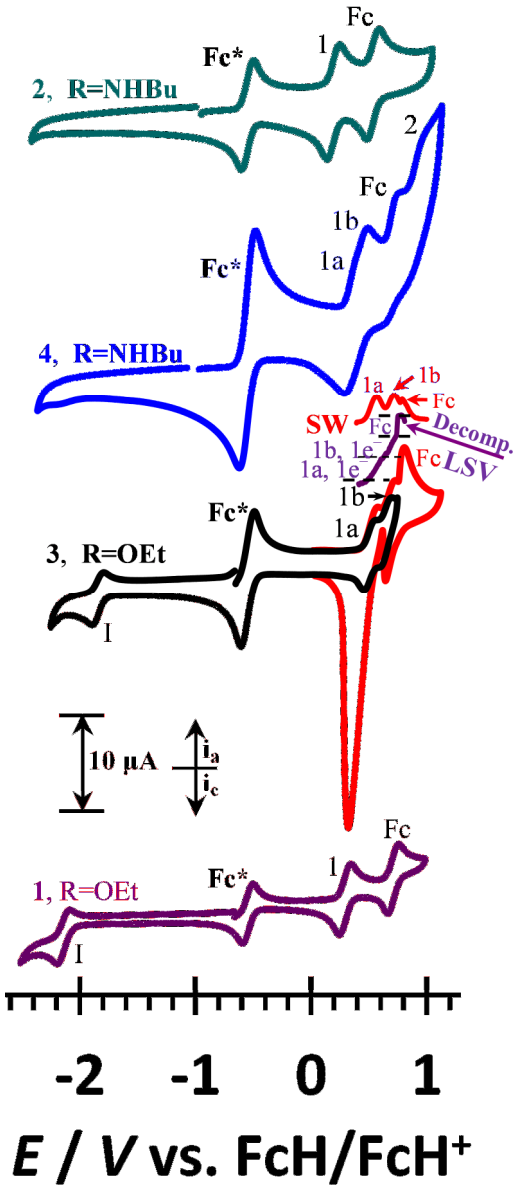

Fig. 4.4 Cyclic voltammograms of 0.5 mmol.dm^{-3} solutions of monocarbene [(OC)5Cr=C(Fc)X] **1** and **2** and biscarbene complexes [(OC)$_5$Cr=C(X)-Fc′-(X)C=Cr(CO)$_5$] **3** and **4** in CH_2Cl_2/0.1 mol.dm^{-3} [N(*n*Bu)$_4$][PF$_6$] on a glassy carbon-working electrode at a scan rate of 200 mV/s. Decamethylferrocene, Fc*, was used as internal standard. For **3**, the black scan was reversed at 880 mV. This excluded oxidation of the ferrocenyl group and no electrode deposition of the substrate on the electrode surface area which led to large cathodic currents at wave 1 as indicated by the red CV was observed.

For **3**, oxidation of both Cr(0) centers (waves 1a and 1b) and the ferrocen-1,1'-diyl group at wave Fc leads to electrode deposition of the substrate as indicated by the large cathodic electrode currents at wave 1 while recording the red CV of **3** in Fig. 4.4. However, when the reverse potential was chosen to be sufficiently small to exclude wave Fc in the CV of **3**, the resolved oxidations of the two chromium centers at waves 1a and 1b (black CV of **3** in Fig. 4.4) exhibited electrochemical reversible behavior with i_{pc}/i_{pa} ratios approaching 1 and ΔE_p about 80 mV at slow scan rates (Table 4.2). Ideally, electrochemical reversible one-electron transfer processes are characterized by $\Delta E_p = E_{pa} - E_{pc} = 59$ mV and peak current ratios approaching one [36]. For **4**, the resolution between the two Cr(0) oxidations were not as good as for **3**, probably as a result of the NHPr conjugation as shown in Fig. 4.1(b) dominating over ferrocenyl conjugation with the carbene double bond as shown in Fig. 4.1(a). This at the same time must also contribute to the absence of noticeable amounts of electrode deposition when the potential was allowed to increase enough to oxidize the ferrocenyl group of **4** compared to what was observed for **3**, (Fig. 4.4).

The third redox process that was observed in **1**– **4** is the one-electron oxidation of the ferrocenyl group (wave Fc in Fig.'s 4.4 and 4.5). This redox process is also electrochemically reversible by virtue of good ΔE_p values at slow scan rates (Table 4.2). Similarly to the electrochemistry of **3** (Fig. 4.3) that has been discussed above, we observed by LSV measurements on **4** that poorly resolved waves 1a and 1b both involve the same numbers of electrons, and also involves the same number of electrons as the Fc wave (Fig. 4.5). Upon recognizing that the ferrocenyl group represents a one electron transfer process, it follows that the current ratio of (wave 1a + wave 1b):Fc should be 2:1.

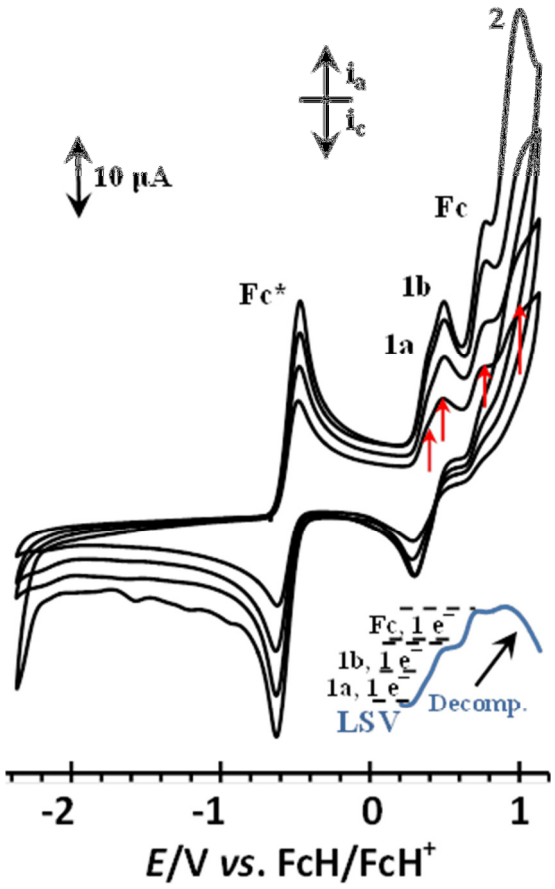

Figure 4.5 An LSV at 2 mV/s as well as CV's of 1.0 mmol.dm^{-3} solutions of the biscarbene $[(OC)_5Cr{=}C(NHPr)\text{-}Fc'\text{-}(PrHN)C{=}Cr(CO)_5]$ **4** in CH_2Cl_2/0.1 mol.dm^{-3} $[N(^nBu)_4][PF_6]$ on a glassy carbon-working electrode at scan rates of 100 (smallest currents), 200, 300 and 400 mV/s. Decamethylferrocene, Fc*, was used as internal standard.

Once the ferrocenyl group has been oxidized to ferrocenium, the group electronegativity of this functionality increased from 1.83 to 2.82 on the Gordy scale [8]. This implies that complexes **1** – **4** are after ferrocenyl oxidation under the influence of an electron-withdrawing substituent almost as strong as a CF_3 group which has a Gordy scale group electronegativity of 3.01 [37]. It is therefore expected that any remaining redox processes will be shifted to much more positive potentials. In our previous studies regarding furyl and thienyl complexes, a one-electron Cr(I) oxidation to Cr(II) was observed at ca. 1.0 volt vs FcH/FcH^+. In the present compound series only the biscarbene complex $[(OC)_5Cr{=}C(NHPr)\text{-}Fc'\text{-}(PrHN)C{=}Cr(CO)_5]$, **4**, exhibited this redox process at E_{pa} = 0.977 V (wave 2 Fig.'s 4.4 and 4.5 and Table 4.2). For compounds **1** - **3**, this fourth redox process fell outside the potential window of the solvent. That wave 2 was observed

for **4** is related to this complex having two amino groups that are involved with stabilization via imine formation, Cr $^{-}$–C=N^{+}HPr, compare Fig. 4.1 for **2**. As with wave I that moved to lower potentials because of this, it is also the case with wave 2. For complex **4** with two amino groups, this negative shift was enough to observe wave 2 in its CV. The number of electrons that are transferred at the redox process associated with wave 2 should be one for each Cr(I) oxidations, but LSV measurements could not confirm this. The complex decomposed on LSV timescale (Fig. 4.5). However, upon comparing the i_{pa} current of wave 2 with that of the one-electron transfer Fc wave and the two one-electron Cr(0) oxidations (Fig. 4.5, Table 4.1), we conclude that the observed current of wave 2 is consistent with two one-electron oxidations occurring simultaneously.

Scheme 4.2 highlights the electrochemical processes associated with **4**. Complexes **2** and **4** undergo essentially the same redox processes, although, of course the monocarbene **2** only show one electron transferred at each wave, rather than two, and wave 1 does not have an "a" and "b" component. Furthermore, wave I was only detected for ethoxy complexes **1** and **3**; for **2** and **4** this electron transfer process fell outside the potential window of the solvent. With respect to wave 2, only compound **4** exhibited Cr(I) oxidation within the potential window of the solvent. For **1**, **2** and **3**, this process occurred at potentials too large to be measurable in CH_2Cl_2.

To verify the electrochemical assignment of the sequence of redox events, the above described oxidation processes were further studied by computational means utilizing **3** and **4** as substrates. As discussed above (Fig. 4.3), the first oxidation reaction of biscarbene complex **3** leads to the radical cation **3**$^{\cdot+}$ where the computed spin density indicates that the unpaired electron is mainly located at one of the two chromium centers. Further calculations suggest the subsequent second oxidation reaction does not occur at this Cr(I) center leading to the closed-shell singlet dication **3**$^{+2}$**(b)** (Fig. 4.6). Instead, the open-shell singlet species **3**$^{+2}$**(a)** is formed in view of the higher stability computed for this complex (ΔE(b-a) = 39.5 kcal/mol). Moreover, the computed spin density for the latter dication indicates that the second oxidation process involves oxidation of the second Cr(0) centre also to Cr(I) rather than oxidation at the ferrocenyl moiety. From the dicationic **3**$^{+2}$**(a)** complex, ferrocenyl oxidation leads to the formation of the tricationic species **3**$^{\cdot+3}$ where the spin densities are located at the two chromium(I) centers and at the newly generated Fe(III) centre (Fig. 4.6).

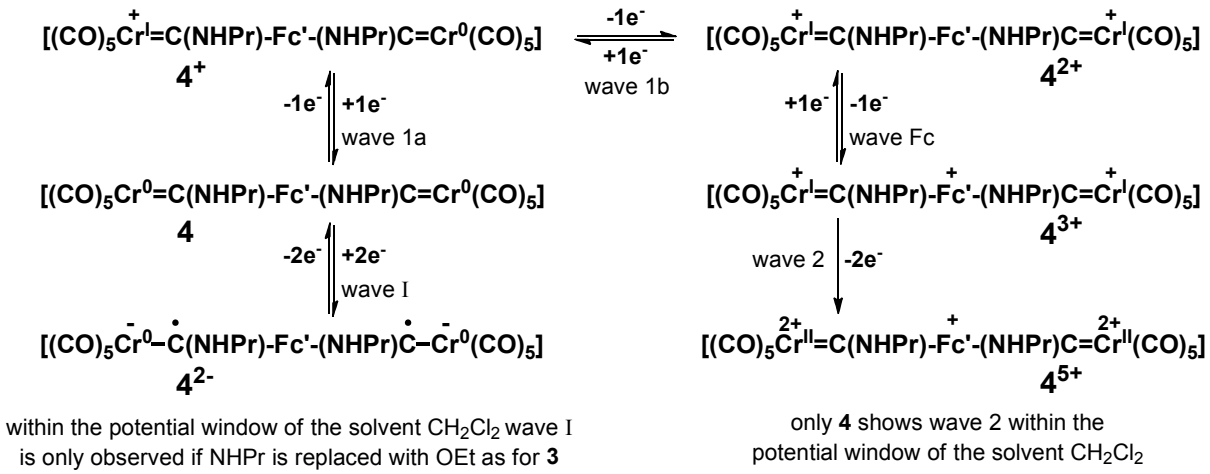

within the potential window of the solvent CH_2Cl_2 wave I is only observed if NHPr is replaced with OEt as for **3**

only **4** shows wave 2 within the potential window of the solvent CH_2Cl_2

Scheme 4.2 Electrochemical processes associated with **4**. Both the final reduction product possessing the $^{-}$Cr-C$^{\bullet}$ radical anions and the final oxidation product possessing the Cr(II) centers are highly reactive and may undergo further chemical decomposition reactions. The formulas do not show the imine isomers (Fig. 4.1); only the carbene isomers are depicted. The dominance of the imine isomers in carbene structures may well be an important contributing reason why wave I is not observed in the potential window of the solvent, CH_2Cl_2.

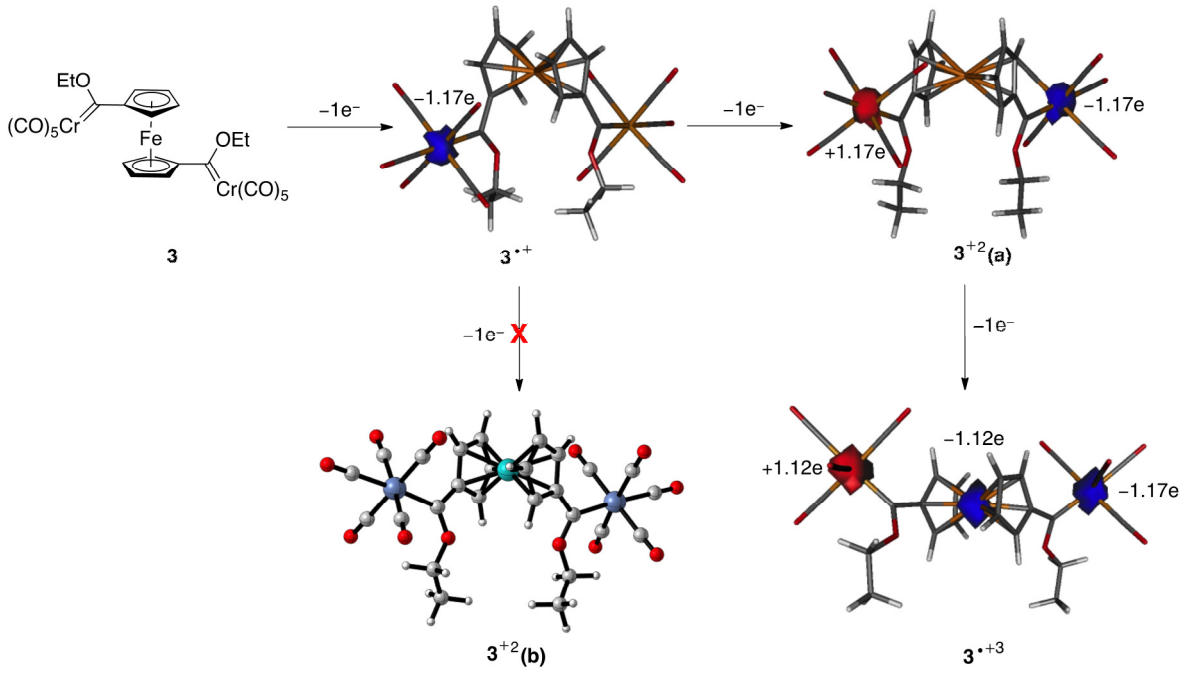

Fig. 4.6 Oxidation process for complex **3**.

As expected, the bis(aminocarbene) complex **4** follows the same sequence of redox events. As shown in Fig. 4.7, the first oxidation process involves the formation of the radical cation $\mathbf{4}^{\bullet+}$ where the computed spin density indicates that the unpaired electron is mainly located at one of the chromium centers (1.17e) thus confirming the Cr(0) to Cr(I) reaction. This species is further oxidized to the dication $\mathbf{4}^{+2}$, an open-shell singlet species whose the spin density is located at both Cr(I) centers (-1.18 and 1.18e, respectively). Further oxidation of the ferrocenyl group of **4** produced the corresponding trication $\mathbf{4}^{\bullet+3}$ and quatercation $\mathbf{4}^{+4}$.

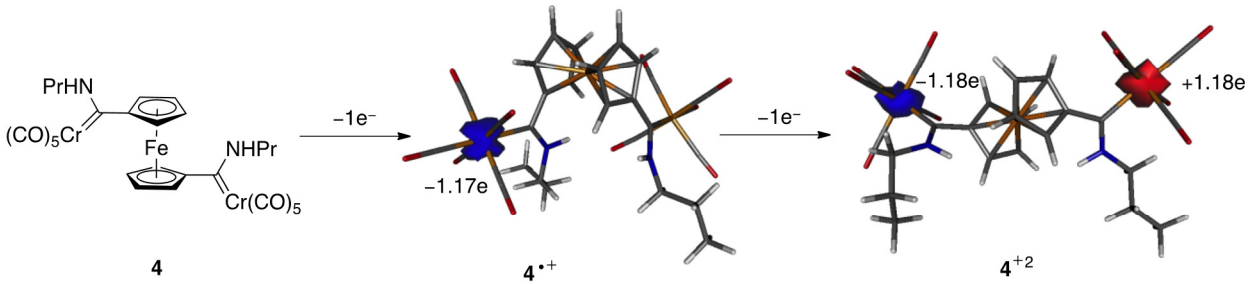

Fig. 4.7. Oxidation process for complex **4**.

We conclude results from our computational study involving **3** and **4** nicely replicate the redox sequence assignment from the electrochemical analysis described above.

4.3 CONCLUSIONS

New ferrocenyl mono- and bisaminocarbene chromium complexes $[(CO)_5Cr{=}C(NHBu)Fc]$, **2**, and $[(CO)_5Cr{=}C(NHPr)\text{-}Fc'\text{-}(NHPr)C{=}Cr(CO)_5]$, **4**, were prepared from their ethoxy precursors. From ^{1}H NMR evidence, only the *syn*-rotamer across the restricted $C_{carbene}$–N bond was formed. An electrochemical study revealed four redox processes. Electrochemical reversible to quasi-reversible reduction of Cr=C to $^-$Cr-C• was only observed for the ethoxy analogues at far negative potentials; -2.148 or -1.845 V vs FcH/FcH^+ for **1** and **3** respectively. This redox process for the amino derivatives **2** and **4** fell outside the negative potential limit of the solvent. Oxidation of Cr(0) to Cr(I) was observed in the 0.196-0.650 V potential range. A striking result of this study is the observation of two resolved $Cr^{0/I}$ couples for the ferrocen-1,1'-diyl biscarbene complexes **2** and **4**. The formal oxidation potentials of these two consecutive Cr(0) oxidations

were 105 and 151 mV apart, indication electronic interaction between the Cr(0) centers. The ferrocenyl group of **1** – **4** is oxidized at larger potentials (0.539-0.730 V) than that of the $Cr^{0/I}$ couple. Irreversible oxidation of Cr(I) to Cr(II) at the positive edge of the solvent potential window was only observed for **4** at 0.977 V. This redox process fell outside the positive solvent potential limit for the other complexes. These redox assignments were mutually consistent with the computational results obtained at the DFT level.

4.4 EXPERIMENTAL SECTION

General Procedures

All manipulations involving organometallic compounds made use of standard Schlenk techniques under inert atmosphere. Solvents were dried over sodium metal (hexane, thf and diethylether) and phosphorouspentoxide (CH_2Cl_2); and distilled under nitrogen gas prior to use. All chemicals were used as purchased without further purification unless stated otherwise. Triethyloxoniumtetrafluoroborate was prepared according to literature procedures [24]. Complexes **1** and **3** were synthesized according to literature procedures [21,22]. Purification of complexes was done with column chromatography using silica gel 60 (0.0063-0.200 mm) as the stationary phase. NMR spectra were recorded on a Bruker AVANCE 500 spectrometer. ^{1}H NMR spectra were recorded at 500.139 MHz and ^{13}C NMR at 125.75 MHz. The signals of the deuterated solvent were used as a reference: ^{1}H $CDCl_3$ at 7.24 ppm and C_6D_6 7.15 ppm; ^{13}C $CDCl_3$ at 77.00 ppm and C_6D_6 128.00 ppm. IR spectra were recorded on a Perkin-Elmer Spectrum RXI FT-IR spectrophotometer in solvent hexanes. Only the vibration bands in the carbonyl-stretching region (ca. 1600-2200 cm^{-1}) were recorded.

Synthesis of complexes

[Cr(CO)$_5${C(NHBu)Fc}] (2)

A diethylether solution of **1** (2 mmol, 0.87g) was stirred at room temperature (rt) and *n*-butylamine (2 mmol, 0.20 mL) was added. The colour changed rapidly from dark red to deep yellow. Purification was performed using column chromatography and a 1:1 mixture of hexane/CH_2Cl_2 as eluent. Yield: 0.72g (78%), yellow solid. Anal. Calcd for $CrFeC_{20}H_{19}NO_5$: C,

52.08; H, 4.16. Found: C, 52.05; H, 4.10. ^{1}HNMR (500 MHz, $CDCl_3$, δ, ppm): 9.48 (s, 1H, N**H**), 4.42 (br, 4H, H_α overlap H_β), 4.17 (s, 5H, Cp), 4.10-3.96 (m, 2H, NC**H**$_2$), 1.85 (p, *J* = 7.5 Hz, 2H, C**H**$_2$CH$_2$), 1.57 (s, 2H, CH$_2$C**H**$_2$), 1.06 (t, *J* = 7.4 Hz, 3H, C**H**$_3$). ^{13}CNMR (125 MHz, $CDCl_3$, δ, ppm): 270.60 ($C_{carbene}$), 223.56 (*trans*-**C**O), 217.81 (*cis*-**C**O) , 99.55 (**C**$_{ipso}$), 70.01 (C_α), 68.29 (C_β) , 69.35 (Cp), 52.62 (N**C**H$_2$), 31.88 (**C**H$_2$CH$_2$), 20.13 (CH$_2$**C**H$_2$), 13.80 (**C**H$_3$). FTIR (hexanes, νCO, cm^{-1}): 2053 s (A″$_1$), 1971 w (B), 1931 s (A′$_1$ overlap E).

[(CO)$_5$Cr{C(NHPr)(Fc′)C(NHPr)}] (4)

Complex **3** (2 mmol, 1.27g) was dissolved in diethylether and *n*-propylamine (2 mmol, 0.16 mL) was added at rt. The colour of the solution turned from dark red to deep yellow and volatiles were removed by reduced pressure. Purification was performed by employing column chromatography with a 1:1 hexane/CH_2Cl_2 solvent mixture. Yield: 0.96g (68%), deep yellow crystals. Anal. Calcd for $Cr_2FeC_{28}H_{24}N_2O_{10}$: C, 56.82; H, 5.08. Found: C, 55.72; H, 4.90. ^{1}HNMR (500 MHz, $CDCl_3$, δ,ppm): 9.38 (s, 2H, **H**N), 4.42 (m, 8H, H_α overlap $H_ß$), 4.01 (m, 4H, NC**H**$_2$), 1.89 (m, 4H, C**H**$_2$CH$_3$), 1.15 (t, *J* = 7.4 Hz, 6H, C**H**$_3$). ^{13}CNMR (125 MHz, $CDCl_3$, δ, ppm): 270.64($C_{carbene}$), 223.12 (CO_{trans}), 217.50 (CO_{cis}), 101.40 (C_{ipso}), 70.94 (C_α), 68.70 ($C_ß$), 54.66 (HN**C**H$_2$), 23.21 (**C**H$_2$CH$_3$), 11.23 (**C**H$_3$). FTIR (hexane, νCO, cm^{-1}): 2051 m (A″$_1$), 1972 w (B), 1925 vs (A′$_1$ overlap E).

Electrochemistry

Cyclic voltammograms (CV's), square wave voltammograms (SW's) and linear sweep voltammograms (LSV's) were recorded on a Princeton Applied Research PARSTAT 2273 voltammograph running PowerSuite (Version 2.58) utilizing a standard three-electrode cell in a M Braun Lab Master SP glovebox filled with high purity argon (H_2O and O_2 < 5 ppm) as described before [19,20]. All electrode potentials are reported *versus* the ferrocene/ferrocenium redox couple (FcH/FcH$^+$, FcH = Fe(η^5-C_5H_5)$_2$, $E^{o\prime}$ = 0.00 V) [38]. However, decamethyl ferrocene, Fc*, was used as internal standard to prevent signal overlap with the ferrocenyl of **1** and **2**. Decamethylferrocene has a potential of -550 mV versus free ferrocene with ΔE = 72 mV and i_{pc}/i_{pa} = 1 under the conditions employed [39].

Computational details

Geometry optimizations without symmetry constraints were carried out using the Gaussian09 suite of programs [40] at the B3LYP (uB3LYP for open-shell species) [41] using the double-□ plus polarization def2-SVP [42] basis set for all atoms. This protocol is denoted B3LYP/def2-SVP. All species were characterized by frequency calculations, and have a positive defined Hessian matrix indicating that they are minima on the potential energy surface. In order to check the reliability of the B3LYP results, different functionals (BP86 [43] and OLYP [41(b),44]) were used as well.

4.5 ACKNOWLEDGEMENTS

This work is supported by the National Research Foundation, South Africa, (DIB, Grant number 76226; JCS, Grant number 81829), and by the Spanish MICINN and CAM (IF, Grants CTQ2010-20714-CO2-01/BQU, Consolider-Ingenio 2010, CSD2007-00006, S2009/PPQ-1634).

4.6 REFERENCES

[1] (a) T.L. Stott, M.O. Wolf, Coord. Chem. Rev. 246 (2003) 89-101; (b) B.J. Holiday, T.M. Swager, Chem. Commun. 1 (2005) 23-36 (c) M.O. Wolf, J. Inorg. Organomet. Polym. Mater. 16 (2006) 189-199.

[2] (a) A. Caballero, A. Espinosa, A. Tarraga, P. Molina, J. Org. Chem. 72 (2007) 6924-6937; (b) M.L. Lage, D. Curiel, I. Fernández, M.J. Mancheño, M. Gómez-Gallego, P. Molina, M.A. Sierra, Organometallics 30 (2011) 1794–1803; (c) G.M. Chu, I. Fernández, M.A. Sierra, Chem. Eur. J. 19 (2013) 5899-5908.

[3] (a) G.M. Chu, I. Fernández, M.A. Sierra, J. Org. Chem. 78 (2013) 865-871; (b) G. Occhipinti, V.R. Jensen, Organometallics 30 (2011) 3522-3529; (c) M.P. López-Alberca, I. Fernández, M.J. Mancheño, M. Gómez-Gallego, L. Casarrubios, M.A. Sierra, Eur. J. Org.

Chem. (2011) 3293-3300; (d) W.I. Dijk, X.P. Zhang, B. de Bruin, Inorg. Chem. 50 (2011) 9896-9903; (e) I. Fernández, M.J. Mancheño, R. Vicente, L.A. López, M.A. Sierra, Chem. Eur. J. 14 (2008) 11222-11230; (f) B. Koo, F.E. McDonald, Org. Lett. 9 (2007) 1737-1740; (g) J.C. del Amo, M.J. Mancheño, M. Gómez-Gallego, M.A. Sierra, Organometallics 23 (2004) 5021-5029; (h) M.A. Sierra, J.C. del Amo, M.J. Mancheño, M. Gómez-Gallego, J. Am. Chem. Soc. 123 (2001) 851-861; (i) For a revision of the catalytic transmetallation to late transition metals, see M. Gómez-Gallego, M.J. Mancheño, M.A. Sierra, Acc. Chem. Res. 38 (2005) 44-53.

[4] For selected reviews, see: (a) J. Barluenga, J. Santamaría, M. Tomás, Chem. Rev. 104 (2004) 2259-2283; (b) K.H. Dötz, J. Stendel, Jr., Chem. Rev. 109 (2009) 3227-3274; (c) M.A. Fernández-Rodríguez, P. García-García, E. Aquilar, Chem. Commun. 46 (2010) 7670-7687; (d) M.A. Sierra, I. Fernández, F.P. Cossío, Chem. Commun. (2008) 4671-4682.

[5] C. Baldoli, P. Cerea, L. Falciola, C. Giannini, F. Licandro, S. Maiorana, P. Mussini, D.J. Perdiccia, Organomet. Chem. 690 (2005) 5777 - 5787.

[6] (a) M.E. Bos, W.D. Wulff, R.A. Miller, S. Chamberlin, T.A. Brandvold, J. Am. Chem. Soc. 113 (1991) 9293 -9319; (b) B.A. Anderson, J. Bao, T.A. Brandvold, C.A. Challener, W.D. Wulff, Y.C. Xu, A.L. Rheingold, J. Am. Chem. Soc. 115 (1993) 10671 - 10687.

[7] (a) L.S. Hegedus, Tetrahedron 53 (1997) 4105-4128; (b) A. Arrieta, F.P. Cossío, I. Fernández, M. Gómez-Gallego, B. Lecea, M.J. Mancheño, M.A. Sierra, J. Am. Chem. Soc. 122 (2000) 11509-11510; (c) I. Fernández, M.A. Sierra, M.J. Mancheño, M. Gómez-Gallego, F.P. Cossío, J. Am. Chem. Soc. 130 (2008) 13892-13899; (d) I. Fernández, M.A. Sierra, M. Gómez-Gallego, M.J. Mancheño, F.P. Cossío, Chem. Eur. J. 11 (2005) 5988-5996; (e) I. Fernández, F.P. Cossío, M.A. Sierra, Acc. Chem. Res. 44 (2011) 479-490 (f) I. Fernández, M.A. Sierra, Top. Heterocycl. Chem. 30 (2013) 65-84.

[8] (a) W.C. Du Plessis, W.L. Davis, S.J. Cronje, J.C. Swarts, Inorg. Chim. Acta 314 (2001) 97-104; (b) S. Otto, A. Roodt, J.J.C. Erasmus, J.C. Swarts, Polyhedron 17 (1998) 2447-2453.

[9] A. Hildebrandt, T. Rüffer, E. Erasmus, J.C. Swarts, H. Lang, Organometallics 29 (2010) 4900-4905.

[10] (a) N.G. Connelly, W.E. Geiger, Chem. Rev. 96 (1996) 877-910; (b) J.M. Speck, R. Claus, A. Hildebrandt, T. Rüffer, E. Erasmus, L. van As, J.C. Swarts, H. Lang, Organometallics 31 (2012) 6373-6380; (c) U. Pfaff, A. Hildebrandt, D. Schaarschmidt, T. Hahn, S. Liebing, J. Kortus, H. Lang, Organometallics 31 (2012) 6761-6771.

[11] A.R. Pike, L.C. Ryder, B.R. Horrocks, W. Clegg, B.A. Connolly, A. Houlton, Chem. Eur. J. 11 (2005) 344-353.

[12] F. Spanig, C. Kolvacs, F. Hauke, K. Ohlubo, F. Fukuzumi, D. Guldi, A. Hirsch, J. Am. Chem. Soc. 131 (2009) 8180-8195.

[13] J. Conradie, J.C. Swarts, Organometallics 28 (2009) 1018-1026.

[14] T.G. Vosloo, W.C. du Plessis, J.C. Swarts, Inorg. Chim. Acta 331 (2002) 188-193.

[15] (a) D. Saravanakumar, N. Sengottuvelan, V. Narayanan, M. Kandaswamy, T.L. Varghese, J. Appl. Polym. Sci. 119 (2011) 2517-2524; (b) H. Jungbluth, G. Lohmann, Nachr. Chem. Tech. Lab. 47 (1999) 532 – 536; (c) P.J. Swarts, M. Immelman, G.J. Lamprecht, S.E. Greyling, J.C. Swarts, S. Afr. J. Chem. 50 (1997) 208-216.

[16] (a) Q. Shen, S. Shekhar, J.P. Stambuli, J.F. Hartwig, Angew. Chem. Int. Ed. 44 (2005) 1371-1375; (b) V. Percec, L.-Y. Bae, D.H. Hill, J. Org. Chem. 60 (1995) 1060-1065; (c) T.J. Colacot, Chem. Rev. 103 (2003) 3101-3118.

[17] (a) C.E.J. van Rensburg, E. Kreft, J.C. Swarts, S.R. Dalrymple, D.M. Macdonald, M.W. Cooke, M.A.S. Aquino, Anticancer Res. 22 (2002) 889-892; (b) J.C. Swarts, T.G. Vosloo, S.J. Cronje, W.C. Du Plessis, C.E.J. van Rensburg, E. Kreft, J.E. van Lier, Anticancer Res. 28 (2008) 2781-2784; (c) R.F. Shago, J.C. Swarts, E. Kreft, C.E.J. van Rensburg, Anticancer Res. 27 (2007) 3431-3434; (d) I. Ott, K. Kowalski, R. Gust, J. Maurer, P. Mücke, R.F. Winter, Bioorg. Med. Chem. Lett. 20 (2010) 866-869; (e) A. Gross, N. Hüsken, J. Schur, L. Raszeja, I. Ott, N. Metzler-Nolte, Bioconjug. Chem. 23 (2012) 1764-1774; (f) J.T. Chantson, M.V.V. Falzacappa, S. Crovella, N. Metzler-Nolte, J. Organomet. Chem. 690 (2005) 4564-4572; (g) M. Maschke, M. Lieb, N. Metzler-Nolte, Eur. J. Inorg. Chem. (2012) 5953-5959.

[18] (a) I. Fernández, M.J. Mancheño, M. Gómez-Gallego, M.A. Sierra, Org. Lett. 5 (2003) 1237-1240; (b) R. Martínez-Álvarez, M. Gómez-Gallego, I. Fernández, M.J. Mancheño, M.A. Sierra, Organometallics 23 (2004) 4647-4654; (c) D.I. Bezuidenhout, W. Barnard, B. van der Westhuizen, E. van der Watt, D.C. Liles, Dalton Trans. 40 (2011) 6711-6721; (d)

D.I. Bezuidenhout, S. Lotz, D.C. Liles, B. van der Westhuizen, Coord. Chem. Rev. 256 (2012) 479-524.

[19] B. van der Westhuizen, P.J. Swarts, I. Strydom, D.C. Liles, I. Fernández, J.C. Swarts, D.I. Bezuidenhout, Dalton Trans. 42 (2013) 5367 -5378.

[20] B. van der Westhuizen, P.J. Swarts, L.M. van Jaarsveld, D.C. Liles, U. Siegert, J.C. Swarts, I. Fernández, D.I. Bezuidenhout, Inorg. Chem. 52 (2013) 6674-6684.

[21] (a) J.G. López-Cortés, L.F. Contreras de la Cruz, M.C. Ortega-Alfaro, R.A. Toscano, C. Alvarez-Toledano, H. Rudler, J. Organomet. Chem. 690 (2005) 2229 – 2237; (b) J.A. Connor, E.M. Jones, J.P. Lloyd, J. Organomet. Chem. 24 (1970) C20-C23.

[22] D.I. Bezuidenhout, E. van der Watt, D.C. Liles, M. Landman, S. Lotz, Organometallics 27 (2008) 2447 -2456 .

[23] H. Sünkel, S.J. Bernhartzeder, J. Organomet. Chem. 696 (2011) 1536 - 1540.

[24] H. Meerwein, Org. Synth. 46 (1966) 113-116.

[25] J.A. Connor, E.M. Jones, J.P. Lloyd, J. Organomet. Chem. 24 (1970) C20-C22 .

[26] M.S. Inkpen, S. Du, M. Driver, T. Albrecht, N.J. Long, Dalton Trans. 42 (2013) 2813 - 2816.

[27] (a) D.I. Bezuidenhout, D.C. Liles, P.H. van Rooyen, S. Lotz, J. Organomet. Chem. 692 (2007) 774 – 783; (b) U. Klabunde, E.O. Fischer, J. Am. Chem. Soc. 89 (1967) 7141 - 7142.

[28] (a) M.L. Lage, I. Fernández, M.J. Mancheño, M.A. Sierra, Inorg. Chem. 47 (2008) 5253 - 5258; (b) R.D. Topsom, Acc. Chem. Res. 16 (1983) 292-298.

[29] (a) P.S. Braterman, Metal Carbonyl Spectra; Academic Press Inc., London, 1975, p 68; (b) D.M. Adams, Metal-Ligand and Related Vibrations; Edward Arnold Publishers Ltd., London, 1967, p 98.

[30] (a) S. Lotz, N.A. van Jaarsveld, D.C. Liles, C. Crause, H. Görls, Y.M. Terblans, Organometallics 31 (2012) 5371-5383; (b) C. Crause, H. Görls, S. Lotz, Dalton Trans. (2005) 1649 -1657; (c) S. Lotz, Y.M. Terblans, J. Chem. Soc., Dalton Trans. (1997) 2177 - 2182.

[31] Reduction in aprotic solvents of alkenes in general and the carbene double bond, Cr=C, in particular, are known to occur at far negative applied potentials [19, 20]. During a one-electron transfer process a radical anion of considerable instability is generated; follow-up

chemical reactions destroy this electrochemically generated species quickly. References to general alkene reduction include (a) A.J. Fry, Synthetic Organic Electrochemistry, 2nd ed., John Wiley and Sons, New York, 1989, p 208, 232; (b) J. Volke, F. Liska, Electrochemistry in Organic Synthesis, Springer-Verlag, Berlin, 1994, p 90.

[32] This situation is usual in Fischer type carbene complexes. See, for instance (a) M. Cases, G. Frenking, M. Duran, M. Solà, Organometallics 21 (2002) 4182-4191; (b) G. Frenking, M. Solà, S.F. Vyboishchikov, J. Organomet. Chem. 690 (2005) 6178-6204; (c) I. Fernández, M.A. Sierra, F.P. Cossío, J. Org. Chem. 71 (2006) 6178-6184; (d) I. Fernández, M.A. Sierra, F.P. Cossío, J. Org. Chem. 73 (2008) 2083-2089; (e) D.M. Andrada, A.M. Granados, M. Solá, I. Fernández, Organometallics 30 (2011) 466-476.

[33] (a) C. Creutz, H. Taube, J. Am. Chem. Soc. 91 (1969) 3988 – 3989; (b) W.E. Geiger, N. van Order, D.T. Pierce, T.E. Bitterwolf, A.L. Reingold, N.D. Chasteen, Organometallics 10 (1991) 2403 – 2411; (c) N. van Order, W.E. Geiger, T.E. Bitterwolf, A.L. Reingold, J. Am. Chem. Soc. 109 (1987) 5680 – 5690; (d) D.T. Pierce, W.E. Geiger, Inorg. Chem. 33 (1994) 373 – 381; (e) K.C. Kemp, E. Fourie, J. Conradie, J.C. Swarts, Organometallics 27 (2008) 353 - 362.

[34] J. March, Advanced Organic Chemistry, 4th ed., John Wiley and Sons, New York, 1992, pp. 17-20, 263-269, 273-275.

[35] D.E. Richardson, H. Taube, Inorg. Chem. 20 (1981) 1278 -1285.

[36] (a) H.J. Gericke, N.I. Barnard, E. Erasmus, J.C. Swarts, M.J. Cook, M.A.S. Aquino, Inorg. Chim. Acta 363 (2010) 2222 – 2232; (b) D.H. Evans, K.M. O'Connell, R.A. Peterson, M.J. Kelly, J. Chem. Educ. 60 (1983) 290-293; (c) P.T. Kissinger, W.R. Heineman, J. Chem. Educ. 60 (1983) 702-706; (d) M. J. Cook, I. Chambrier, G. F. White, E. Fourie, J. C. Swarts, Dalton Trans. (2009) 1136-1144; (e) J.J. van Benshoten, L.Y. Lewis, W.J. Heineman, J. Chem. Educ. 60 (1983) 772-776; (f) G.A. Mobbott, J. Chem. Educ. 60 (1983) 697-702.

[37] W.C. du Plessis, J.J.C. Erasmus, G.J. Lamprecht, J. Conradie, T.S. Cameron, M.A.S. Aquino, J.C. Swarts, Can. J. Chem. 77 (1999) 378 - 386.

[38] (a) G. Gritzner, J. Kuta, J. Pure Appl. Chem. 56 (1984) 461 – 466; (b) R.R. Gagne, C.A. Koval, G.C. Lisensky, Inorg. Chem. 19 (1980) 2854 - 2855.

[39] Leading references describing the electrochemical activity and behavior of ferrocene and decamethylferrocene in a multitude of organic solvents are: (a) I. Noviandri, K.N. Brown, D.S. Fleming, P.T. Gulyas, P.A. Lay, A.F. Masters, L. Phillips, J. Phys. Chem. B 103 (1999) 6713 – 6722; (b) N.G. Connelly, W.E. Geiger, Chem. Rev. 96 (1996) 877-910; (c) J. Ruiz, D. Astruc, C.R. Acad. Sci. (Paris), Ser. IIc 1 (1998) 21; (d) R.J. Aranzaes, M.C. Daniel, D. Astruc, Can. J. Chem. 84 (2006) 288 – 299; (e) E. Fourie, J.C. Swarts, I. Chambrier, M.J. Cook, Dalton Trans. (2009) 1145 - 1154.

[40] Gaussian 09, Revision B.1, M.J. Frisch, G.W. Trucks, H.B. Schlegel, G.E. Scuseria, M.A. Robb, J.R. Cheeseman, G. Scalmani, V. Barone, B. Mennucci, G.A. Petersson, H. Nakatsuji, M. Caricato, X. Li, H.P. Hratchian, A.F. Izmaylov, J. Bloino, G. Zheng, J.L. Sonnenberg, M. Hada, M. Ehara, K. Toyota, R. Fukuda, J. Hasegawa, M. Ishida, T. Nakajima, Y. Honda, O. Kitao, H. Nakai, T. Vreven, J.A. Montgomery, Jr., J.E. Peralta, F. Ogliaro, M. Bearpark, J.J. Heyd, E. Brothers, K.N. Kudin, V.N. Staroverov, R. Kobayashi, J. Normand, K. Raghavachari, A. Rendell, J.C. Burant, S.S. Iyengar, J. Tomasi, M. Cossi, N. Rega, N.J. Millam, M. Klene, J.E. Knox, J.B. Cross, V. Bakken, C. Adamo, J. Jaramillo, R. Gomperts, R.E. Stratmann, O. Yazyev, A.J. Austin, R. Cammi, C. Pomelli, J.W. Ochterski, R.L. Martin, K. Morokuma, V.G. Zakrzewski, G.A. Voth, P. Salvador, J.J. Dannenberg, S. Dapprich, A.D. Daniels, Ö. Farkas, J.B. Foresman, J.V. Ortiz, J. Cioslowski, D.J. Fox, Gaussian, Inc., Wallingford CT, 2009.

[41] (a) A.D. Becke, J. Chem. Phys. 98 (1993) 5648-5661; (b) C. Lee, W. Yang, R.G. Parr, Phys. Rev. B 37 (1988) 785-789.

[42] F. Weigend, R. Ahlrichs, Phys. Chem. Chem. Phys. 7 (2005) 3297-3305.

[43] (a) A.D. Becke, Phys. Rev. A 38 (1988) 3098-3100; (b) J.P. Perdew, Phys. Rev. B 33 (1986) 8822-8824.

[44] N.C. Handy, A. Cohen, J. Mol. Phys. 99 (2001) 403-412.

CHAPTER 5

An Electrochemical and computational study of tungsten(0) ferrocene complexes: observation of the mono-oxidized tungsten(0) ferrocenium species and intramolecular electronic interactions

This chapter was published in Organometallics. The format reflects the style set by the journal.

Daniela I. Bezuidenhout,[a] Israel Fernández,[b] Belinda van der Westhuizen,[a] Pieter J. Swarts,[c] Jannie C. Swarts,[c] *Organometallics,* **2013**, *32(24)*, 7334-7344.

Author contributors

Synthetic work: B. van der Westhuizen

Cyclic voltammetry and data analysis: P. J. Swarts, J. C. Swarts

Computational work: I. Fernández

Article written, submitted and response to reviewers: B. van der Westhuizen, D. I. Bezuidenhout, J. C. Swarts, I. Fernández.

[a] *Chemistry Department, University of Pretoria, Private Bag X20, Hatfield, 0028, South Africa. Fax: +27-(0)12-420-4687; Tel: +27-(0)12- 420-2626; E-mail: daniela.bezuidenhout@up.ac.za*
[b] *Departamento de Química Orgánica I, Facultad de Química, Universidad Complutense,28040-Madrid,Spain.*
[c] *Chemistry Department, University of the Free State, PO Box 339, Bloemfontein 9300, South Africa. Fax:+27-(0)51-444-6384; Tel: +27-(0)51-401-2781; E-mail: swartsjc@ufs.ac.za*

Supplementary information: The LSV and CV of complexes **1 - 4**, (**Appendix 4a**) and Cartesian coordinates and energies of all the stationary species discussed in the text are included. This material is available free of charge via the Internet at http://pubs.acs.org. (**Appendix 4b, CD**)

ABSTRACT

The series [$(CO)_5W$=C(XR)Fc], **1** (XR = OEt) and **3** (XR = NHBu) as well as [$(CO)_5W$=C(XR)-Fc'-(XR)C=$W(CO)_5$], **2** (XR = OEt) and **4** (XR = NHBu) of mono- and biscarbene tungsten(0) complexes with Fc = $Fe^{II}(C_5H_5)(C_5H_4)$ for monosubstituted derivatives and Fc′ = $Fe^{II}(C_5H_4)_2$ for disubstituted derivatives were synthesized and characterized spectroscopically. The oxidized ferrocenium complex [$\mathbf{1}^+$]•PF_6 was also synthesized and characterized. Electrochemical and computational studies were mutually consistent in confirming the sequence of redox events for the carbene derivatives **1** – **4** as first a carbene double bond reduction to a radical anion, $^-$W-C•, at peak cathodic potentials smaller than -2 V, then a ferrocenyl group oxidation in the range $0.206 < E^{o'} < 0.540$ V and finally an electrochemically irreversible three-electron W(0) oxidation at $E_{pa} > 0.540$ V vs. FcH/FcH^+ in CH_2Cl_2 / [(^{n}Bu$_4$)N][PF_6]. This contrasts the sequence of oxidation events in ferrocenylcarbene complexes of chromium where Cr(0) is first oxidised in a one electron transfer process, then the ferrocenyl group, and finally formation of a Cr(II) species. The unpaired electron of the reductively formed radical anion is mainly located on the carbene carbon atom. Electronic interactions between two carbene double bonds (for biscarbenes **2** and **4**) as well as between two W centers (for **4**) were evident. Differences in redox potentials between the "a" and "b" components of the three-electron W oxidation of **4** in CH_2Cl_2 or CH_3CN / [(^{n}Bu$_4$)N][PF_6] are $\Delta E^{o'} = E_{pa\ W(0)\ oxd\ 1b} - E_{pa\ W(0)\ oxd\ 1a}$ = ca. 51 and 337 mV respectively. Tungsten oxidation was restricted to a $W^{0/II}$ couple in CH_2Cl_2 / [(^{n}Bu$_4$)N][$B(C_6F_5)_4$]. From the computational results, the short-lived W(II) species were observed to be stabilized by agostic CH···W interactions.

5.1 INTRODUCTION

Based on its reversible electrochemical signature, ferrocene derivatives are researched as molecular sensors,[1] in energy transfer processes,[2] as catalysts[3] and even in anticancer research.[4] Fischer carbene complexes are versatile organometallics with valuable applications in organic and organometallic synthesis as well as in the fields of bioorganometallics and materials chemistry.[5] Recently, computational studies especially enhanced the understanding of this group of organometallic compounds substantially.[6]

The first examples of ferrocenyl carbene complexes of the group 6 transition metals, $[(CO)_5Cr=C(OR)Fc]$ (R = Me, Et), were synthesized to study the electronic effects of the ferrocenyl substituent on the carbene ligand as part of an investigation into the electron withdrawing nature of metal carbonyl carbene groups.[7] Early hints of the increased stability and chemodirecting steric effect of ferrocenyl carbene complexes were reported by Dötz *et al.*[8] Reaction of these ferrocenyl carbene complexes with tolane gave unexpected furanoid products over the customary Dötz benzannulation that yields chromium-coordinated hydroquinones.[9]

Our recent investigation into the electrochemical behavior of Fischer carbene complexes of the type $[(CO)_5Cr=C(XR)Ar]$ (XR = OEt, NHBu or NHPr; Ar = 2-thienyl (Th), 2-furyl (Fu) or ferrocenyl (Fc)), revealed the formation of dicationic Cr(II) species formed upon two consecutive one-electron oxidation processes.[10] These dicationic carbene complexes are characterized by an unusual bonding situation as they are stabilized by CH···Cr agostic interactions.[11] Strikingly, for the biscarbene complexes $[(CO)_5Cr=C(OEt)\text{-}Fc'\text{-}(OEt)C=Cr(CO)_5]$ (Fc' = ferrocen-1,1'-diyl), two resolved $Cr^{0/I}$ couples were observed. It was observed that intramolecular electronic interactions between the two Cr(0) centers is much more effective in biscarbene complexes linked together by a ferrocen-1,1′-diyl functionality,[12] since the biscarbene complexes with 2,5-thiendiyl or 2,5-furadiyl spacers did not display the split of the $Cr^{0/I}$ couple into two components. Rather, the redox processes in these heteroaryl biscarbene complexes are two-electron transfer processes that comprise two simultaneously occurring but independent one-electron transfer steps, one for each Cr(0) center.

In contrast to our findings that the $Cr^{I/0}$ and $Cr^{II/I}$ redox couples in Fischer carbene complexes are at potentials that may differ as much as 0.75 V,[10,11] tungsten(0) carbene complexes were reported to be oxidized to tungsten(II) carbene complexes either by a single two-electron transfer process or by two unresolved (overlapping) one electron transfer processes.[13] Previous electrochemical studies[14] on the redox behavior for chromium(0) and tungsten(0) carbene complexes did not identify a $Cr^{II/I}$ couple, nor did they comment on the now firmly established reduction of the chromium carbene double bond, Cr=C to the radical anion $^{-}$Cr-C•.[10,11] It is clear that the electrochemical behavior of chromium(0) and tungsten(0) Fischer carbene complexes and the driving forces behind it may not be so similar as was accepted till now. To probe the differences between chromium and tungsten carbenes, including the possibility of metal-metal

communication between the tungsten pentacarbonyl termini, we synthesized the ethoxycarbene complexes $[(CO)_5W{=}C(OEt)Fc]$ (**1**),[15] $[(CO)_5W{=}C(OEt)Fc'(OEt)C{=}W(CO)_5]$ (**2**), and the new aminocarbene analogues, $[(CO)_5W{=}C(NHBu)Fc]$ (**3**), and $[(CO)_5W{=}C(NHPr)Fc'(NHPr)C{=}(CO)_5]$ (**4**) (Scheme 5.1). In addition, the isolation of the monocationic salt, $[\mathbf{1}^+]\cdot\mathbf{PF_6}$, was achieved. An electrochemical analysis, supported by density functional theory (DFT) calculations and spectroscopic analyses, are reported and results are compared to highlight the differences between Cr and W analogues.

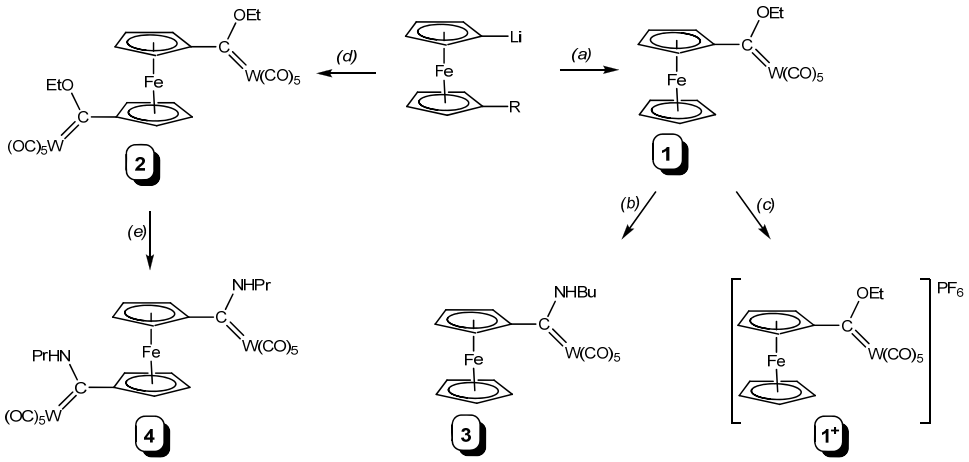

Scheme 5.1 Synthesis of ferrocenyl mono- and biscarbene tungsten complexes; Reagents and conditions: (a) (i) 1 eq FcLi (R = H), 1eq $[W(CO)_6]$, thf, -50°C; (ii) 1.3eq Et_3OBF_4, CH_2Cl_2, -30°C; (b) 1.1eq NH_2Bu, Et_2O, rt; (c) 1eq $AgPF_6$, CH_2Cl_2, -35°C; (d) (i) 1eq $Fc'Li_2$ (R = Li), 2eq $[W(CO)_6]$, thf, -50°C; (ii) 2.5eq Et_3OBF_4, CH_2Cl_2, -30°C; (e) 2.2eq NH_2Pr, Et_2O, rt.

5.2 RESULTS AND DISCUSSION

*Synthesis and spectroscopic characterization of complexes **1 - 4**.*

Ferrocenyllithium[16] was reacted with $[W(CO)_6]$ in the classic Fischer route to carbene complexes (Scheme 5.1), followed by alkylation with Et_3OBF_4[17] to yield the known complex **1** $[(CO)_5W{=}C(OEt)Fc]$.[15] Following the procedure described for the synthesis of the chromium analogues, reaction of two equivalents of tungsten carbonyl and 1,1'-dilithioferrocene[18] yielded the tungsten bisacylate. Quenching of the reaction was achieved with excess of oxonium salt, to

yield the novel bridging ferrocen-1,1'-diyl biscarbene complex, **2** [$(CO)_5W$=C(OEt)Fc′(OEt)C=$W(CO)_5$]. Both the monocarbene complex **1** and biscarbene complex **2** were aminolysed[19] with *n*-butylamine or *n*-propylamine, respectively, to yield the new complexes [$(CO)_5W$=C(NHBu)Fc] (**3**) and [$(CO)_5W$=C(NHPr)Fc′(NHPr)C=$W(CO)_5$] (**4**). These tungsten carbene complexes displayed NMR and FTIR spectroscopic properties similar to that observed for their chromium analogues.[10,11] Upfield shifts of the ferrocenyl-H_α in the case of the aminocarbene complexes **3** and **4** (4.24 and 4.56 ppm, respectively) compared to the ethoxycarbenes **1** and **2** (4.98 and 5.02 ppm, respectively), upfield ^{13}C NMR shifts of the carbene carbon resonances of the aminocarbenes compared to the ethoxycarbenes (eg. **3**, 249.1 ppm compared to **1**, 304.3 ppm) and decreased carbonyl stretching frequencies of the overlapping A'_1 and E-modes for the aminocarbenes compared to the ethoxy analogues (**3**, 1922 cm^{-1}; **4**, 1920 cm^{-1} vs. **1**, 1932 cm^{-1}; **2**, 1935 cm^{-1}) are all indicators of the increased donating ability of the amino-substituents towards stabilizing the electrophilic carbene carbon atom.[19] This is due to the contribution of imine formation to the $C_{carbene}$-N bond (Figure 5.1), which results in the formation of both *syn*- and *anti*-configurational isomers around the abovementioned $C_{carbene}$-N bond.[10,11] However, as for the Cr-derivatives, the steric bulk of the ferrocenyl carbene substituent precludes the formation of both isomers, and only the *syn*-isomer can be observed by NMR. [20]

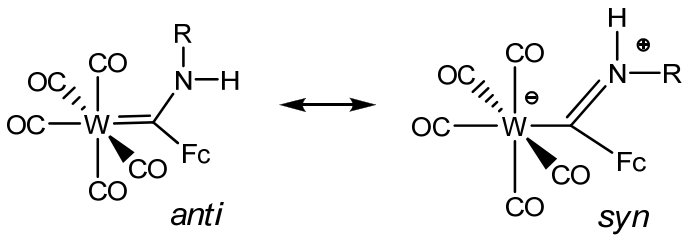

Figure 5.1 Stabilization of Fischer aminocarbene complexes via imine formation. For both **3** and **4**, only the *syn* rotamer is observed.

During the electrochemical investigation, we observed more positive oxidation potentials for the tungsten carbene complexes compared to the chromium analogues, in accordance with the higher hyperpolarizability of the tungsten complexes.[13] For our bimetallic complexes, however, this

meant that in contrast to the chromium ferrocenyl complexes,[10] the first oxidation process corresponds to the $Fe^{II/III}$ couple and not to the tungsten carbonyl moiety (see Electrochemistry Section). This encouraged us to perform the chemical oxidation of **1** with $AgPF_6$ (see Scheme 5.1) to gain insight into the properties of the ferrocenium cation $\mathbf{1}^+$. For the Cr-analogues, although this first $Cr^{0/I}$ oxidation proved reversible, the formed chromium +1 cation could not be isolated. After the addition of 1 equivalent of $AgPF_6$ to a solution of **1** in CH_2Cl_2 at -35 °C, an immediate color change from red to brown was observed. While the solution was allowed to warm to room temperature, IR and NMR data had to be collected for $\mathbf{[1^+]\bullet PF_6}$ within 10 minutes before decomposition of $\mathbf{1}^+$ occurred. Spectroscopically it could be seen (Figure 5.2) that much of $\mathbf{1}^+$ reverted back to **1**, probably by the capture of an electron from any electron-rich species in solution such as the free electron pairs on CO or OEt. To the best of our knowledge, no other isolated example of such a chemically oxidized ferrocenium Fischer carbene complex has been reported.

The IR spectra (Figure 5.2) clearly illustrate the shift of the carbonyl stretching frequencies from 1932, 1976 and 2063 cm^{-1} for **1** to 1953, 1998 and 2074 cm^{-1} for $\mathbf{1}^+$. The magnitude of the wavenumber shifts (21, 22 and 11 cm^{-1} for the E overlapping with A'_1, B and A''_1 bands respectively), is smaller than the shift of more than 100 cm^{-1} that is expected for oxidation of metal-carbonyl-based W(0) to W(I). Instead, it corresponds to an inductive effect accompanying the oxidation of the ferrocenyl Fe(II) substituent to a ferrocenium Fe(III) species. During this oxidation, the highly electron donating ferrocenyl group having a group electronegativity of $\chi_{Fc} = 1.87$ converted to an electron-withdrawing ferrocenium species ($\chi_{Fc+} = 2.82$) almost as strong as the CF_3 group ($\chi_{CF3} = 3.01$).[21] This observation is corroborated by the electrochemical data presented below. In addition, previous calculations reported the stabilization of the partially empty carbene carbon p_z atomic orbital by donation from a doubly-occupied d-orbital of iron.[22] Thus, with the removal of an electron from this atomic orbital, the donation is lowered, reducing the electron density of the W=C bond. Consequently, the π-backdonation to the π* orbital of the CO is also reduced with resulting higher C=O bond strength and higher CO stretching frequencies. The ^1H NMR spectrum recorded did not show any ferrocenyl resonances, even when recorded in a spectral window of up to 50 ppm, although the ferrocenium chemical shift is reported at δ31 ppm.[23] Presumably this can be ascribed to the paramagnetic nature of cation $\mathbf{1}^+$. The presence of the PF_6 counter anion is confirmed by the

upfield shifts of the resonances in the ^{31}P and ^{19}F NMR spectra in CD_2Cl_2, where for **[1$^+$]•PF$_6$** δ ^{31}P = -149.6 and δ ^{19}F = -85.4 ppm. The characteristic pentacarbonyl metal υ(CO)-pattern[24] indicates that no CO-ligand had been substituted by a coordinating PF_6-moiety.

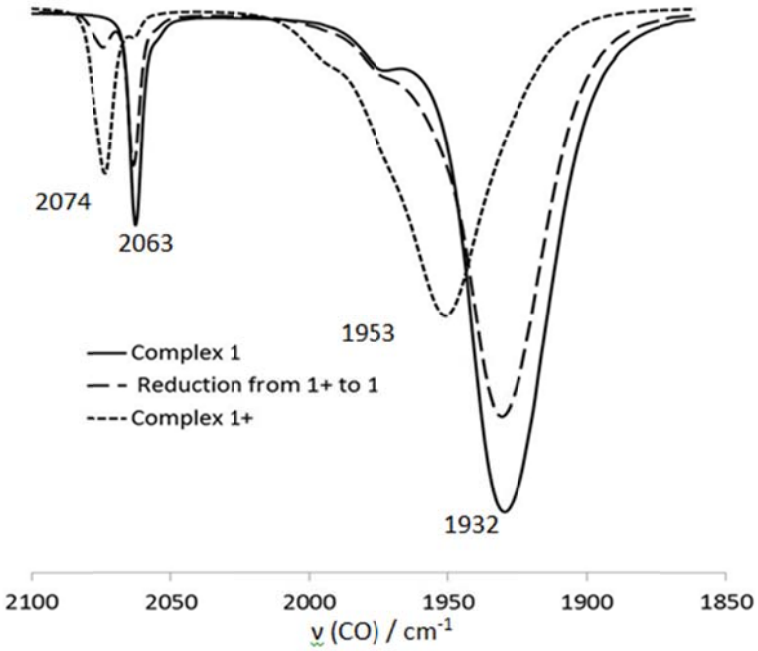

Figure 5.2 IR spectra demonstrating the carbonyl vibrations observed for complexes **1**, **[1$^+$]•PF$_6$** and the regeneration of **1**.

Electrochemistry and computational analyses

Cyclic voltammetry (CV), linear sweep voltammetry (LSV), and Osteryoung Square Wave voltammetry (SW) were first conducted on 0.5 mmol·dm^{-3} solutions of **1** – **4** in dry, oxygen-free CH_2Cl_2 utilizing 0.1 mol·dm^{-3} [N(^{n}Bu)$_4$][PF$_6$] as supporting electrolyte. Data are summarized in Table 5.1, CV's are shown in Figures 5.4 - 5.6.

At far negative potentials, the carbene double bond of the mono-ethoxycarbene derivative **1** was reduced electrochemically reversibly (ΔE = 63 mV), but chemically irreversibly (i_{pa}/i_{pc} = 0.56) in a one-electron transfer redox process to a radical anion at $E^{o'}$ = ½(E_{pa} + E_{pc}) = -2.076 V vs. FcH/FcH$^+$ (Table 5.1, Figure 5.4). Electrochemical and chemical reversibility is theoretically characterized by peak potential differences of ΔE = E_{pa} – E_{pc} = 59 mV and current ratios i_{pa}/i_{pc} approaching unity.[25] As is usual for Fischer carbene complexes,[6] the LUMO of complex **1** is

mainly located at the p_z atomic orbital of the carbene carbon atom (Figure 5.3). Therefore, it should be expected that the one-electron reduction process should lead to the radical anion **1**$^{\cdot-}$ whose unpaired electron remains mainly located on that carbon atom. Indeed, the computed spin density on **1**$^{\cdot-}$ indicates a value of 0.57 e on the carbene carbon atom thus suggesting a $^{-}$W-C$^{\cdot}$ species as reduction product. The remaining electron density is mainly localized at the iron center (0.27e) which further confirms the orbital interaction between the ferrocenyl group and the carbene carbon atom.[22] Similar electron density was computed for the analogous $(CO)_5Cr{=}C(OEt)Fc$ carbene complex at the same level of theory (0.57e at the carbene carbon atom), thus indicating that the one-electron reduction process is similar in both types of complexes.

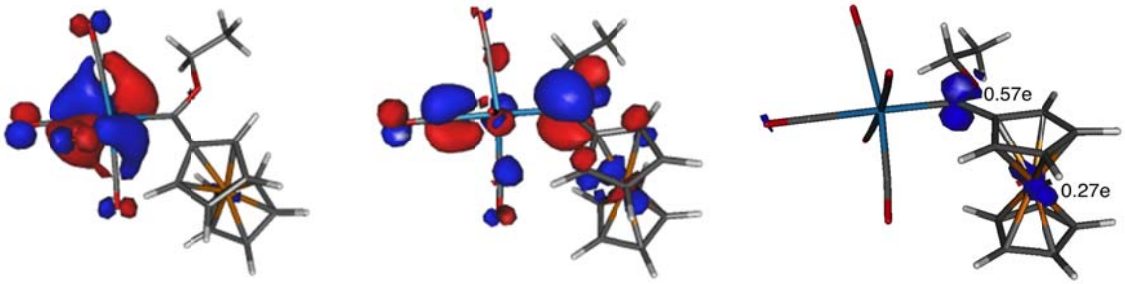

HOMO (1) **LUMO (1)** **1**$^{\cdot-}$

Figure 5.3 Frontier Molecular Orbitals of **1** and computed spin density on **1**$^{\cdot-}$.

The bisethoxy complex **2** exhibited two W=C reductions at waves I_a and I_b in the CV's shown in Figure 5.4 to $^{-}$W-C$^{\cdot}$ with formal reductions potentials being separated by $\Delta E^{o'} = E^{o'}_{\text{wave Ib}} - E^{o'}_{\text{wave Ia}} = 433$ mV. This relatively large separation in reduction potentials illustrates noticeable interactions between the two carbene moieties and leads to the general reductive scheme shown in equation 1. The first carbene reduction associated with wave I_a is electrochemically reversible but the second is not (Figure 5.4 and Table 5.1).

$$\mathbf{2}^{2\bullet,2-} \underset{+e^-}{\overset{\text{wave } I_b}{\longleftarrow}} \mathbf{2}^{\bullet,-} \underset{+e^-}{\overset{\text{wave } I_a \; -e^-}{\rightleftharpoons}} \mathbf{2} \qquad (1)$$

The radical anion notation in equation 1 is explained by noting that $\mathbf{2}^{\bullet -}$ = [(CO)$_5$(¯W-C$^{\bullet}$)(OEt)-Fc′-(OEt)C=W(CO)$_5$]. Different reduction potentials for symmetrical complexes in which mixed-valent intermediates are generated (for **2,** this refers to $\mathbf{2}^{\bullet -}$) are well known in systems that allow some form of electronic interaction between the redox centers; these may include electrostatic or through-bond conjugated paths.[26]

In contrast to the OEt derivatives **1** and **2**, the new NHBu monocarbene **3** showed no carbene reduction within the potential window of the solvent in the presence of [N(^{n}Bu)$_4$][PF$_6$]. This agrees with the computed energy of the corresponding LUMO (-2.64 and -2.25 eV for **1** and **3**, respectively) which suggests that the less negative energy of the LUMO of **3** is translated into a more negative reduction potential. The biscarbene-NHPr derivative **4**, showed a single carbene reduction at -2.293 V in the CV at wave I (Figure 5.4), but the current was more than four times (3.71/0.90) larger than that expected for a one-electron transfer processes. A one-electron transfer process in this system requires ½[i(wave Fc+1a)/4+i(wave 1b)/3] = 0.90 µA. The large observed current (3.71 µA) is thought to be due to significant amounts of substrate being deposited on the surface of the electrode during reduction but because this wave is close to the potential at which cathodic discharge caused by solvent reduction takes place, the large increase in current may also originate from an E_rC_{cat} process by which **4** catalyses the reduction of CH_2Cl_2. A repeat experiment utilizing **4** as analyte in CH_3CN as solvent (Figure S3, Appendix 4a, Table 5.1) confirmed the second carbene moiety is reduced at a potential ca. 0.27 V lower than the first. This observation also suggests some form of electronic interaction between two carbene moieties observed for **2** but completely contrasts the observations described for the chromium complex [(CO)$_5$Cr=C(OEt)-Fc′-(OEt)C=Cr(CO)$_5$].[10,11] For this analogous Cr carbene complex, under the same experimental conditions, no splitting of Cr=C carbene reduction into two components “a” and “b” could be detected. Very few studies describe the electrochemical reduction of the W=C double bond,[14] although the *in situ* generation of the radical anion by chemical single electron transfer agents have been reported.[27] Consistent with NHR (R = Bu, Pr) being a more powerful electron-donating group than OEt, the NHPr group shifted the wave I_a peak cathodic potential, E_{pc}, of the bis W=C species **4** compared to **2** with $\Delta E_{pc} = E_{pc,\ OEt,\ \mathbf{2}} - E_{pc,\ NHBu,\ \mathbf{4}} = -1.773 - (-2.293) = 0.520$ to more negative potentials.

The next redox process observed for **1 – 4** is the chemically and electrochemically one-electron reversible oxidation of ferrocene which is associated with wave Fc in Figure's 5.4 – 5.6, and Table 5.1. The Fc wave in these CV's is followed by the W oxidation processes (wave 1) which in CH_2Cl_2 / $[(^nBu_4)N][PF_6]$ involves a three-electron transfer process (Figure 5.4). This oxidation of the ferrocenyl group in tungsten carbenes at lower potentials than that of W oxidation contrasts with the behavior of the analogues chromium carbenes $[(OC)_5Cr=C(Fc)(OEt)]$ and $[(OC)_5Cr=C(OEt)\text{-}Fc'\text{-}(OEt)C=Cr(CO)_5]$ where the ferrocenyl group was oxidized *after* oxidation of the Cr(0) center to Cr(I).[10,11] The second oxidation of Cr(I) to Cr(II) follows after the ferrocenyl oxidation, and also contrasts with the three-electron closely-overlapping W oxidation under the same experimental conditions. The resolution between Fc and tungsten (wave 1) oxidation processes, expressed as $\Delta E_{pa} = E_{pa,\ W} - E_{pa,\ Fc}$, is better in mono- than in biscarbene tungsten complexes, and also in OEt than in NHR complexes. For **4**, the Fc wave was superimposed onto a W-oxidation wave (Figure 5.4).

An important consequence of the ferrocenyl moiety being oxidized before the W center is that when the W center is oxidized, it is under the influence of the ferrocenium species, Fc^+, which is almost as electron-withdrawing as a CF_3 group ($\chi_{Fc} = 2.82$; $\chi_{CF3} = 3.01$).[21] This shifts the W redox process to more positive potentials than would be expected for other compounds where the linking group is not so strongly electron-withdrawing, e.g. for $-CH_2-$. The one-electron ferrocenyl oxidation process was useful to identify the number of electrons that is transferred during tungsten oxidation.

Tungsten oxidation is associated with wave 1 in Figures 5.4 – 5.6 and Table 5.1. Since the peak anodic current ratio between wave Fc and wave 1 in the CV of **1** was 10.01/3.38 = 2.96 = 3, indications are that W(0) is oxidized irreversibly (no i_{pc} detected) in three consecutive and overlapping one-electron transfer steps, apparently to a W(III) species (Figure 5.4, Table 5.1).

Table 5.1. Cyclic voltammetry data of 0.5 mmol·dm^{-3} solutions of the monocarbene [(OC)$_5$W=C(Fc)(X)] complexes **1** and **3** and biscarbene [(OC)$_5$W=C(X)-Fc'-(X)C=W(CO)$_5$] complexes **2** and **4** in CH_2Cl_2 containing 0.1 mol·dm^{-3} [N(^{n}Bu)$_4$][PF$_6$] or 0.2 mol·dm^{-3} [N(^{n}Bu)$_4$][B(C$_6$F$_5$)$_4$] as supporting electrolyte at a scan rate of 100 mV s^{-1} and 20 °C. Potentials are relative to the FcH/FcH$^+$ couple.

Complex	Peak no.	i_{pa}/μA, i_{pc}/i_{pa} [N(^{n}Bu)$_4$][PF$_6$]	$E^{o'}$/V, ΔE/mV [N(^{n}Bu)$_4$][PF$_6$]	$E^{o'}$/V, ΔE/mV [N(^{n}Bu)$_4$][B(C$_6$F$_5$)$_4$]	i_{pa}/μA, i_{pc}/i_{pa} [N(^{n}Bu)$_4$][B(C$_6$F$_5$)$_4$]
1, Fc	I(=)	3.23,[b] 0.56	-2.076, 63	-2.119, 100	7.02,[b] 0.71
X = OEt	(Fc)	3.38, 0.85	0.285, 90	0.307, 82	5.61 0.93
	1(W$^{0/III}$)	10.01, -	0.809,[d] -	(W$^{0/II}$)1.105,[d,i] -	11.58, -
2, Fc'	D[f]	0.76,[b] -	-2.409,[c] -		
X = OEt	Ib(=)	1.64,[b] -	-2.206,[c] -	-2.222,[c] -	2.80,[b] -
	Ia(=)	1.73,[b] 0.40	-1.773, 67	-1.811, 74	3.02,[b] 0.51
	(Fc)	1.62, 0.84	0.510, 86	0.513, 82	2.82, 0.64
	1(2xW$^{0/III}$)	9.56, 0.15	0.766, 142	(2xW$^{0/II}$) 0.922,[i] -	(2xW$^{0/II}$) 9.99, -
3, Fc	I(=)	-[a], -[a]	-[a], -[a]	-2.580,[c] -	9.71,[b] -
X =NHBu	(Fc)	2.67, 0.88	0.206, 92	0.289, 80	4.23, 0.67
	1(W$^{0/III}$)	7.94, 0.11	0.611, 293	(W$^{0/II}$) 0.950,[d,i] -	(W$^{0/II}$) 8.10,[d] -
4, Fc'	I(=)	3.71,[b] -	-2.293,[c] -	-2.285,[c] -	6.84[b], -
X = NHPr	(Fc)+1$_a$(W$^{0/1II}$)	3.53, -	0.540,[e,h] -	(Fc)+1$_a$(W$^{0/1II}$)	7.20, -
	1$_b$(W$^{0/III}$)	2.76, -	0.591,[d] -	0.580,[d,e,h] -	(2xW$^{0/II}$)
	D[f]	0.55, -	1.000,[d] -	(1$_b$ W$^{0/II}$) 0.792,[d,i] -	5.45, -
4,[g] Fc'	I$_b$(=)	1.30[b], -	-2.458,[c] -		
X = NHPr	I$_a$(=)	3.38[b], -	-2.185,[c] -		
CH_3CN[g]	(Fc)+1$_a$(W$^{0/1II}$)[i]	3.40, 0.31	0.408, 80		
	1$_b$(W$^{0/III}$)[i]	4.69, 0.21	0.745, 100		

(a) No peak detected within the solvent potential window; (b) i_{pc} and i_{pa}/i_{pc} values to maintain the current ratio convention of i(forward scan)/i(reverse scan); (c) E_{pc} value, no E_{pa} detected. (d) E_{pa} value, no E_{pc} detected; (e) Estimations only; (f) Peaks labeled "D" represent decomposition processes of either the $^-$W-C· radical anions that was generated at the redox processes labeled "I" or of W(III) generated at wave "1b"; (g) The supporting electrolyte changed to BARF = [NBu$_4$][B(C$_6$F$_5$)$_4$] (0.2 mol·dm^{-3}) or the solvent changed to CH_3CN; (h) a very weak Fc reduction peak was observed at E_{pc} = 0.357, i_{pa} = 0.3 μA. In the presence of [NBu$_4$][B(C$_6$F$_5$)$_4$] a much stronger Fc reduction wave was observed at E_{pa} = 0.497, i_{pa} = 3.75 μA. (i) In the presence of [NBu$_4$][B(C$_6$F$_5$)$_4$] (0.2 mol·dm^{-3}) W oxidation is a two-electron transfer process, while in the presence of CH_3CN, or [N(^{n}Bu)$_4$][PF$_6$] it is a three-electron transfer process.

This contrasts a study by Maiorana and co-workers who reported a few years ago that W in $[(OC)_5W{=}C(CH_3)(X)]$ with X = substituted morpholino and other amine derivatives undergo a two-electron oxidation in CH_2Cl_2 in the presence of 0.1 mol·dm^{-3} $[(^nBu_4)N][ClO_4]$ as supporting electrolyte.[13] Figure 5.5 highlights the CV's of **1** at different scan rates, and more importantly, the LSV at 1mV·s^{-1}. The LSV was mutually consistent with CV i_{pa} current ratios between wave Fc and wave 1 at scan rates of 100, 200, 300, 400 and 500 mV·s^{-1} in indicating that the total W oxidation involves the flow of three electrons. With our observation of a three-electron transfer W oxidation, it follows that in the biscarbene **2**, possessing two tungsten centers, a total of six electrons being transferred during tungsten oxidation should be observed. This was confirmed by the measured i_{pa} values (Figure 5.4, $i_{pa,wave\ 1}/i_{pa,wave\ Fc}$ = 9.56/1.62 = 5.90 ≈ 6, Table 5.1). Although the CV of **2** showed electronic interactions between the two carbene double bond centers by means of the splitting of wave I into two components "a" and "b", no resolution between the irreversible oxidations of the two W centers of **2** could be detected (Figure 5.4). However, a very weak reduction of oxidized W was detected at wave 1_r during the cathodic sweep, Figure 5.4, Table 5.1. The current was, however, small with i_{pc}/i_{pa} = 0.15; ΔE = 143 mV.

An LSV of **2** (Figure S1, Appendix 4a) showed that the oxidation of the second tungsten center results in a species that is unstable on LSV time scale. Only the first 3-electron oxidation could be detected before compound decomposition took place. The peak anodic current of wave 1 in the CV of the mono NHBu tungsten carbene **3** also estimates a three electron transfer step during W oxidations but the LSV shown in Figure 5.4 highlights new information. On LSV timescale, the first two electrons during W oxidation are transferred fast in two unresolved one-electron redox processes, but the different slope observed for the third electron that was transferred shows this redox step to be slower than the first two electron transfer steps. The LSV splitting of wave 1 (W-oxidation) into two components "a" (a two electron process) and "b" (a one-electron process) for **3** allows for a meaningful comparison with chromium carbene analogues $[(OC)_5Cr{=}C(XR)(Ar)]$ and $[(OC)_5Cr{=}C(XR)\text{-}Ar'\text{-}(XR)C{=}Cr(CO)_5]$ with XR = OEt , NHBu or NHPr and Ar or Ar' = thienyl, furyl or ferrocenyl.[10,11] In these Cr carbene derivatives, Cr(0) is oxidized in two separate one-electron transfer steps and exhibits $\Delta E_{pa} = E_{pa,Cr(I/II)} - E_{pa,Cr(0/I)}$ peak potential separations larger than 0.5 V.[10,11] For the present W-series, indications are that W(0) is first oxidized in a two electron step followed by a second one-electron oxidation. In all

compounds studied, these steps overlap on CV timescale, but on LSV timescale, for **3**, ΔE_{pa} = $E_{pa,W(II/III)}$ - $E_{pa,W(0/II)}$ peak separations are estimated from Figure 5.4 to be approximately 90 mV.

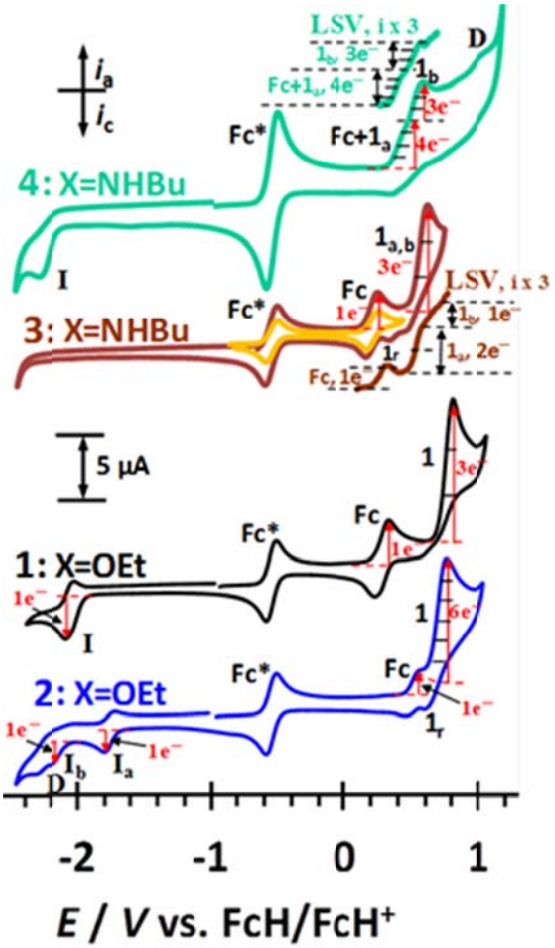

Figure 5.4 CV's of 0.5 mmol.dm^{-3} solutions of the monocarbene $[(OC)_5W=C(Fc)(XR)]$ complexes **1** (black) and **3** (brown) and biscarbene complexes $[(OC)_5W=C(XR)\text{-}Fc'\text{-}(XR)C=W(CO)_5]$ **2** (blue) and **4** (green) in CH_2Cl_2 containing 0.1 mol.dm^{-3} $[N(^nBu)_4][PF_6]$ as supporting electrolyte at a scan rate of 100 mV s^{-1} and 20 ^oC. LSV's are also shown for **3** and **4**. Fc* = decamethylferrocene = internal standard. Under these conditions, each W center is ultimately involved in a three-electron transfer redox process.

A small cathodic peak associated with wave 1 was also observed for **3** at wave 1_r but again irreversible W oxidation was implied by virtue of i_{pc}/i_{pa} = 0.11 and ΔE = 293 mV. The CV's of

the NHBu biscarbene **4** showed oxidation of the ferrocenyl group and one of the two W centers occurred simultaneously. For **4**, the oxidation of the second W center was resolved from the first by ca. $\Delta E_{pa} = E_{pa,\ wave\ (1b+Fc)} - E_{pa,\ wave\ 1a} = 51$ mV. The ratio $i_{pa,\ wave\ (1b+Fc)} : i_{pa,\ wave\ 1a}$ in the CV as well as the LSV (Figure 5.4) was found to be 4:3 which again showed W oxidation involves three electrons.

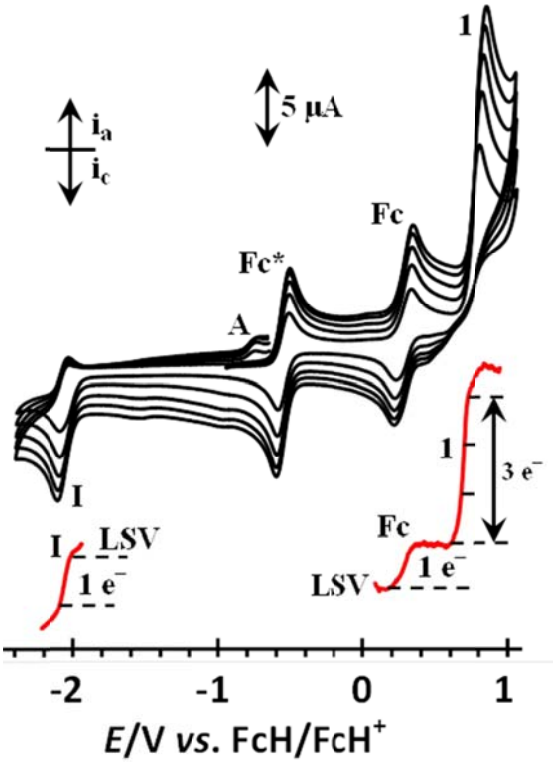

Figure 5.5 CV's of 0.5 mmol·dm^{-3} solutions of the [(OC)$_5$W=C(Fc)(OEt)], **1**, in CH_2Cl_2 containing 0.1 mol·dm^{-3} [N(^{n}Bu)$_4$][PF$_6$] as supporting electrolyte at a scan rate of 100 (smallest currents), 200, 300, 400 and 500 mV·s^{-1} and 20 °C. The LSV's show that the W center is involved in a three-electron transfer redox process, while both the ferrocenyl group and the carbene double bond involves one-electron flow. Fc* = decamethylferrocene. A = decomposition product peak.

To understand why our results indicating an irreversible three-electron W(0) oxidation differed from those of Maiorana, who observed a two-electron W oxidation,[13] complexes **1** – **4** were also studied under different conditions utilizing first 0.1 mol·dm^{-3} [(^{n}Bu$_4$)N][B(C$_6$F$_5$)$_4$] as supporting electrolyte, see Table 5.1 for electrochemical data. The Geiger electrolyte, [(^{n}Bu$_4$)N][B(C$_6$F$_5$)$_4$],

is known to minimize ion pair formations of the type $(cation)^{+\cdots\cdots-}[B(C_6F_5)_4]$ where $(cation)^+$ represents any electrochemically generated cation. Such ion pair formations frequently cause oxidation potentials of cationic species to move to different values.[28] In addition, use of this electrolyte allows the observation of unstable intermediate redox states of, for example, the ruthenocenium species $[Ru^{III}(C_5H_5)_2]^+$. [29] Use of other solvents or electrolytes invariably causes over oxidation of ruthenocene to a Ru(IV) species.[30]

Figure 5.6 shows a CV and LSV's of **2** utilizing 0.1 mol·dm^{-3} $[(^nBu_4)N][B(C_6F_5)_4]$ as supporting electrolyte. The first obvious difference is that in CH_2Cl_2, but in the presence of $[(^nBu_4)N][B(C_6F_5)_4]$ as supporting electrolyte, resolution between the ferrocenyl oxidation and the two overlapping W(0) oxidations are markedly increased. The differences in the oxidation potentials of these two processes are $\Delta E^{o\prime} = E_{pa,W(0)\ oxd,\ 1} - E_{pa,Fc\ oxd} = 284$ mV in CH_2Cl_2 containing $[(^nBu_4)N][PF_6]$ and 368 mV in CH_2Cl_2 containing $[(^nBu_4)N][B(C_6F_5)_4]$. More importantly, the LSV as well as i_{pa} current ratios for waves Fc and 1 in the presence of $[(^nBu_4)N][B(C_6F_5)_4]$, shows a two-electron tungsten oxidation, the same as reported by Maiorana.[13] All the other complexes in the present compound series **1** – **4** also showed the two-electron $W^{0/II}$ couple when the supporting electrolyte was $[(^nBu_4)N][B(C_6F_5)_4]$, see Table 5.1 and Figures S3 and S4 (Appendix 4a).

An additional experiment utilizing CH_3CN as solvent was also performed on **4** because the coordination power of acetonitrile (Gutmann donor number = 14.1, while for CH_2Cl_2 it is ranges from 0 to 1)[31,32] frequently leads to interactions with cationic species. This results in different oxidation potentials, or even differences in the number of electrons being transferred during redox processes. Such solvent effects are highlighted by the electrochemical oxidation of, for example, Rh^I(β-diketonato)(CO)(PPh_3)] in a one-electron transfer process to a Rh(II) species in CH_2Cl_2 / $[(^nBu_4)N][BF_4]$,[33] but in a two-electron transfer process to a Rh(III) species in CH_3CN / $[(^nBu_4)N][PF_6]$.[34] Potential referencing in different solvents and electrolytes has to be made with care. Results in this work are referenced to FcH/FcH^+ as required by IUPAC, but the internal standard was not free ferrocene to prevent peak overlaps with **1 – 4**. Hence decamethylferrocene, Fc^* was used as internal standard and potentials was thereafter adjusted to be versus FcH/FcH^+. Under our conditions the formal reduction potential of Fc* vs. FcH/FcH^+ is -550 mV in CH_2Cl_2 / $[(^nBu_4)N][PF_6]$, -610 mV in CH_2Cl_2 / $[(^nBu_4)N][B(C_6F_5)_4]$ and -510 mV in CH_3CN /

[(^{n}Bu$_4$)N][PF$_6$].[35] It was found that in CH$_3$CN, **4** tungsten(0) oxidation is also a three electron transfer process, See Table 5.1 and Figure S3, Appendix 4a.

Scheme 5.2 shows the observed redox processes of **2** in the presence of [(^{n}Bu$_4$)N][PF$_6$]. This electrochemical scheme would also fit **4** if wave 1 is split into an "a" and "b" component. The monocarbene complexes **1** and **3** would fit the scheme if waves I_a and/or I_b are removed as required, and if wave 1 for **2** is rewritten to accommodate only one three electron transfer process rather than two. In the presence of [(^{n}Bu$_4$)N][B(C$_6$F$_5$)$_4$], the scheme would fit if the three-electron $W^{0/III}$ coupled is replaced with a two-electron $W^{0/II}$ couple.

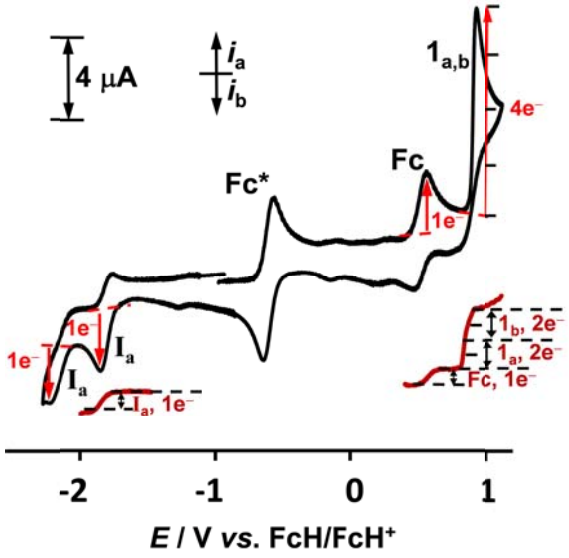

Figure 5.6 CV and LSV (brown curves) at 20 °C of 0.5 mmol·dm^{-3} solutions of **2** in CH$_2$Cl$_2$ / 0.2 mol·dm^{-3} [N(^{n}Bu)$_4$][B(C$_6$F$_5$)$_4$]. The number of electrons involved in each redox process is indicated next to the relevant waves. Each W is oxidized in a two-electron transfer process in this medium. Fc* = decamethylferrocene.

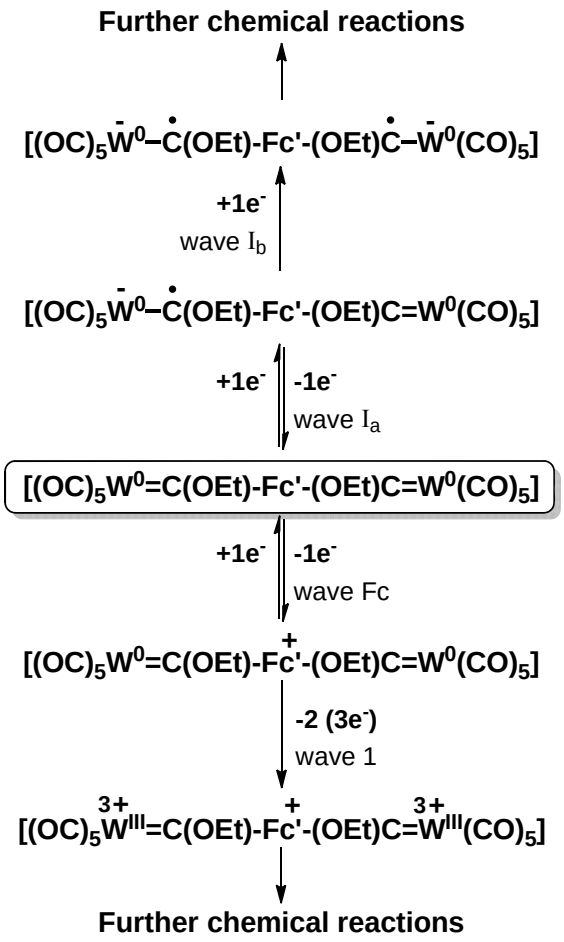

Scheme 5.2 Electrochemical reactions associated with **2**. Both the final reduction product possessing $^{-}$W-C$^{\bullet}$ radical anions and the final oxidation product possessing two W(III) centers are highly reactive and undergo further chemical decomposition reactions.

The above described redox processes were finally addressed by means of a computational-DFT study. As shown in Figure 5.7, complex **1** is electrochemically oxidized to radical cation **1**$^{\cdot +}$**.** The computed spin density of this species indicates that the unpaired electron is located at the iron atom (1.26e), thus confirming that the first one-electron oxidation does not involve the tungsten center but the Fe(II) to Fe(III) reaction.

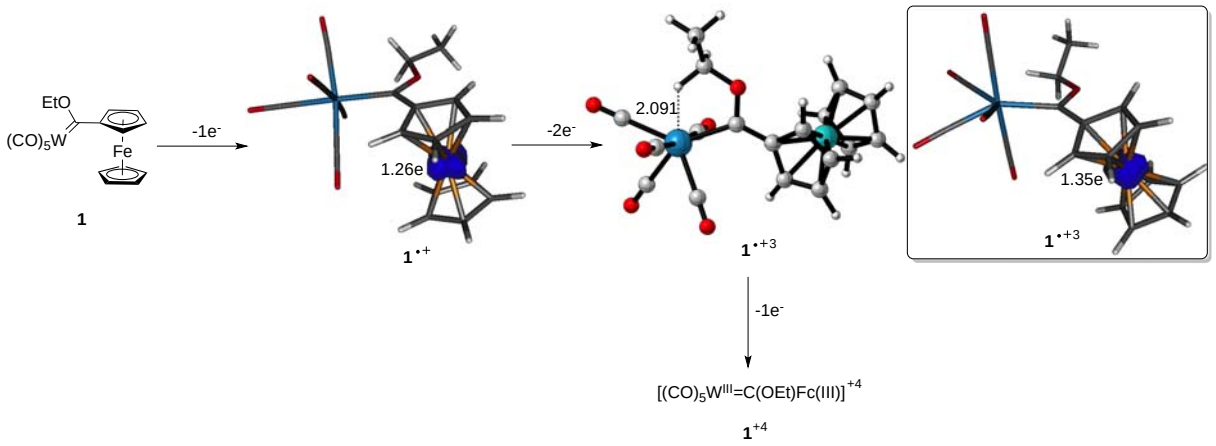

Figure 5.7 Computed oxidation process of complex **1** at the B3LYP/def2-SVP level. W···H bond distance in $\mathbf{1}^{\bullet+3}$ is given in angstroms.

Subsequent 2-electron oxidation leads to the trication $\mathbf{1}^{\bullet+3}$ whose unpaired electron remains at the iron atom (computed electron density on Fe of 1.35e). This indicates that the oxidation process involves the W(0) to W(II) reaction. As described above, the total three-electron tungsten oxidation process ends up with the third and final one-electron oxidation at the tungsten center (W(II) to W(III)) to form the corresponding tetracation $\mathbf{1}^{+4}$. Unfortunately, the structure of this open-shell singlet species (whose unpaired electrons are located at the iron and tungsten centers) could not be located on the potential energy surface (even using different functionals) due to convergence problems.

The structure of the trication $\mathbf{1}^{\bullet+3}$ deserves further analysis. As shown in Figure 5.7, a hydrogen atom of the ethoxy substituent is found in close proximity to the tungsten atom (W···H distance of 2.091 Å), pointing to possible C−H···W agostic interaction. Indeed, the Laplacian distribution of $\mathbf{1}^{\bullet+3}$ in the W···H−C plane (Figure 5.8) clearly reveals the occurrence of a bond critical point located between the transition metal and the hydrogen atom, which is associated with a bond path running between the corresponding two atoms. This proves the existence of a direct interaction between both atoms. Moreover, the computed value of 0.045 e·Å^{-3} for the electron density at the bond critical point, is in the range expected for CH agostic interactions.[36] The structure of this species resembles that found for oxidised products of related chromium(0) carbene complexes upon 2-electron oxidation of the transition metal.[11] This peculiar bonding

situation seems to be general for oxidized products of Fischer carbene complexes regardless of the transition metal involved and it implies the normal carbene structure is not retained after oxidation.

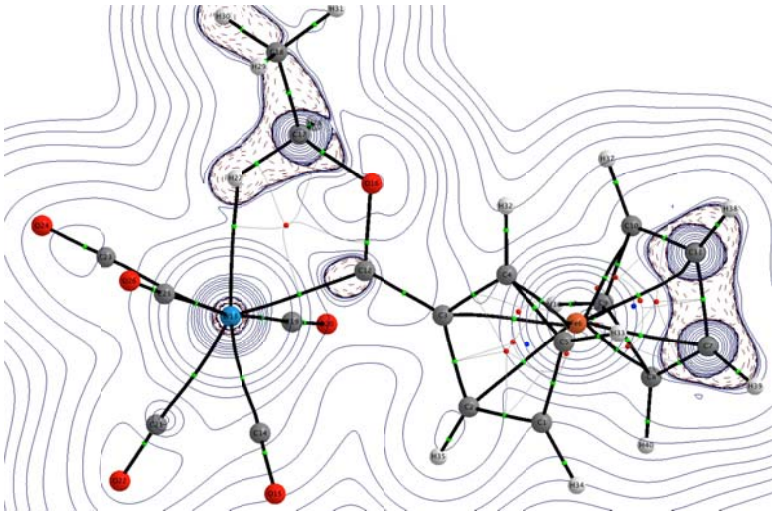

Figure 5.8 Contour line diagrams $\nabla^2\rho(r)$ for complex $\mathbf{1}^{\cdot+3}$ in the W−H−C plane. Solid lines indicate areas of charge concentration ($\nabla^2\rho(r) < 0$) while dashed lines show areas of charge depletion ($\nabla^2\rho(r) > 0$). The solid lines connecting the atomic nuclei are the bond paths while the small red spheres indicate the corresponding bond critical points. The solid lines separating the atomic basins indicate the zero-flux surfaces crossing the molecular plane.

5.3 CONCLUSION

Mono- and bis-ethoxycarbene and –butyl(or propyl)aminocarbene tungsten(0) complexes $[(CO)_5W{=}C(XR)Fc]$, **1** and **3**, and $[(CO)_5W{=}C(XR)\text{-}Fc'\text{-}(XR)C{=}W(CO)_5]$, **2** and **4** were prepared. For the aminocarbenes **3** and **4**, only the *syn*-rotamer possessing restricted rotation about the $C_{carbene}$-N bond was observed by ^{1}H NMR due to the steric bulk of the ferrocenyl carbene substituent. The chemically oxidized but short-lived ferrocenium complex $[\mathbf{1}^+]\bullet\mathbf{PF_6}$ was also synthesized. From an electrochemical study in CH_2Cl_2 / $[(^nBu_4)N][PF_6]$ it was found that the electron-rich carbene double bond functionality of all complexes were reduced from W=C to $^-$W-C• at potentials < –2.0 V vs FcH/FcH^+. This assignment was confirmed by DFT calculations, which indicate that the unpaired electron of the formed radical anion is mainly located on the carbene carbon atom. For the two biscarbene complexes **2** and **4**, reduction potentials of the two

W=C functionalities were resolved which is indicative of good interactions between the formally carbene double bonds. The ferrocenyl group was electrochemically reversibly oxidized before W oxidation at potentials $0.206 < E^{o'} < 0.540$ V vs FcH/FcH^+. These potentials were continuously more than 250 mV smaller than those measured for the analogues Cr compounds. Tungsten(0) was oxidized in three consecutive but unresolved one-electron transfer steps to a W(III) species in the presence of $[N(^nBu)_4][PF_6]$ as supporting electrolyte, or in CH_3CN as solvent. In CH_2Cl_2 containing $[(^nBu_4)N][B(C_6F_5)_4]$ as supporting electrolyte, tungsten(0) oxidation was found to be a two-electron transfer process. The structure of this tricationic W(II) species has been highlighted with DFT calculations. Complex **4** showed identifiable resolution between the oxidation of each W center. This also argued for a weak interaction between the two W centers. All redox assignments were mutually consistent with the computational data obtained at the DFT level, which suggest a peculiar bonding situation (i.e. stabilized by C−H···W agostic interaction) in the tricationic species formed upon the oxidation process which involves the W(0) to W(II) reaction.

5.4 EXPERIMENTAL SECTION

General Procedures.

All manipulations involving organometallic compounds made use of standard Schlenk techniques under inert atmosphere. Solvents were dried over sodium metal (hexane, thf and diethylether) and phosphorouspentoxide (CH_2Cl_2); and distilled under nitrogen gas prior to use. All chemicals were used as purchased without further purification unless stated otherwise. Triethyloxoniumtetrafluoroborate was prepared according to literature procedures.[17] Purification of complexes was done with column chromatography using silica gel 60 (0.0063-0.200 mm) as the stationary phase. NMR spectra were recorded on a Bruker AVANCE 500 spectrometer. ^1H NMR spectra were recorded at 500.139 MHz and ^{13}C NMR at 125.75 MHz. The signals of the deuterated solvent were used as a reference: ^1H $CDCl_3$ at 7.24 ppm and C_6D_6 at 7.15 ppm; ^{13}C $CDCl_3$ at 77.00 ppm and C_6D_6 128.00 ppm. IR spectra were recorded on a Perkin-Elmer Spectrum RXI FT-IR spectrophotometer in solvent (hexane or DCM) as indicated. Only the vibration bands in the carbonyl-stretching region (ca. 1600-2200 cm^{-1}) were recorded.

[(CO)$_5$W=C(OEt)Fc] (**1**) was prepared according to previously reported methods.[15]

[(CO)$_5$W=C(OEt)Fc′(OEt)C=W(CO)$_5$] (**2**)

Dilithioferrocene was prepared according to literature procedures:[16] to a solution of ferrocene (4 mmol, 0.74g) in hexane was added TMEDA (8.2 mmol, 1.23 mL) and *n*BuLi in hexane (8.2 mmol) and stirred while heating to 60°C. After formation of the orange precipitate, the solvent was removed *via* cannula filtration, and the precipitate redissolved in thf. W(CO)$_6$ (8 mmol, 2.81g) was added at -78°C, and stirred for 1 hour while allowing the reaction mixture to reach room temperature. The solvent thf was removed by reduced pressure and Et_3OBF_4 (8.2 mmol), dissolved in CH_2Cl_2, added at -30°C. After reaction completion, the solvent was evaporated. Column chromatography was used for purification and the dark red fraction collected. Yield: 2.65g (70%), black red crystals. Anal. Calcd for $W_2FeC_{26}H_{18}O_{12}$: C, 33.01; H, 1.92. Found: C, 31.98; H, 1.88. ^{1}H NMR ($CDCl_3$): δ 5.02 (m, 4H, H$_\alpha$), 4.89 (q, *J* = 7.0 Hz, 4H, C**H**$_2$CH$_3$), 4.81 (m, 4H, H$_ß$), 1.61 (t, *J* = 7.1 Hz, 6H, CH$_2$C**H**$_3$). ^{13}C NMR ($CDCl_3$): δ n.o. (C$_{carbene}$), 201.91 (*trans*-**C**O), 197.58 (*cis*-**C**O) , 98.82 (**C**$_{ipso}$) , 74.52 (C$_\alpha$), 69.15 (C$_\beta$) , 77.20 O**C**H$_2$), 14.12 (**C**H$_3$). IR (ν_{CO}, cm^{-1}, CH_2Cl_2): 2060 m (A″$_1$), 1978 w (B), 1935 vs (A′$_1$ overlap E).

[(CO)$_5$W=C(NHBu)Fc] (**3**)

A diethylether solution of **1** (2 mmol, 1.13 g) was stirred at room temperature (rt) and *n*-butylamine (2 mmol, 0.20 mL) was added. The color changed rapidly from dark red to deep yellow. Purification was performed using column chromatography and a 1:1 mixture of hexane/CH_2Cl_2 as eluent. Yield: 0.90g (76%), yellow solid. Anal. Calcd for $WFeC_{20}H_{19}NO_5$: C, 40.50; H, 3.24. Found: C, 40.23; H, 3.09. ^{1}H NMR (C_6D_6): δ 8.91 (s, 1H, N**H**), 4.24 (br, 2H, H$_\alpha$), 4.02 (br, 2H, H$_ß$), 3.86 (s, 5H, Cp), 3.53 (m, 2H, NC**H**$_2$), 1.35 (m, 2H, C**H**$_2$CH$_2$), 1.17 (m, 2H, CH$_2$C**H**$_2$), 0.78 (m, 3H, C**H**$_3$). ^{13}C NMR (C_6D_6): δ 249.14 (C$_{carbene}$), 203.27 (*trans*-**C**O), 199.27 (*cis*-**C**O) , 97.12 (**C**$_{ipso}$) , 71.12 (C$_\alpha$), 69.86 (C$_\beta$ overlap Cp), 54.95 (N**C**H$_2$), 31.54 (**C**H$_2$CH$_2$), 20.07 (CH$_2$**C**H$_2$), 13.72 (**C**H$_3$). IR (ν_{CO}, cm^{-1}, CH_2Cl_2): 2060 m (A″$_1$), 1966 w (B), 1922 vs (A′$_1$ overlap E).

[(CO)$_5$W=C(NHPr)Fc′(NHPr)C=W(CO)$_5$] (4)

Complex **2** (2 mmol, 1.89g) was dissolved in diethylether and *n*-propylamine (2 mmol, 0.16 mL) was added at rt. The color of the solution turned from dark red to deep yellow and volatiles were removed by reduced pressure. Purification was performed by employing column chromatography with a 1:1 hexane/CH_2Cl_2 solvent mixture.

Yield: 1.46g (75%), deep yellow crystals. Anal. Calcd for $W_2FeC_{28}H_{24}N_2O_{10}$: C, 34.59; H, 2.49. Found: C, 33.42; H, 2.35. ^{1}H NMR ($CDCl_3$): 8.96 (s, 2H, **H**N), 4.56 (m, 4H, H$_\alpha$), 4.48 (m, 4H, H$_ß$), 3.88 (m, 4H, NC**H**$_2$), 1.86 (h, *J* = 7.4 Hz, 4H, C**H**$_2$CH$_3$), 1.13 (t, *J* = 7.4 Hz, 6H, C**H**$_3$). ^{13}C NMR (CDCl3): 249.58(C$_{carbene}$), 202.81 (CO$_{trans}$), 198.45 (CO$_{cis}$), 99.19 (C$_{ipso}$), 72.23 (C$_\alpha$), 70.15(C$_ß$), 56.96 (HN**C**H$_2$), 23.01 (**C**H$_2$CH$_3$), 11.23 (**C**H$_3$). IR (ν_{CO}, cm^{-1}, CH_2Cl_2): 2060 m (A″$_1$), 1963 w (B), 1920 vs (A′$_1$ overlap E).

[(CO)$_5$W=C(OEt)Fc][PF$_6$] ([1$^+$]•PF$_6$)

Complex **1** (0.02g, 0.035 mmol) was dissolved in dichloromethane and cooled to -35^{o}C. Silver hexafluorophosphate (0.009g, 0.035 mmol) was added and the solution changed from red to deep brown. The cold bath was removed and the brown solution was stirred at RT for 10 min. Cannula filtration was used to separate solids from the solution. ^{31}P NMR (CD_2Cl_2): δ -149.63 (h, *J* = 716.9, 706.7 Hz); ^{19}F NMR (CD_2Cl_2): δ -85.38 (d, *J* = 967.0 Hz); IR (ν_{CO}, cm^{-1}, CH_2Cl_2): 2074 (A$_1$", m), 1996 (B, w), 1952 (A$_1$' overlap E, vs).

Electrochemistry

Cyclic voltammograms (CV's), square wave voltammograms (SW's) and linear sweep voltammograms (LSV's) were recorded on a Princeton Applied Research PARSTAT 2273 voltammograph running PowerSuite (Version 2.58) utilizing a standard three-electrode cell in a M Braun Lab Master SP glovebox filled with high purity argon (H_2O and O_2 < 5 ppm) as described before.[10,11] To establish whether the electrolyte used, [(^{n}Bu$_4$)N][PF$_6$], and also the solvent influenced the number of electrons transferred at the tungsten center, **4** was also studied in the presence of 0.2 mol dm^{-3} [(^{n}Bu$_4$)N][B(C$_6$F$_5$)$_4$][37] as supporting electrolyte and in CH_3CN as solvent. All electrode potentials are reported versus the ferrocene/ferrocenium redox couple (FcH/FcH$^+$, FcH = Fe(η^5-C$_5$H$_5$)$_2$, E$^{o'}$ = 0.00 V) as reference.[38] However, decamethylferrocene,

Fc*, was used as internal standard to prevent signal overlap with the ferrocenyl of **1** – **4**. Decamethylferrocene has a formal reduction potential of -550 mV versus free ferrocene with ΔE = 72 mV and i_{pc}/i_{pa} = 1 under the prevailing conditions utilizing CH_2Cl_2 / $[(^nBu_4)N][PF_6]$ as solvent / supporting electrolyte.[36] In the presence of $[(^nBu_4)N][B(C_6F_5)_4]$ as electrolyte, the decamethylferrocene potential moves to -610 mV versus free ferrocene, while in CH_3CN / $[(^nBu_4)N][PF_6]$ it moves to -510 mV.[36]

Computational details

Geometry optimizations without symmetry constraints were carried out using the Gaussian09 suite of programs[39] at the B3LYP (uB3LYP for open-shell species)[40] using the double-ζ plus polarization def2-SVP[41] basis set for all atoms. This protocol is denoted B3LYP/def2-SVP. All species were characterized by frequency calculations, and have a positive defined Hessian matrix indicating that they are minima on the potential energy surface.

All Atoms in Molecules (AIM)[42] results described in this work correspond to calculations performed at the B3LYP/6-31G(d)&WTBS level on the optimized geometries obtained at the B3LYP/def2-SVP level. The WTBS (well-tempered basis sets)[43], used herein to describe Fe and W, have been recommended for AIM calculations involving transition metals.[44] The topology of the ED was conducted using the AIMAll program package. [45]

5.5 ACKNOWLEDGMENT

This work is supported by the National Research Foundation, South Africa, (DIB, Grant number 76226; JCS, Grant number 81829), and by the Spanish MICINN and CAM (IF, Grants CTQ2010-20714-CO2-01/BQU, Consolider-Ingenio 2010, CSD2007-00006, S2009/PPQ-1634).

5.6 REFERENCES

(1) Pike A. R.; Ryder, L. C.; Horrocks, B. R.; Clegg, W.; Connolly, B. A.; Houlton, A. *Chem. Eur. J.* **2004**, *11*, 344-353.

(2) Spanig, F.; Kolvacs, C.; Hauke, F.; Ohlubo, K.; Fukuzumi, F.; Guldi, D. M.; Hirsch, A. *J. Am. Chem. Soc.* **2009**, *131*, 8180-8195.

(3) (a) Saravanakumar, D.; Sengottuvelan, N.; Narayanan, V.; Kandaswamy, M.; Varghese, T. L. *J. Appl. Polym. Sci.* **2011**, *119*, 2517-2524; (b) Jungbluth, H.; Lohmann, G. *Nachr. Chem. Tech. Lab*. **1999**, *47*, 534-538; (c) Swarts, P. J.; Immelman, M.; Lamprecht, G. J.; Greyling, S. E.; Swarts, J. C. *S. Afr. J. Chem.* **1997**, *50*, 208-216; (d) Shen, Q. L.; Shekhar, S.; Stambuli, J. P.; Hartwig, J. F. *Angew. Chem. Int. Ed.* **2005**, *44*, 1371-1375; (e) Conradie, J.; Swarts, J. C. *Organometallics*, **2009**, *28*, 1018-1026. (4) (a) Shago, R. F.; Swarts, J. C.; Kreft, E.; Van Rensburg, C. E. J. *Anticancer Res*. **2007**, *27*, 3431-3434; (b) Van Rensburg, C. E. J.; Kreft, E.; Swarts, J. C.; Dalrymple, S. R.; Macdonald, D. M.; Cooke, M. W.; Aquino, M. A. S. *Anticancer Res*. **2002**, *22*, 889-892. (c) Gross, A.; Hüsken, N.; Schur, J.; Raszeja, L.; Ott, I.; Metzler-Nolte, N. *Bioconjugate Chemistry*, **2012**, *23*, 1764-1774. (d) Swarts, J. C.; Vosloo, T. G.; Cronje, S. J.; Du Plessis, W. C.; Van Rensburg, C. E. J.; Kreft, E.; Van Lier, J. E. *Anticancer Res.* **2008**, *28*, 2781-2784; (e) Ott, I.; Kowalski, K.; Gust, R.; Maurer, J.; Mücke, P.; Winter, R. F. *Bioorg. Med. Chem. Lett.* **2010**, *20*, 866-869.

(5) Recent reviews on the chemistry and applications of Fischer carbenes include: (a) Wu, Y.-T.; Kurahashi, T.; De Meijere, A. *J. Organomet. Chem.* **2005**, *690*, 5900-5911; (b) Gómez-Gallego, M.; Mancheño, M. J.; Sierra, M. A. *Acc. Chem. Res*. **2005**, *38*, 44-53; (c) Sierra, M. A.; Gómez-Gallego, M.; Martínez-Ávarez, R. *Chem.–Eur. J.* **2007**, *13*, 736-744; (d) Sierra, M. A.; Fernández, I.; Cossío, F. P. *Chem. Commun*. **2008**, 4671-4682; (e) Dötz, K. H.; Stendel, J. *Chem. Rev*. **2009**, *109*, 3227-3274; (f) Herndon, J. W. *Coord. Chem. Rev*. **2010**, *254*, 103-194; (g) Fernández-Rodríguez, M. A.; García-García, P.; Aguilar, E. *Chem. Comm*. **2010**, *46*, 7670-7687; (h) Fernández, I.; Cossío, F. P.; Sierra, M. A. *Acc. Chem. Res.* **2011**, *44*, 479-490; (i) Bezuidenhout, D. I.; Lotz, S.; Liles, D. C.; Van der Westhuizen, B. *Coord. Chem. Rev.* **2012**, *256*, 479-524; (j) Fernández, I.; Sierra, M. A. *Top. Heterocycl. Chem*. **2013**, *30*, 65-84.

(6) Representative examples: (a) Cases, M.; Frenking, G.; Duran, M.; Solà, M. *Organometallics,* **2002**, *21*, 4182-4191; (b) Poater, J.; Cases, M.; Fradera, X.; Duran, M.; Solà, M. *Chem. Phys.*

2003, *294*, 129-139; (c) Fernández, I.; Cossío, F. P.; Arrieta, A.; Lecea, B.; Mancheño, M. J.; Sierra, M. A. *Organometallics* **2004**, *23,* 1065-1071; (d) Frenking, G.; Solà, M.; Vyboishchikov, S. F. *J. Organomet. Chem.* **2005**, *690*, 6178-6204; (e) Fernández, I.; Sierra, M. A.; Mancheño, M. J.; Gómez-Gallego, M.; Cossío, F. P. *Chem. Eur. J*. **2005**, *11*, 5988-5996; (f) Fernández, I.; Sierra, M. A.; Cossío, F. P. *J. Org. Chem.* **2008**, *73*, 2083-2089; (g) Valyaev, D. A.; Brousses, R.; Lugan, N.; Fernández, I.; Sierra, M. A. *Chem. Eur. J.* **2011**, *17*, 6602-6605; (h) Andrada, D. M.; Granados, A. M.; Solá, M.; Fernández, I. *Organometallics*, **2011**, *30*, 466-476.

(7) Connor, J. A.; Jones, E. M.; Lloyd, J. P. *J. Organomet. Chem.* **1970**, *24*, C20-C22.

(8) (a) Dötz, K. H.; Dietz, R.; Neugebauer, D. *Chem. Ber.* **1979**, *112*, 1486-1490; (b) Bennewits, J.; Nieger, M.; Lewall, B.; Dötz, K. H. *J. Organomet. Chem.* **2005**, *690*, 5892-5899.

(9) (a) Dötz, K. H. *Angew. Chem. Int. Ed. Engl*. **1975**, *14*, 644-645; (b) Wulff, W. D. in *Comprehensive Organic Synthesis*, Vol. 5 (Eds.: B. M. Trost, I. Fleming), Pergamon, Oxford, **1991**, p. 1065; (c) Minatti, A.; Dötz, K. H. *Top. Organomet. Chem*. **2004**, *13*, 123; (d) Waters, M. L.; Wulff, W. D. *Org. React*. **2008**, *70*, 121.

(10) Van der Westhuizen, B.; Swarts, P. J.; Strydom, I.; Liles, D. C.; Fernández, I.; Swarts, J. C.; Bezuidenhout, D. I. *Dalton Trans.* **2013**, *42*, 5367-5378.

(11) Van der Westhuizen, B.; Swarts, P. J.; Van Jaarsveld, L. M.; Liles, D. C.; Siegert, U.; Swarts, J. C.; Fernández, I.; Bezuidenhout, D. I. *Inorg. Chem.* **2013**, *52*, 6674-6684.

(12) (a) Bezuidenhout, D. I.; Van der Watt, E.; Liles, D. C.; Landman, M.; Lotz, S. *Organometallics*, **2008**, *27*, 2447-2456; (b) Bezuidenhout, D. I.; Lotz, S.; Landman, M.; Liles, D. C. *Inorg. Chem.* **2011**, *50*, 1521-1533.

(13) Baldoli, C.; Cerea, P.; Falciola, L.; Giannini, C.; Licandro, E.; Maiorana, S.; Mussini, P.; Perdicchia, D. *J. Organomet. Chem.* **2005**, *690*, 5777-5787.

(14) (a) Chu, G. M.; Fernández, I.; Sierra, M. A. *Chem. Eur. J*. **2013**, *19*, 5899-5908; (b) López-Alberca, M. P.; Mancheño, M. J.; Fernández, I.; Gómez-Gallego, M.; Sierra, M. A.; Hemmert, C.; Gornitzka, H. *Eur. J. Inorg. Chem.* **2011**, 842-849; (c) Bezuidenhout, D. I.; Barnard, W.; Van der Westhuizen, B.; Van der Watt, E.; Liles, D. C. *Dalton Trans.* **2011,** *40*, 1-11; (d) Schobert, R.; Kempe, R,; Schmalz, T.; Gmeiner, A. *J. Organomet. Chem.* **2006**, *691*, 859-868; (e) Pombeiro, A. J. L. *J. Organomet. Chem.* **2005**, *690*, 6021-6040; (f) Fernández, I.; Mancheño, M. J.; Gómez-Gallego, M.; Sierra, M. A. *Org. Lett*. **2003**, *5*, 1237-1240; (g) Jayaprakash, K. N.; Ray, P. C.; Matsuoka, I.; Bhadbhade, M. M.; Puranik, V. G.; Das, P. K.; Nishihara, H.; Sarkar,

A. *Organometallics* **1999**, *18*, 3851-3858; (h) Casey, C. P.; Albin, L. D.; Saeman, M. C.; Evans, D. H. *J. Organomet. Chem.* **1978**, *155*, C37-C40; (i) Lloyd, M. K.; McCleverty, J. A.; Orchard, D. G.; Connor, J. A.; Hall, M. B.; Hillier, I. H.; Jones, E. M.; McEwen, G. K. *J. Chem. Soc., Dalton* **1973**, 1743-1747.

(15) López-Cortés, J. G.; Contreras de la Cruz, L. F.; Ortega-Alfaro, M. C.; Toscano, R. A.; Alvarez-Toledano, C.; Rudler, H. *J. Organomet. Chem.* **2005**, *690*, 2229-2237.

(16) Sünkel, H.; Bernhartzeder, S. *J. Organomet. Chem*. **2011**, *696*, 1536-1540.

(17) Meerwein, H. *Org. Synth*. **1966**, *46*, 113–115.

(18) Inkpen, M. S.; Du, S.; Driver, M.; Albrecht, T.; Long, N. J. *Dalton Trans.* **2013**, *42*, 2813-2816.

(19) (a) Bezuidenhout, D. I.; Liles, D. C.; Van Rooyen, P. H.; Lotz, S. *J. Organomet. Chem*., **2007**, *692*, 774-783; (b) Klabunde, U.; Fischer, E. O. *J. Am. Chem. Soc*. **1967**, *89*, 7141-7142.

(20) (a) Post, E. W.; Watters, K. L. *Inorg. Chim. Acta,* **1978**, *26*, 29-36; (b) Moser, E.; Fischer, E. O. *J. Organomet. Chem.*, **1968**, *15*, 147-155.

(21) (a) Kemp, K. C.; Fourie, E.; Conradie, J.; Swarts, J. C. *Organometallics,* **2008**, *27*, 353-362; (b) Du Plessis, W. C.; Davis, W. L.; Cronje, S. J.; Swarts, J. C. *Inorg. Chim. Acta* **2001**, *314*, 97-104.

(22) Lage, M. L.; Fernández, I.; Mancheño, M. J.; Sierra, M. A. *Inorg. Chem.* **2008**, *47*, 5253-5258.

(23) Venkatasubbaiah, K.; Nowik, I.; Herber, R. H.; Jäkle, F. *Chem. Commun.* **2007**, 2154-2156.

(24) (a) Braterman, P. S. *Metal Carbonyl Spectra*; Academic Press Inc., London, **1975**, p 68. (b) Adams, D. M. *Metal-Ligand and Related Vibrations;* Edward Arnold Publishers Ltd., London, **1967**, p 98.

(25) (a) Gericke, H. J.; Barnard, N. I.; Erasmus, E.; Swarts, J. C.; Cook, M. J.; Aquino, M. A. S. *Inorg. Chim. Acta,* **2010**, *363*, 2222-2232; (b) Evans, D. H.; O'Connell, K. M.; Peterson, R. A.; Kelly, M. J. *J. Chem. Educ.*, **1983**, *60*, 290-293; *(c)* Kissinger, P. T.; Heineman, W. R. *J. Chem. Educ.* **1983**, *60*, 702-706. *(d)* Van Benschoten, J. J.; Lewis, J. Y.; Heineman, W. R. *J. Chem. Educ.*, **1983**, *60*, 772-776; *(e)* Mobbott, G. A. *J. Chem. Educ.*, **1983**, *60*, 697-702.

(26) Leading references are (a) Creutz, C.; Taube, H. *J. Am. Chem. Soc.* **1969**, *91*, 3988-3989. (b) Geiger, W. E.; Van Order, N.; Pierce, D. T.; Bitterwolf, T. E.; Reingold, A. L.; Chasteen, N. D. *Organometallics* **1991**, *10*, 2403-2411. (c) Van Order, N.; Geiger, W. E.; Bitterwolf, T. E.;

Reingold, A. L. *J. Am. Chem. Soc.* **1987**, *109*, 5680-5690. (d) Pierce, D. T.; Geiger, W. E. *Inorg. Chem.* **1994**, *33*, 373-381. (e) Cook, M. J.; Chambrier, I.; White, G. F.; Fourie, E.; Swarts, J. C. *Dalton Trans.* **2009**, 1136-1144.

(27) For a review, see: Sierra, M. A.; Gómez-Gallego, M.; Martínez-Álvarez, R. *Chem-Eur. J.* **2007**, *13*, 736-744.

(28) Leading publications demonstrating the influence and use of [(*n*Bu4)N][B(C6F5)4] and the complimentary role of associated *cations* with different charge densities may be found in (a) Barriere, F.; Kirss, R. U.; Geiger, W. E. *Organometallics* **2005**, *24*, 48-52 and references therein; (b) Hildebrandt, A.; Rüffer, T.; Erasmus, E.; Swarts, J. C.; Lang, H. *Organometallics* **2010**, *29*, 4900-4905; (c) Barriere, F.; Camire, N.; Geiger, W. E.; Mueller-Westerhoff, U. T.; Sanders, R. *J. Am. Chem. Soc.* **2002**, *124*, 7262-7263; (d) Barriere, F.; Geiger, W. E. *J. Am. Chem. Soc.* **2006**, *128*, 3980-3989; (e) Nafady, A.; Chin, T. T.; Geiger, W. E. *Organometallics* **2006** *25*, 1654-1663; (f) Chong, D. S.; Slote, J.; Geiger, W. E. *J. Electroanal. Chem.*, **2009**, *630*, 28-34.

(29) Swarts, J. C.; Nafady, A.; Roudebush, J. H.; Trupia, S.; Geiger, W. E. *Inorg. Chem.* **2009**, *48*, 2156-2165.

(30) Ruthenocene and osmocene behave quite similarly in that oxidation generates a Ru(IV) and Os(IV) species: (a) Watanabe, M.; Motoyama, I.; Takayama, T.; Sato, M. *J. Organomet. Chem.* **1997**, *549*, 13-23; (b) Watanabe, M.; Motoyama, I.; Shimoi, M.; Sano, H. *J. Organomet. Chem.* **1996**, *517*, 115-121; (c) Smith, T. P.; Iverson, D. J.; Droege, M. W.; Kwan, K. S.; Taube, H. *Inorg. Chem.* **1987**, *26*, 2882-2884.

(31) The donor number of CH2Cl2 is difficult to find in literature, it is always listed as an undetermined quantity. However, a Google search of the World Wide Web gave a value of 1, see http://www.stenutz.eu/chem/solv21.php. Leading references to Gutmann donor numbers include: (a) Gutmann, V. *Coord. Chem. Rev.*, **1976**, *18*, 225-255; (b) Gutmann, V. *The Donor-acceptor Approach to Molecular Interactions*, Plenum Press, New York, **1978**, p.20; (c) Huheey, J. E. *Inorganic Chemistry: Principles of structure and reactivity*, 3rd Ed., Harper, Cambridge, **1983**, p340.

(32) For a scale of donor numbers referenced to 1,2-dichloroethane, where CH2Cl2 has DN = 0 and MeCN has DN = 0.36, see: Reichardt, C. *Solvents and Solvent-Effects in Organic Chemistry,* 3rd Ed., Wiley-VCH, Weinheim, **2003**.

(33) Da Silva, M. F. C. G.; Trzeciak, A. M.; Ziolkowski, J. J.; Pombeiro, A. J. L. *J. Organomet. Chem.* **2001**, *620*, 174-181.

(34) (a) Conradie, J.; Swarts, J. C. *Eur. J. Inorg. Chem.* **2011**, 2439-2449; (b) Conradie, J.; Cameron, T. S.; Aquino, M. A. S.; Lamprecht, G. J.; Swarts, J. C. *Inorg. Chim. Acta* **2005**, 2530-2542.

(35) Leading references describing the electrochemical activity and behaviour of ferrocene and decamethylferrocene in a multitude of organic solvents are (a) Noviandri, I.; Brown, K. N.; Fleming, D. S.; Gulyas, P. T.; Lay, P. A.; Masters, A. F.; Phillips, L. *J. Phys. Chem. B* **1999**, *103*, 6713-6722; (b) Connelly, N. G.; Geiger, W. E. *Chem. Rev.* **1996**, *96*, 877-910; (c) Ruiz, J.; Astruc, D. *C.R. Acad. Sci.* (Paris), Ser. IIc 1, **1998**, 21-27; (d) Aranzaes, R. J.; Daniel, M. C.; Astruc, D. *Can. J. Chem.* **2006**, *84*, 288-299; (e) Fourie, E.; Swarts, J. C.; Chambrier, I.; Cook, M. J. *Dalton Trans.*, **2009**, 1145-1154.

(36) Lein, M. *Coord. Chem. Rev.* **2009**, *253*, 625-634.

(37) LeSuer, R. J.; Buttolph, C.; Geiger, W. E. *Anal. Chem.* **2004**, *76*, 6395-6401.

(38) (a) Gritzner, G.; Kuta, J. *Pure Appl. Chem.* **1984**, *56*, 461-466; (b) Gagne, R. R.; Koval, C. A.; Lisensky, G. C. *Inorg. Chem.* **1980**, *19*, 2854-2855.

(39) *Gaussian 09*, Revision B.1, Frisch, M. J.; Trucks, G. W.; Schlegel, H. B.; Scuseria, G. E.; Robb, M. A.; Cheeseman, J. R.; Scalmani, G.; Barone, V.; Mennucci, B.; Petersson, G. A.; Nakatsuji, H.; Caricato, M.; Li, X.; Hratchian, H. P.; Izmaylov, A. F.; Bloino, J.; Zheng, G.; Sonnenberg, J. L.; Hada, M.; Ehara, M.; Toyota, K.; Fukuda, R.; Hasegawa, J.; Ishida, M.; Nakajima, T.; Honda, Y.; Kitao, O.; Nakai, H.; Vreven, T.; Montgomery, Jr., J. A.; Peralta, J. E.; Ogliaro, F.; Bearpark, M.; Heyd, J. J.; Brothers, E.; Kudin, K. N.; Staroverov, V. N.; Kobayashi, R.; Normand, J.; Raghavachari, K.; Rendell, A.; Burant, J. C.; Iyengar, S. S.; Tomasi, J.; Cossi, M.; Rega, N.; Millam, N. J.; Klene, M.; Knox, J. E.; Cross, J. B.; Bakken, V.; Adamo, C.; Jaramillo, J.; Gomperts, R.; Stratmann, R. E.; Yazyev, O.; Austin, A. J.; Cammi, R.; Pomelli, C.; Ochterski, J. W.; Martin, R. L.; Morokuma, K.; Zakrzewski, V. G.; Voth, G. A.; Salvador, P.; Dannenberg, J. J.; Dapprich, S.; Daniels, A. D.; Farkas, Ö.; Foresman, J. B.; Ortiz, J. V.; Cioslowski, J.; Fox, D. J. Gaussian, Inc., Wallingford CT, **2009**.

(40) (a) Becke, A. D. *J. Chem. Phys.* **1993**, *98*, 5648-5652. (b) Lee, C.; Yang, W.; Parr, R. G. *Phys. Rev. B* **1988**, *37*, 785-789.

(41) Weigend, F.; Ahlrichs, R. *Phys. Chem. Chem. Phys.* **2005**, *7*, 3297-3305.

(42) Bader, R. F. W. *Atoms in Molecules. A Quantum Theory*; Oxford University Press: Oxford, U.K., **1990**.

(43) (a) Huzinaga, S.; Miguel, B. *Chem. Phys. Lett*. **1990**, *175*, 289-291. (b) Huzinaga, S.; Klobukowski, M. *Chem. Phys. Lett*. **1993**, *212*, 260-264.

(44) (a) Cabeza, J. A.; Van der Maelen, J. F.; García-Granda, S. *Organometallics* **2009**, *28*, 3666-3672. (b) Buil, M. L.; Esteruelas, M. A.; Fernández, I.; Izquierdo, S.; Oñate, E. *Organometallics* **2013**, *32*, 2744-2752.

(45) Keith, T. A. AIMAll, 2010, http://tkgristmill.com

CHAPTER 5

An Electrochemical and computational study of tungsten(0) ferrocene complexes: observation of the mono-oxidized tungsten(0) ferrocenium species and intramolecular electronic interactions

This chapter was published in Organometallics. The format reflects the style set by the journal.

Daniela I. Bezuidenhout,[a] Israel Fernández,[b] Belinda van der Westhuizen,[a] Pieter J. Swarts,[c] Jannie C. Swarts,[c] *Organometallics,* **2013**, *32(24)*, 7334-7344.

Author contributors

Synthetic work: B. van der Westhuizen

Cyclic voltammetry and data analysis: P. J. Swarts, J. C. Swarts

Computational work: I. Fernández

Article written, submitted and response to reviewers: B. van der Westhuizen, D. I. Bezuidenhout, J. C. Swarts, I. Fernández.

[a] *Chemistry Department, University of Pretoria, Private Bag X20, Hatfield, 0028, South Africa. Fax: +27-(0)12-420-4687; Tel: +27-(0)12- 420-2626; E-mail: daniela.bezuidenhout@up.ac.za*
[b] *Departamento de Química Orgánica I, Facultad de Química, Universidad Complutense,28040-Madrid,Spain.*
[c] *Chemistry Department, University of the Free State, PO Box 339, Bloemfontein 9300, South Africa. Fax:+27-(0)51-444-6384; Tel: +27-(0)51-401-2781; E-mail: swartsjc@ufs.ac.za*

Supplementary information: The LSV and CV of complexes **1 - 4**, (**Appendix 4a**) and Cartesian coordinates and energies of all the stationary species discussed in the text are included. This material is available free of charge via the Internet at http://pubs.acs.org. (**Appendix 4b, CD**)

ABSTRACT

The series [$(CO)_5W$=C(XR)Fc], **1** (XR = OEt) and **3** (XR = NHBu) as well as [$(CO)_5W$=C(XR)-Fc'-(XR)C=$W(CO)_5$], **2** (XR = OEt) and **4** (XR = NHBu) of mono- and biscarbene tungsten(0) complexes with Fc = $Fe^{II}(C_5H_5)(C_5H_4)$ for monosubstituted derivatives and Fc′ = $Fe^{II}(C_5H_4)_2$ for disubstituted derivatives were synthesized and characterized spectroscopically. The oxidized ferrocenium complex [$\mathbf{1}^+$]•PF_6 was also synthesized and characterized. Electrochemical and computational studies were mutually consistent in confirming the sequence of redox events for the carbene derivatives **1** – **4** as first a carbene double bond reduction to a radical anion, $^-$W-C•, at peak cathodic potentials smaller than -2 V, then a ferrocenyl group oxidation in the range $0.206 < E^{o'} < 0.540$ V and finally an electrochemically irreversible three-electron W(0) oxidation at $E_{pa} > 0.540$ V vs. FcH/FcH^+ in CH_2Cl_2 / [(^{n}Bu$_4$)N][PF_6]. This contrasts the sequence of oxidation events in ferrocenylcarbene complexes of chromium where Cr(0) is first oxidised in a one electron transfer process, then the ferrocenyl group, and finally formation of a Cr(II) species. The unpaired electron of the reductively formed radical anion is mainly located on the carbene carbon atom. Electronic interactions between two carbene double bonds (for biscarbenes **2** and **4**) as well as between two W centers (for **4**) were evident. Differences in redox potentials between the "a" and "b" components of the three-electron W oxidation of **4** in CH_2Cl_2 or CH_3CN / [(^{n}Bu$_4$)N][PF_6] are $\Delta E^{o'} = E_{pa\ W(0)\ oxd\ 1b} - E_{pa\ W(0)\ oxd\ 1a}$ = ca. 51 and 337 mV respectively. Tungsten oxidation was restricted to a $W^{0/II}$ couple in CH_2Cl_2 / [(^{n}Bu$_4$)N][$B(C_6F_5)_4$]. From the computational results, the short-lived W(II) species were observed to be stabilized by agostic CH···W interactions.

5.1 INTRODUCTION

Based on its reversible electrochemical signature, ferrocene derivatives are researched as molecular sensors,[1] in energy transfer processes,[2] as catalysts[3] and even in anticancer research.[4] Fischer carbene complexes are versatile organometallics with valuable applications in organic and organometallic synthesis as well as in the fields of bioorganometallics and materials chemistry.[5] Recently, computational studies especially enhanced the understanding of this group of organometallic compounds substantially.[6]

The first examples of ferrocenyl carbene complexes of the group 6 transition metals, $[(CO)_5Cr=C(OR)Fc]$ (R = Me, Et), were synthesized to study the electronic effects of the ferrocenyl substituent on the carbene ligand as part of an investigation into the electron withdrawing nature of metal carbonyl carbene groups.[7] Early hints of the increased stability and chemodirecting steric effect of ferrocenyl carbene complexes were reported by Dötz *et al.*[8] Reaction of these ferrocenyl carbene complexes with tolane gave unexpected furanoid products over the customary Dötz benzannulation that yields chromium-coordinated hydroquinones.[9]

Our recent investigation into the electrochemical behavior of Fischer carbene complexes of the type $[(CO)_5Cr=C(XR)Ar]$ (XR = OEt, NHBu or NHPr; Ar = 2-thienyl (Th), 2-furyl (Fu) or ferrocenyl (Fc)), revealed the formation of dicationic Cr(II) species formed upon two consecutive one-electron oxidation processes.[10] These dicationic carbene complexes are characterized by an unusual bonding situation as they are stabilized by CH···Cr agostic interactions.[11] Strikingly, for the biscarbene complexes $[(CO)_5Cr=C(OEt)\text{-}Fc'\text{-}(OEt)C=Cr(CO)_5]$ (Fc' = ferrocen-1,1'-diyl), two resolved $Cr^{0/I}$ couples were observed. It was observed that intramolecular electronic interactions between the two Cr(0) centers is much more effective in biscarbene complexes linked together by a ferrocen-1,1′-diyl functionality,[12] since the biscarbene complexes with 2,5-thiendiyl or 2,5-furadiyl spacers did not display the split of the $Cr^{0/I}$ couple into two components. Rather, the redox processes in these heteroaryl biscarbene complexes are two-electron transfer processes that comprise two simultaneously occurring but independent one-electron transfer steps, one for each Cr(0) center.

In contrast to our findings that the $Cr^{I/0}$ and $Cr^{II/I}$ redox couples in Fischer carbene complexes are at potentials that may differ as much as 0.75 V,[10,11] tungsten(0) carbene complexes were reported to be oxidized to tungsten(II) carbene complexes either by a single two-electron transfer process or by two unresolved (overlapping) one electron transfer processes.[13] Previous electrochemical studies[14] on the redox behavior for chromium(0) and tungsten(0) carbene complexes did not identify a $Cr^{II/I}$ couple, nor did they comment on the now firmly established reduction of the chromium carbene double bond, Cr=C to the radical anion $^{-}$Cr-C•.[10,11] It is clear that the electrochemical behavior of chromium(0) and tungsten(0) Fischer carbene complexes and the driving forces behind it may not be so similar as was accepted till now. To probe the differences between chromium and tungsten carbenes, including the possibility of metal-metal

communication between the tungsten pentacarbonyl termini, we synthesized the ethoxycarbene complexes $[(CO)_5W{=}C(OEt)Fc]$ (**1**),[15] $[(CO)_5W{=}C(OEt)Fc'(OEt)C{=}W(CO)_5]$ (**2**), and the new aminocarbene analogues, $[(CO)_5W{=}C(NHBu)Fc]$ (**3**), and $[(CO)_5W{=}C(NHPr)Fc'(NHPr)C{=}(CO)_5]$ (**4**) (Scheme 5.1). In addition, the isolation of the monocationic salt, $[\mathbf{1}^+]\cdot\mathbf{PF_6}$, was achieved. An electrochemical analysis, supported by density functional theory (DFT) calculations and spectroscopic analyses, are reported and results are compared to highlight the differences between Cr and W analogues.

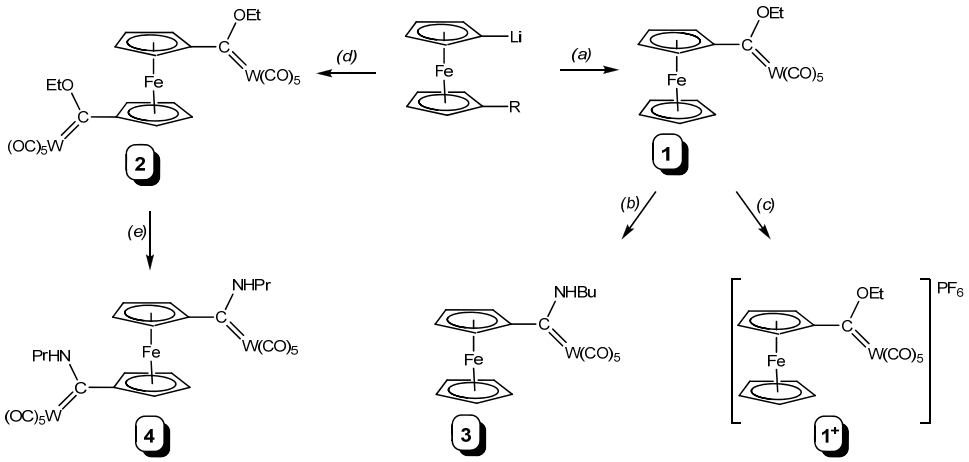

Scheme 5.1 Synthesis of ferrocenyl mono- and biscarbene tungsten complexes; Reagents and conditions: (a) (i) 1 eq FcLi (R = H), 1eq $[W(CO)_6]$, thf, -50°C; (ii) 1.3eq Et_3OBF_4, CH_2Cl_2, -30°C; (b) 1.1eq NH_2Bu, Et_2O, rt; (c) 1eq $AgPF_6$, CH_2Cl_2, -35°C; (d) (i) 1eq $Fc'Li_2$ (R = Li), 2eq $[W(CO)_6]$, thf, -50°C; (ii) 2.5eq Et_3OBF_4, CH_2Cl_2, -30°C; (e) 2.2eq NH_2Pr, Et_2O, rt.

5.2 RESULTS AND DISCUSSION

*Synthesis and spectroscopic characterization of complexes **1 - 4**.*

Ferrocenyllithium[16] was reacted with $[W(CO)_6]$ in the classic Fischer route to carbene complexes (Scheme 5.1), followed by alkylation with Et_3OBF_4[17] to yield the known complex **1** $[(CO)_5W{=}C(OEt)Fc]$.[15] Following the procedure described for the synthesis of the chromium analogues, reaction of two equivalents of tungsten carbonyl and 1,1'-dilithioferrocene[18] yielded the tungsten bisacylate. Quenching of the reaction was achieved with excess of oxonium salt, to

yield the novel bridging ferrocen-1,1'-diyl biscarbene complex, **2** [$(CO)_5W$=C(OEt)Fc′(OEt)C=$W(CO)_5$]. Both the monocarbene complex **1** and biscarbene complex **2** were aminolysed[19] with *n*-butylamine or *n*-propylamine, respectively, to yield the new complexes [$(CO)_5W$=C(NHBu)Fc] (**3**) and [$(CO)_5W$=C(NHPr)Fc′(NHPr)C=$W(CO)_5$] (**4**). These tungsten carbene complexes displayed NMR and FTIR spectroscopic properties similar to that observed for their chromium analogues.[10,11] Upfield shifts of the ferrocenyl-H_α in the case of the aminocarbene complexes **3** and **4** (4.24 and 4.56 ppm, respectively) compared to the ethoxycarbenes **1** and **2** (4.98 and 5.02 ppm, respectively), upfield ^{13}C NMR shifts of the carbene carbon resonances of the aminocarbenes compared to the ethoxycarbenes (eg. **3**, 249.1 ppm compared to **1**, 304.3 ppm) and decreased carbonyl stretching frequencies of the overlapping A'_1 and E-modes for the aminocarbenes compared to the ethoxy analogues (**3**, 1922 cm^{-1}; **4**, 1920 cm^{-1} vs. **1**, 1932 cm^{-1}; **2**, 1935 cm^{-1}) are all indicators of the increased donating ability of the amino-substituents towards stabilizing the electrophilic carbene carbon atom.[19] This is due to the contribution of imine formation to the $C_{carbene}$-N bond (Figure 5.1), which results in the formation of both *syn*- and *anti*-configurational isomers around the abovementioned $C_{carbene}$-N bond.[10,11] However, as for the Cr-derivatives, the steric bulk of the ferrocenyl carbene substituent precludes the formation of both isomers, and only the *syn*-isomer can be observed by NMR. [20]

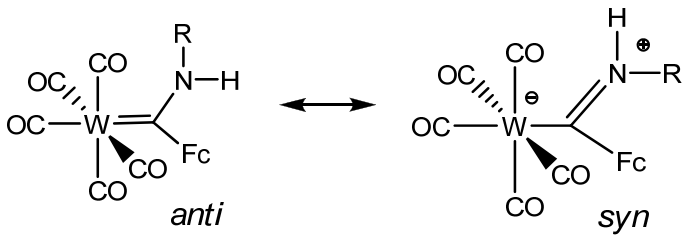

Figure 5.1 Stabilization of Fischer aminocarbene complexes via imine formation. For both **3** and **4**, only the *syn* rotamer is observed.

During the electrochemical investigation, we observed more positive oxidation potentials for the tungsten carbene complexes compared to the chromium analogues, in accordance with the higher hyperpolarizability of the tungsten complexes.[13] For our bimetallic complexes, however, this

meant that in contrast to the chromium ferrocenyl complexes,[10] the first oxidation process corresponds to the $Fe^{II/III}$ couple and not to the tungsten carbonyl moiety (see Electrochemistry Section). This encouraged us to perform the chemical oxidation of **1** with $AgPF_6$ (see Scheme 5.1) to gain insight into the properties of the ferrocenium cation $\mathbf{1}^+$. For the Cr-analogues, although this first $Cr^{0/I}$ oxidation proved reversible, the formed chromium +1 cation could not be isolated. After the addition of 1 equivalent of $AgPF_6$ to a solution of **1** in CH_2Cl_2 at -35 °C, an immediate color change from red to brown was observed. While the solution was allowed to warm to room temperature, IR and NMR data had to be collected for $\mathbf{[1^+]\bullet PF_6}$ within 10 minutes before decomposition of $\mathbf{1}^+$ occurred. Spectroscopically it could be seen (Figure 5.2) that much of $\mathbf{1}^+$ reverted back to **1**, probably by the capture of an electron from any electron-rich species in solution such as the free electron pairs on CO or OEt. To the best of our knowledge, no other isolated example of such a chemically oxidized ferrocenium Fischer carbene complex has been reported.

The IR spectra (Figure 5.2) clearly illustrate the shift of the carbonyl stretching frequencies from 1932, 1976 and 2063 cm^{-1} for **1** to 1953, 1998 and 2074 cm^{-1} for $\mathbf{1}^+$. The magnitude of the wavenumber shifts (21, 22 and 11 cm^{-1} for the E overlapping with A'_1, B and A''_1 bands respectively), is smaller than the shift of more than 100 cm^{-1} that is expected for oxidation of metal-carbonyl-based W(0) to W(I). Instead, it corresponds to an inductive effect accompanying the oxidation of the ferrocenyl Fe(II) substituent to a ferrocenium Fe(III) species. During this oxidation, the highly electron donating ferrocenyl group having a group electronegativity of $\chi_{Fc} = 1.87$ converted to an electron-withdrawing ferrocenium species ($\chi_{Fc+} = 2.82$) almost as strong as the CF_3 group ($\chi_{CF3} = 3.01$).[21] This observation is corroborated by the electrochemical data presented below. In addition, previous calculations reported the stabilization of the partially empty carbene carbon p_z atomic orbital by donation from a doubly-occupied d-orbital of iron.[22] Thus, with the removal of an electron from this atomic orbital, the donation is lowered, reducing the electron density of the W=C bond. Consequently, the π-backdonation to the π* orbital of the CO is also reduced with resulting higher C=O bond strength and higher CO stretching frequencies. The ^1H NMR spectrum recorded did not show any ferrocenyl resonances, even when recorded in a spectral window of up to 50 ppm, although the ferrocenium chemical shift is reported at δ31 ppm.[23] Presumably this can be ascribed to the paramagnetic nature of cation $\mathbf{1}^+$. The presence of the PF_6 counter anion is confirmed by the

upfield shifts of the resonances in the ^{31}P and ^{19}F NMR spectra in CD_2Cl_2, where for **[1$^+$]•PF$_6$** δ ^{31}P = -149.6 and δ ^{19}F = -85.4 ppm. The characteristic pentacarbonyl metal υ(CO)-pattern[24] indicates that no CO-ligand had been substituted by a coordinating PF_6-moiety.

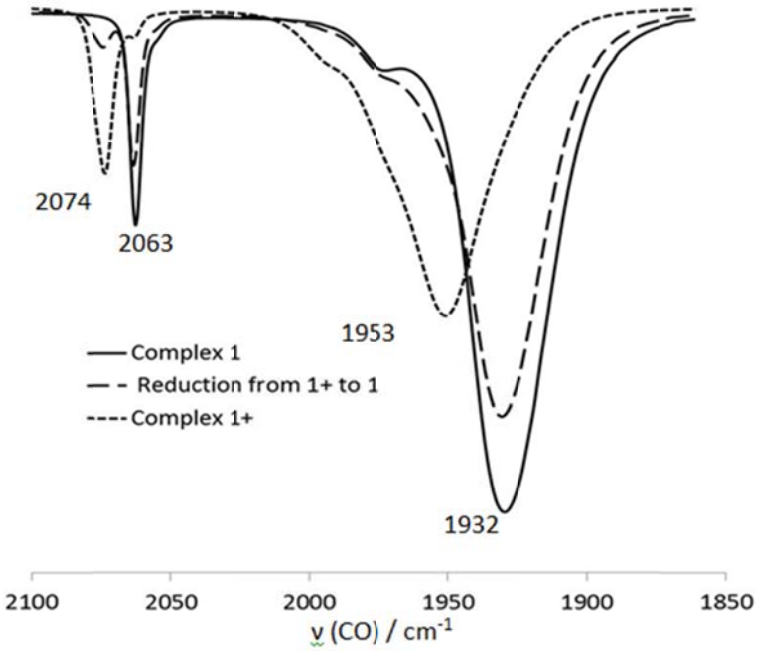

Figure 5.2 IR spectra demonstrating the carbonyl vibrations observed for complexes **1**, **[1$^+$]•PF$_6$** and the regeneration of **1**.

Electrochemistry and computational analyses

Cyclic voltammetry (CV), linear sweep voltammetry (LSV), and Osteryoung Square Wave voltammetry (SW) were first conducted on 0.5 mmol·dm^{-3} solutions of **1** – **4** in dry, oxygen-free CH_2Cl_2 utilizing 0.1 mol·dm^{-3} [N(^{n}Bu)$_4$][PF$_6$] as supporting electrolyte. Data are summarized in Table 5.1, CV's are shown in Figures 5.4 - 5.6.

At far negative potentials, the carbene double bond of the mono-ethoxycarbene derivative **1** was reduced electrochemically reversibly (ΔE = 63 mV), but chemically irreversibly (i_{pa}/i_{pc} = 0.56) in a one-electron transfer redox process to a radical anion at $E^{o'}$ = ½(E_{pa} + E_{pc}) = -2.076 V vs. FcH/FcH$^+$ (Table 5.1, Figure 5.4). Electrochemical and chemical reversibility is theoretically characterized by peak potential differences of ΔE = E_{pa} – E_{pc} = 59 mV and current ratios i_{pa}/i_{pc} approaching unity.[25] As is usual for Fischer carbene complexes,[6] the LUMO of complex **1** is

mainly located at the p_z atomic orbital of the carbene carbon atom (Figure 5.3). Therefore, it should be expected that the one-electron reduction process should lead to the radical anion **1**$^{\cdot-}$ whose unpaired electron remains mainly located on that carbon atom. Indeed, the computed spin density on **1**$^{\cdot-}$ indicates a value of 0.57 e on the carbene carbon atom thus suggesting a $^{-}$W-C$^{\cdot}$ species as reduction product. The remaining electron density is mainly localized at the iron center (0.27e) which further confirms the orbital interaction between the ferrocenyl group and the carbene carbon atom.[22] Similar electron density was computed for the analogous $(CO)_5Cr{=}C(OEt)Fc$ carbene complex at the same level of theory (0.57e at the carbene carbon atom), thus indicating that the one-electron reduction process is similar in both types of complexes.

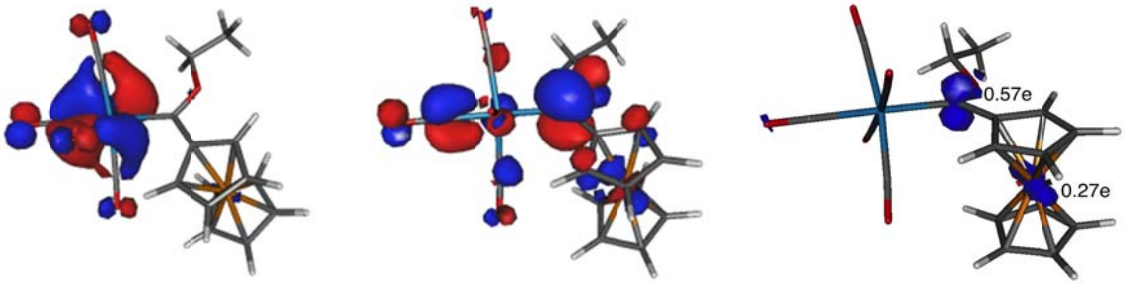

HOMO (1) **LUMO (1)** **1**$^{\cdot-}$

Figure 5.3 Frontier Molecular Orbitals of **1** and computed spin density on **1**$^{\cdot-}$.

The bisethoxy complex **2** exhibited two W=C reductions at waves I_a and I_b in the CV's shown in Figure 5.4 to $^{-}$W-C$^{\cdot}$ with formal reductions potentials being separated by $\Delta E^{o'} = E^{o'}_{\text{wave Ib}} - E^{o'}_{\text{wave Ia}} = 433$ mV. This relatively large separation in reduction potentials illustrates noticeable interactions between the two carbene moieties and leads to the general reductive scheme shown in equation 1. The first carbene reduction associated with wave I_a is electrochemically reversible but the second is not (Figure 5.4 and Table 5.1).

$$\mathbf{2}^{2\bullet,2-} \underset{+e^-}{\overset{\text{wave } I_b}{\longleftarrow}} \mathbf{2}^{\bullet,-} \underset{+e^-}{\overset{\text{wave } I_a \; -e^-}{\rightleftharpoons}} \mathbf{2} \qquad (1)$$

The radical anion notation in equation 1 is explained by noting that $\mathbf{2}^{\bullet -}$ = [(CO)$_5$(¯W-C$^{\bullet}$)(OEt)-Fc′-(OEt)C=W(CO)$_5$]. Different reduction potentials for symmetrical complexes in which mixed-valent intermediates are generated (for **2,** this refers to $\mathbf{2}^{\bullet -}$) are well known in systems that allow some form of electronic interaction between the redox centers; these may include electrostatic or through-bond conjugated paths.[26]

In contrast to the OEt derivatives **1** and **2**, the new NHBu monocarbene **3** showed no carbene reduction within the potential window of the solvent in the presence of [N(^{n}Bu)$_4$][PF$_6$]. This agrees with the computed energy of the corresponding LUMO (-2.64 and -2.25 eV for **1** and **3**, respectively) which suggests that the less negative energy of the LUMO of **3** is translated into a more negative reduction potential. The biscarbene-NHPr derivative **4**, showed a single carbene reduction at -2.293 V in the CV at wave I (Figure 5.4), but the current was more than four times (3.71/0.90) larger than that expected for a one-electron transfer processes. A one-electron transfer process in this system requires ½[i(wave Fc+1a)/4+i(wave 1b)/3] = 0.90 µA. The large observed current (3.71 µA) is thought to be due to significant amounts of substrate being deposited on the surface of the electrode during reduction but because this wave is close to the potential at which cathodic discharge caused by solvent reduction takes place, the large increase in current may also originate from an E_rC_{cat} process by which **4** catalyses the reduction of CH_2Cl_2. A repeat experiment utilizing **4** as analyte in CH_3CN as solvent (Figure S3, Appendix 4a, Table 5.1) confirmed the second carbene moiety is reduced at a potential ca. 0.27 V lower than the first. This observation also suggests some form of electronic interaction between two carbene moieties observed for **2** but completely contrasts the observations described for the chromium complex [(CO)$_5$Cr=C(OEt)-Fc′-(OEt)C=Cr(CO)$_5$].[10,11] For this analogous Cr carbene complex, under the same experimental conditions, no splitting of Cr=C carbene reduction into two components “a” and “b” could be detected. Very few studies describe the electrochemical reduction of the W=C double bond,[14] although the *in situ* generation of the radical anion by chemical single electron transfer agents have been reported.[27] Consistent with NHR (R = Bu, Pr) being a more powerful electron-donating group than OEt, the NHPr group shifted the wave I_a peak cathodic potential, E_{pc}, of the bis W=C species **4** compared to **2** with $\Delta E_{pc} = E_{pc,\ OEt,\ \mathbf{2}} - E_{pc,\ NHBu,\ \mathbf{4}} = -1.773 - (-2.293) = 0.520$ to more negative potentials.

The next redox process observed for **1 – 4** is the chemically and electrochemically one-electron reversible oxidation of ferrocene which is associated with wave Fc in Figure's 5.4 – 5.6, and Table 5.1. The Fc wave in these CV's is followed by the W oxidation processes (wave 1) which in CH_2Cl_2 / $[(^nBu_4)N][PF_6]$ involves a three-electron transfer process (Figure 5.4). This oxidation of the ferrocenyl group in tungsten carbenes at lower potentials than that of W oxidation contrasts with the behavior of the analogues chromium carbenes $[(OC)_5Cr=C(Fc)(OEt)]$ and $[(OC)_5Cr=C(OEt)\text{-}Fc'\text{-}(OEt)C=Cr(CO)_5]$ where the ferrocenyl group was oxidized *after* oxidation of the Cr(0) center to Cr(I).[10,11] The second oxidation of Cr(I) to Cr(II) follows after the ferrocenyl oxidation, and also contrasts with the three-electron closely-overlapping W oxidation under the same experimental conditions. The resolution between Fc and tungsten (wave 1) oxidation processes, expressed as $\Delta E_{pa} = E_{pa,\ W} - E_{pa,\ Fc}$, is better in mono- than in biscarbene tungsten complexes, and also in OEt than in NHR complexes. For **4**, the Fc wave was superimposed onto a W-oxidation wave (Figure 5.4).

An important consequence of the ferrocenyl moiety being oxidized before the W center is that when the W center is oxidized, it is under the influence of the ferrocenium species, Fc^+, which is almost as electron-withdrawing as a CF_3 group ($\chi_{Fc} = 2.82$; $\chi_{CF3} = 3.01$).[21] This shifts the W redox process to more positive potentials than would be expected for other compounds where the linking group is not so strongly electron-withdrawing, e.g. for $-CH_2-$. The one-electron ferrocenyl oxidation process was useful to identify the number of electrons that is transferred during tungsten oxidation.

Tungsten oxidation is associated with wave 1 in Figures 5.4 – 5.6 and Table 5.1. Since the peak anodic current ratio between wave Fc and wave 1 in the CV of **1** was 10.01/3.38 = 2.96 = 3, indications are that W(0) is oxidized irreversibly (no i_{pc} detected) in three consecutive and overlapping one-electron transfer steps, apparently to a W(III) species (Figure 5.4, Table 5.1).

Table 5.1. Cyclic voltammetry data of 0.5 mmol·dm^{-3} solutions of the monocarbene [(OC)$_5$W=C(Fc)(X)] complexes **1** and **3** and biscarbene [(OC)$_5$W=C(X)-Fc'-(X)C=W(CO)$_5$] complexes **2** and **4** in CH_2Cl_2 containing 0.1 mol·dm^{-3} [N(^{n}Bu)$_4$][PF$_6$] or 0.2 mol·dm^{-3} [N(^{n}Bu)$_4$][B(C$_6$F$_5$)$_4$] as supporting electrolyte at a scan rate of 100 mV s^{-1} and 20 °C. Potentials are relative to the FcH/FcH$^+$ couple.

Complex	Peak no.	i_{pa}/μA, i_{pc}/i_{pa} [N(^{n}Bu)$_4$][PF$_6$]	$E^{o'}$/V, ΔE/mV [N(^{n}Bu)$_4$][PF$_6$]	$E^{o'}$/V, ΔE/mV [N(^{n}Bu)$_4$][B(C$_6$F$_5$)$_4$]	i_{pa}/μA, i_{pc}/i_{pa} [N(^{n}Bu)$_4$][B(C$_6$F$_5$)$_4$]
1, Fc	I(=)	3.23,[b] 0.56	-2.076, 63	-2.119, 100	7.02,[b] 0.71
X = OEt	(Fc)	3.38, 0.85	0.285, 90	0.307, 82	5.61 0.93
	1(W$^{0/III}$)	10.01, -	0.809,[d] -	(W$^{0/II}$)1.105,[d,i] -	11.58, -
2, Fc'	D[f]	0.76,[b] -	-2.409,[c] -		
X = OEt	Ib(=)	1.64,[b] -	-2.206,[c] -	-2.222,[c] -	2.80,[b] -
	Ia(=)	1.73,[b] 0.40	-1.773, 67	-1.811, 74	3.02,[b] 0.51
	(Fc)	1.62, 0.84	0.510, 86	0.513, 82	2.82, 0.64
	1(2xW$^{0/III}$)	9.56, 0.15	0.766, 142	(2xW$^{0/II}$) 0.922,[i] -	(2xW$^{0/II}$) 9.99, -
3, Fc	I(=)	-[a], -[a]	-[a], -[a]	-2.580,[c] -	9.71,[b] -
X =NHBu	(Fc)	2.67, 0.88	0.206, 92	0.289, 80	4.23, 0.67
	1(W$^{0/III}$)	7.94, 0.11	0.611, 293	(W$^{0/II}$) 0.950,[d,i] -	(W$^{0/II}$) 8.10,[d] -
4, Fc'	I(=)	3.71,[b] -	-2.293,[c] -	-2.285,[c] -	6.84[b], -
X = NHPr	(Fc)+1$_a$(W$^{0/1II}$)	3.53, -	0.540,[e,h] -	(Fc)+1$_a$(W$^{0/1II}$)	7.20, -
	1$_b$(W$^{0/III}$)	2.76, -	0.591,[d] -	0.580,[d,e,h] -	(2xW$^{0/II}$)
	D[f]	0.55, -	1.000,[d] -	(1$_b$ W$^{0/II}$) 0.792,[d,i] -	5.45, -
4,[g] Fc'	I$_b$(=)	1.30[b], -	-2.458,[c] -		
X = NHPr	I$_a$(=)	3.38[b], -	-2.185,[c] -		
CH_3CN[g]	(Fc)+1$_a$(W$^{0/1II}$)[i]	3.40, 0.31	0.408, 80		
	1$_b$(W$^{0/III}$)[i]	4.69, 0.21	0.745, 100		

(a) No peak detected within the solvent potential window; (b) i_{pc} and i_{pa}/i_{pc} values to maintain the current ratio convention of i(forward scan)/i(reverse scan); (c) E_{pc} value, no E_{pa} detected. (d) E_{pa} value, no E_{pc} detected; (e) Estimations only; (f) Peaks labeled "D" represent decomposition processes of either the $^-$W-C· radical anions that was generated at the redox processes labeled "I" or of W(III) generated at wave "1b"; (g) The supporting electrolyte changed to BARF = [NBu$_4$][B(C$_6$F$_5$)$_4$] (0.2 mol·dm^{-3}) or the solvent changed to CH_3CN; (h) a very weak Fc reduction peak was observed at E_{pc} = 0.357, i_{pa} = 0.3 μA. In the presence of [NBu$_4$][B(C$_6$F$_5$)$_4$] a much stronger Fc reduction wave was observed at E_{pa} = 0.497, i_{pa} = 3.75 μA. (i) In the presence of [NBu$_4$][B(C$_6$F$_5$)$_4$] (0.2 mol·dm^{-3}) W oxidation is a two-electron transfer process, while in the presence of CH_3CN, or [N(^{n}Bu)$_4$][PF$_6$] it is a three-electron transfer process.

This contrasts a study by Maiorana and co-workers who reported a few years ago that W in $[(OC)_5W{=}C(CH_3)(X)]$ with X = substituted morpholino and other amine derivatives undergo a two-electron oxidation in CH_2Cl_2 in the presence of 0.1 mol·dm^{-3} $[(^nBu_4)N][ClO_4]$ as supporting electrolyte.[13] Figure 5.5 highlights the CV's of **1** at different scan rates, and more importantly, the LSV at 1mV·s^{-1}. The LSV was mutually consistent with CV i_{pa} current ratios between wave Fc and wave 1 at scan rates of 100, 200, 300, 400 and 500 mV·s^{-1} in indicating that the total W oxidation involves the flow of three electrons. With our observation of a three-electron transfer W oxidation, it follows that in the biscarbene **2**, possessing two tungsten centers, a total of six electrons being transferred during tungsten oxidation should be observed. This was confirmed by the measured i_{pa} values (Figure 5.4, $i_{pa,wave\ 1}/i_{pa,wave\ Fc}$ = 9.56/1.62 = 5.90 ≈ 6, Table 5.1). Although the CV of **2** showed electronic interactions between the two carbene double bond centers by means of the splitting of wave I into two components "a" and "b", no resolution between the irreversible oxidations of the two W centers of **2** could be detected (Figure 5.4). However, a very weak reduction of oxidized W was detected at wave 1_r during the cathodic sweep, Figure 5.4, Table 5.1. The current was, however, small with i_{pc}/i_{pa} = 0.15; ΔE = 143 mV.

An LSV of **2** (Figure S1, Appendix 4a) showed that the oxidation of the second tungsten center results in a species that is unstable on LSV time scale. Only the first 3-electron oxidation could be detected before compound decomposition took place. The peak anodic current of wave 1 in the CV of the mono NHBu tungsten carbene **3** also estimates a three electron transfer step during W oxidations but the LSV shown in Figure 5.4 highlights new information. On LSV timescale, the first two electrons during W oxidation are transferred fast in two unresolved one-electron redox processes, but the different slope observed for the third electron that was transferred shows this redox step to be slower than the first two electron transfer steps. The LSV splitting of wave 1 (W-oxidation) into two components "a" (a two electron process) and "b" (a one-electron process) for **3** allows for a meaningful comparison with chromium carbene analogues $[(OC)_5Cr{=}C(XR)(Ar)]$ and $[(OC)_5Cr{=}C(XR)\text{-}Ar'\text{-}(XR)C{=}Cr(CO)_5]$ with XR = OEt , NHBu or NHPr and Ar or Ar' = thienyl, furyl or ferrocenyl.[10,11] In these Cr carbene derivatives, Cr(0) is oxidized in two separate one-electron transfer steps and exhibits $\Delta E_{pa} = E_{pa,Cr(I/II)} - E_{pa,Cr(0/I)}$ peak potential separations larger than 0.5 V.[10,11] For the present W-series, indications are that W(0) is first oxidized in a two electron step followed by a second one-electron oxidation. In all

compounds studied, these steps overlap on CV timescale, but on LSV timescale, for **3**, ΔE_{pa} = $E_{pa,W(II/III)}$ - $E_{pa,W(0/II)}$ peak separations are estimated from Figure 5.4 to be approximately 90 mV.

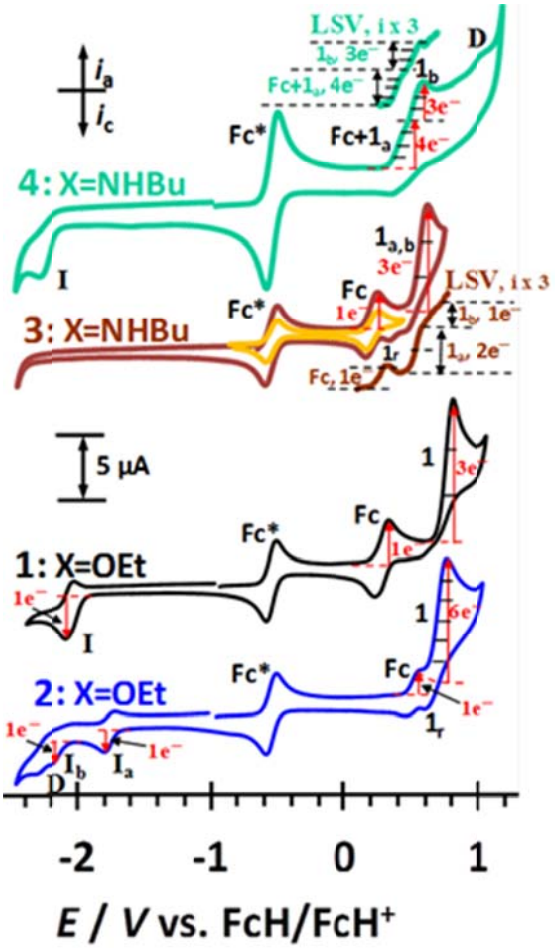

Figure 5.4 CV's of 0.5 mmol.dm^{-3} solutions of the monocarbene $[(OC)_5W=C(Fc)(XR)]$ complexes **1** (black) and **3** (brown) and biscarbene complexes $[(OC)_5W=C(XR)\text{-}Fc'\text{-}(XR)C=W(CO)_5]$ **2** (blue) and **4** (green) in CH_2Cl_2 containing 0.1 mol.dm^{-3} $[N(^nBu)_4][PF_6]$ as supporting electrolyte at a scan rate of 100 mV s^{-1} and 20 ^oC. LSV's are also shown for **3** and **4**. Fc* = decamethylferrocene = internal standard. Under these conditions, each W center is ultimately involved in a three-electron transfer redox process.

A small cathodic peak associated with wave 1 was also observed for **3** at wave 1_r but again irreversible W oxidation was implied by virtue of i_{pc}/i_{pa} = 0.11 and ΔE = 293 mV. The CV's of

the NHBu biscarbene **4** showed oxidation of the ferrocenyl group and one of the two W centers occurred simultaneously. For **4**, the oxidation of the second W center was resolved from the first by ca. $\Delta E_{pa} = E_{pa,\ wave\ (1b+Fc)} - E_{pa,\ wave\ 1a} = 51$ mV. The ratio $i_{pa,\ wave\ (1b+Fc)} : i_{pa,\ wave\ 1a}$ in the CV as well as the LSV (Figure 5.4) was found to be 4:3 which again showed W oxidation involves three electrons.

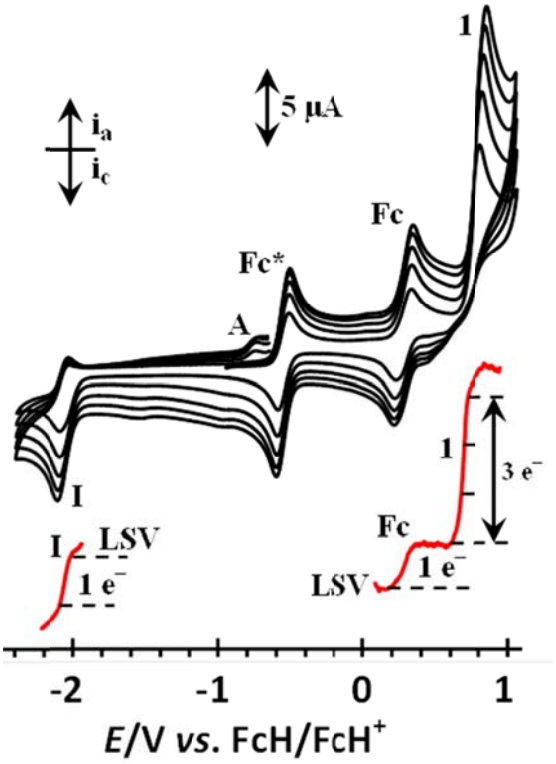

Figure 5.5 CV's of 0.5 mmol·dm^{-3} solutions of the [(OC)$_5$W=C(Fc)(OEt)], **1**, in CH_2Cl_2 containing 0.1 mol·dm^{-3} [N(^{n}Bu)$_4$][PF$_6$] as supporting electrolyte at a scan rate of 100 (smallest currents), 200, 300, 400 and 500 mV·s^{-1} and 20 °C. The LSV's show that the W center is involved in a three-electron transfer redox process, while both the ferrocenyl group and the carbene double bond involves one-electron flow. Fc* = decamethylferrocene. A = decomposition product peak.

To understand why our results indicating an irreversible three-electron W(0) oxidation differed from those of Maiorana, who observed a two-electron W oxidation,[13] complexes **1** – **4** were also studied under different conditions utilizing first 0.1 mol·dm^{-3} [(^{n}Bu$_4$)N][B(C$_6$F$_5$)$_4$] as supporting electrolyte, see Table 5.1 for electrochemical data. The Geiger electrolyte, [(^{n}Bu$_4$)N][B(C$_6$F$_5$)$_4$],

is known to minimize ion pair formations of the type $(cation)^{+\cdots\cdots-}[B(C_6F_5)_4]$ where $(cation)^+$ represents any electrochemically generated cation. Such ion pair formations frequently cause oxidation potentials of cationic species to move to different values.[28] In addition, use of this electrolyte allows the observation of unstable intermediate redox states of, for example, the ruthenocenium species $[Ru^{III}(C_5H_5)_2]^+$. [29] Use of other solvents or electrolytes invariably causes over oxidation of ruthenocene to a Ru(IV) species.[30]

Figure 5.6 shows a CV and LSV's of **2** utilizing 0.1 mol·dm^{-3} $[(^nBu_4)N][B(C_6F_5)_4]$ as supporting electrolyte. The first obvious difference is that in CH_2Cl_2, but in the presence of $[(^nBu_4)N][B(C_6F_5)_4]$ as supporting electrolyte, resolution between the ferrocenyl oxidation and the two overlapping W(0) oxidations are markedly increased. The differences in the oxidation potentials of these two processes are $\Delta E^{o\prime} = E_{pa,W(0)\ oxd,\ 1} - E_{pa,Fc\ oxd} = 284$ mV in CH_2Cl_2 containing $[(^nBu_4)N][PF_6]$ and 368 mV in CH_2Cl_2 containing $[(^nBu_4)N][B(C_6F_5)_4]$. More importantly, the LSV as well as i_{pa} current ratios for waves Fc and 1 in the presence of $[(^nBu_4)N][B(C_6F_5)_4]$, shows a two-electron tungsten oxidation, the same as reported by Maiorana.[13] All the other complexes in the present compound series **1** – **4** also showed the two-electron $W^{0/II}$ couple when the supporting electrolyte was $[(^nBu_4)N][B(C_6F_5)_4]$, see Table 5.1 and Figures S3 and S4 (Appendix 4a).

An additional experiment utilizing CH_3CN as solvent was also performed on **4** because the coordination power of acetonitrile (Gutmann donor number = 14.1, while for CH_2Cl_2 it is ranges from 0 to 1)[31,32] frequently leads to interactions with cationic species. This results in different oxidation potentials, or even differences in the number of electrons being transferred during redox processes. Such solvent effects are highlighted by the electrochemical oxidation of, for example, Rh^I(β-diketonato)(CO)(PPh_3)] in a one-electron transfer process to a Rh(II) species in CH_2Cl_2 / $[(^nBu_4)N][BF_4]$,[33] but in a two-electron transfer process to a Rh(III) species in CH_3CN / $[(^nBu_4)N][PF_6]$.[34] Potential referencing in different solvents and electrolytes has to be made with care. Results in this work are referenced to FcH/FcH^+ as required by IUPAC, but the internal standard was not free ferrocene to prevent peak overlaps with **1 – 4**. Hence decamethylferrocene, Fc^* was used as internal standard and potentials was thereafter adjusted to be versus FcH/FcH^+. Under our conditions the formal reduction potential of Fc* vs. FcH/FcH^+ is -550 mV in CH_2Cl_2 / $[(^nBu_4)N][PF_6]$, -610 mV in CH_2Cl_2 / $[(^nBu_4)N][B(C_6F_5)_4]$ and -510 mV in CH_3CN /

[(^{n}Bu$_4$)N][PF$_6$].[35] It was found that in CH$_3$CN, **4** tungsten(0) oxidation is also a three electron transfer process, See Table 5.1 and Figure S3, Appendix 4a.

Scheme 5.2 shows the observed redox processes of **2** in the presence of [(^{n}Bu$_4$)N][PF$_6$]. This electrochemical scheme would also fit **4** if wave 1 is split into an "a" and "b" component. The monocarbene complexes **1** and **3** would fit the scheme if waves I_a and/or I_b are removed as required, and if wave 1 for **2** is rewritten to accommodate only one three electron transfer process rather than two. In the presence of [(^{n}Bu$_4$)N][B(C$_6$F$_5$)$_4$], the scheme would fit if the three-electron $W^{0/III}$ coupled is replaced with a two-electron $W^{0/II}$ couple.

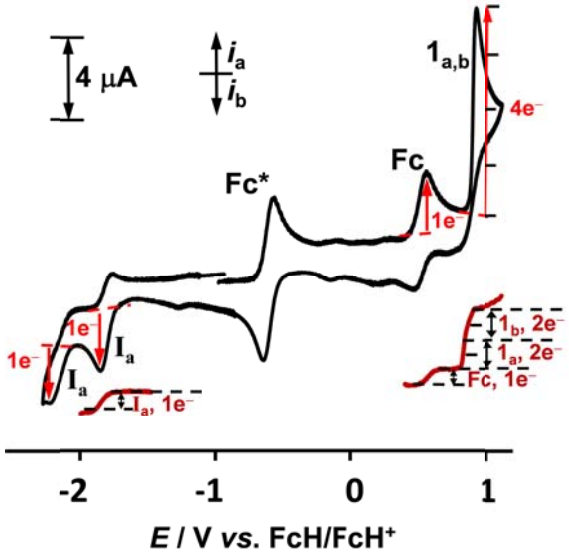

Figure 5.6 CV and LSV (brown curves) at 20 °C of 0.5 mmol·dm^{-3} solutions of **2** in CH$_2$Cl$_2$ / 0.2 mol·dm^{-3} [N(^{n}Bu)$_4$][B(C$_6$F$_5$)$_4$]. The number of electrons involved in each redox process is indicated next to the relevant waves. Each W is oxidized in a two-electron transfer process in this medium. Fc* = decamethylferrocene.

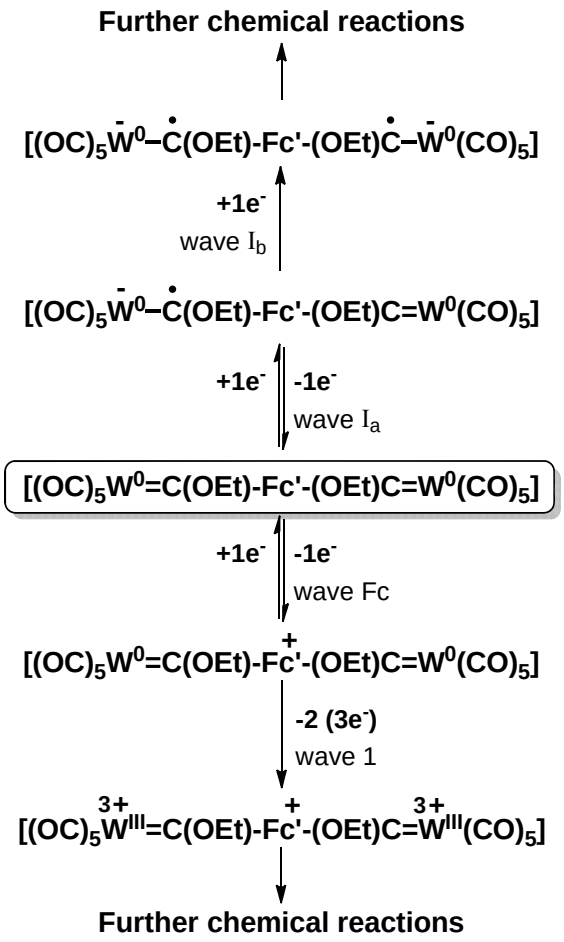

Scheme 5.2 Electrochemical reactions associated with **2**. Both the final reduction product possessing $^{-}$W-C$^{\bullet}$ radical anions and the final oxidation product possessing two W(III) centers are highly reactive and undergo further chemical decomposition reactions.

The above described redox processes were finally addressed by means of a computational-DFT study. As shown in Figure 5.7, complex **1** is electrochemically oxidized to radical cation **1**$^{\cdot +}$**.** The computed spin density of this species indicates that the unpaired electron is located at the iron atom (1.26e), thus confirming that the first one-electron oxidation does not involve the tungsten center but the Fe(II) to Fe(III) reaction.

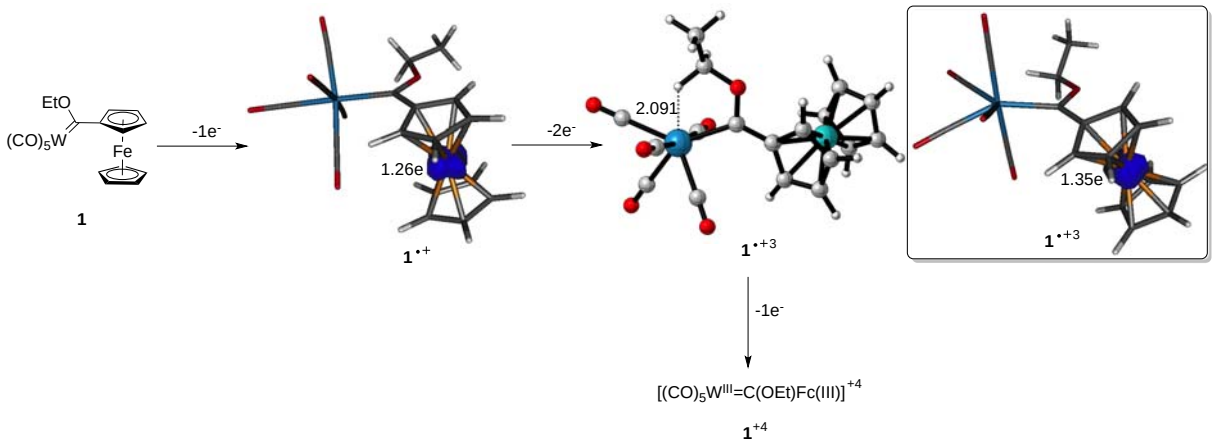

Figure 5.7 Computed oxidation process of complex **1** at the B3LYP/def2-SVP level. W···H bond distance in $\mathbf{1}^{\bullet+3}$ is given in angstroms.

Subsequent 2-electron oxidation leads to the trication $\mathbf{1}^{\bullet+3}$ whose unpaired electron remains at the iron atom (computed electron density on Fe of 1.35e). This indicates that the oxidation process involves the W(0) to W(II) reaction. As described above, the total three-electron tungsten oxidation process ends up with the third and final one-electron oxidation at the tungsten center (W(II) to W(III)) to form the corresponding tetracation $\mathbf{1}^{+4}$. Unfortunately, the structure of this open-shell singlet species (whose unpaired electrons are located at the iron and tungsten centers) could not be located on the potential energy surface (even using different functionals) due to convergence problems.

The structure of the trication $\mathbf{1}^{\bullet+3}$ deserves further analysis. As shown in Figure 5.7, a hydrogen atom of the ethoxy substituent is found in close proximity to the tungsten atom (W···H distance of 2.091 Å), pointing to possible C−H···W agostic interaction. Indeed, the Laplacian distribution of $\mathbf{1}^{\bullet+3}$ in the W···H−C plane (Figure 5.8) clearly reveals the occurrence of a bond critical point located between the transition metal and the hydrogen atom, which is associated with a bond path running between the corresponding two atoms. This proves the existence of a direct interaction between both atoms. Moreover, the computed value of 0.045 e·Å^{-3} for the electron density at the bond critical point, is in the range expected for CH agostic interactions.[36] The structure of this species resembles that found for oxidised products of related chromium(0) carbene complexes upon 2-electron oxidation of the transition metal.[11] This peculiar bonding

situation seems to be general for oxidized products of Fischer carbene complexes regardless of the transition metal involved and it implies the normal carbene structure is not retained after oxidation.

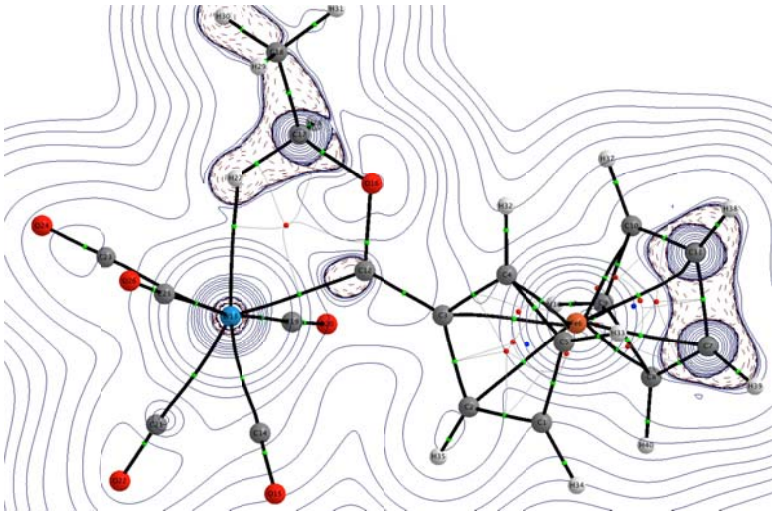

Figure 5.8 Contour line diagrams $\nabla^2\rho(r)$ for complex $\mathbf{1}^{\cdot+3}$ in the W−H−C plane. Solid lines indicate areas of charge concentration ($\nabla^2\rho(r) < 0$) while dashed lines show areas of charge depletion ($\nabla^2\rho(r) > 0$). The solid lines connecting the atomic nuclei are the bond paths while the small red spheres indicate the corresponding bond critical points. The solid lines separating the atomic basins indicate the zero-flux surfaces crossing the molecular plane.

5.3 CONCLUSION

Mono- and bis-ethoxycarbene and –butyl(or propyl)aminocarbene tungsten(0) complexes $[(CO)_5W{=}C(XR)Fc]$, **1** and **3**, and $[(CO)_5W{=}C(XR)\text{-}Fc'\text{-}(XR)C{=}W(CO)_5]$, **2** and **4** were prepared. For the aminocarbenes **3** and **4**, only the *syn*-rotamer possessing restricted rotation about the $C_{carbene}$-N bond was observed by ^{1}H NMR due to the steric bulk of the ferrocenyl carbene substituent. The chemically oxidized but short-lived ferrocenium complex $[\mathbf{1}^+]\bullet\mathbf{PF_6}$ was also synthesized. From an electrochemical study in CH_2Cl_2 / $[(^nBu_4)N][PF_6]$ it was found that the electron-rich carbene double bond functionality of all complexes were reduced from W=C to $^-$W-C• at potentials < –2.0 V vs FcH/FcH^+. This assignment was confirmed by DFT calculations, which indicate that the unpaired electron of the formed radical anion is mainly located on the carbene carbon atom. For the two biscarbene complexes **2** and **4**, reduction potentials of the two

W=C functionalities were resolved which is indicative of good interactions between the formally carbene double bonds. The ferrocenyl group was electrochemically reversibly oxidized before W oxidation at potentials $0.206 < E^{o'} < 0.540$ V vs FcH/FcH^+. These potentials were continuously more than 250 mV smaller than those measured for the analogues Cr compounds. Tungsten(0) was oxidized in three consecutive but unresolved one-electron transfer steps to a W(III) species in the presence of $[N(^nBu)_4][PF_6]$ as supporting electrolyte, or in CH_3CN as solvent. In CH_2Cl_2 containing $[(^nBu_4)N][B(C_6F_5)_4]$ as supporting electrolyte, tungsten(0) oxidation was found to be a two-electron transfer process. The structure of this tricationic W(II) species has been highlighted with DFT calculations. Complex **4** showed identifiable resolution between the oxidation of each W center. This also argued for a weak interaction between the two W centers. All redox assignments were mutually consistent with the computational data obtained at the DFT level, which suggest a peculiar bonding situation (i.e. stabilized by C−H···W agostic interaction) in the tricationic species formed upon the oxidation process which involves the W(0) to W(II) reaction.

5.4 EXPERIMENTAL SECTION

General Procedures.

All manipulations involving organometallic compounds made use of standard Schlenk techniques under inert atmosphere. Solvents were dried over sodium metal (hexane, thf and diethylether) and phosphorouspentoxide (CH_2Cl_2); and distilled under nitrogen gas prior to use. All chemicals were used as purchased without further purification unless stated otherwise. Triethyloxoniumtetrafluoroborate was prepared according to literature procedures.[17] Purification of complexes was done with column chromatography using silica gel 60 (0.0063-0.200 mm) as the stationary phase. NMR spectra were recorded on a Bruker AVANCE 500 spectrometer. ^1H NMR spectra were recorded at 500.139 MHz and ^{13}C NMR at 125.75 MHz. The signals of the deuterated solvent were used as a reference: ^1H $CDCl_3$ at 7.24 ppm and C_6D_6 at 7.15 ppm; ^{13}C $CDCl_3$ at 77.00 ppm and C_6D_6 128.00 ppm. IR spectra were recorded on a Perkin-Elmer Spectrum RXI FT-IR spectrophotometer in solvent (hexane or DCM) as indicated. Only the vibration bands in the carbonyl-stretching region (ca. 1600-2200 cm^{-1}) were recorded.

[(CO)$_5$W=C(OEt)Fc] (**1**) was prepared according to previously reported methods.[15]

[(CO)$_5$W=C(OEt)Fc′(OEt)C=W(CO)$_5$] (**2**)

Dilithioferrocene was prepared according to literature procedures:[16] to a solution of ferrocene (4 mmol, 0.74g) in hexane was added TMEDA (8.2 mmol, 1.23 mL) and *n*BuLi in hexane (8.2 mmol) and stirred while heating to 60°C. After formation of the orange precipitate, the solvent was removed *via* cannula filtration, and the precipitate redissolved in thf. W(CO)$_6$ (8 mmol, 2.81g) was added at -78°C, and stirred for 1 hour while allowing the reaction mixture to reach room temperature. The solvent thf was removed by reduced pressure and Et_3OBF_4 (8.2 mmol), dissolved in CH_2Cl_2, added at -30°C. After reaction completion, the solvent was evaporated. Column chromatography was used for purification and the dark red fraction collected. Yield: 2.65g (70%), black red crystals. Anal. Calcd for $W_2FeC_{26}H_{18}O_{12}$: C, 33.01; H, 1.92. Found: C, 31.98; H, 1.88. ^{1}H NMR ($CDCl_3$): δ 5.02 (m, 4H, H$_\alpha$), 4.89 (q, *J* = 7.0 Hz, 4H, C**H**$_2$CH$_3$), 4.81 (m, 4H, H$_ß$), 1.61 (t, *J* = 7.1 Hz, 6H, CH$_2$C**H**$_3$). ^{13}C NMR ($CDCl_3$): δ n.o. (C$_{carbene}$), 201.91 (*trans*-**C**O), 197.58 (*cis*-**C**O) , 98.82 (**C**$_{ipso}$) , 74.52 (C$_\alpha$), 69.15 (C$_\beta$) , 77.20 O**C**H$_2$), 14.12 (**C**H$_3$). IR (ν_{CO}, cm^{-1}, CH_2Cl_2): 2060 m (A″$_1$), 1978 w (B), 1935 vs (A′$_1$ overlap E).

[(CO)$_5$W=C(NHBu)Fc] (**3**)

A diethylether solution of **1** (2 mmol, 1.13 g) was stirred at room temperature (rt) and *n*-butylamine (2 mmol, 0.20 mL) was added. The color changed rapidly from dark red to deep yellow. Purification was performed using column chromatography and a 1:1 mixture of hexane/CH_2Cl_2 as eluent. Yield: 0.90g (76%), yellow solid. Anal. Calcd for $WFeC_{20}H_{19}NO_5$: C, 40.50; H, 3.24. Found: C, 40.23; H, 3.09. ^{1}H NMR (C_6D_6): δ 8.91 (s, 1H, N**H**), 4.24 (br, 2H, H$_\alpha$), 4.02 (br, 2H, H$_ß$), 3.86 (s, 5H, Cp), 3.53 (m, 2H, NC**H**$_2$), 1.35 (m, 2H, C**H**$_2$CH$_2$), 1.17 (m, 2H, CH$_2$C**H**$_2$), 0.78 (m, 3H, C**H**$_3$). ^{13}C NMR (C_6D_6): δ 249.14 (C$_{carbene}$), 203.27 (*trans*-**C**O), 199.27 (*cis*-**C**O) , 97.12 (**C**$_{ipso}$) , 71.12 (C$_\alpha$), 69.86 (C$_\beta$ overlap Cp), 54.95 (N**C**H$_2$), 31.54 (**C**H$_2$CH$_2$), 20.07 (CH$_2$**C**H$_2$), 13.72 (**C**H$_3$). IR (ν_{CO}, cm^{-1}, CH_2Cl_2): 2060 m (A″$_1$), 1966 w (B), 1922 vs (A′$_1$ overlap E).

[(CO)$_5$W=C(NHPr)Fc′(NHPr)C=W(CO)$_5$] (4)

Complex **2** (2 mmol, 1.89g) was dissolved in diethylether and *n*-propylamine (2 mmol, 0.16 mL) was added at rt. The color of the solution turned from dark red to deep yellow and volatiles were removed by reduced pressure. Purification was performed by employing column chromatography with a 1:1 hexane/CH_2Cl_2 solvent mixture.

Yield: 1.46g (75%), deep yellow crystals. Anal. Calcd for $W_2FeC_{28}H_{24}N_2O_{10}$: C, 34.59; H, 2.49. Found: C, 33.42; H, 2.35. ^{1}H NMR ($CDCl_3$): 8.96 (s, 2H, **H**N), 4.56 (m, 4H, H$_\alpha$), 4.48 (m, 4H, H$_ß$), 3.88 (m, 4H, NC**H**$_2$), 1.86 (h, *J* = 7.4 Hz, 4H, C**H**$_2$CH$_3$), 1.13 (t, *J* = 7.4 Hz, 6H, C**H**$_3$). ^{13}C NMR (CDCl3): 249.58(C$_{carbene}$), 202.81 (CO$_{trans}$), 198.45 (CO$_{cis}$), 99.19 (C$_{ipso}$), 72.23 (C$_\alpha$), 70.15(C$_ß$), 56.96 (HN**C**H$_2$), 23.01 (**C**H$_2$CH$_3$), 11.23 (**C**H$_3$). IR (ν_{CO}, cm^{-1}, CH_2Cl_2): 2060 m (A″$_1$), 1963 w (B), 1920 vs (A′$_1$ overlap E).

[(CO)$_5$W=C(OEt)Fc][PF$_6$] ([1$^+$]•PF$_6$)

Complex **1** (0.02g, 0.035 mmol) was dissolved in dichloromethane and cooled to -35^{o}C. Silver hexafluorophosphate (0.009g, 0.035 mmol) was added and the solution changed from red to deep brown. The cold bath was removed and the brown solution was stirred at RT for 10 min. Cannula filtration was used to separate solids from the solution. ^{31}P NMR (CD_2Cl_2): δ -149.63 (h, *J* = 716.9, 706.7 Hz); ^{19}F NMR (CD_2Cl_2): δ -85.38 (d, *J* = 967.0 Hz); IR (ν_{CO}, cm^{-1}, CH_2Cl_2): 2074 (A$_1$", m), 1996 (B, w), 1952 (A$_1$' overlap E, vs).

Electrochemistry

Cyclic voltammograms (CV's), square wave voltammograms (SW's) and linear sweep voltammograms (LSV's) were recorded on a Princeton Applied Research PARSTAT 2273 voltammograph running PowerSuite (Version 2.58) utilizing a standard three-electrode cell in a M Braun Lab Master SP glovebox filled with high purity argon (H_2O and O_2 < 5 ppm) as described before.[10,11] To establish whether the electrolyte used, [(^{n}Bu$_4$)N][PF$_6$], and also the solvent influenced the number of electrons transferred at the tungsten center, **4** was also studied in the presence of 0.2 mol dm^{-3} [(^{n}Bu$_4$)N][B(C$_6$F$_5$)$_4$][37] as supporting electrolyte and in CH_3CN as solvent. All electrode potentials are reported versus the ferrocene/ferrocenium redox couple (FcH/FcH$^+$, FcH = Fe(η^5-C$_5$H$_5$)$_2$, E$^{o'}$ = 0.00 V) as reference.[38] However, decamethylferrocene,

Fc*, was used as internal standard to prevent signal overlap with the ferrocenyl of **1** – **4**. Decamethylferrocene has a formal reduction potential of -550 mV versus free ferrocene with ΔE = 72 mV and i_{pc}/i_{pa} = 1 under the prevailing conditions utilizing CH_2Cl_2 / $[(^nBu_4)N][PF_6]$ as solvent / supporting electrolyte.[36] In the presence of $[(^nBu_4)N][B(C_6F_5)_4]$ as electrolyte, the decamethylferrocene potential moves to -610 mV versus free ferrocene, while in CH_3CN / $[(^nBu_4)N][PF_6]$ it moves to -510 mV.[36]

Computational details

Geometry optimizations without symmetry constraints were carried out using the Gaussian09 suite of programs[39] at the B3LYP (uB3LYP for open-shell species)[40] using the double-ζ plus polarization def2-SVP[41] basis set for all atoms. This protocol is denoted B3LYP/def2-SVP. All species were characterized by frequency calculations, and have a positive defined Hessian matrix indicating that they are minima on the potential energy surface.

All Atoms in Molecules (AIM)[42] results described in this work correspond to calculations performed at the B3LYP/6-31G(d)&WTBS level on the optimized geometries obtained at the B3LYP/def2-SVP level. The WTBS (well-tempered basis sets)[43], used herein to describe Fe and W, have been recommended for AIM calculations involving transition metals.[44] The topology of the ED was conducted using the AIMAll program package. [45]

5.5 ACKNOWLEDGMENT

This work is supported by the National Research Foundation, South Africa, (DIB, Grant number 76226; JCS, Grant number 81829), and by the Spanish MICINN and CAM (IF, Grants CTQ2010-20714-CO2-01/BQU, Consolider-Ingenio 2010, CSD2007-00006, S2009/PPQ-1634).

5.6 REFERENCES

(1) Pike A. R.; Ryder, L. C.; Horrocks, B. R.; Clegg, W.; Connolly, B. A.; Houlton, A. *Chem. Eur. J.* **2004**, *11*, 344-353.

(2) Spanig, F.; Kolvacs, C.; Hauke, F.; Ohlubo, K.; Fukuzumi, F.; Guldi, D. M.; Hirsch, A. *J. Am. Chem. Soc.* **2009**, *131*, 8180-8195.

(3) (a) Saravanakumar, D.; Sengottuvelan, N.; Narayanan, V.; Kandaswamy, M.; Varghese, T. L. *J. Appl. Polym. Sci.* **2011**, *119*, 2517-2524; (b) Jungbluth, H.; Lohmann, G. *Nachr. Chem. Tech. Lab*. **1999**, *47*, 534-538; (c) Swarts, P. J.; Immelman, M.; Lamprecht, G. J.; Greyling, S. E.; Swarts, J. C. *S. Afr. J. Chem.* **1997**, *50*, 208-216; (d) Shen, Q. L.; Shekhar, S.; Stambuli, J. P.; Hartwig, J. F. *Angew. Chem. Int. Ed.* **2005**, *44*, 1371-1375; (e) Conradie, J.; Swarts, J. C. *Organometallics*, **2009**, *28*, 1018-1026. (4) (a) Shago, R. F.; Swarts, J. C.; Kreft, E.; Van Rensburg, C. E. J. *Anticancer Res*. **2007**, *27*, 3431-3434; (b) Van Rensburg, C. E. J.; Kreft, E.; Swarts, J. C.; Dalrymple, S. R.; Macdonald, D. M.; Cooke, M. W.; Aquino, M. A. S. *Anticancer Res*. **2002**, *22*, 889-892. (c) Gross, A.; Hüsken, N.; Schur, J.; Raszeja, L.; Ott, I.; Metzler-Nolte, N. *Bioconjugate Chemistry*, **2012**, *23*, 1764-1774. (d) Swarts, J. C.; Vosloo, T. G.; Cronje, S. J.; Du Plessis, W. C.; Van Rensburg, C. E. J.; Kreft, E.; Van Lier, J. E. *Anticancer Res.* **2008**, *28*, 2781-2784; (e) Ott, I.; Kowalski, K.; Gust, R.; Maurer, J.; Mücke, P.; Winter, R. F. *Bioorg. Med. Chem. Lett.* **2010**, *20*, 866-869.

(5) Recent reviews on the chemistry and applications of Fischer carbenes include: (a) Wu, Y.-T.; Kurahashi, T.; De Meijere, A. *J. Organomet. Chem.* **2005**, *690*, 5900-5911; (b) Gómez-Gallego, M.; Mancheño, M. J.; Sierra, M. A. *Acc. Chem. Res*. **2005**, *38*, 44-53; (c) Sierra, M. A.; Gómez-Gallego, M.; Martínez-Ávarez, R. *Chem.–Eur. J.* **2007**, *13*, 736-744; (d) Sierra, M. A.; Fernández, I.; Cossío, F. P. *Chem. Commun*. **2008**, 4671-4682; (e) Dötz, K. H.; Stendel, J. *Chem. Rev*. **2009**, *109*, 3227-3274; (f) Herndon, J. W. *Coord. Chem. Rev*. **2010**, *254*, 103-194; (g) Fernández-Rodríguez, M. A.; García-García, P.; Aguilar, E. *Chem. Comm*. **2010**, *46*, 7670-7687; (h) Fernández, I.; Cossío, F. P.; Sierra, M. A. *Acc. Chem. Res.* **2011**, *44*, 479-490; (i) Bezuidenhout, D. I.; Lotz, S.; Liles, D. C.; Van der Westhuizen, B. *Coord. Chem. Rev.* **2012**, *256*, 479-524; (j) Fernández, I.; Sierra, M. A. *Top. Heterocycl. Chem*. **2013**, *30*, 65-84.

(6) Representative examples: (a) Cases, M.; Frenking, G.; Duran, M.; Solà, M. *Organometallics,* **2002**, *21*, 4182-4191; (b) Poater, J.; Cases, M.; Fradera, X.; Duran, M.; Solà, M. *Chem. Phys.*

2003, *294*, 129-139; (c) Fernández, I.; Cossío, F. P.; Arrieta, A.; Lecea, B.; Mancheño, M. J.; Sierra, M. A. *Organometallics* **2004**, *23,* 1065-1071; (d) Frenking, G.; Solà, M.; Vyboishchikov, S. F. *J. Organomet. Chem.* **2005**, *690*, 6178-6204; (e) Fernández, I.; Sierra, M. A.; Mancheño, M. J.; Gómez-Gallego, M.; Cossío, F. P. *Chem. Eur. J*. **2005**, *11*, 5988-5996; (f) Fernández, I.; Sierra, M. A.; Cossío, F. P. *J. Org. Chem.* **2008**, *73*, 2083-2089; (g) Valyaev, D. A.; Brousses, R.; Lugan, N.; Fernández, I.; Sierra, M. A. *Chem. Eur. J.* **2011**, *17*, 6602-6605; (h) Andrada, D. M.; Granados, A. M.; Solá, M.; Fernández, I. *Organometallics*, **2011**, *30*, 466-476.

(7) Connor, J. A.; Jones, E. M.; Lloyd, J. P. *J. Organomet. Chem.* **1970**, *24*, C20-C22.

(8) (a) Dötz, K. H.; Dietz, R.; Neugebauer, D. *Chem. Ber.* **1979**, *112*, 1486-1490; (b) Bennewits, J.; Nieger, M.; Lewall, B.; Dötz, K. H. *J. Organomet. Chem.* **2005**, *690*, 5892-5899.

(9) (a) Dötz, K. H. *Angew. Chem. Int. Ed. Engl*. **1975**, *14*, 644-645; (b) Wulff, W. D. in *Comprehensive Organic Synthesis*, Vol. 5 (Eds.: B. M. Trost, I. Fleming), Pergamon, Oxford, **1991**, p. 1065; (c) Minatti, A.; Dötz, K. H. *Top. Organomet. Chem*. **2004**, *13*, 123; (d) Waters, M. L.; Wulff, W. D. *Org. React*. **2008**, *70*, 121.

(10) Van der Westhuizen, B.; Swarts, P. J.; Strydom, I.; Liles, D. C.; Fernández, I.; Swarts, J. C.; Bezuidenhout, D. I. *Dalton Trans.* **2013**, *42*, 5367-5378.

(11) Van der Westhuizen, B.; Swarts, P. J.; Van Jaarsveld, L. M.; Liles, D. C.; Siegert, U.; Swarts, J. C.; Fernández, I.; Bezuidenhout, D. I. *Inorg. Chem.* **2013**, *52*, 6674-6684.

(12) (a) Bezuidenhout, D. I.; Van der Watt, E.; Liles, D. C.; Landman, M.; Lotz, S. *Organometallics*, **2008**, *27*, 2447-2456; (b) Bezuidenhout, D. I.; Lotz, S.; Landman, M.; Liles, D. C. *Inorg. Chem.* **2011**, *50*, 1521-1533.

(13) Baldoli, C.; Cerea, P.; Falciola, L.; Giannini, C.; Licandro, E.; Maiorana, S.; Mussini, P.; Perdicchia, D. *J. Organomet. Chem.* **2005**, *690*, 5777-5787.

(14) (a) Chu, G. M.; Fernández, I.; Sierra, M. A. *Chem. Eur. J*. **2013**, *19*, 5899-5908; (b) López-Alberca, M. P.; Mancheño, M. J.; Fernández, I.; Gómez-Gallego, M.; Sierra, M. A.; Hemmert, C.; Gornitzka, H. *Eur. J. Inorg. Chem.* **2011**, 842-849; (c) Bezuidenhout, D. I.; Barnard, W.; Van der Westhuizen, B.; Van der Watt, E.; Liles, D. C. *Dalton Trans.* **2011,** *40*, 1-11; (d) Schobert, R.; Kempe, R,; Schmalz, T.; Gmeiner, A. *J. Organomet. Chem.* **2006**, *691*, 859-868; (e) Pombeiro, A. J. L. *J. Organomet. Chem.* **2005**, *690*, 6021-6040; (f) Fernández, I.; Mancheño, M. J.; Gómez-Gallego, M.; Sierra, M. A. *Org. Lett*. **2003**, *5*, 1237-1240; (g) Jayaprakash, K. N.; Ray, P. C.; Matsuoka, I.; Bhadbhade, M. M.; Puranik, V. G.; Das, P. K.; Nishihara, H.; Sarkar,

A. *Organometallics* **1999**, *18*, 3851-3858; (h) Casey, C. P.; Albin, L. D.; Saeman, M. C.; Evans, D. H. *J. Organomet. Chem.* **1978**, *155*, C37-C40; (i) Lloyd, M. K.; McCleverty, J. A.; Orchard, D. G.; Connor, J. A.; Hall, M. B.; Hillier, I. H.; Jones, E. M.; McEwen, G. K. *J. Chem. Soc., Dalton* **1973**, 1743-1747.

(15) López-Cortés, J. G.; Contreras de la Cruz, L. F.; Ortega-Alfaro, M. C.; Toscano, R. A.; Alvarez-Toledano, C.; Rudler, H. *J. Organomet. Chem.* **2005**, *690*, 2229-2237.

(16) Sünkel, H.; Bernhartzeder, S. *J. Organomet. Chem*. **2011**, *696*, 1536-1540.

(17) Meerwein, H. *Org. Synth*. **1966**, *46*, 113–115.

(18) Inkpen, M. S.; Du, S.; Driver, M.; Albrecht, T.; Long, N. J. *Dalton Trans.* **2013**, *42*, 2813-2816.

(19) (a) Bezuidenhout, D. I.; Liles, D. C.; Van Rooyen, P. H.; Lotz, S. *J. Organomet. Chem*., **2007**, *692*, 774-783; (b) Klabunde, U.; Fischer, E. O. *J. Am. Chem. Soc*. **1967**, *89*, 7141-7142.

(20) (a) Post, E. W.; Watters, K. L. *Inorg. Chim. Acta,* **1978**, *26*, 29-36; (b) Moser, E.; Fischer, E. O. *J. Organomet. Chem.*, **1968**, *15*, 147-155.

(21) (a) Kemp, K. C.; Fourie, E.; Conradie, J.; Swarts, J. C. *Organometallics,* **2008**, *27*, 353-362; (b) Du Plessis, W. C.; Davis, W. L.; Cronje, S. J.; Swarts, J. C. *Inorg. Chim. Acta* **2001**, *314*, 97-104.

(22) Lage, M. L.; Fernández, I.; Mancheño, M. J.; Sierra, M. A. *Inorg. Chem.* **2008**, *47*, 5253-5258.

(23) Venkatasubbaiah, K.; Nowik, I.; Herber, R. H.; Jäkle, F. *Chem. Commun.* **2007**, 2154-2156.

(24) (a) Braterman, P. S. *Metal Carbonyl Spectra*; Academic Press Inc., London, **1975**, p 68. (b) Adams, D. M. *Metal-Ligand and Related Vibrations;* Edward Arnold Publishers Ltd., London, **1967**, p 98.

(25) (a) Gericke, H. J.; Barnard, N. I.; Erasmus, E.; Swarts, J. C.; Cook, M. J.; Aquino, M. A. S. *Inorg. Chim. Acta,* **2010**, *363*, 2222-2232; (b) Evans, D. H.; O'Connell, K. M.; Peterson, R. A.; Kelly, M. J. *J. Chem. Educ.*, **1983**, *60*, 290-293; *(c)* Kissinger, P. T.; Heineman, W. R. *J. Chem. Educ.* **1983**, *60*, 702-706. *(d)* Van Benschoten, J. J.; Lewis, J. Y.; Heineman, W. R. *J. Chem. Educ.*, **1983**, *60*, 772-776; *(e)* Mobbott, G. A. *J. Chem. Educ.*, **1983**, *60*, 697-702.

(26) Leading references are (a) Creutz, C.; Taube, H. *J. Am. Chem. Soc.* **1969**, *91*, 3988-3989. (b) Geiger, W. E.; Van Order, N.; Pierce, D. T.; Bitterwolf, T. E.; Reingold, A. L.; Chasteen, N. D. *Organometallics* **1991**, *10*, 2403-2411. (c) Van Order, N.; Geiger, W. E.; Bitterwolf, T. E.;

Reingold, A. L. *J. Am. Chem. Soc.* **1987**, *109*, 5680-5690. (d) Pierce, D. T.; Geiger, W. E. *Inorg. Chem.* **1994**, *33*, 373-381. (e) Cook, M. J.; Chambrier, I.; White, G. F.; Fourie, E.; Swarts, J. C. *Dalton Trans.* **2009**, 1136-1144.

(27) For a review, see: Sierra, M. A.; Gómez-Gallego, M.; Martínez-Álvarez, R. *Chem-Eur. J.* **2007**, *13*, 736-744.

(28) Leading publications demonstrating the influence and use of [(*n*Bu4)N][B(C6F5)4] and the complimentary role of associated *cations* with different charge densities may be found in (a) Barriere, F.; Kirss, R. U.; Geiger, W. E. *Organometallics* **2005**, *24*, 48-52 and references therein; (b) Hildebrandt, A.; Rüffer, T.; Erasmus, E.; Swarts, J. C.; Lang, H. *Organometallics* **2010**, *29*, 4900-4905; (c) Barriere, F.; Camire, N.; Geiger, W. E.; Mueller-Westerhoff, U. T.; Sanders, R. *J. Am. Chem. Soc.* **2002**, *124*, 7262-7263; (d) Barriere, F.; Geiger, W. E. *J. Am. Chem. Soc.* **2006**, *128*, 3980-3989; (e) Nafady, A.; Chin, T. T.; Geiger, W. E. *Organometallics* **2006** *25*, 1654-1663; (f) Chong, D. S.; Slote, J.; Geiger, W. E. *J. Electroanal. Chem.*, **2009**, *630*, 28-34.

(29) Swarts, J. C.; Nafady, A.; Roudebush, J. H.; Trupia, S.; Geiger, W. E. *Inorg. Chem.* **2009**, *48*, 2156-2165.

(30) Ruthenocene and osmocene behave quite similarly in that oxidation generates a Ru(IV) and Os(IV) species: (a) Watanabe, M.; Motoyama, I.; Takayama, T.; Sato, M. *J. Organomet. Chem.* **1997**, *549*, 13-23; (b) Watanabe, M.; Motoyama, I.; Shimoi, M.; Sano, H. *J. Organomet. Chem.* **1996**, *517*, 115-121; (c) Smith, T. P.; Iverson, D. J.; Droege, M. W.; Kwan, K. S.; Taube, H. *Inorg. Chem.* **1987**, *26*, 2882-2884.

(31) The donor number of CH2Cl2 is difficult to find in literature, it is always listed as an undetermined quantity. However, a Google search of the World Wide Web gave a value of 1, see http://www.stenutz.eu/chem/solv21.php. Leading references to Gutmann donor numbers include: (a) Gutmann, V. *Coord. Chem. Rev.*, **1976**, *18*, 225-255; (b) Gutmann, V. *The Donor-acceptor Approach to Molecular Interactions*, Plenum Press, New York, **1978**, p.20; (c) Huheey, J. E. *Inorganic Chemistry: Principles of structure and reactivity*, 3rd Ed., Harper, Cambridge, **1983**, p340.

(32) For a scale of donor numbers referenced to 1,2-dichloroethane, where CH2Cl2 has DN = 0 and MeCN has DN = 0.36, see: Reichardt, C. *Solvents and Solvent-Effects in Organic Chemistry,* 3rd Ed., Wiley-VCH, Weinheim, **2003**.

(33) Da Silva, M. F. C. G.; Trzeciak, A. M.; Ziolkowski, J. J.; Pombeiro, A. J. L. *J. Organomet. Chem.* **2001**, *620*, 174-181.

(34) (a) Conradie, J.; Swarts, J. C. *Eur. J. Inorg. Chem.* **2011**, 2439-2449; (b) Conradie, J.; Cameron, T. S.; Aquino, M. A. S.; Lamprecht, G. J.; Swarts, J. C. *Inorg. Chim. Acta* **2005**, 2530-2542.

(35) Leading references describing the electrochemical activity and behaviour of ferrocene and decamethylferrocene in a multitude of organic solvents are (a) Noviandri, I.; Brown, K. N.; Fleming, D. S.; Gulyas, P. T.; Lay, P. A.; Masters, A. F.; Phillips, L. *J. Phys. Chem. B* **1999**, *103*, 6713-6722; (b) Connelly, N. G.; Geiger, W. E. *Chem. Rev.* **1996**, *96*, 877-910; (c) Ruiz, J.; Astruc, D. *C.R. Acad. Sci.* (Paris), Ser. IIc 1, **1998**, 21-27; (d) Aranzaes, R. J.; Daniel, M. C.; Astruc, D. *Can. J. Chem.* **2006**, *84*, 288-299; (e) Fourie, E.; Swarts, J. C.; Chambrier, I.; Cook, M. J. *Dalton Trans.*, **2009**, 1145-1154.

(36) Lein, M. *Coord. Chem. Rev.* **2009**, *253*, 625-634.

(37) LeSuer, R. J.; Buttolph, C.; Geiger, W. E. *Anal. Chem.* **2004**, *76*, 6395-6401.

(38) (a) Gritzner, G.; Kuta, J. *Pure Appl. Chem.* **1984**, *56*, 461-466; (b) Gagne, R. R.; Koval, C. A.; Lisensky, G. C. *Inorg. Chem.* **1980**, *19*, 2854-2855.

(39) *Gaussian 09*, Revision B.1, Frisch, M. J.; Trucks, G. W.; Schlegel, H. B.; Scuseria, G. E.; Robb, M. A.; Cheeseman, J. R.; Scalmani, G.; Barone, V.; Mennucci, B.; Petersson, G. A.; Nakatsuji, H.; Caricato, M.; Li, X.; Hratchian, H. P.; Izmaylov, A. F.; Bloino, J.; Zheng, G.; Sonnenberg, J. L.; Hada, M.; Ehara, M.; Toyota, K.; Fukuda, R.; Hasegawa, J.; Ishida, M.; Nakajima, T.; Honda, Y.; Kitao, O.; Nakai, H.; Vreven, T.; Montgomery, Jr., J. A.; Peralta, J. E.; Ogliaro, F.; Bearpark, M.; Heyd, J. J.; Brothers, E.; Kudin, K. N.; Staroverov, V. N.; Kobayashi, R.; Normand, J.; Raghavachari, K.; Rendell, A.; Burant, J. C.; Iyengar, S. S.; Tomasi, J.; Cossi, M.; Rega, N.; Millam, N. J.; Klene, M.; Knox, J. E.; Cross, J. B.; Bakken, V.; Adamo, C.; Jaramillo, J.; Gomperts, R.; Stratmann, R. E.; Yazyev, O.; Austin, A. J.; Cammi, R.; Pomelli, C.; Ochterski, J. W.; Martin, R. L.; Morokuma, K.; Zakrzewski, V. G.; Voth, G. A.; Salvador, P.; Dannenberg, J. J.; Dapprich, S.; Daniels, A. D.; Farkas, Ö.; Foresman, J. B.; Ortiz, J. V.; Cioslowski, J.; Fox, D. J. Gaussian, Inc., Wallingford CT, **2009**.

(40) (a) Becke, A. D. *J. Chem. Phys.* **1993**, *98*, 5648-5652. (b) Lee, C.; Yang, W.; Parr, R. G. *Phys. Rev. B* **1988**, *37*, 785-789.

(41) Weigend, F.; Ahlrichs, R. *Phys. Chem. Chem. Phys.* **2005**, *7*, 3297-3305.

(42) Bader, R. F. W. *Atoms in Molecules. A Quantum Theory*; Oxford University Press: Oxford, U.K., **1990**.

(43) (a) Huzinaga, S.; Miguel, B. *Chem. Phys. Lett*. **1990**, *175*, 289-291. (b) Huzinaga, S.; Klobukowski, M. *Chem. Phys. Lett*. **1993**, *212*, 260-264.

(44) (a) Cabeza, J. A.; Van der Maelen, J. F.; García-Granda, S. *Organometallics* **2009**, *28*, 3666-3672. (b) Buil, M. L.; Esteruelas, M. A.; Fernández, I.; Izquierdo, S.; Oñate, E. *Organometallics* **2013**, *32*, 2744-2752.

(45) Keith, T. A. AIMAll, 2010, http://tkgristmill.com

CHAPTER 6

Metal–Metal Interaction in Fischer Carbene Complexes – A Study on Ferrocenyl and Biferrocenyl Tungsten Alkylidene Complexes

This chapter was published in Inorganic Chemistry. The format reflects the style set by the journal.

Belinda van der Westhuizen,[a] J. Matthäus Speck,[b] Marcus Korb,[b] Joachim Friedrich,[c] Daniela I. Bezuidenhout[a*] and Heinrich Lang[b*], *Inorg. Chem.*, **2013**, *52(24)*, 14255-14263. DOI:10.1021/ic402202w.

Author contributors

Synthetic work: Belinda van der Westhuizen

Cyclic voltammetry and data analysis: Matthäus Speck

Computational work: Joachim Friedrich

Crystallography: Marcus Korb

Article written, submitted and response to reviewers: Belinda van der Westhuizen, J. Matthäus Speck, Marcus Korb, Joachim Friedrich, Daniela I. Bezuidenhout and Heinrich Lang

[a] *Chemistry Department, University of Pretoria, Private Bag X20, Hatfield, 0028, South Africa. Fax: +27-(0)12-420-4687; Tel: +27-(0)12- 420-2626; E-mail: daniela.bezuidenhout@up.ac.za*
[b] *Technische Universität Chemnitz, Fakultät für Naturwissenschaften, Institut für Chemie, Anorganische Chemie, D-09107 Chemnitz, Germany.*
[c] *Technische Universität Chemnitz, Fakultät für Naturwissenschaften, Institut für Chemie, Theoretische Chemie, D-09107 Chemnitz, Germany.*

Supporting Information. UV-Vis/NIR spectra in dichloromethane and crystal structure details for **1** - **4** as well as calculated infrared spectra of **1** and $\mathbf{1}^{+}$ are given. This material is available free of charge via the Internet at http://pubs.acs.org. (**Appendix 5**)

ABSTRACT

A series of ferrocenyl (Fc = ferrocenyl; fc = ferrocen-1,1'-diyl) and biferrocenyl (Bfc = 1',1''-biferrocenyl; bfc = 1',1''-biferrocen-1,1'''diyl) mono- and biscarbene tungsten(0) complexes of the type $[(CO)_5W{=}C(OMe)R]$ (**1**, R = Fc; **3**, R = Bfc) and $[(CO)_5W{=}C(OMe)\text{-}R'\text{-}(OMe)C{=}W(CO)_5]$ (**2**, R' = fc; **4**, R' = bfc) were synthesized according to the classical synthetic methodology by reacting $W(CO)_6$ with LiR (R = Fc, fc, bfc), followed by a subsequent alkylation using methyl trifluoromethanesulfonate. Electrochemical investigations were carried out on these complexes to get a closer insight into the electronic properties of **1** - **4**. The ferrocenyl and biferrocenyl moieties in **1** – **4** show reversible one electron redox events. It was further found that the Fischer carbene unit is reducible in an electrochemical one electron transfer process. For the tungsten carbonyl moieties, irreversible oxidation processes were found. In addition, charge transfer studies were performed on **1** - **4** by the use of *in situ* UV-Vis-NIR and infrared spectroelectrochemical techniques. During the UV-Vis-NIR investigations typical low energy transitions for the mixed-valent biferrocenyl unit were found. A further observed high energy NIR absorption is attributed to a metal-metal charge transfer transition between the tungsten carbonyl fragment and the ferrocenyl/biferrocenyl group in the corresponding oxidized state, which can be described as class II systems according to Robin and Day. This assignment was verified by infrared spectroelectrochemical studies and is reported herein for the first time. The electrochemical investigations are supported by DFT calculations. The structural properties of **1** - **4** in the solid state were investigated by single-crystal X-ray diffraction studies showing no substituent effects on bond lengths and angles. The biferrocenyl derivatives exhibit *syn*-conformation of the ferrocenyl and carbene building blocks.

6.1 INTRODUCTION

Since the first synthesis of transition metal alkyidene complexes of type $(CO)_5M{=}C(OMe)R$ (M = Cr, W) by Fischer and Maasböl in the early-1960s, this family of compounds received popularity, as they are fascinating molecules and powerful tools in organic and organometallic chemistry.[1] The Dötz benzannulation reaction and the Aumann reaction procedure, a simple approach for metallaolefins, are examples of their varied application in chemistry.[2] By incorporating a ferrocenyl substituent with known applications in molecular sensors,[3] energy

transfer processes[4] and anti-cancer drugs,[5] the application of Fischer carbene complexes could be extended beyond their traditional use as ligands employed for organic transformations[6] and as auxiliary ligands in catalysis,[7] to design new push-pull systems with interesting non-linear optical (NLO) properties.[8]

It is well known that the ferrocenyl moiety as a redox-active group displays high stability in the neutral as well as oxidized state during one-electron transfer processes.[9] Such ferrocenyl systems are ideal for studying electronic interactions by applying electrochemical and spectroelectrochemical techniques; these are efficient instruments to investigate charge transfer transitions between the separated metal entities.[10] This phenomenon is almost unexplored in Fischer carbene complexes.[11] Moreover, studies in general concerning ferrocenyl- and biferrocenyl-functionalized Fischer carbene complexes are limited in the literature.[12,13]

We report herein the synthesis and characterization of a series of ferrocenyl (**1**, **2**) and biferrocenyl (**3**, **4**) tungsten(0) Fischer carbene complexes. Concerning the investigation of charge transfer transitions between the metallocenyl increments and the Fischer carbene units, the electrochemical and spectroelectrochemical properties of these species are discussed. These investigations are supported by computational studies.

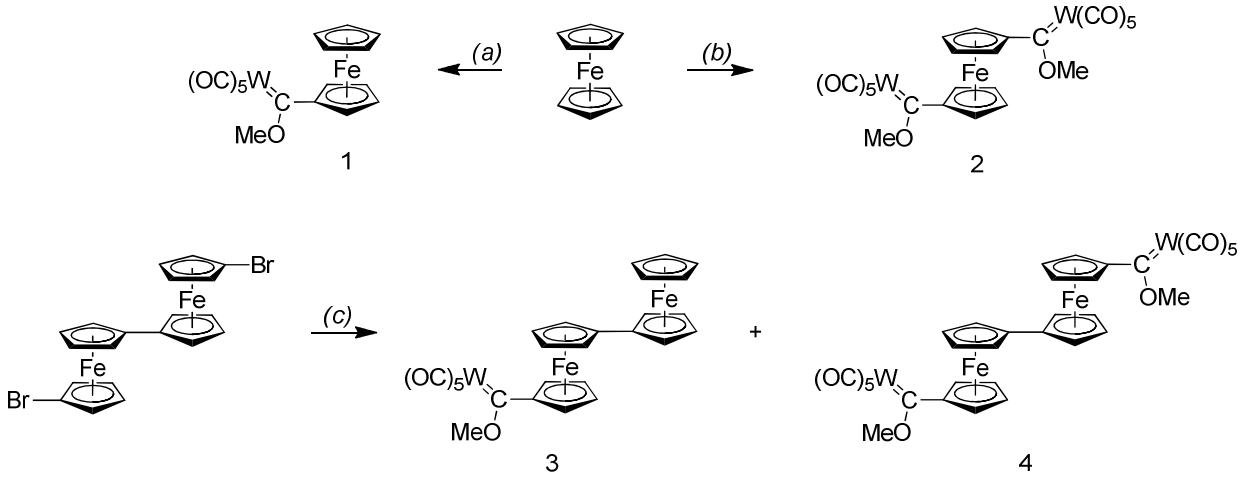

Scheme 6.1. Reaction conditions: (a) (i) tetrahydrofuran (thf), -80 °C, 1.06 eq ^{t}BuLi, 1 eq $W(CO)_6$; (ii) dichloromethane (CH_2Cl_2), -50 °C, 3 eq MeOTf. (b) (i) *n*-hexane, 2 eq ^{n}BuLi/TMEDA (1:1); (ii) thf, -60 °C, 2 eq $W(CO)_6$; (iii) CH_2Cl_2, -30 °C, 6 eq MeOTf. (c) (i) thf, -40 °C, 2.0 eq ^{n}BuLi; (ii) 2 eq $W(CO)_6$; (iii) CH_2Cl_2, -30 °C, 6 eq MeOTf.

6.2 RESULTS AND DISCUSSION

Synthesis and Characterization. The tungsten Fischer carbene complexes **1** – **4** were prepared using the classical Fischer carbene synthetic methodology in which $W(CO)_6$ was reacted with LiR (R = Fc, fc, bfc; Fc = ferrocenyl, fc = ferrocen-1,1'-diyl, bfc = 1',1''-biferrocen-1,1'''diyl) to form the corresponding metal acylate, followed by a subsequent alkylation via addition of methyl trifluoromethanesulfonate (MeOTf) (Scheme 6.1, Experimental Section). Complex **1** has been previously prepared,[14] although single x-ray diffraction data have not been reported.

The lithiated ferrocenyl/biferrocenyl species were generated *in situ* from ferrocene or dibromobiferrocene by lithiation or lithium-bromine exchange reaction according to literature procedures (Scheme 6.1). [15,16] After purification by column chromatography, complexes **1** - **4** could be isolated as deep red to dark maroon solids and are very stable in the solid state as well as in solution toward moisture and air.

Complexes **1** - **4** were characterized by elemental analysis, IR and NMR (^{1}H, ^{13}C{^{1}H}) spectroscopy, X-ray diffraction and mass spectrometry. Electronic effects of the carbene substituents can be followed in solution by IR and especially NMR spectroscopy. The electron withdrawing effect of the pentacarbonyl metal carbene moiety leads to a significant downfield shift of the resonances for the H_α protons (Figure 6.1) in **1** – **4** (4.80 – 5.00 ppm), compared to the value for ferrocene (4.15 ppm).[17] This is attributed to the π-delocalization of the aryl group in stabilizing the electrophilic carbene carbon atom, in addition to its inductive donating effect (Figure 6.1).

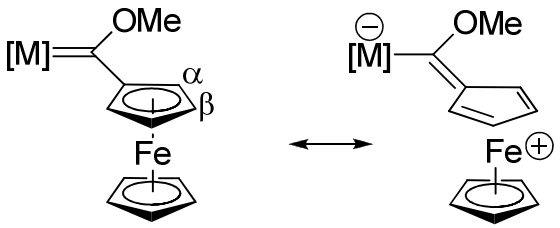

Figure 6.1. Stabilization of Fischer carbene complexes with a ferrocenyl group.

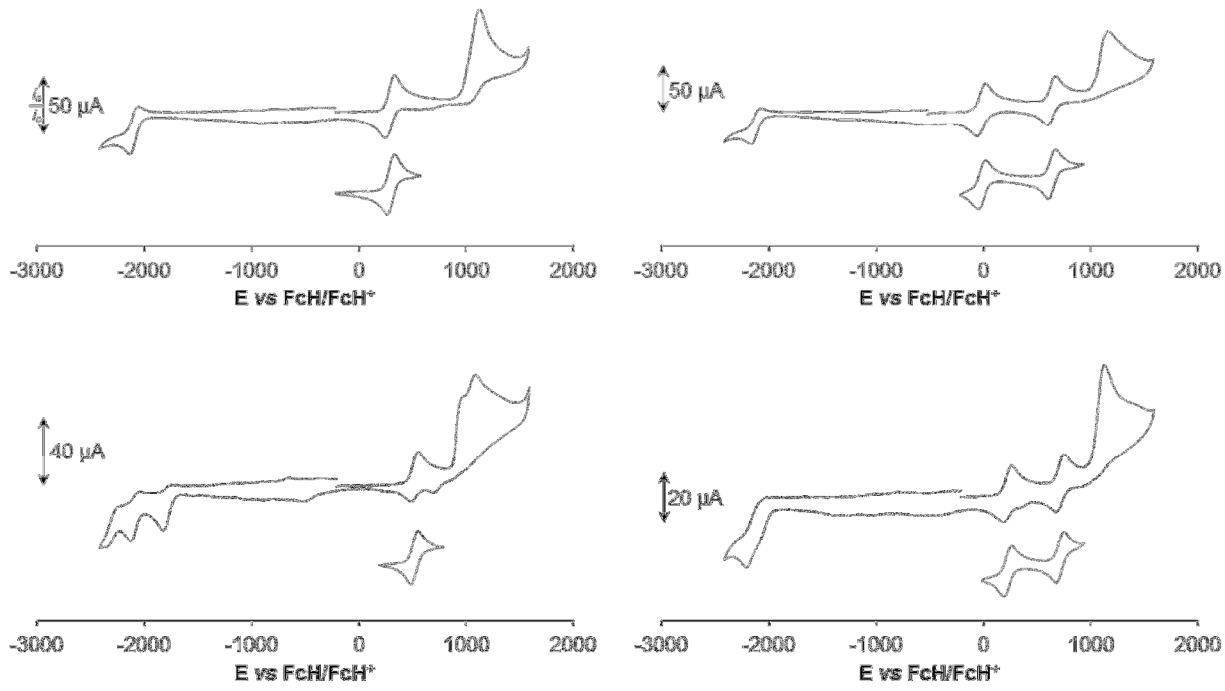

Figure 6.2 Cyclic voltammograms of Fischer carbenes **1** (left top), **2** (left bottom), **3** (right top) and **4** (right bottom). Scan rate: 100 mVs^{-1} in dichloromethane solutions (1.0 $mmol{\cdot}L^{-1}$) at 25 °C, supporting electrolyte $[N^{n}Bu_4][B(C_6F_5)_4]$ (0.1 M). In case of the full range cyclic voltammograms the initial cycle is shown. For cyclic voltammetry data see Table 6.2.

A comparison of the H_α ^1H NMR signals between complexes **1** – **4** as well as the ν(CO) stretching frequencies (A_1") reveal no significant differences, due to similarity of the carbene complexes (Table 6.1).

Table 6.1 Selected NMR data and the infrared ν(CO) stretching frequencies (A_1'') of Fischer carbenes **1** – **4** (Figure SI-5, Appendix 5).

Compd.	H_α δ ^1H [ppm]	$C_{carbene}$ δ $^{13}C\{^1H\}$ [ppm]	A_1''ν(CO) [cm^{-1}]
1	4.99	307.73	2063
2	5.01	310.72	2063
3	4.83	307.36	2062
4	4.83	308.72	2062

Electrochemistry and Molecular Orbital Analysis. The electrochemical studies of Fischer carbene complexes **1** – **4** were carried out under an argon atmosphere in dichloromethane solutions containing $[N^nBu_4][B(C_6F_5)_4]$ (0.1 M) as supporting electrolyte and were supported by DFT calculations (computational details are given in the Experimental Section). Spectroelectrochemical investigations of **1** - **4** were carried out using an OTTLE[18] (= Optically Transparent Thin Layer Electrochemistry) cell (Experimental Section).

During the electrochemical studies of **1**, three significant redox events could be observed. One reversible event was detected for **1** at $E^{0'}$ = 300 mV, similar as detected previously,[11] which can be assigned to the ferrocenyl/ferrocenium (Fc/Fc^+) redox process (Table 6.2, Figures 6.2 and SI-1). The significant anodic shift of this redox event, relative to ferrocene, demonstrates the electron withdrawing effect of the Fischer carbene moiety. Computational studies were carried out to verify the nature of the observed redox processes. The solvent effects on the ionization energies were taken into account with the conductor like screening model (COSMO) using ε = ∞ (Table 6.3, Figure 6.3).

As a result from the DFT calculations, the oxidation potential for the first oxidation in **1** was calculated to 0.3 V (Table 6.3). Considering the moderate level of theory, the theoretical value is in good agreement compared with the experimental value ($E_{ox\text{-}onset}$ = 0.22 V) as well as with

other considerations regarding a correlation between the electrochemical measurement and ionization energies.[19]

Table 6.2 Cyclic voltammetry data (potentials *vs* FcH/FcH^+) of 1.0 $mmol{\cdot}L^{-1}$ solutions of **1** – **4** in dry dichloromethane containing $[N^nBu_4][B(C_6F_5)_4]$ (0.1 M) as supporting electrolyte at 25 °C. [a] i_{pa}/i_{pc}. [b] ΔE_{pc}.

Compd.	$E_{pa}/E_{pc}/\Delta E_p/E^{0'}/\Delta E^{0'}$ [mV] (i_{pc}/i_{pa}) Wave (no.)				
	(1)	(2)	(3)	(4)	(5)
1	-2053/-2133/80/-2093 (0.46)[a]	266/334/68/ 300 (0.95)	1125/ -		
2	- /-2124	- /-1823/ 301[b]	554/484/70/ 519 (0.99)	989/ -	1086/ -
3	-2072/-2166/94/ -2119 (0.54)[a]	20/-48/68/-14 (0.98)	671/604/67/ 637/651 (0.98)	1161/ -	
4	- /-2213	- /-2100/ 113[b]	261/191/70/ 226 (0.99)	750/679/71/ 715/489 (0.98)	1127/ -

Furthermore, the spin density distribution of $\mathbf{1}^{+}$ offers a localization (Mulliken spin density of 1.25) around the iron center and thus verifies the assignment to a Fc/Fc^{+} redox event (*vide supra*, Figure 6.3).

Table 6.3 Calculated ionization energies and oxidation/reduction potentials of **1** (computational details are given in the Experimental Section).
[a] The ionization energy of ferrocene was calculated to 4.3 eV (414.9 kJ/mol).

Compd.	B3LYP Ionization Energy [kJ/mol]	Incremental Ionization Energy [kJ/mol]	*E vs* FcH/FcH^{+} [V][a]
$\mathbf{1}^{-}$	-273.7		
1	0.0	273.7	-1.5
$\mathbf{1}^{+}$	447.0	447.0	0.3
$\mathbf{1}^{2+}$	988.6	541.6	1.3
$\mathbf{1}^{3+}$	1632.8	644.2	2.4

Further increasing the potential leads to an irreversible oxidation process at E_{pa} = 1.13 V, which is associated with an oxidation of the tungsten carbonyl moiety (Figures 6.2 and SI-1(Appendix 5)). The peak current for this oxidation was observed as 2.5 times higher as for the ferrocenyl unit, similar as observed previously.[20,21] If an one step electrochemical process is assumed, the observed current reveals a two electron oxidation process, according to the Randles-Sevcik equation. However, the large differences between the calculated oxidation potentials (Table 6.3) suggest well-separated oxidation events during the generation of the oligocationic species. To determine the flown charge equivalents, chronocoulometric measurements were carried out. Assuming a reversible one electron redox event for the Fc/Fc^{+} couple (1 eq), the charge equivalents can be determined from the slope of the Anson plot, charge (*Q*) *vs* square root of time ($t^{1/2}$), with the Anson equation.[22] For the tungsten oxidation a value of 2.9 eq was obtained and suggests an electrode mediated successive three electron oxidation process, formal from

W(0) to W(III). Nevertheless, such results should be handled with caution, due to irreversibility of the oxidation process.

Furthermore, a partial reversible reduction (Figures 6.2 and SI-1 (Appendix 5)) could be found in the cathodic end of the electrochemical window at E_{pc} = –2.09 V (theoretical value: E = -1.5 V, Table 6.3). This redox process is associated to a carbene center reduction/reoxidation process (Table 6.2, Figure 6.2).[23]

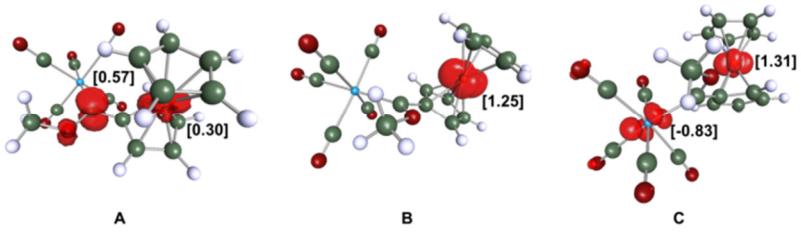

Figure 6.3 Computed spin density plots of $\mathbf{1}^-$ (**A**), $\mathbf{1}^+$ (**B**) and $\mathbf{1}^{2+}$ (**C**). For computational details see Experimental Section. Numbers in brackets indicate the computed Mulliken spin densities.

The cyclic voltammetric as well as the chronocoulometric (1.1 eq) studies suggest a one electron redox process. From the spin density distribution in Figure 6.3 (A) localization around the carbene carbon can be seen.

A further tungsten carbene substituent on the ferrocenyl unit (complex **2**) leads to an anodic shifting of the Fc/Fc^+ redox process to $E^{0'}$ = 519 mV. Within this context, the first carbene reduction should be easier than in **1** and was observed 170 mV less cathodic compared to the carbene reduction in the ferrocenyl monocarbene complex (Table 6.2, Figure 6.2). A second carbene reduction could be found at E_{pc} = –2.12 V, 300 mV more cathodic as the generation of $\mathbf{1}^-$ (Table 6.2, Figures 6.2 and SI-2 (Appendix 5)). The observation of two separated carbene reduction events leads to the conclusion that the first reduction process has an influence on the second, depending on the bridging unit (in comparison with **4**, *vide infra*). A similar observation was made during the oxidation events of the tungsten centers, two separated peaks at E_{pa} = 0.99 V and 1.09 V were found (Table 6.2). However, the oxidation potential of the 1st process was found more cathodic as observed for **1**.

Table 6.4 NIR data of **1** – **4** in dry dichloromethane containing $[N^nBu_4][B(C_6F_5)_4]$ (0.1 M) as supporting electrolyte at 25 °C.
[a] $\lambda = \nu_{max} - \Delta G^0$. [b] $\lambda = \nu_{max}$. [c] $\Delta G^0 = 5900\ cm^{-1}$. [d] $\Delta G^0 = 2420\ cm^{-1}$.

Compd.	Transition	ν_{max} [cm^{-1}] (ε_{max} [$Lmol^{-1}cm^{-1}$])	$\Delta\nu_{1/2}$ [cm^{-1}]	$\Delta\nu_{1/2(theo)}$ [cm^{-1}] {$\Delta\nu_{1/2(theo)} = (2310\lambda)^{1/2}$}[a]
$\mathbf{1}^+$	MMCT	9270 (340)	4660	2790[c] (4630[b])
	LF	3930 (50)	1280	
$\mathbf{2}^+$	MMCT	8000 (470)	5070	2200[c] (4300[b])
	LF	3670 (70)	1010	
$\mathbf{3}^+$	MMCT	8930 (65)	2510	2650[c]
	IVCT	5580 (930)	3640	2700[d] (3590[b])
	IBT	3790 (340)	820	1780[d]
$\mathbf{3}^{2+}$	MMCT	8190 (280)	4860	2300[c] (4140[b])
	LF	3510 (120)	1590	
$\mathbf{4}^+$	MMCT	8870 (500)	3170	2620[c]
	IVCT	4320 (1290)	3720	3160[b]
	IBT	3320 (720)	900	2770[b]
$\mathbf{4}^{2+}$	MMCT	7870 (570)	9030	2133[b] (4260[b])
	LF	3600 (200)	700	

In the case of the biferrocenyl Fischer carbene complex **3**, one redox event was detected at E_{pc} = –2.12 V and is also assigned to the carbene reduction electrode reaction (vide supra). For the biferrocenyl unit itself, two well separated ($\Delta E^{0'}$ = 651 mV) reversible one electron redox events at $E^{0'}$ = -14 mV and 637 mV were found (Table 6.2, Figure 6.2). A comparison of the first Bfc redox process with the corresponding event in biferrocene itself reveals an anodic shift of approx. 110 mV for the $\mathbf{3/3}^+$ redox couple, only one third as observed for the corresponding process in **1**.[23] Thus, the influence of the tungsten carbene moiety on the first biferrocenyl redox process in **3** is significantly lower as on the ferrocenyl redox event in **1**.

In addition, an oxidation peak at E_{pa} = 1.16 V was noticed and is assigned to the irreversible tungsten carbonyl oxidation (vide supra, Table 6.2, Figure 6.2). The electrochemical investigation of the biferrocenyl carbene complex **4** revealed two carbene reduction processes with a smaller separation (ΔE_{pc} = 113 mV) as observed for **2**, due to the larger biferrocenyl bridge between the Fischer carbene units (vide supra). For the biferrocenyl increment, two reversible redox events were observed, which are separated by $\Delta E^{0'}$ = 489 mV. Hence $\Delta E^{0'}$ was observed as smaller as detected for biferrocene ($\Delta E^{0'}$ = 530 mV) under similar experimental conditions.[24] A comparison of formal potentials from the first biferrocenyl redox processes of compounds **3** and **4** shows again the anodic potential shift, due to the installation of a second Fischer carbene substituent. Finally, the irreversible oxidation of the tungsten carbonyl fragments was found at ΔE_{pa} = 1.13 V, even slightly more cathodic than for **3**.

In order to get more insight into the oxidation process of **1** - **4** spectroelectrochemical studies were carried out by an stepwise increase of the potential *vs* Ag/AgCl in an OTTLE cell (= Optically Transparent Thin Layer Electrochemistry)[18] using a 0.1 M dichloromethane solution of $[N^nBu_4][B(C_6F_5)_4]$ as supporting electrolyte. This procedure allows the *in situ* generation of mixed-valent species such as $\mathbf{1}^+$, $\mathbf{2}^+$, $\mathbf{3}^{n+}$ and $\mathbf{4}^{n+}$ (n = 1, 2). If deconvolution of NIR absorptions was used, transitions with Gaussian shapes were taken to get fits good enough to allow an almost exact overlay of the sum of the spectral components with the experimental spectra. All neutral Fischer carbene complexes do not display, as expected, any absorptions in the NIR range. The corresponding UV-Vis spectra are presented in Appendix 5 (Figures SI-3, SI-6 to SI-8). For calculation of the theoretical bandwidth at half height ($\Delta\nu_{1/2(theo)}$) in asymmetric systems, the energy gap between the diabatic states (ΔG^0) could be estimated, using the difference in oxidation potentials of the two redox sites. Regarding this, the oxidation potential of $(CO)_5W{=}C(OMe)Me$[20] as well as the formal potential of the $\mathbf{1/1}^+$ redox process were used (Table 6.4). Furthermore, an experimental $\Delta\nu_{1/2}$ value equal or larger as the theoretical width for symmetrical systems verifies clearly a class II assignment according to Robin and Day, since theoretical $\Delta\nu_{1/2}$ values for asymmetrical systems are generally smaller as the corresponding widths for the symmetrical case.[25]

During the oxidation of **1** typical absorptions in the UV-Vis region of inner ferrocenyl transitions (π-π^* and MLCT/d-d) were observed (Appendix 5).[26] Upon successive increasing the potential,

two main absorptions at 9270 cm^{-1} and 3930 cm^{-1} could be detected in the NIR range during the generation of $\mathbf{1}^+$ (in comparison with FcH^+, Table 6.4 and Figure 6.4).[27] The latter very weak absorption is attributed to an iron-based forbidden ligand field (LF) transition as described previously.[9f,10b,28] The weak high energy NIR absorption band around 9300 cm^{-1} can be assigned to a metal-metal charge transfer transition (MMCT) between the tungsten carbonyl fragment and the ferrocenium unit. To verify an interaction between the tungsten and the ferrocenyl building blocks, infrared spectroelectrochemical measurements monitoring the shift of ν(CO) stretching frequencies during the oxidation process were carried out (Figures 6.5 and SI-4 (Appendix 5)).

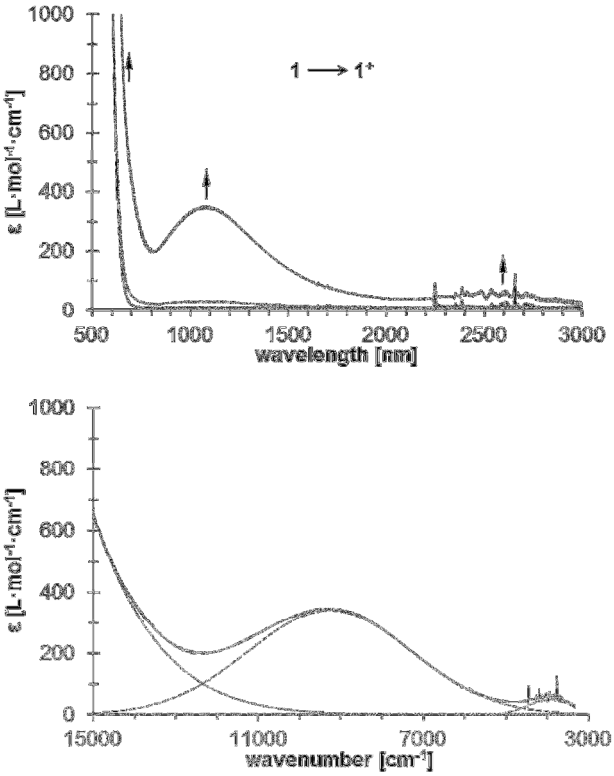

Figure 6.4 UV-Vis/NIR spectra of **1** at rising potentials (0 to 700 mV). Top: 500 – 3000 nm. Bottom: deconvolution of NIR absorptions at 700 mV using three distinct overlapping transitions with Gaussian shapes (dashed line indicates MMCT absorptions, dotted line corresponds to absorptions caused by interactions between ligand and metal, dotted-dashed line represents ligand field transitions). All potentials *vs* Ag/AgCl at 25 °C in dichloromethane, supporting electrolyte $[N^nBu_4][B(C_6F_5)_4]$ (0.1 M). Arrows indicate increasing or decreasing as well as shifting absorptions.

For carbene **1**, absorptions could be found at 1930 cm^{-1} and 2063 cm^{-1}, respectively (Experimental Section). Upon generation of the monocationic species $\mathbf{1}^+$ a decrease of these

bands takes place together with an increase of absorptions at 1953 cm^{-1} and 2076 cm^{-1}, respectively (Figure 6.5). The limited shift of the $W(CO)_5$ carbonyl stretching frequencies on oxidation is the result of conjugative and inductive effects that operate in stabilizing the positive charge on the iron nucleus by the metal carbene. Hence, a reduced back bonding behavior to the carbonyl carbon atoms leads to an increasing of the CO bond strengths and results in larger stretching frequencies (Figure 6.5). The observed carbonyl stretching frequencies are in good agreement with the calculated infrared spectra for **1** and the corresponding monocation (Figure SI-4 (Appendix 5)), whereas the difference between the two observed frequencies (2063 cm^{-1} and 2076 cm^{-1}) for the total symmetrical carbonyl stretching mode (A_1", vide supra, Figure SI-5 (Appendix 5)) during the oxidation of **1** ($\Delta\nu$ = 13 cm^{-1}) differs only slightly from the corresponding value for the predicted vibrations of **1** and $\mathbf{1}^+$ ($\Delta\nu$ = 19 cm^{-1}, Figure SI-4 (Appendix 5)). Furthermore, the small magnitude of the carbonyl band shifts, compared to shifts of more than 100 cm^{-1} for metal carbonyl-based oxidation, indicates an iron based oxidation process. Moreover, the existence of the initial A_1" ν(CO) stretching frequencies at 1953 cm^{-1} as well as 2076 cm^{-1} in the final spectra (bold line, Figure 5, top left) clarifies the valence trapped situation in $\mathbf{1}^+$. Calculation of the spin density distribution for $\mathbf{1}^+$ confirms this conclusion (Figure 6.3). Thus, the interaction between the ferrocenyl unit and the tungsten carbene increment can be described with a weakly coupled class II system according to Robin and Day.[25]

The absorption behavior of $\mathbf{2}^+$ during the oxidation of molecule **2** is similar to the corresponding Fischer monocarbene complex **1** (Table 6.4, Figure SI-6 (Appendix 5)). Absorptions at 3670 cm^{-1} and 8000 cm^{-1} could be noticed and are assigned to ligand field transition and an electronic interaction between the tungsten carbene units and the iron center, too (MMCT, vide supra). The latter transition was observed as more intense as the corresponding absorption for $\mathbf{1}^+$, due to the 2nd Fischer carbene substituent on the ferrocenyl moiety. During the infrared spectroelectrochemical investigations of **2**, a double band (1935 cm^{-1} and 1958 cm^{-1}) as well as a broad absorption at 2071 cm^{-1}, the carbonyl stretching frequency (A_1", *vide supra*), could be found upon generation of $\mathbf{2}^+$ (Figure 6.4). However, the width of the latter band suggests a superposition of two absorptions close together (Figure 6.5) and would be consistent with a class II electronic coupling behavior according to Robin and Day (*vide supra*).[25] A comparison between the observed ($\Delta\nu_{1/2}$) and the calculated band width at half height ($\Delta\nu_{1/2(theo)}$) of the MMCT absorption supports this classification (Table 6.4).

An enhancement of ferrocenyl complex **1** to a biferrocenyl Fischer carbene complex **3** leads to an occurrence of two (Figure SI-7, Appendix 5) absorptions in the NIR range during the generation of cation $\mathbf{3}^{+}$. Characteristic for biferrocenyl systems is the observation of an inter valence charge transfer (IVCT) band close together with another absorption on the low energy side of the ICVT absorption (Table 6.4, Figure SI-7 (Appendix 5)). Tuczek *et al.* attributed this intrabiferrocenyl transition (IBT), around 3800 cm^{-1} for $\mathbf{3}^{+}$, to a further intervalence charge transfer transition.[27,30] However, the latter absorption is very narrow compared to the corresponding value of $\Delta\nu_{1/2(theo)}$ (Table 6.4, Figure SI-7 (Appendix 5)). An assignment to a LMCT or a charge transfer assisted ligand field transition is also not uncommon.[26,31] Furthermore, a similar absorption band, which was found for $\mathbf{1}^{+}$ and $\mathbf{2}^{+}$, attributed to an electronic interaction between the tungsten carbonyl moiety and the iron center, is observed as very weak or negligible (Table 6.4, Figure SI-7 (Appendix 5)). The infrared spectroelectrochemical investigations of **3** support this observation, since upon formation of $\mathbf{3}^{+}$ the initial ν(CO) frequencies (1930 cm^{-1} and 2061 cm^{-1}) shift only a few wavenumbers to higher energies (1935 cm^{-1} and 2065 cm^{-1}, Figure 6.5). Thus, in combination with the electrochemical results, the first oxidation in **3** takes primarily place at the terminal ferrocenyl unit. During the generation of $\mathbf{3}^{2+}$ the low energy absorptions in the NIR range disappear and further transitions could be detected at 3510 cm^{-1} (LF) and around 8200 cm^{-1} (Table 6.4, Figure SI-7 (Appendix 5)). The latter transition is also associated to a metal-metal charge transfer between the tungsten increment and the Bfc unit. The corresponding infrared absorption behavior during the formation of $\mathbf{3}^{2+}$ verifies this conclusion, similar as observed for $\mathbf{1}^{+}$ (*vide supra*, Figure 6.5).

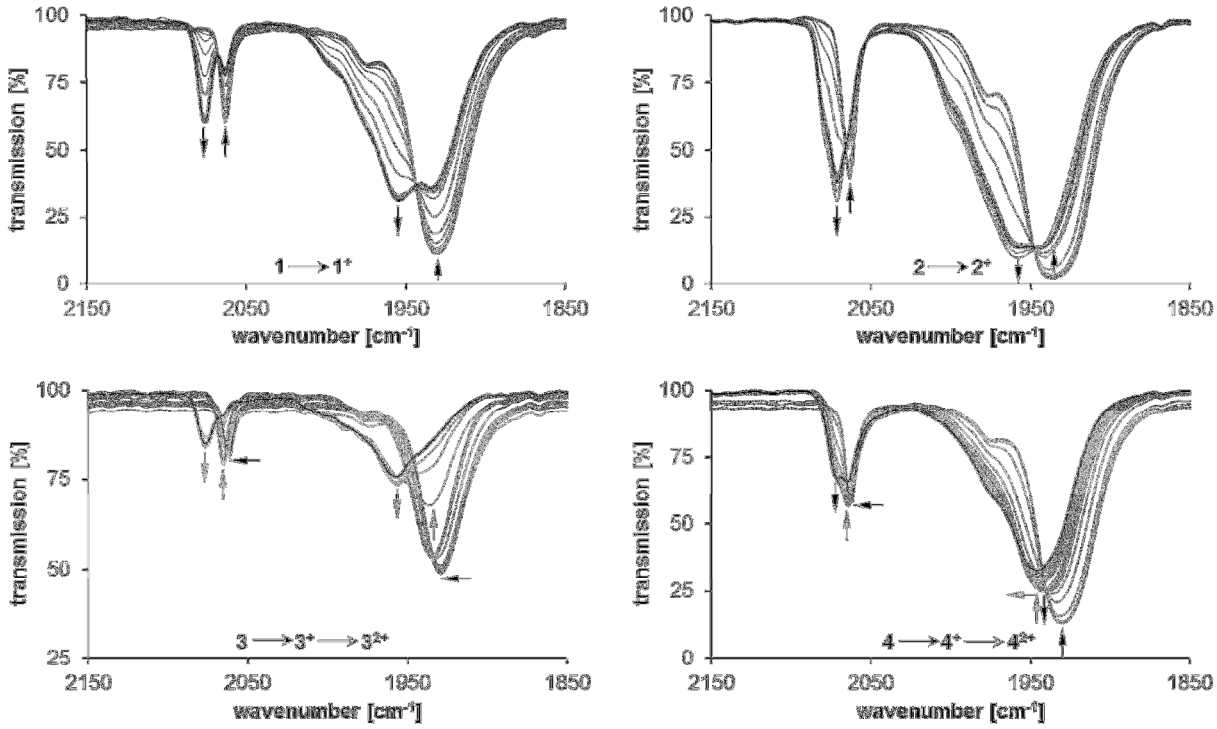

Figure 6.5 Infrared spectra of **1** - **4** at rising potentials (left top: -200 to 950 mV; right top: -200 to 1350 mV; left bottom: -100 to 1350 mV; right bottom: -100 to 1600 mV). All potentials *vs* Ag/AgCl at 25 °C in dichloromethane on 5 mM analyte solutions, supporting electrolyte $[N^nBu_4][B(C_6F_5)_4]$ (0.1 M). Arrows indicate increasing or decreasing as well as shifting absorptions.

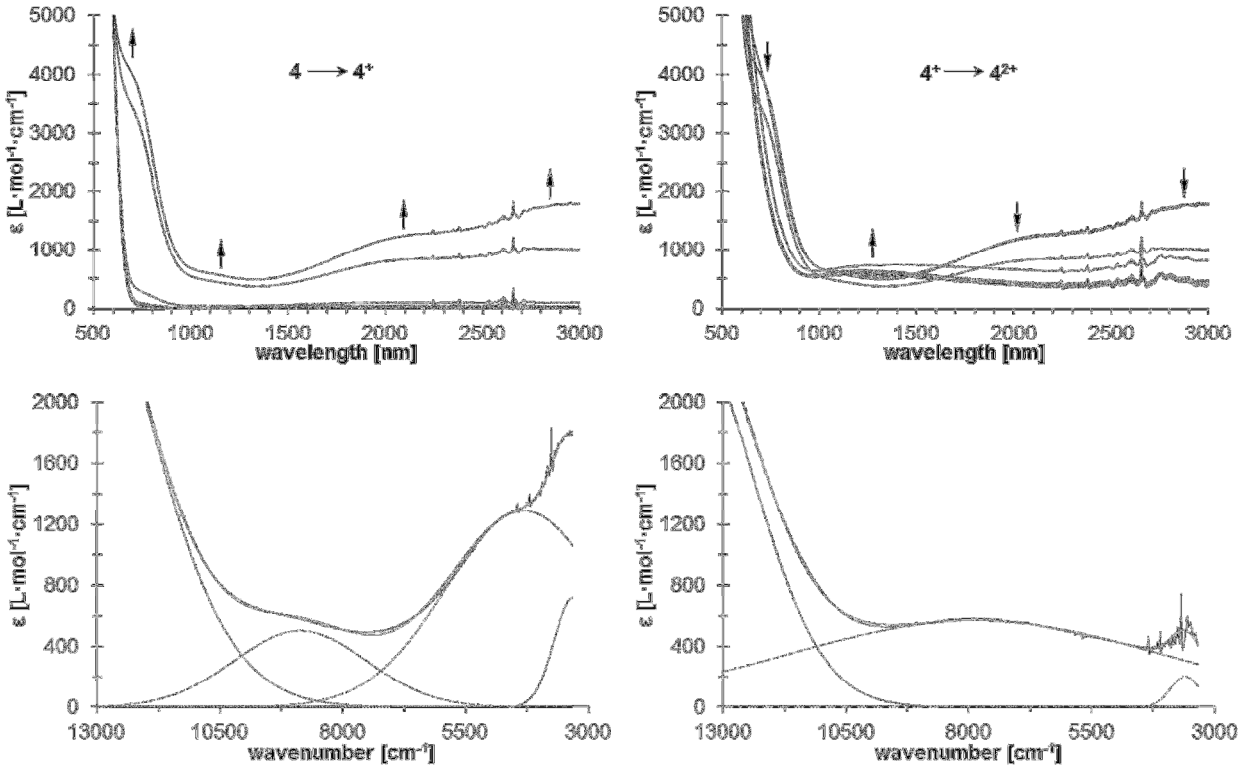

Figure 6.6 UV-Vis/NIR spectra of **4** at rising potentials (left: -100 to 600 mV; right: 600 to 1050 mV). Top: 500 – 3000 nm. Bottom (left): deconvolution of NIR absorptions at 600 mV using four distinct overlapping transitions with Gaussian shapes. Bottom (right): deconvolution of NIR absorptions at 1050 mV, using three distinct overlapping transitions with Gaussian shapes (dashed line indicates IVCT (grey) or MMCT (black) absorptions, dotted line corresponds to absorptions caused by interactions between ligand and metal (black) as well as intrabiferrocenyl transitions (IBT, grey), dotted-dashed line represents ligand field transitions). All potentials *vs* Ag/AgCl at 25 °C in dichloromethane, supporting electrolyte $[N^{n}Bu_4][B(C_6F_5)_4]$ (0.1 M). Arrows indicate increasing or decreasing as well as shifting absorption.

A second tungsten Fischer complex fragment on the biferrocenyl building block leads to three NIR absorptions for monocationic $\mathbf{4}^{+}$ (Table 6.4, Figure 6.6). The two transitions at lower energies are typical for such mixed-valent biferrocenyl species (*vide supra*). The intensities are higher as observed for $\mathbf{3}^{+}$ but weaker than for symmetrical electron donor substituted biferrocenyl systems.[32] The third absorption around 8900 cm^{-1} can be assigned again to a MMCT transition, caused by an electronic interaction between the tungsten unit and the ferrocenyl group in $\mathbf{4}^{+}$. Within the infrared spectroelectrochemical studies of **4**, a shifting of the initial ν(CO) stretching frequencies from 1930 cm^{-1} and 2063 cm^{-1} to formal 1941 cm^{-1} and 2065 cm^{-1} is characteristic, whereas an increase of a shoulder at 2071 cm^{-1} could be observed (Figure 6.5). This suggests a main localization of positive charge in the biferrocenyl fragment within the infrared timescale corresponding to a weakly coupled class II system according to Robin and Day.[25] Further oxidation to dicationic $\mathbf{4}^{2+}$ leads to absorptions at 1945 cm^{-1} and a double band around 2070 cm^{-1} (A_1", 2063 cm^{-1} and 2071 cm^{-1}) offering the valence trapped behavior between the biferrocenyl bridge and both tungsten Fischer carbene fragments (*vide supra*). This is consistent with the detection of an increasing NIR absorption at 7870 cm^{-1} (MMCT) upon decreasing of the low energy transitions, caused from intra biferrocenyl electronic interactions, during the formation of $\mathbf{4}^{2+}$ (Table 6.3, Figure 6.6). Finally, a low intense ligand field transition could be observed at 3600 cm^{-1}, similar as described previously (*vide supra*, Table 6.4 and Figure 6.6).[9f,10b,28]

Crystallography. The molecular structures of **1**[11,26] and **2** – **4** in the solid state have been determined by single-crystal X-ray diffraction analysis.

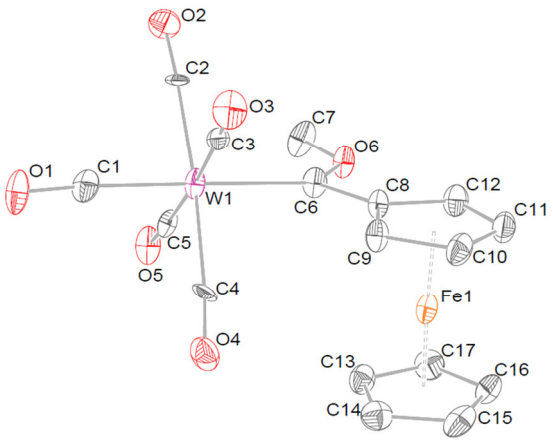

Figure 6.7 Single crystal X-ray structure analysis of **1** with the atom numbering scheme. Ellipsoids represent 50 % probability levels. Hydrogen atoms are omitted for clarity. Selected bond lengths (Å), angles (°), and torsion angles (°): W1–C1 1.981(14), W1-C6 2.211(13), C6-O6 1.339(15), C6-C8 1.458(19), D1–Fe1 1.652(19), D2–Fe1 1.656(17), O6-C6-W1 128.33(92), C8-C6-W1 126.39(93), O6-C6-C8 105.24(11), D1–Fe1–D2 176.77(18), C8–D1–D2–C13 –13.31(10), W1–C6–O6–C7 –1.67(19), C8–C6–O6–C7 –179.67(12), O6–C6–W1–C2 –46.63(13), C8–C6–W1–C2 –130.97(12), O6–C6–C8–C9 –178.96(14), W1–C6–C8–C9 3.00(21). D1: C8–C9–C10–C11–C12, D2: C13–C14–C15–C16–C17.

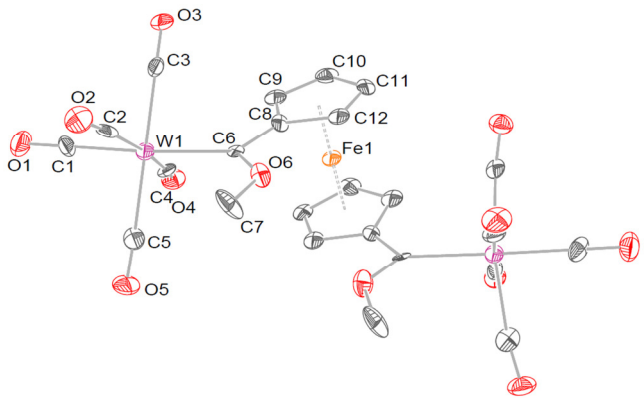

Figure 6.8 Single crystal X-ray structure analysis of **2** with the atom numbering scheme. Equivalent atoms are generated by the following symmetry operation: –x+1, y, –z+3/2. Ellipsoids represent 50 % probability levels. Disordered and hydrogen atoms are omitted for clarity. Selected bond lengths (Å), angles (°), and torsion angles (°): W1–C1 1.987(11), W1-C6 2.204(99), C6-O6 1.353(12), C6-C8 1.443(12), D1–Fe1 1.657, O6-C6-W1 127.84(57), C8-C6-W1 125.54(61), O6-C6-C8 106.49(81), D1–Fe1–D1_$1 176.95(12), C8–D1–D1_$1–C12_$1 3.69(63), W1–C6–O6–C7 –4.45(12), C8–C6–O6–C7 171.66(95), O6–C6–W1–C2 44.08(61), C8–C6–W1–C2 –131.33(54), O6–C6–C8–C9 174.36(61), W1–C6–C8–C9 –9.41(91). D1: C8–C9–C10–C11–C12.

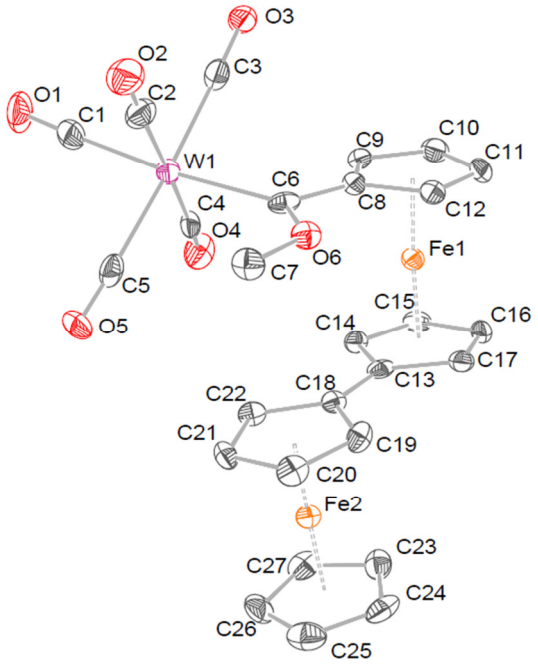

Figure 6.9 Single crystal X-ray structure analysis of **3** with the atom numbering scheme. Ellipsoids represent 50 % probability levels. Hydrogen atoms are omitted for clarity. Selected bond lengths (Å), angles (°), and torsion angles (°): W1–C1 2.034(56), W1-C6 2.207(49), C6-O6 1.335(51), C6-C8 1.457(71), D1–Fe1 1.653(7), D2–Fe1 1.662(7), O6-C6-W1 129.14(37), C8-C6-W1 123.69(31), O6-C6-C8 106.83(41), D1–Fe1–D2 176.25(5), C8–D1–D2–C13 –21.58(31), C18–D3–D4–C23 –0.27(33), D3–Fe2 1.6426(7), D4–Fe2 1.695(7), D3–Fe2–D4 166.47(5), W1–C6–O6–C7 6.92(58), C8–C6–O6–C7 –179.65(37), O6–C6–W1–C2 47.81(40), C8–C6–W1–C2 –124.63(38), O6–C6–C8–C9 172.42(41), W1–C6–C8–C9 –13.70(65), D1: C8–C9–C10–C11–C12, D2: C13–C14–C15–C16–C17, D3: C18–C19–C20–C21–C22, D4: C23–C24–C25–C26–C27.

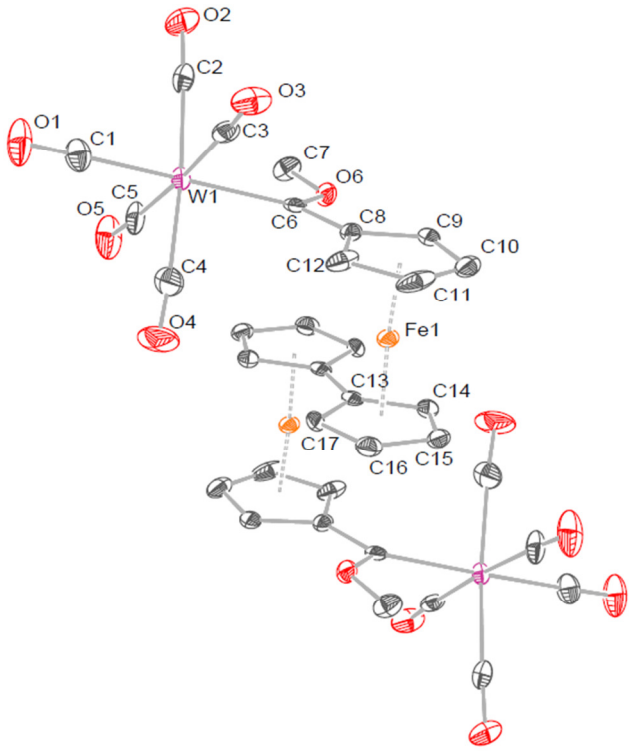

Figure 6.10 Single crystal X-ray structure analysis of **4** with the atom numbering scheme. Equivalent atoms are generated by the following symmetry operation: –x+2, –y, –z. Ellipsoids represent 50 % probability levels. Hydrogen atoms are omitted for clarity. Selected bond lengths (Å), angles (°), and torsion angles (°): W1–C1 2.022(37), W1-C6 2.217(31), C6-O6 1.317(38), C6-C8 1.456(44), D1–Fe1 1.649(5), D2–Fe1 1.658(5), O6-C6-W1 128.60(22), C8-C6-W1 123.87(23), O6-C6-C8 107.22(27), D1–Fe1–D2 175.72(4), C8–D1–D2–C13 22.60(22), W1–C6–O6–C7 –5.69(40), C8–C6–O6–C7 –179.39(26), O6–C6–W1–C2 –44.36(28), C8–C6–W1–C2 128.38(25), O6–C6–C8–C9 6.14(41), W1–C6–C8–C9 –167.93(23), D1: C8–C9–C10–C11–C12, D2: C13–C14–C15–C16–C17.

Suitable single crystals of **1** - **4** were obtained by slow evaporation of a saturated dichloromethane solution of the respective complex layered with *n*-hexane at –5 ^{o}C. The *ORTEP* diagrams with selected bond lengths (Å), bond angles (°), and torsion angles (°) are shown in Figures 6.7 – 6.10. The appropriate complexes crystallize in the orthorhombic space groups *Pca*2$_1$ (**1**) and *Pbcn* (**2**), the triclinic space group *P*–1 (**3**) and the monoclinic space group *P*2$_1$/*n* (**4**) with one (**1**), a half (**2**,**4**) and four (**3**) molecules in the asymmetric unit.

Regarding the numerous solid state structures of Fischer carbene complexes, only six group VI alkoxyferrocenyl-substituted derivatives have been reported so far, whereby just one contains tungsten.[12c, 13b, 33]

In a comparison of the angles and bond distances (Figures 6.7 – 6.10) at the trigonal-planar carbene carbon, no further differences, not for the ferrocenyl unit nor for the biferrocenyls can be identified. W1–C1 distances are equal for all four complexes and coincide with the corresponding ethoxy-substituted derivative of **1**.[33] The free electron pairs at O6 are always directed to the ferrocenyl moiety of the molecules, due to the electronic interaction with the carbonyl groups.[34] Thus, to avoid electronic interactions, the bonded methyl group C6 shields the oxygen atom O6. The carbene carbon and the C_5H_4 plane of the ferrocenyl moieties extend their π-system by arranging almost coplanar to each other. The highest deviations of the corresponding O6–C6–C8–C9 torsion angles can be found for one molecule in the asymmetric unit of **3** (10.99(39) °). Additionally, this plane shows a staggered orientation related to the carbonyl groups. The highest deviations from an ideally assumed angle (45 °) can be found in carbene **3**, which shows differences of 5.43(40) ° and 10.37(38) ° for the representing torsion angle O6–C6–W1–C2 and O6–C6–W1–C2, respectively.

For the biferrocenyl complexes **3** and **4**, both ferrocenyl units are antiparallel oriented with nearly coplanar C_5H_4 rings (highest deviation: 17.73(25) ° for **3** and 0.00(24) ° for **4**, respectively). Interestingly, carbene fragments are disposed synclinal and synperiplanar to the ferrocenyl substituent. This conformation strongly depends on the rotation of the cyclopentadienyl rings. Fischer carbenes **1** and **4** exhibit rather eclipsed than staggered torsion angles (–13.31(101) ° for **1** and 22.60(22) ° for **4**). In contrast, complex **2** with two tungsten carbene building blocks nearly shows an eclipsed conformation (3.69(63) °) for both C_5H_4 rings, whereby both fragments show synclinal orientation. The same conformation can also be found for the corresponding chromium complex with ^{n}propoxy substituents.[12] Torsion angles of both entities in the biferrocenyl unit of complex **3** are summarized in Table 6.5 showing great differences between the molecules (Table 6.5, A - D) of the asymmetric unit for the 1,1'-disubstituted moiety. Molecules B and C exhibit a nearly synclinal orientation, whereas A and D rather are arranged synperiplanar. However, all monosubsituted ferrocenyl fragments are synperiplanar oriented with small deviations for molecule B and D (Table 6.5).

Table 6.5 Torsion angles (°) for **3**.

Molecule	**C8–CT1–CT2–C13**	**C18–CT3–CT4–C23**
A	–21.61(29)	–0.70(31)
B	62.44(34)	–14.08(42)
C	–61.49(32)	–4.27(39)
D	15.65(29)	–16.22(29)

6.3 CONCLUSION

Within this study, a series of ferrocenyl (Fc = ferrocenyl; fc = ferrocen-1,1'-diyl) and biferrocenyl Bfc = 1',1''-biferrocenyl; bfc = 1',1''-biferrocen-1,1'''diyl) tungsten Fischer carbene complexes, of type $[(CO)_5W{=}C(OMe)R]$ (**1**, R = Fc; **3**, R = Bfc) and $[(CO)_5W{=}C(OMe)\text{-}R'\text{-}(OMe)C{=}W(CO)_5]$ (**2**, R' = fc; **4**, R' = bfc), is reported with the aim of investigating low energy charge transfer transitions between the carbene substituents and the transition metal carbonyl fragment. For this reason, ferrocenyl and biferrocenyl mono- and bismethoxycarbene tungsten(0) complexes **1** – **4** were prepared and characterized spectroscopically in solution. Furthermore, the structural properties of **1** - **4** in the solid state were investigated by single-crystal X-ray diffraction studies whereby the biferrocenyl derivatives **3** and **4** exhibit a *syn*-conformation of ferrocenyl and carbene moiety. The results reveal no substituent effects in the bond-lengths and angles.

The electrochemical studies reveal reversible one electron redox events for the ferrocenyl/biferrocenyl moieties. Moreover, an electrochemical one electron transfer reaction could be found for the reduction of the Fischer carbene units. For the tungsten carbonyl moieties, irreversible oxidation processes could be detected. During the UV-Vis-NIR spectroelectrochemical investigations typical low energy absorptions for the mixed-valent biferrocenyl unit were found. A further observed high energy NIR absorption was attributed to a metal-metal charge transfer transition between the tungsten carbonyl increment and the

ferrocenyl/biferrocenyl unit in the corresponding oxidized state and is reported herein for the first time. Finally, verification was made within infrared spectroelectrochemical studies by which the electronic interactions in the corresponding cationic species can be described with weakly coupled class II systems according to Robin and Day.

6.4 EXPERIMENTAL SECTION

General Information

All operations were carried out under an inert atmosphere of nitrogen or argon gas using standard Schlenk techniques. Solvents were dried by refluxing over sodium metal (*n*-hexane and tetrahydrofuran) or phosphorous pentoxide (dichloromethane) and were distilled under nitrogen prior to use. Chemicals were used without further purification unless stated elsewhere. Dibromobiferrocene was synthesized according to a literature procedure.[15] Tetra-*n*-butylammonium tetrakis(pentafluorophenyl)borate was prepared by metathesis of lithium tetrakis(pentafluorophenyl)borate etherate (Boulder Scientific) with tetra-*n*-butylammonium bromide according the a published procedure.[35] Purification with column chromatography was done using Silica gel 60 (0.0063 – 0.200mm) as stationary phase. A Bruker AVANCE 500 spectrometer was used for NMR recordings. ^{1}H NMR spectra were recorded at 500.30 MHz and ^{13}C{^{1}H} NMR spectra at 125.80 MHz. The signal of the solvent was used as reference: ^{1}H, $CDCl_3$ at 7.26 ppm and ^{13}C{^{1}H}, $CDCl_3$ at 77.16 ppm. Infrared spectra were obtained with a Thermo Nicolet 200 FT-IR spectrometer using a NaCl cell and dichloromethane as solvent. Only the vibration bands in the carbonyl stretching region (1600 - 2200 cm^{-1}) were recorded. The melting points were determined using a Gallenkamp MFB 595 010 M melting point apparatus. Microanalyses were performed by using a Thermo FLASHEA 1112 Series instrument. High-resolution mass spectra were recorded with a Bruker micrOTOF QII with an Apollo II ESI source.

Synthesis of Fischer carbene complexes 1 – 4

$[(CO)_5W{=}C(OMe)Fc]$ (**1**)

Ferrocene (3.0 mmol, 0.56 g) was monolithiated according to a literature procedure in tetrahydrofuran (thf) with ^{t}BuLi (3.2 mmol).[14] The solution was cooled to -80 ^{o}C and $W(CO)_6$ (3.0 mmol, 1.06 g) was added in a single portion. The color of the solution turned deep red upon addition. The reaction mixture was stirred isotherm for 30 min and then allowed to reach room temperature within 1 h. The solvent was changed to dichloromethane (CH_2Cl_2), cooled to -50 ^{o}C and methyl trifluoromethanesulfonate (9.9 mmol, 1.09 mL) added. The reaction mixture was removed from the cold bath and stirred overnight at ambient temperature. Purification of the product was performed by using column chromatography and *n*-hexane as initial eluent. The polarity of the eluent was increased by adding small portions of CH_2Cl_2. Yield 1.44g (87%), dark red crystals. Anal. Calcd. for $C_{17}H_{12}FeO_6W$ (551.98): C, 36.99; H, 2.20; found C, 36.94; H, 2.12. Mp: 153°C. NMR ($CDCl_3$) ^{1}H: 4.99 (m, 2H, H_α), 4.84 (m, 2H, $H_ß$), 4.27 (s, 5H, Cp), 4.53 (s, 3H, CH_3). $^{13}C\{^{1}H\}$: 307.73($C_{carbene}$), 202.34(C_{trans}), 198.03(C_{cis}), 95.23(C_{ipso}), 75.06(C_α), 73.25($C_ß$), 70.80(Cp), 68.60(CH_3). IR ν(CO) (*n*-hexane): 2063 m (A″1), 1974 w (B), 1946 s (A′1), 1935 vs (E). FAB-MS [m/z]: 551.95 [M^+].

$[\{(CO)_5W{=}C(OMe)\}_2fc]$ (**2**)

Dilithiation of ferrocene (3.0 mmol, 0.56 g) was done according to methods previously reported with an 1:1 ^{n}BuLi/TMEDA solution in *n*-hexane (6.5 mmol) overnight at ambient temperature. Afterward, the solvent was removed by filtration via cannula and the remaining dilithioferrocene was redissolved in tetrahydrofuran. The resulting solution was cooled to -60 ^{o}C and $W(CO)_6$ (6.0 mmol, 2.11 g) was added in a single portion. After 1 h of isothermal stirring the solution was warmed up to room temperature within 60 min. All volatiles were removed, the residue was redissolved in CH_2Cl_2 and methyl trifluoromethanesulfonate (20.0 mmol, 2.41 mL) was added at -30 ^{o}C after which the reaction solution darkened. The resulting mixture was stirred overnight at ambient temperature. Purification of the crude product was performed by column chromatography using *n*-hexane as initial eluent. The polarity of the eluent was increased by adding small portions of dichloromethane. Yield 1.51g (85%), dark purple solid. Anal. Calcd. for $C_{24}H_{14}FeO_{12}W_2$ (917.91): C, 31.40; H, 1.54; found C, 30.92; H, 1.42. Mp: 195°C. NMR ($CDCl_3$)

^{1}H: 5.01 (m, 4H, H_{α}), 4.82 (m, 4H, $H_{ß}$), 4.54 (s, 6H, CH_3). $^{13}C\{^{1}H\}$: 310.72 ($C_{carbene}$), 202.07 (C_{trans}), 197.66 (C_{cis}), 96.07 (C_{ipso}), 76.58 (C_{α}), 74.93 ($C_{ß}$), 69.09 (CH_3). IR ν(CO) (*n*-hexane): 2063 m (A″1), 1974 w (B), 1940 vs (A′1 overlap E). FAB-MS [m/z]: 917.89 [M+].

[$(CO)_5$W=C(OMe)Bfc] (**3**) and [{$(CO)_5$W=C(OMe)}$_2$Bfc] (**4**)

Dibromobiferrocene[14,15] (3.0 mmol, 1.58 g) was dissolved in 50 mL of tetrahydrofuran and ^{n}BuLi (6.0 mmol) was added slowly at -40 ^{o}C. After 30 min of isothermal stirring, W$(CO)_6$ (6.0 mmol, 2.11 g) was added in a single portion. The solution was kept at -40 °C for an additional hour and then allowed to reach room temperature within 1 h. Afterward, the solvent was changed to dichloromethane and methyl trifluoromethanesulfonate (20.0 mmol, 2.41 mL) was added at -30 ^{o}C. The reaction mixture was removed from the cold bath and stirred overnight at ambient temperature. Purification of the product was performed by column chromatography using *n*-hexane as initial eluent. The polarity of the eluent was increased by adding small portions of dichloromethane. Complexes **3** and **4** were purified and separated with column chromatography and gradient elution.

Compound **3**: Yield 0.96g (40%), red brown crystals. Anal. Calcd. for $C_{27}H_{20}Fe_2O_6W$ (736.01): C, 44.06; H, 2.74; found C, 43.95; H, 2.68. Mp: 166°C. NMR ($CDCl_3$) ^{1}H: 4.83 (m, 2H, $H_{ipso1\alpha}$), 4.64 (m, 2H, $H_{ipso1ß}$), 4.47 (m, 2H, $H_{ipso2\alpha}$), 4.32 (m, 2H, $H_{ipso2ß}$), 4.27 (m, 2H, $H_{ipso3\alpha}$), 4.26 (m, 2H, $H_{ipso3ß}$), 3.97 (s, 5H, Cp), 4.24 (s, 3H, CH_3). $^{13}C\{^{1}H\}$: 307.36($C_{carbene}$), 202.48(C_{trans}), 198.13(C_{cis}), 95.96(C_{ipso1}),88.24 (C_{ipso2}), 80.67 (C_{ipso3}), 75.06 ($C_{ipso1\alpha}$), 73.25($C_{ipso1ß}$), 70.17 ($C_{ipso2\alpha}$), 68.47($C_{ipso2ß}$), 68.12 ($C_{ipso3\alpha}$), 66.46($C_{ipso3ß}$), 69.43(Cp), 53.47(CH_3). IR ν(CO) (*n*-hexane): 2062 m (A″1), 1972 w (B), 1943 s (A′1), 1932 vs (E). FAB-MS [m/z]: 735.95 [M+].

Compound **4**: Yield 0.99g (30%), dark brown crystals. Anal. Calcd. for $C_{36}H_{26}Fe_2O_{12}W_2$ (1101.94): C, 37.06; H, 2.02; found C, 37.08; H, 2.05. Mp: 232°C (decomp.). NMR ($CDCl_3$) ^{1}H: 4.83 (m, 4H, $H_{ipso1\alpha}$), 4.62 (m, 4H, $H_{ipso1ß}$), 4.44 (m, 4H, $H_{ipso2\alpha}$), 4.32 (m, 4H, $H_{ipso2ß}$), 4.30 (s, 6H, CH_3). $^{13}C\{^{1}H\}$: 308.72($C_{carbene}$), 202.29(C_{trans}), 198.03(C_{cis}), 96.05(C_{ipso1}),84.98 (C_{ipso2}), 75.98 ($C_{ipso1\alpha}$), 74.12($C_{ipso1ß}$), 70.70 ($C_{ipso2\alpha}$), 68.43($C_{ipso2ß}$), 67.97(CH_3). IR ν(CO) (*n*-hexane): 2062 m (A″1), 1972 w (B), 1943 s (A′1), 1932 vs (E). FAB-MS [m/z]: 1101.88 [M+].

Electrochemistry. The electrochemical measurements were carried out under an argon atmosphere on 1.0 mmol·L^{-1} dichloromethane solutions containing 0.1 mol·L^{-1} of $[N^nBu_4][B(C_6F_5)_4]$ as supporting electrolyte utilizing a Voltalab 10 electrochemical laboratory from Radiometer analytical.[35] Furthermore, an OTTLE (= Optically Transparent Thin Layer Electrochemistry) cell placed in a Varian Cary 5000 UV-VIS/NIR absorption spectrometer or in a Thermo Nicolet 200 FT-IR spectrometer was used in spectroelectrochemical measurements.[18] For voltammetry, a three electrode cell with a platinum counter electrode, a glassy carbon working electrode and a Ag/Ag^+ reference electrode was used. The working electrode was prepared by polishing with a Buehler micro cloth using Buehler diamond pastes with decreasing sizes (1 to 0.25 μm). The Ag/Ag^+ reference electrode was constructed from a silver wire inserted into a luggin capillary with a vycor tip containing a solution of 0.01 mol·L^{-1} $AgNO_3$ as well as 0.1 mol·L^{-1} $[N^nBu_4][B(C_6F_5)_4]$ in acetonitrile. This luggin capillary was inserted into a second luggin capillary with vycor tip filled with a 0.1 mol·L^{-1} $[N^nBu_4][B(C_6F_5)_4]$ solution in dichloromethane. Successive experiments under the same experimental conditions showed that all formal reduction and oxidation potentials were reproducible within 5 mV. Experimentally potentials were referenced against a Ag/Ag^+ reference electrode but the results are presented referenced against the FcH/FcH^+ couple ($E_{1/2}$ = 0.0 V) as required by IUPAC.[36] When decamethylferrocene was used as an internal standard, the experimentally measured potential was converted in to *E vs* FcH/FcH^+ by addition of -0.61 V.[37] The cyclovoltammograms were taken after typical two scans and are considered to be steady state cyclovoltammograms, in which the signal pattern differs not from the initial sweep. Finally, the experimental data were processed on Microsoft Excel worksheets.

Computational Details. All quantum chemical calculations were performed with TURBOMOLE 6.3.1.[38] After the initial guess the Kohn-Sham equations were converged in the small def-SV(P)[39] basis set using a damping factor of 20 and Fermi smearing. After this step a geometry optimization was performed. Next the structures were optimized at the PB86/def2-TZVP[38,40] level of theory using the m5 grid. In all calculations density fitting was applied.[41] The final stationary points were characterized by analyzing the hessian matrix.[42] The final energy evaluations were performed with the B3LYP[39,43] hybrid functional in combination with the def2-TZVP basis set. To include the solvent effects the COSMO[44] solvation model with $\varepsilon = \infty$ was

applied. The reported relative energies include the zero point energy correction from the gas phase at the BP86/def2-TZVP level of theory.

Single-Crystal X-ray Diffraction Analysis. Crystal data for **1** – **4** are summarized in Table SI-1 (Appendix 5). Data were collected with an Oxford Gemini S diffractometer at 100 K using Mo-Kα (λ = 0.71073 Å) radiation. The structures were solved by direct methods using SHELXS-97 and refined by full matrix least-square procedures on F2 using SHELXL-97.[45,46] All non-hydrogen atoms were refined anisotropically and a riding model was employed in the refinement of the hydrogen atom positions.

Crystallographic data (excluding structure factors) for the structures in this paper have been deposited with the Cambridge Crystallographic Data Centre, CCDC, 12 Union Road, Cambridge CB21EZ, UK. Copies of the data can be obtained free of charge on quoting the depository numbers CCDC-949877 (**1**), 949876 (**2**), 949878 (**3**) and 949875 (**4**) (Fax: +44-1223-336-033; E-Mail: deposit@ccdc.cam.ac.uk, http://www.ccdc.cam.ac.uk).

6.5 ACKNOWLEDGMENT

D.I.B. and B.v.d.W. acknowledge the National Research foundation, South Africa for financial support (Grant number 76226). We are grateful to the Fonds der Chemischen Industrie for financial support. J.M.S. and M.K. thank the FCI for Chemiefonds Fellowships.

6.6 REFERENCES

(1) (a) Fischer, E. O.; Maasböl, A. *Angew. Chem., Int. Ed. Engl.* **1964**, *3*, 580-581; (b) Bezuidenhout, D. I.; Lotz, S.; Liles, D. C.; van der Westhuizen, B.; *Coord. Chem. Rev.*, **2012**, *51*, 479-524; (c) Astruc, D. *Electron Transfer and Radical Processes in Transition Metal Chemistry*, VCH, New York, **1995**; (d) Astruc, D. *Acc. Chem. Res.*, **1997**, *30*, 383-391; (e) Long, N. J. *Angew. Chem.,* **1995**, *34*, 21-38; (f) Behrens, U.; Brussaard, H.; Hagenau, U.; Heck, J.; Hendrickx, E.; Kornich, J.; van der Linden, J. G. M.; Persoons, A.; Spek, A. L.; Veldman, N.; Voss, B.; Wong, H. *Chem. Eur. J.* **1996**, *2*, 98-103.

(2) (a) Dötz, K. H. *Angew. Chem., Int. Ed. Engl.* **1975**, *14*, 644-645; (b) Aumann, R.; Heinen, H. *Chem. Ber.* **1987**, *120*, 537-540.

(3) Pike, A. R.; Ryder, L. C.; Horrocks, B. R.; Clegg, W.; Connolly, B. A.; Houlton, A. *Chem. Eur. J.*, **2004**, *11*, 344-353.

(4) Spanig, F.; Kolvacs, C.; Hauke, F.; Ohlubo, K.; Fukuzumi, F.; Guldi, D. M.; Hirsch, A. *J. Am. Chem. Soc.* **2009**, *131*, 8180-8195.

(5) (a) Shago, R. F.; Swarts, J. C.; Kreft, E.; Van Rensburg, C. E. J.; *Anticancer Res*. **2007**, *27*, 3431-3434; (b) Van Rensburg, C. E. J.; Kreft, E.; Swarts, J. C.; Dalrymple, S. R.; Macdonald, D. M.; Cooke, M. W.; Aquino, M. A. S. *Anticancer Res*. **2002**, *22*, 889-892; (c) Gross, A.; Hüsken, N.; Schur, J.; Raszeja, L.; Ott, I.; Metzler-Nolte, N. *Bioconjugate Chemistry*, **2012**, *23*, 1764-1774; (d) Swarts, J. C.; Vosloo, T. G.; Cronje, S. J.; Du Plessis, W. C.; Van Rensburg, C. E. J.; Kreft, E.; Van Lier, J. E. *Anticancer Res.* **2008**, *28*, 27812784; (e) Ott, I.; Kowalski, K.; Gust, R.; Maurer, J.; Mücke, P.; Winter, R. F. *Bioorg. Med. Chem. Lett.* **2010**, *20*, 866-869.

(6) See annual reviews by: Herndon, J. W. *Coord. Chem. Rev.,* 2002 – 2012.

(7) (a) Wulff, W. D. in *Advances in Metal-Organic Chemistry*; Liebeskind, L. S., Ed.; JAI Press Inc.: Greenwich, Conn, 1989; Vol. 1; b) Wulff, W. D., in "*Comprehensive Organic Synthesis*", Trost, B. M.; Fleming, I., Eds., Pergamon Press, 1990, Vol 5. c) Wulff, W. D. in *Comprehensive Organometallic Chemistry II*, Abel, E.W.; Stone, R.G.A.; Wilkinson, G., Eds.; Pergamon Press, 1995, *Vol. 12*, 469. d) Wulff, W. D., *Organometallics*, **1998**, *17*, 3116-3134.

(8) (a) Leroux, F.; Stumpt, R.; Fischer, H.; *Eur. J. Inorg. Chem.* **1998**, 1225-1234. (b) Licandro, E.; Maiorana, S.; Papagani, A.; Hellier, P.; Capella, L.; Persoons, A.; Houbrechts, S. *J. Organomet. Chem.* **1999**, *583*, 111-119. (c) Robin-Le Guen, F.; Le Poul, P.; Caro, B.; Pichon, R.; Kervarec, N.; *J. Organomet. Chem.* **2001**, *626*, 37-42. (d) Faux, N.; Caro, B.; Robin-Le Guen, F.;

Le Poul, P.; Nakatani, K.; Ishow, E. *J. Organomet. Chem.* **2005**, *690*, 4982-4988. (e) Baldoli, C.; Cerea, P.; Falciola, L.; Giannini, C.; Licandro, F.; Maiorana, S.; Mussini, P.; Perdiccia, D.; *J. Organomet. Chem.* **2005**, *690*, 5777-5787.

(9) (a)Chandrasekhar, V.; Thirumoorthi, R. *Organometallics*, **2007**, *26*, 5415-5422; (b) Ogawa, S.; Muroaka, H.; Kikuta,K.; Saito, F.; Sato, R. *J. Organomet. Chem.*, **2007**, *692*, 60-69; (c) *Ferrocenes,* Stepnicka, P. Ed.; John Wiley & Sons, 2008; (d) Ludvik, J.; Stepnicka, P. *ECS Trans.,* **2007**, *2*, 17-25; (e) Hildebrandt, A.; Rüffer, T.; Erasmus, E.; Swarts, J. C.; Lang, H. *Organometallics*, **2010**, *29*, 4900-4905; (f) Speck, J. M.; Schaarschmidt, D.; Lang, H. *Organometallics* **2012**, *31*, 1975-1982.

(10) (a) Hildebrandt, A.; Lang, H. *Dalton Trans.* **2011**, *40*, 11831-11837; (b) Speck, J.M., Claus, R., Hildebrandt, A., Rüffer, T., Erasmus, E., van As, L., Swarts, J.C., Lang, H., *Organometallics*, **2012**, *31*, 6373-6380.

(11) (a) Connor, J. A.; Jones, E. M.; Lloyd, J. P. *J. Organomet. Chem.* **1970**, *24*, C20-C22; (b) Lloyd, M. K.; McCleverty, J. A.; Orchard, D. G.; Connor, J. A.; Hall, M. B.; Hillier, I. H.; Jones, E. M.; McEwen, G. K. *J. Chem. Soc., Dalton Trans.* **1973**, 1743-1747; (c) Casey, C. P.; Albin, L. D.; Saeman, M. C.; Evans, D. H. *J. Organomet. Chem.*, **1978**, *155*, C37-C40; (d) Limberg, A.; Lemos, M. A. N. D. A.; Pombeiro, A. J. L.; Maiorana, S.; Papagni, A.; Licandro, E.; *Port. Electrochim. Acta,* **1995**, *13*, 319-323; (e) Pombeiro, A. J. L. *New J. Chem.*, **1997**, *21*, 649-660; (f) Fernández, I.; Mancheño, M. J.; Gómez-Gallego, M.; Sierra, M. A.; *Org. Lett.*, **2003**, *5*, 1237-1240; (g) MartínezÁlvarez, R.; Gómez-Gallego, M.; Fernández, I.; Mancheño, M. J.; Sierra, M. A. *Organometallics*, **2004**, *23*, 4647-4654; (h) Wulff, W. D.; Korthals, K. A.; Martínez-Álvarez, R.; Gómez-Gallego, M.; Fernández, I.; Sierra, M. A. *J. Org. Chem.*, **2005**, *70*, 5269-5277; (i) López-Alberca, M. P.; Mancheño, M. J.; Fernández, I.; Gómez-Gallego, M.; Sierra, M. A.; Hemmert, C.; Gornitzka, K. H. *Eur. J. Inorg. Chem.*, **2011**, 842-849; (j) van der Westhuizen, B.; Swarts, P. J.; Strydom, I.; Liles, D. C.; Fernández, I.; Swarts, J. C.; Bezuidenhout, D. I. *Dalton Trans.* **2013**, 42, 5367-5378 (k) van der Westhuizen, B.; Swarts, P. J.; van Jaarsveld, L. M.; Liles, D. C.; Siegert, U.; Swarts, J. C.; Fernández, I.; Bezuidenhout, D. I. *Inorg. Chem.* **2013**, *52*, 6674-6684.

(12) (a) Bezuidenhout, D.I.; Lotz, S.; Landman, M.; Liles, D.C. *Inorg. Chem.* **2011**, *50*, 1521-1533; (b) Helten, H.; Beckman, M.; Schnakenburg, G.; Streubel, R. *Eur. J. Inorg. Chem.* **2010**, *16*, 2337-2341; (c) Bezuidenhout, D.I.; van der Watt, E.; Liles, D.C.; Landman, M.; Lotz, S.

Organometallics, **2008**, *27*, 2447-2456; (d) Fischer, E.O.; Postnov, V.N.; Kreissl, F.R. *J. Organomet. Chem.*, **1982**, *23,* C73-C77.

(13) (a) Meca, L.; Dvorak, D.; Ludvik, J.; Cisarova, I.; Stepnicka, P. *Organometallics* **2004**, *23*, 2541-2551; (b) Butler, I.R.; Cullen, W.R.; Einstein, F.W.B.; Willis, A.C. *Organometallics*, **1985**, *4*, 603-604; (c) Fischer, E.O.; Gammel, F.J.; Besenhard, J.O.; Frank, A.; Neugebauer, D. *J. Organomet. Chem.,* **1980**, *191,* 261-282.

(14) R. Schobert, R. Kempe, T. Schmalz, A. Gmeiner, *J. Organomet. Chem*., **2006**, *691*, 859-868.

(15) Sünkel, K.; Bernhartzeder, S. *J. Organomet. Chem.* **2011**, *696*, 1536-1540.

(16) Dong, T.Y.; Chang, C.K.; Lee, S.H.; Lai, L.L.; Chiang, M.Y.N.; Lin, K.L. *Organometallics,* **1997**, *16*, 5816-5825.

(17) *Spectral Database for Organic Compounds (SDBS)*; 1H NMR spectrum (No. 6650HPM-00-130); SDBS No.: 6650; RN: 102-54-5; http://riodb01.ibase.aist.go.jp/sdbs/.

(18) Krejčik, M.; Daněk, M.; Hartl, F. *J. Electroanal. Chem.* **1991**, *317*, 179-187.

(19) Cardona, C. M.; Li, W.; Kaifer, A. E.; Stockdale, D.; Bazan, G. C. *Adv. Mater.* **2011**, *23*, 2367-2371.

(20) Baldoli, C.; Cerea, P.; Falciola, L.; Giannini, C.; Licandro, E.; Maiorana, S.; Mussini, P.; Perdicchia, D. *J. Organomet. Chem.* **2005**, *690*, 5777-5787.

(21) In related alkoxy- and aminocarbene tungsten complexes of ferrocene, 3-electron oxidation was observed when employing [(*n*Bu)4N][PF6] as electrolyte, while use of [(*n*Bu)4N]{B(C6H5)4] yielded a two-electron oxidation; Bezuidenhout, D. I.; Fernández, I.; van der Westhuizen, B.; Swarts, P. J.; Swarts, J. C. *unpublished results*.

(22) (a) Bott, A. W.; Heineman, W. R. *Curr. Sep.* **2004**, *20*, 121-126; (b) Anson, F. C.; Christie, J. H.; Osteryoung, R. A. *J. Electroanal. Chem.* **1967**, *13*, 343-353.

(23) Bezuidenhout, D. I.; Barnard, W.; Van der Westhuizen, B.; Van der Watt, E.; Liles, D. C. *Dalton Trans.* **2011**, *40*, 6711-6721.

(24) Camire, N.; Mueller-Westerhoff, U. T.; Geiger, W. E. *J. Organomet. Chem.* **2001**, *637*, 823-826.

(25) Robin, M. B.; Day, P. *Adv. Inorg. Chem. Radiochem.* **1968**, *10*, 247-422.

(26) (a) Connor, J. A.; Lloyd, J. P. *J. Chem. Soc., Dalton Trans.* **1972**, 1470-1476; (b) Rosenblum, M.; Santer, J. O.; Howells, W. G. *J. Am. Chem. Soc.* **1957**, *85*, 1450-1458; (c) Sohn, Y. S.; Hendrickson, D. N.; Gray, H. B. *J. Am. Chem. Soc.* **1971**, *93*, 3603-3612.

(27) Warratz, R.; Aboulfadl, H.; Bally, T.; Tuczek, F. *Chem. Eur. J.* **2009**, *15*, 1604-1617.

(28) (a) Atwood, C. G.; Geiger, W. E. *J. Am. Chem. Soc.* **1994**, *116*, 10849-10850; (b) Lohan, M.; Ecorchard, P.; Rüffer, T.; Justaud, F.; Lapinte, C.; Lang, H. *Organometallics* **2009**, *28*, 1878-1890; (c) Paul, F.; Toupet, L.; Thépot, J.-Y.; Costuas, K.; Halet, J.-F.; Lapinte, C. *Organometallics* **2005**, *24*, 5464-5478.

(29) (a) D'Alessandro, D. M.; Keene, F. R. *Chem. Soc. Rev.* **2006**, *35*, 424-440; (b) Brunschwig, B. S.; Creutz, C.; Sutin, N. *Chem. Soc. Rev.* **2002**, *31*, 168-184.

(30) Warratz, R.; Tuczek, F. *Inorg. Chem.* **2009**, *48*, 3591-3607.

(31) (a) Siebler, D.; Förster, C.; Gasi, T.; Heinze, K. *Organometallics* **2011**, *30*, 313-327; (b) Lohan, M.; Justaud, F.; Roisnel, T.; Ecorchard, P.; Lang, H.; Lapinte, C. *Organometallics* **2010**, *29*, 4804-4817.

(32) Dong, T.-Y.; Lee, T.-Y.; Lee, S.-H.; Lee, G.-H.; Peng, S.-M. *Organometallics* **1994**, *13*, 2337-2348.

(33) López-Cortés, J. G.; Contreras de la Cruz, L. F.; Ortega-Alfaro, M. C.; Toscano, R. A.; Alvarez-Toledano, C.; Rudler, H. *J. Organomet. Chem.* **2005**, *690*, 2229-2237.

(34) Fernández, I.; Cossío, F. P.; Arrieta, A.; Lecea, B.; Mancheño, M. J.; Sierra, M. A. *Organometallics* **2004**, *23*, 1065-1071.

(35) (a) LeSuer, R. J.; Buttolph, C.; Geiger, W. E. *Anal. Chem.* **2004**, *76*, 6395-6401; (b) Barrière, F.; Camire, N.; Geiger, W. E.; Mueller-Westerhoff, U. T.; Sanders, R. *J. Am. Chem. Soc.* **2002**, *124*, 7262-7263; (c) Barrière, F.; Geiger, W. E. *J. Am. Chem. Soc.* **2006**, *128*, 3980-3989.

(36) Gritzner, G.; Kuta, J. *Pure Appl. Chem.* **1984**, *56*, 461-466.

(37) Nafady, A.; Geiger, W. E. *Organometallics* **2008**, *27*, 5624-5631.

(38) (a) TURBOMOLE V6.3 2011, a development of University of Karlsruhe and Forschungszentrum Karlsruhe GmbH, since 2007; available from http://www.turbomole.com., 1989-2007; (b) Haser, M.; Ahlrichs, R. *J. Comput. Chem.* **1989**, *10*, 104-111; (c) Deglmann, P.; Furche, F.; Ahlrichs, R. *Chem. Phys. Lett.* **2002**, *362*, 511-518; (d) van Wüllen, C. *J. Comp. Chem.* **2002**, *32*, 1195-1201.

(39) (a) Weigend, F.; Ahlrichs, R. *Phys. Chem. Chem. Phys.* **2005** , *7*, 3297-3305; (b) Weigend, F.; Häser, M.; Patzelt, H.; Ahlrichs, R. *Chem. Phys. Lett.* **1998**, *294*, 143-152; (c) Schäfer, A.; Horn, H.; Ahlrichs, R. *J. Chem. Phys.* **1992** , *97*, 2571-2522.

(40) (a) Becke, A. D. *Phys. Rev. A* **1988**, *38*, 3098-3100; (b) Perdew, J.P. *Phys. Rev. B* **1986**, *33*, 8822-8824.

(41) (a) Weigend, F. *Phys. Chem. Chem. Phys.* **2006**, *8*, 1057-1065; (b) Eichkorn, K.; Treutler, O.; Oehm, H.; Häser, M.; Ahlrichs, R. *Chem. Phys. Lett.* **1995**, *242*, 652-660; (c) Eichkorn, K.; Weigand, F.; Treutler, O.; Ahlrichs, R. *Theo. Chem. Acc.* **1997**, *97*, 119-124.

(42) (a) Treutler, O.; Ahlrichs, R. *J. Chem. Phys.* **1995**, *102*, 346-354; (b) v. Arnim, M.; Ahlrichs, R. *J. Chem. Phys.* **1999**, *111*, 9183-9190.

(43) (a) Lee, C.; Yang, W.; Parr, R. G. *Phys. Rev. B* **1988**, *37*, 785-789; (b) Becke, A. D. *J. Chem. Phys.* **1993**, *98*, 5648-5652.

(44) Klamt, A.; Schüürmann, G. *J. Chem. Soc., Perkin Trans.* **1993**, *2*, 799-805.

(45) Sheldrick, G. M. *Acta Crystallogr., Sect. A* **1990**, *46*, 467.

(46) Sheldrick, G. M. SHELXL-97, Program for Crystal Structure Refinement; Universität Göttingen, Göttingen, Germany, 1997.

CHAPTER 7

(Spectro)electrochemical Investigations on (Ferrocenyl)thiophenes modified by Tungsten Fischer Carbenes.

A manuscript of this chapter has been submitted to Organometallics. The format reflects the style set by the journal.

Belinda van der Westhuizen,[a] J. Matthäus Speck,[b] Marcus Korb,[b] Daniela I. Bezuidenhout[a*] and Heinrich Lang[b*], *Organometallics*, **2013**.

Author contributors

Synthetic work: Belinda van der Westhuizen

Cyclic voltammetry and data analysis: Matthäus Speck

Crystallography: Marcus Korb

Article written: Belinda van der Westhuizen, J. Matthäus Speck, Marcus Korb

[a] *Chemistry Department, University of Pretoria, Private Bag X20, Hatfield, 0028, South Africa. Fax: +27-(0)12-420-4687; Tel: +27-(0)12- 420-2626; E-mail: daniela.bezuidenhout@up.ac.za*
[b] *Technische Universität Chemnitz, Fakultät für Naturwissenschaften, Institut für Chemie, Anorganische Chemie, D-09107 Chemnitz, Germany.*

Supporting Information. UV-Vis/NIR spectra in dichloromethane and crystal structure details for **1** - **4** as well as calculated infrared spectra of **1** and $\mathbf{1}^{+}$ are given. This material is available free of charge via the Internet at http://pubs.acs.org. (**Appendix 6**)

ABSTRACT: A series of thiophene tungsten Fischer carbene complexes of type [$(CO)_5$W=C(OMe)R] (**1**, R = 2-Th; **3**, R = fcthFc) and [$(CO)_5$W=C(OMe)-R'-(OMe)C=W$(CO)_5$] (**2**, R' = th; **5**, R' = fcthfc) was synthesized for investigating low energy charge transfer interactions between the carbene substituents and the transition metal carbonyl fragment incorporating the thiophene heterocyclic system (Th = Thienyl; th = 2,5-thiendiyl; Fc = ferrocenyl; fc = 1,1'-ferrocenediyl). Electrochemical investigations were carried out on these complexes for a closer insight into the electronic properties of **1**, **2**, **4** and **5**. They reveal reversible one electron redox events for the ferrocenyl moieties. Moreover, typical electrode reactions could be found for the carbene reductions itself and for the tungsten carbonyl oxidation processes. However, for the thiophene complex **2** two well separated one-electron reduction events could be found. During the UV-Vis-NIR spectroelectrochemical investigations typical low energy absorptions for the mixed-valent *α,α'*-diferrocenyl thiophene increment were found, as well as high energy NIR absorptions which were attributed to metal-metal charge transfer transition between the tungsten carbonyl increment and the ferrocenyl units in the corresponding species. Further infrared spectroelectrochemical studies reveal that the electronic interactions in the corresponding cationic species can be described with weakly coupled class II systems according to Robin and Day.

7.1 INTRODUCTION

In recent years the application of Fischer carbene complexes has expanded from catalysis, auxiliary ligands and application in organic chemistry to electronic probes and potential molecular wires.[1] These applications have mostly evolved around the M=C carbene double bond but interest in the electrochemical properties of carbene complexes was the prelude to new applications, especially in the field of catalysis.[2] Fischer carbene complexes are excellent candidates for electrochemical studies as redox centra can be extended from mono- to polymetallic[3] and organic or organometallic π-conjugated linkers can be used to separate transition metal moieties.[4] Combining the properties of Fischer carbenes with π-conjugated bridges could result in the design of new push-pull systems with novel non-linear optical (NLO) character. In our recent papers we paid attention to metal-metal interaction in Fischer carbenes on ferrocenyl and biferrocenyl tungsten alkylidene complexes.[5] UV-Vis-NIR

spectroelectrochemical investigations revealed a high energy NIR absorption which was attributed to a metal-metal charge transfer transition (MMCT) between the tungsten and ferrocenyl/biferrocenyl moieties. Within this context, the use of redox active metal-based temini offers the possibility to design new materials, such as semiconducting polymers and molecular wires.

In this study we describe synthesis and characterization of tungsten thienyl (Th) novel and 2,5-diferrocenylthiophenes mono- and biscarbene Fischer complexes (Scheme 7.1). Electrochemical and spectroelectrochemical properties were investigated.

7.2 RESULTS AND DISCUSSION

Synthesis and Characterization. The tungsten Fischer carbene complexes **1**, **2**, **4** and **5** were prepared employing the classical Fischer carbene synthesis: $W(CO)_6$ was reacted with relevant lithiated species of Th, 2,5-dibromothiophene (2,5-$ThBr_2$) and 2,5-di(1'-bromoferrocenyl)thiophene ($Fc_2Th'Br_2$) to form the respective metal acylates. After alkylation with methyl trifluoromethanesulfonate (MeOTf), neutral complexes were isolated as red/purple – dark brown solids. Complex **1** was previously synthesized and spectroscopically characterized, but single x-ray diffraction data was not reported.[6] The ethoxy-analogue of compound **1** has also recently been electrochemically characterized.[7]

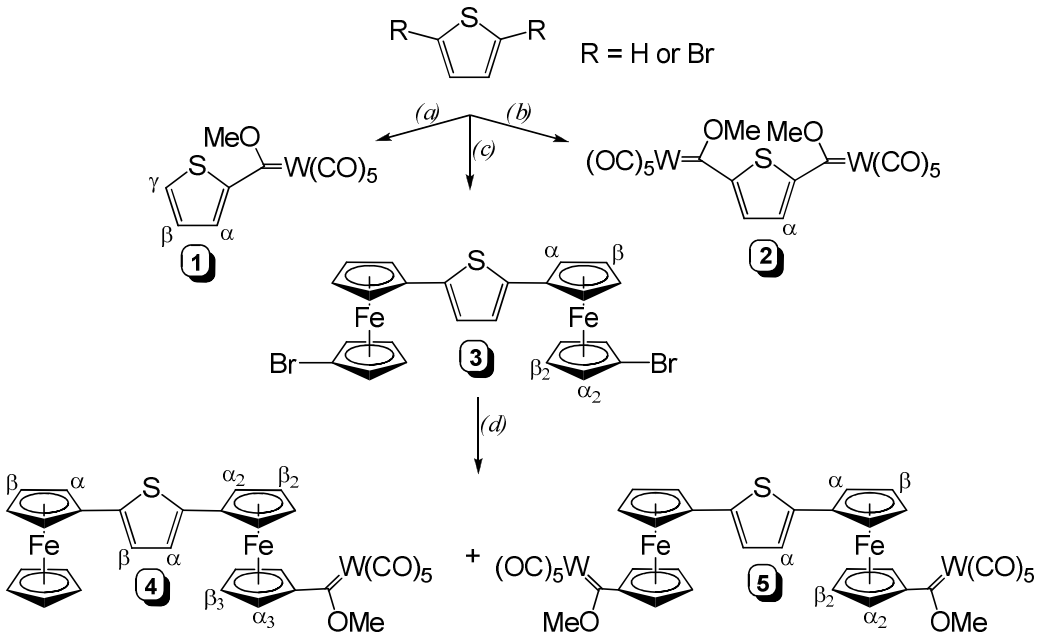

Scheme 7.1 Atom numbering system used for the series of complexes studied. Reaction conditions: (a) (i) R = H, thf, -80°C, ^{n}BuLi; (ii) $W(CO)_6$, -50°C; (iii) dcm, -50°C, MeOTf. (b) (i) R = Br, thf, -40°C, ^{n}BuLi; (ii) $W(CO)_6$, -40°C; (iii) dcm, -30°C, MeOTf. (c) (i) thf, $FcBr_2$, -100°C, ^{n}BuLi; (ii) $ZnCl_2 \cdot 2thf$, 0°C; (iii) 2,5-$ThBr_2$, [Pd], 55°C. (d) (i) thf, -40°C, ^{n}BuLi; (ii) $W(CO)_6$, -40°C; (iii) dcm, -30°C, MeOTf.

Lithiated thienyl/biferrocenylthiophenes were generated *in situ* from respective brominated precursors by lithiation or lithium-bromine exchange reaction according to literature procedures.[8] Purification of these complexes was done by column chromatography and were very stable toward moisture and air in the solid state and in solution. Compound **3** were synthesized by employing the palladium-promoted Negishi C-C cross-coupling protocol[9] using dibromoferrocene ($FcBr_2$) and 2,5-dibromothiophene. The catalyst used was [$Pd(CH_2CMe_2P^tBu_2)(\mu$-Cl).[10]

Table 7.1 Selected NMR data and the infrared ν(CO) stretching frequencies (A_1'') of Fischer carbenes **1**, **2**, **4**, **5**.

Compd.	$H_\alpha\ \delta^a$ ^1H [ppm]	$C_{carbene}\ \delta^a$ $^{13}C\{^1H\}$ [ppm]	$A_1''\nu(CO)^b$ [cm^{-1}]
1	8.17	293.39	2069
2	7.95	296.50	2062
4	4.93	307.75	2062
5	4.93	308.47	2060

Solvent used: a) $CDCl_3$ b) dichloromethane

The electronic effects of the carbene substituents in the compounds synthesized can be followed in solution by both NMR and IR spectroscopy. The proton α to the carbene substituent in thienyl and ferrocenethiophenes experiences the greatest deshielding (Table 7.1) and corresponds well to the substituent effect of, for example, an ester functionality instead of a metal carbonyl fragment.[11] Stabilization of the electrophilic carbene carbon also occurs in a similar way as with the ester analogues: via π-delocalisation of the heteroaryl ring. As expected, this effect is also seen in the *trans*-CO stretching frequency which decreases as stabilization from the heteroatom increases.[12] Due to the relative insensitivity of the carbonyl stretches toward the changes on the carbene substituents,[13] little difference is observed in the measured IR frequencies for these series of complexes.

Electrochemistry. The electrochemical studies of complexes **1**, **2**, **4** and **5** were carried out under an argon atmosphere in dichloromethane solutions containing $[N^nBu_4][B(C_6F_5)_4]$ (0.1 M) as supporting electrolyte, an OTTLE[14] (= Optically Transparent Thin Layer Electrochemistry) cell was used during the spectroelectrochemical investigations (Experimental Section).

During the electrochemical study of **1**, two significant redox events could be detected. A reduction process at E_{pc} = -1746 mV, which is associated with the reduction of the carbene center itself, and a tungsten carbonyl oxidation reaction at E_{pa} = 819 mV (Table 7.2 and Figure 7.1). Similar observations were made for other Fischer carbene complexes previously.[5] Furthermore, a second tungsten carbene moiety on the thiophene system (**2**) results in an more anodic, irreversible tungsten oxidation process starting from E_{pa} = 851 mV (Table 7.2 and Figure 7.1). In contrast to the latter electrode reaction, two reversible one-electron reduction events could be detected for **2** at $E^{0'}$ = -1319 mV and -1061 mV, in which the generation of the monoanion takes place around 600 mV more anodic as observed for molecule **1** (Table 7.2, Figure 7.1). The corresponding redox separation ($\Delta E^{0'}$ = 258 mV) suggests an interaction of the Fischer carbene moieties in $\mathbf{2}^{-}$ over the thiophene bridge (*vide infra*).

A combination of the 2,5-diferrocenyl thiophene[15] system with one carbene fragment (**4**) results also in a significant anodic shift for the first ferrocenyl redox process compared the 2,5-diferrocenyl thiophene.[15] The second iron based oxidation process for compound **4** could be observed at 419 mV, further increasing of the potential leads to the typical irreversible tungsten carbonyl oxidation process around 1100 mV *vs* FcH/FcH^{+} (Table 7.2 and Figure 7.1). The generation of $\mathbf{4}^{-}$ could be detected at $E_{pc} \approx$ -2.1 V. In case of the biscarbene **5**, the first ferrocenyl redox event was observed at $E^{0'}$ = 230 mV, approximately 0.22 V more anodic as detected for the corresponding $\mathbf{4/4}^{+}$ redox process, but even slightly more cathodic as for the previously described ferrocenyl tungsten Fischer carbene system.[5] The redox potential of the $\mathbf{5}^{+}/\mathbf{5}^{2+}$ process was determined to $E^{0'}$ = 473 mV *vs* FcH/FcH^{+}. Hence, the corresponding redox separation is only slightly lower as observed for the 2,5-diferrocenyl thiophene system itself under similar conditions (Table 7.2 and Figure 7.1).[15] Furthermore, the reduction events of the Fischer carbene centers as well as the tungsten carbonyl electrode reactions of molecule **5** were detected in the same potential range as observed for ferrocenyl thiophene **4** (Table 7.2, Figure 7.1).

In order to get more insight into the oxidation process of **2**, **4** and **5** spectroelectrochemical studies were carried out by an stepwise increase of the potential *vs* Ag/AgCl in an OTTLE cell (= Optically Transparent Thin Layer Electrochemistry)[14] using a 0.1 M dichloromethane solution of $[N^{n}Bu_4][B(C_6F_5)_4]$ as supporting electrolyte. This procedure allows for the *in situ* generation of intervalent species such as $\mathbf{2}^{n-}$, $\mathbf{4}^{n+}$ and $\mathbf{5}^{n+}$ (n = 1, 2). If deconvolution of NIR absorptions was

used, transitions with Gaussian shapes were taken to get fits good enough to allow an almost exact overlay of the sum of the spectral components with the experimental spectra.

Table 7.2 Cyclic voltammetry data (potentials *vs* FcH/FcH^+) of 1.0 $mmol{\cdot}L^{-1}$ solutions of **1**, **2**, **4** and **5** in dry dichloromethane containing 0.1 $mol{\cdot}L^{-1}$ of $[N^nBu_4][B(C_6F_5)_4]$ as supporting electrolyte at 25 °C. [a] *300 mVs*$^{-1}$

Compd.	$E_{pa}/E_{pc}/\Delta E_p/E^{0'}/\Delta E^{0'}$ [mV] Wave (no.) (1)	(2)	(3)	(4)
1	-1666/-1746/78/-1707	819/726/93/773		
2	-1286/-1351/65/-1319	-1030/-1091/61 -1061/258	851[a]/ -	
4	- /-2093	44/-26/70/9	453/385/68/419/410	1134/ -
5	- /-2095[a]	263/198/65/230	507/438/69/473/243	1134[a]/ -

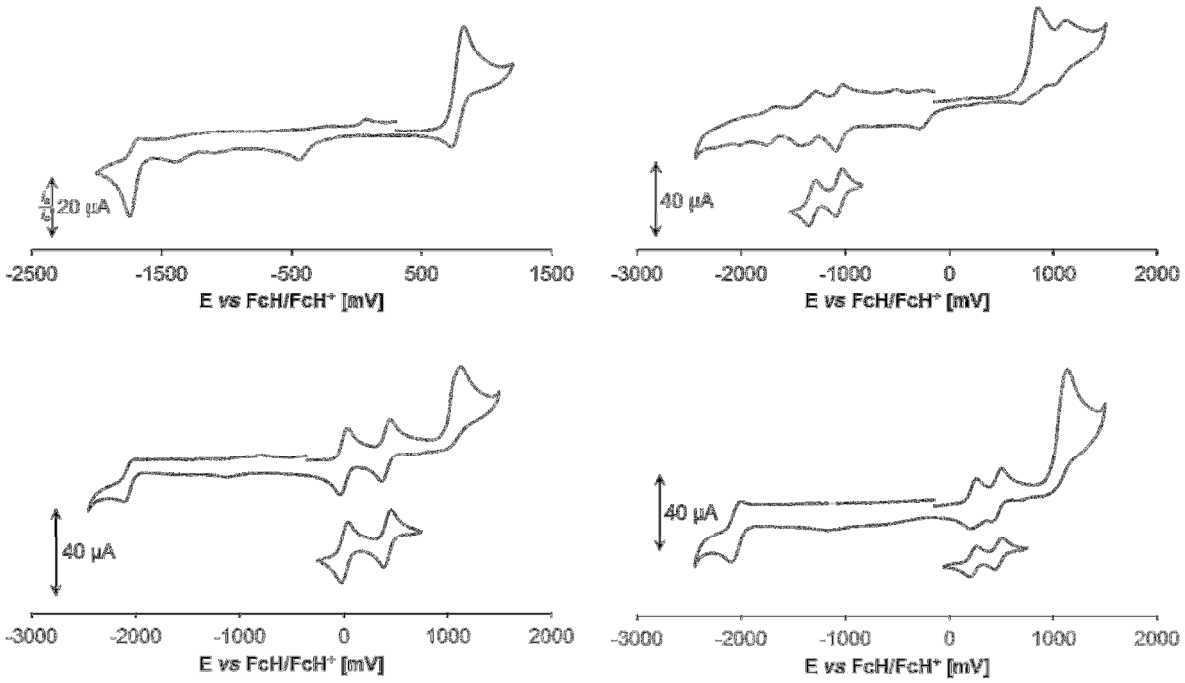

Figure 7.1 Cyclic voltammograms of Fischer type carbenes **1** (left top), **2** (right top), **4** (left bottom) and **5** (right bottom). Scan rate: 100 mVs^{-1} (full range cyclic voltammograms of **2** and **5** at 300 mVs^{-1}) in dichloromethane solutions (1.0 $mmol{\cdot}L^{-1}$) at 25 °C, supporting electrolyte $[N^nBu_4][B(C_6F_5)_4]$ (0.1 $mol{\cdot}L^{-1}$). In case of the full range cyclic voltammograms the initial cycle is shown. For cyclic voltammetry data see Table 7.2.

All neutral Fischer carbene complexes do not display, as expected, any absorptions in the NIR range. The corresponding UV-Vis/NIR spectra **4** and **5** are presented in the Supporting Information (Figures SI-1 and SI-2, Appendix 6). For calculation of the theoretical bandwidth at half height ($\Delta\nu_{1/2(theo)}$) in asymmetric systems, the energy gap between the diabatic states (ΔG^0) could be estimated, using the difference in oxidation potentials of the two redox sites. Regarding this, the oxidation potential of $(CO)_5W{=}C(OMe)Me$[16] as well as the formal potential of the Fc/Fc^+ redox process of $(CO)_5W{=}C(OMe)Fc$[5] were used (Table 7.3).

Within the UV-Vis/NIR spectroelectrochemical investigations of **2** no noteworthy absorptions could be recorded in the NIR range. In contrast, significant changes in ν(CO) stretching frequencies could be detected during the successive *in situ* generation of $\mathbf{2}^-$ (Figure 7.2). Thus,

the absorption of the original A_1" mode, at 2062 cm^{-1} decreases together with an rising absorption band at 2045 cm^{-1} (Figure 7.2). This suggests a significant interaction between the two Fischer carbene increments over the thiophene bridge within the infrared timescale. Furthermore, the ν(CO) stretching frequencies of **2** at 1947 cm^{-1} shift formal to 1920 cm^{-1} upon generation of the monoanion (Figure 7.2). Further reduction to $\mathbf{2^{2-}}$ leads to a decrease of the A_1" ν(CO) stretching frequencies in combination with a formal splitting of the band at 1920 cm^{-1} to 1928 cm^{-1} and 1905 cm^{-1} (Figure 7.2). However, under our conditions a slow decomposition process could be observed during the generation of $\mathbf{2^{2-}}$, and hence the corresponding absorption behavior should be handled with caution. During the infrared spectroelectrochemical study of ferrocenyl thiophene **4**, ν(CO) stretching frequencies were observed at 2063 cm^{-1} and 1930 cm^{-1} (Figure 7.2).

Upon increasing the potential, the original absorptions shift only slightly to higher wavenumbers during the generation of $\mathbf{4^{+}}$ (2064 cm^{-1} and 1932 cm^{-1}, Figure 7.2). This observation reveals that the first oxidation is mostly based on the non-substituted ferrocenyl unit and the interaction with the Fischer carbene moiety is nearly negligible. Further increasing the potential leads to a decrease of the latter absorption bands and ν(CO) stretching frequencies at 2075 cm^{-1} and 1953 cm^{-1} could be detected for the dication of **4**. Within this regard, shift in ν(CO) stretching frequencies upon generation of $\mathbf{4^{2+}}$ is comparable with the corresponding behavior of the ferrocenyl tungsten Fischer carbene complex itself during the Fc/Fc^{+} redox process.[5] Thus, the interaction between the ferrocenyl unit and the Fischer carbene moiety should be very similar in both cases. Regarding this, UV-Vis/NIR spectroelectrochemical studies of **4** were carried out. Thus, during the oxidation process of **4** typical absorptions in the UV-Vis region of inner ferrocenyl transitions (π-π^{*} and MLCT/d-d) were observed (Figure SI-1, Appendix 6).[17] Upon generation of $\mathbf{4^{+}}$ three main absorptions could be detected in the NIR range. A high energy near infrared absorptions was observed around 10500 cm^{-1} and is assigned to a ligand to metal charge transfer (LMCT) transition, similar as observed for the monocationic intermediate of 2,5-diferrocenyl thiophene as well as for other ferrocenyl substituted heterocycles.[15,18] An observation of an absorption, caused by an ferrocenyl-tungsten interaction (MMCT), is not expected and can be excluded for $\mathbf{4^{+}}$, due to very small shift in ν(CO) stretching frequencies

(*vide supra*). Furthermore, the relative strong absorption at 6600 cm^{-1} is assigned to an intervalence charge transfer (IVCT) between the iron centers in $\mathbf{4}^{+}$ (Table 7.3).

The significant blue shift of the latter transition together with the significant smaller bandwidth at half height, as we would observe for a symmetrical system in the same energy range, compared with the corresponding absorption of the monocationic 2,5-diferrocenyl thiophene is caused by the asymmetry in **4** ($\mathbf{4}^{+}$, Table 7.3). From the fact that delocalization is not favored in asymmetrical systems, and together with the estimation of the corresponding theoretical value of the bandwidth at half height for such species, the metal-metal interaction in $\mathbf{4}^{+}$ can be assigned to a class II system according to Robin and Day.[19] The low energy absorption which was detected at 4080 cm^{-1}, which is too intense for an ligand field transition, is often ascribed to a further LMCT absorption, since the experimental determined bandwidth at half height would be too small as expected from the hush theory, however Tuczek *et al.* have proposed an IVCT character for such absorptions in intervalent non-bridged biferrocene species, similar as common accepted for bifulvalene diiron systems (Table 7.3, Figure SI-1 (Appendix 6)).[20]

Further increasing of the potential leads to a decrease of the low energy absorptions upon generation of $\mathbf{4}^{2+}$ together with an increasing LMCT absorption band around 11000 cm^{-1}. Furthermore, an absorption band at 7220 cm^{-1} could be detected and assigned to a MMCT between ferrocenyl unit and its tungsten Fischer carbene substituent, similar as observed for the corresponding ferrocenyl and biferrocenyl systems previously.[5] The weak absorption around 4000 cm^{-1} is ascribed to formal forbidden ligand field transitions.[15,21]

A second tungsten Fischer complex fragment on the α,α'-diferrocenyl thiophene building block (**5**) leads to three NIR absorptions for $\mathbf{5}^{+}$ at 9170 cm^{-1}, around 4700 cm^{-1} and at 3610 cm^{-1} (Table 7.3, Figure SI-2(Appendix 6)). The latter transition is assigned again to a low energy LMCT/IVCT (*vide supra*). The more intense absorption at 4660 cm^{-1} is described with the well-known iron-iron inter valence charge transfer similar as observed previously.[15] A comparison of the corresponding bandwidth at half height with the theoretical value reveals also a class II assignment, according to Robin and Day.[19] The third near infrared transition around 9200 cm^{-1} for $\mathbf{5}^{+}$ could ascribed with an LMCT transition (*vide supra*) between the thiophene core and the ferrocenyls, however it can also be an combination together with a ferrocenyl-tungsten MMCT transition (Table 7.3 and Figure SI-2 (Appendix 6)).

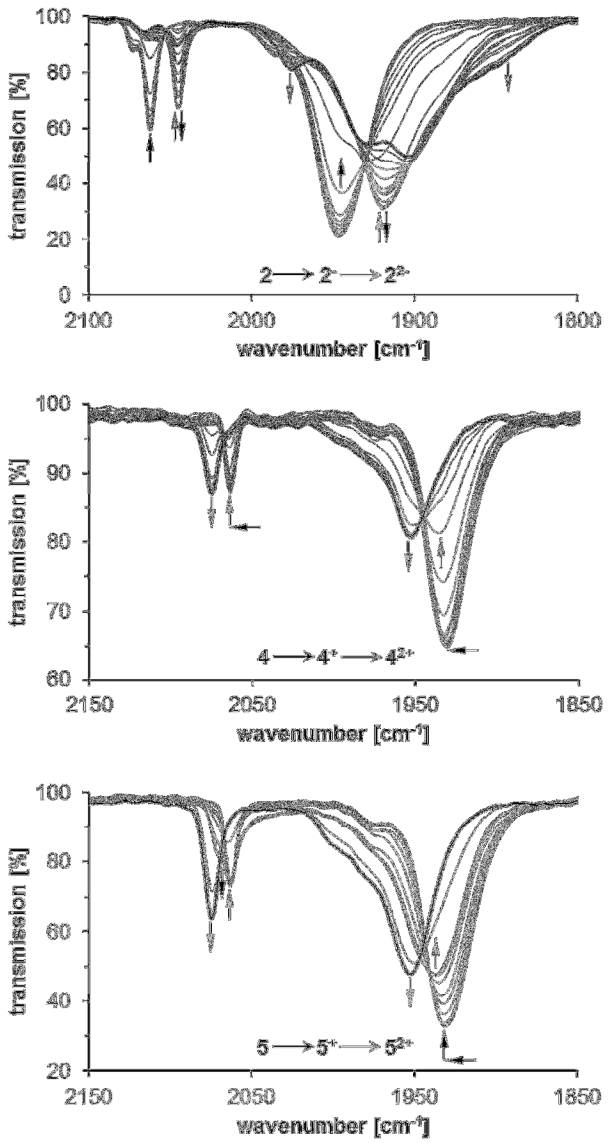

Figure 7.2 Infrared spectra of **2**, **4** and **5** at rising potentials (top: -200 to -750 mV; middle: -100 to 650 mV; bottom: -100 to 710 mV). All potentials *vs* Ag/AgCl at 25 °C in dichloromethane on 5 mM analyte solutions, supporting electrolyte $[N^nBu_4][B(C_6F_5)_4]$ (0.1 M). Arrows indicate increasing or decreasing as well as shifting absorptions.

During the successive generation of the monocationic **5** the ν(CO) stretching frequencies at 1931 cm^{-1} shifts formally to higher energy at 1937 cm^{-1} together with an occurrence of a double band for the A_1" ν(CO) stretching frequencies (2070 cm^{-1} and 2063 cm^{-1}), verifying the valence

trapped situation in $\mathbf{5}^{+}$ (Figure 7.2). Upon oxidation of $\mathbf{5}^{+}$, the low NIR absorptions decreases and the high energy absorption bands around 1000 nm become more intense (Table 7.3, Figure SI-2 (Appendix 6)). Furthermore, absorption bands at 6970 cm^{-1} (MMCT) and around 4000 cm^{-1} (LF) could be detected (Table 7.3 and Figure SI-2 (Appendix 6)). However, a slow decomposition of $\mathbf{5}^{2+}$ could be observed during the spectroelectrochemical measurements, thus the corresponding absorption behavior should be handled with caution.

Table 7.3 NIR data of **4** and **5** in dry dichloromethane containing $[N^{n}Bu_4][B(C_6F_5)_4]$ (0.1 M) as supporting electrolyte at 25 °C.

[a] $\Delta\nu_{1/2(theo)} = (2310\lambda)^{1/2}$. [b] $\lambda = \nu_{max} - \Delta G^0$. [c] $\lambda = \nu_{max}$. [d] $\Delta G^0 = 5900\ cm^{-1}$. [e] $\Delta G^0 = 2420\ cm^{-1}$.

Compd.	Transition	ν_{max} [cm^{-1}]	$\Delta\nu_{1/2}$ [cm^{-1}]	$\Delta\nu_{1/2(theo)}$ [cm^{-1}][a]
4^{+}	LMCT	10460	3280	
	IVCT	6600	3220	3100[e]
	LF	5140	720	
	LMCT/IVCT	4080	730	
4^{2+}	LMCT	10800	n. a.	
	MMCT	7220	3130	1750[d]
	LF	3950	1240	
5^{+}	LMCT/MMCT	9170	2920	2750[d]
	IVCT	4660	4200	3280[c]
	LMCT/IVCT	3610	900	
5^{2+}	LMCT	10200	n. a.	
	MMCT	6970	3800	1572[d]
	LF	4000	1000	

In the infrared range, the ν(CO) stretching frequencies at 2070 cm^{-1}, 2063 cm^{-1} and 1937 cm^{-1} decrease upon generation of $\mathbf{5}^{2+}$ together with increasing absorptions at 2075 cm^{-1} and 1953 cm^{-1}, very similar as observed during the generation of the cation of $(CO)_5W{=}C(OMe)Fc$.[5] Hence, a class II assignment according to Robin and Day should be also valid.[19]

Crystallography. The molecular structures of **1**, **4** and **5** in the solid state have been determined by single-crystal X-ray diffraction analysis. Suitable single crystals of **1**, **4** and **5** were obtained by slow evaporation of a saturated dichloromethane solution of the respective complex layered with *n*-hexane at –5 °C. The *ORTEP* diagrams with selected bond lengths (Å), bond angles (°), and torsion angles (°) are shown in Figures 7.3 – 7.5.

Compounds **1**, **4** and **5** crystallize in the triclinic space group *P*–1 (**5**) or in the monoclinic space group $P2_1/n$ (**4**,**1**) with one (**4**,**1**) or a half molecule (**5**) in the asymmetric unit. The thiophene in **5** is refined disordered on two positions with an occupation of 50 % for each orientation and is omitted for clarity in Figure 7.5. The ferrocenyl containing derivatives **4** and **5** show an almost planar conformation between the thiophene and the cyclopentadienyl cycles (**5**: C14–C13–C18–C19 –16(3) °, **4**: C14–C13–C18–C19 176.6(5) ° and C20–C21–C22–C26 1.1(8) °) and also to the planar carbene substituent (**5**: O6–C6–C8–C9 1.3(9) °, **4**: O6–C6–C8–C9 –0.2(6) °). A directly bonded heterocycle (**1**) also obtains a planar conformation between carbene and thiophene π-system (O6–C6–C8–C9 –170.9(4) °).

The ferrocenyls themselves are almost eclipsed (**5**: C8–D1–D2–C17 –4(1) °, **4**: C22–D3–D4–C27 3.8(4) °) or between eclipsed and staggered (**4**: C8–D1–D2–C17 –16.8(3) °) with a gauche conformation for 1,1'-substituted fragments.

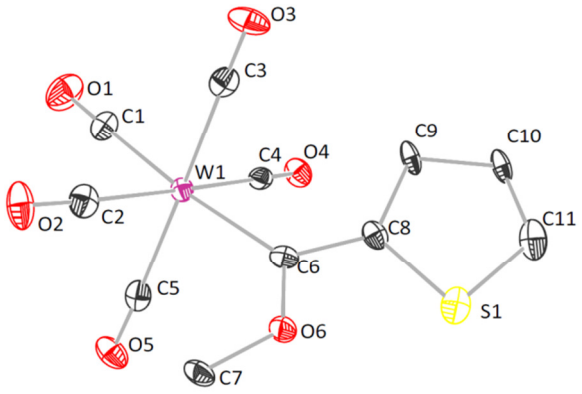

Figure 7.3 ORTEP diagram (50% probability level) of the molecular structure of **1** with the atom-numbering scheme. All hydrogen atoms have been omitted for clarity. Selected bond distances (Å), angles (°), and torsion angles (°): C1−O1 1.140(6), C1–W1 2.030(5), C6–O6 1.330(5), C6–C8 1.461(6), C6–W1 2.180(5), O6–C7 1.449(5), C8–C9 1.476(6), C9–C10 1.436(6), C10–C11 1.354(5), C11–S1 1.678(5), C8–S1 1.725(5), O1–C1–W1 177.8(4), O6–C6–C8 105.1(4), O6–C6–W1 130.1(3), C8–C6–W1 124.8(3), C11–S1–C8 92.1(2), O6–C6–C8–C9 –170.9(4), W1–C6–C8–C9 11.6(6), C8–C6–O6–C7 179.3(3), O6–C6–W1–C5 –49.7(4)

The substituents at the carbene carbon C6 influence the W1–C6 distance. Electron rich metallocenyl moieties extend the formal double bond to a maximum of 2.222(7) Å (**5**), whereas the thiophene derivative **1** significantly shortens the bond to 2.180(5) Å. In compound **4** the distances are averaged to 2.202(4) Å. A further influence to the W1–C1 distance is not detectable.

Regarding the bond lengths in the thiophene core for unsymmetrical **1**, the carbene carbon influences the C–S bonds. The bond length from S1 to C8 is extended to 1.725(5) Å, whereas to the non-substituted C11 is 1.678(5) Å.

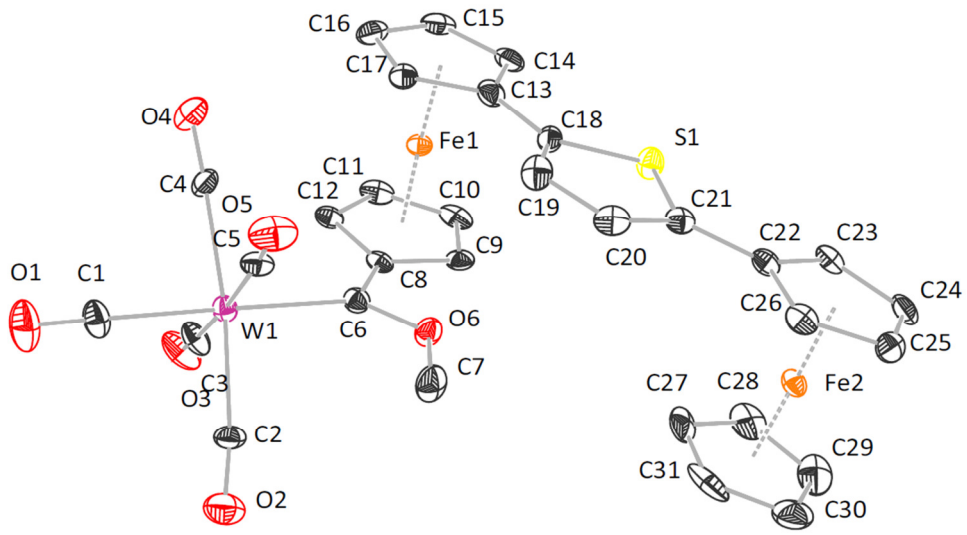

Figure 7.4 ORTEP diagram (50% probability level) of the molecular structure of **4** with the atom-numbering scheme. All hydrogen atoms have been omitted for clarity. Selected bond distances (Å), angles (°), and torsion angles (°): C1−O1 1.129(6), C1–W1 2.046(5), C6–W1 2.202(4), C6–O6 1.334(5), O6–C7 1.436(6), C6–C8 1.453(6), C13–C18 1.458(7), C18–C19 1.361(7), C19–C20 1.417(7), C20–C21 1.357(7), C18–S1 1.725(5), C21–S1 1.741(4), C21–C22 1.446(6), D1–Fe1 1.6467(7), D2–Fe1 1.6558(7), D3–Fe2 1.6328(7), D4–Fe2 1.6425(7), O1–C1–W1 176.6(4), O6–C6–C8 105.6(4), O6–C6–W1 128.9(3), C8–C6–W1 125.4(3), C18–S1–C21 92.4(2), D1–Fe1–D2 177.17(5), D3–Fe2–D4 179.00(5), O6–C6–C8–C9 –0.2(6), W1–C6–O6–C7 1.0(6), C14–C13–C18–C19 176.6(5), C20–C21–C22–C26 1.1(8), O6–C6–W1–C2 –41.3(4), C8–D1–D2–C17 –16.8(3), C8–D1–D2–C13 55.2(3), C22–D3–D4–C27 3.8(4), Fe–Fe 7.4837(10) (D denote the centroids of: D1: C8–C12, D2 C13–C17, D3 C22–C26, D4 C27–C31).

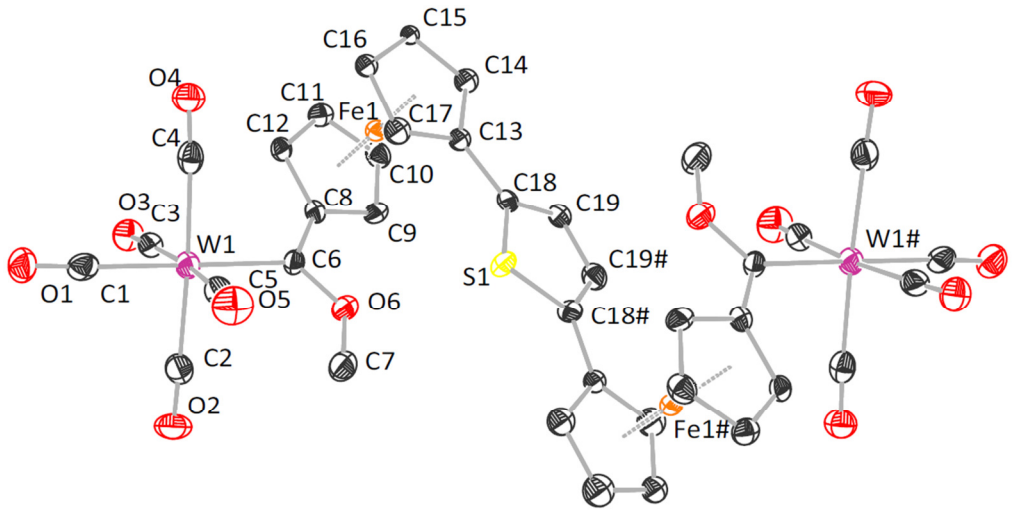

Figure 7.5 ORTEP diagram (50% probability level) of the molecular structure of **5** with the atom-numbering scheme. All hydrogen atoms have been omitted for clarity. Selected bond distances (Å), angles (°), and torsion angles (°): C1−O1 1.139(9), C1–W1 2.030(8), C6–W1 2.222(7), C6–O6 1.328(8), C6–C8 1.461(9), O6–C7 1.425(8), C13–C18 1.45(2), C18–C19 1.406(19), C18–S1 1.707(13), C19–C19# 1.367(19), D1–Fe1 1.6552(9), D2–Fe1 1.6990(9), O1–C1–W1 177.0(6), C18–S1–C18# 93.3(7), C8–C6–W1 124.9(5), O6–C6–W1 128.5(5), O6–C6–C8 106.3(6), D1–Fe1–D2 178.76(7), C8–D1–D2–C17 –4(1), C8–D1–D2–C13 67.2(8), C8–C6–O6–C7 178.2(6), O6–C6–W1–C2 –41.5(6), O6–C6–C8–C9 1.3(9), C14–C13–C18–C19 –16(3), Fe1–Fe1# 8.4367(2) (D1 denotes the centroid of C8–C12; D2 denotes the centroid of C13–C17).

Symmetry operation for the generation of equivalent atoms: –x–1, –y, –z.

The free electron pairs of O6 are oriented away from the carbonyls for all three compounds to avoid an electronic interaction. The steric interaction of the methyl group at C7 to the $W(CO)_5$ fragment is prevented by a staggered conformation between two carbonyls (**5**: O6–C6–W1–C2 –41.5(6) °, **4**: O6–C6–W1–C2 –41.3(4) °, **1**: O6–C6–W1–C5 –49.7(4) °).

The $W(CO)_5$ fragment decreases the O6–C6–C8 angle from ideal 120 ° to 106.3(6) (**5**), 105.6(4) (**4**) and 105.1(4) (**1**).

7.3 CONCLUSION

Within this study, a series of thiophene tungsten Fischer carbene complexes, of type $[(CO)_5W{=}C(OMe)R]$ (**1**, R = 2-Th; **3**, R = fcthFc) and $[(CO)_5W{=}C(OMe)\text{-}R'\text{-}(OMe)C{=}W(CO)_5]$ (**2**, R' = th; **5**, R' = fcthfc), is reported with the aim of investigating low energy charge transfer transitions between the carbene substituents and the transition metal carbonyl fragment incorporating the thiophene system (Th = Thienyl; th = 2,5-thiendiyl; Fc = ferrocenyl; fc = 1,1'-ferrocenediyl). For this reason, tungsten Fischer carbene functionalized thiophene and *α,α'*-diferrocenyl thiophene complexes **1**, **2**, **4** and **5** were prepared and characterized spectroscopically in solution. The structural properties of **1**, **4** and **5** in the solid state were investigated by single-crystal X-ray diffraction studies.

The electrochemical studies reveal reversible one electron redox events for the ferrocenyl moieties. Moreover, typical electrode reactions could be found for the carbene reductions itself and for the tungsten carbonyl oxidation processes. However, for the biscarbene **2** two well separated one-electron reduction events could be found. During the UV-Vis-NIR spectroelectrochemical investigations typical low energy absorptions for the mixed-valent *α,α'*-diferrocenyl thiophene increment were found, as well as high energy NIR absorptions which were attributed to metal-metal charge transfer transition between the tungsten carbonyl increment and the ferrocenyl units in the corresponding species. Further infrared spectroelectrochemical studies reveal that the electronic interactions in the corresponding cationic species can be described with weakly coupled class II systems according to Robin and Day.[19]

7.4 EXPERIMENTAL SECTION

General. Inert Schlenk techniques were employed in all operations and syntheses were done under argon or nitrogen. Solvents were distilled over sodium/benzophenone (hexane, tetrahydrofuran(thf)) or phosphorpentoxide (dichloromethane (dcm)) and collected under nitrogen or argon gas. Chemicals were used as purchased without any further purification unless

stated otherwise. Purification with column chromatography was done using silica gel 60 (0.0063–0.200 mm) as stationary phase. A Bruker AVANCE 500 spectrometer was used for NMR recordings. ^{1}H NMR spectra were recorded at 500.139 MHz and ^{13}C NMR spectra at 125.75 MHz. The signal of the solvent was used as reference: ^{1}H $CDCl_3$ at 7.26 ppm and ^{13}C $CDCl_3$ at 77.16 ppm. IR spectra were recorded on a Perkin-Elmer Spectrum RXI FT-IR spectrophotometer in solvent as specified. Only the vibration bands in the carbonyl-stretching region (ca. 1600–2200 cm^{-1}) were recorded.

Synthesis of complex **1**

To a thf solution of thiophene (3 mmol, 0.24 mL), ^{n}BuLi (3.3 mmol) was slowly added at -80^{o}C. After 1hr the cold bath was removed and the reaction mixture allowed to reach room temperature (rt). It was cooled to -50^{o}C and $W(CO)_6$ (3 mmol, 1.06g) was added in solid form. The colour of the solution turned red upon addition. The reation mixture was stirred at cold temperature for 30 min after which it was stirred for an additional hr at rt. Volatiles were removed by reduced pressure and the residue redissolved in DCM. Again it was cooled to -50^{o}C and methyl trifluorosulfonate (9.9 mmol, 1.09 mL) after which the solution darkened. The mixture was removed from the cold bath and stirred overnight at rt. Purification of the product was performed by using column chromatography and hexane as initial eluent. The polarity of the eluent was increased by adding small portions of DCM. Yield 1.23g (88%), red crystals. Anal. Calcd. for $WC_{11}H_6O_6S$ (450.08): C:29.35%; H:1.35%. Found: C:29.11%; H:1.20%. Mp: 102^{o}C. NMR ($CDCl_3$) ^{1}H: 8.17 (dd, J = 4.0, 1.1 Hz, 1H,H_α), 7.83 (dd, J = 4.9, 1.1 Hz, 1H, H_γ), 7.23 (dd, J = 5.0, 4.1 Hz, 1H, H_β), 4.68 (s, 3H, CH_3). ^{13}C: 293.39($C_{carbene}$), 202.63(C_{trans}), 197.80(C_{cis}), 158.45(C_{ipso}), 141.90(C_α), 136.33(C_γ), 129.20(C_β), 68.93(CH_3). IR(dcm) ν(cm^{-1}): 2069 (m), 1988 (w), 1963 (m), 1948 (vs). **Crystal data for 1.** Suitable single crystals of **1** were obtained by solution containing **1** at ambient temperature. $C_{11}H_6O_6SW$, M_r = 450.07 g·mol^{-1}, crystal dimension 0.20 x 0.20 x 0.10 mm, monoclinic, $P2_1/n$, λ = 0.71073 Å, a = 10.9273(5) Å, b = 11.1569(3) Å, c = 11.7633(4) Å, β = 116.617(5) °, V = 1282.13(8) Å^3, Z = 4, ρ_{calcd} = 2.332 g·cm^{-3}, μ = 9.190 mm^{-1}, T = 100(2) K, Θ *range* = 3.42 – 25.25 °, reflections collected 8217, independent 2309 (R_{int} = 0.0316), R_1 = 0.0215, wR_2 = 0.0494 [$I \geq 2\sigma(I)$].

Synthesis of complex **2**

2,5-dibromothiophene (3 mmol, 0.34 mL) was added to 50 mL thf in a Schlenk and ^{n}BuLi (7 mmol) was slowly added at -40^{o}C. The reaction mixture was left to stir for 30 min in the cold after which $W(CO)_6$ (6 mmol, 2.11g) was added in solid form. The solution was kept at cold temperature for 1hr and then allowed to reach rt for an additional hr. The solvent was removed and the residue redissolved in dcm. Methyl trifluorosulfonate (20 mmol, 2.41 mL) was added at -30^{o}C after which the solution darkened. The mixture was removed from the cold bath and stirred overnight at rt. Purification of the product was performed by using column chromatography and hexane as initial eluent. The polarity of the eluent was increased by adding small portions of dcm. Yield 1.51g (55%), purple solid. Anal. Calcd. for $W_2C_{18}H_8O_{12}S$ (917.91): C:23.55%; H:0.88%. Found: C:23.43%; H:0.73%. Mp: 264^{o}C (decomp.). NMR ($CDCl_3$) ^{1}H: 7.95 (s, 2H, H_α), 4.67 (s, 6H, CH_3). ^{13}C: 296.50 ($C_{carbene}$), 202.64 (C_{trans}), 196.92 (C_{cis}), 162.53 (C_{ipso}), 137.26 (C_α), 69.09 (CH_3). IR(dcm) ν(cm^{-1}): 2062 (m), 1974 (w), 1948 (vs), 1935 (s).

Synthesis of 2,5-Di(1'-bromoferrocenyl)thiophene **3**

Dibromoferrocene (Br_2Fc') (5.1g, 14.8 mmol) was dissolved in thf and cooled to -100^{o}C. ^{n}BuLi (6 mL, 14.8 mmol) was slowly added and the mixture left to stir at this temperature for 45min. Dry $ZnCl_2\cdot$2thf (4.2g, 15 mmol) was added in solid form and the reaction was kept at 0^{o}C for 30 min. 2,5-dibromothiophene (0.83 mL, 6.45 mmol) and $[Pd(CH_2CMe_2P^tBu_2)(\mu\text{-}Cl)]_2$ (0.025g, 0.25% to Br_2Fc') was added to the solution. The reaction mixture was heated to 55^{o}C and stirred for 36 hrs at this temperature. After cooling the mixture to ambient temperature, the product was adsorped on aluminiumoxide (alox) then purified using column chromatography with alox and a 4:1 hexane/toluene mixture. Yield 1.60g (43%), dark orange solid. Anal. Calcd. for $Fe_2C_{24}H_{18}Br_2$ (609.98): C:47.24%; H:2.98%; Found: C:47.16%; H:2.99%. Mp:220^{o}C. NMR ($CDCl_3$) ^{1}H: 6.90 (s, 2H, Th_α), 4.98 (m, 4H, H_α), 4.35 (m, 4H, $H_ß$), 4.30 (m, 4H, $H_{\alpha2}$), 4.06 (m, 4H, $H_{ß2}$). ^{13}C: 139.49(Th_{ipso}), 123.42(Th_α), 82.52(Fc_{ipso2}), 78.97(Fc_{ipso}), 72.22($Fc_{\alpha2}$), 71.28($Fc_{ß2}$), 69.23(Fc_α), 68.97($Fc_ß$).

Synthesis of complex **4** and **5**

FcTh'Br2 (3 mmol, 0.34 mL) was dissolved in 50 mL thf and ^{n}BuLi (7 mmol) was slowly added at -40^{o}C. The reaction mixture was left to stir for 30 min in the cold after which $W(CO)_6$ (6 mmol, 2.11g) was added in solid form. The solution was kept at cold temperature for 1hr and then allowed to reach rt for an additional hr. The solvent was removed and the residue redissolved in DCM. Methyl trifluorosulfonate (20 mmol, 2.41 mL) was added at -30^{o}C after which the solution darkened. The mixture was removed from the cold bath and stirred overnight at rt. Purification of the product was performed by using column chromatography and hexane as initial eluent. The polarity of the eluent was increased by adding small portions of dcm. Compound **4** eluted first as a dark-red fraction followed by compound **5** (brown-red).

Compound **4**: Yield 0.96g (40%), red brown crystals. Anal. Calcd. for $WFe_2C_{27}H_{20}O_6$ (736.01): C, 45.51; H, 2.72; found C, 45.59; H, 2.79. Mp: 237°C (decomp.). NMR ($CDCl_3$) ^{1}H: 6.83 (m, 2H, Th_α), 4.93 (m, 2H, $H_{\alpha3}$), 4.74 (m, 2H, $H_{ß3}$), 4.66 (m, 2H, $H_{\alpha2}$), 4.58 (m, 2H, $\mathbf{H}_{ß2}$), 4.39(m, 2H, $\mathbf{H}_\alpha$), 4.35 (s, 3H, C$\mathbf{H}_3$), 4.31 (m, 2H, $\mathbf{H}_ß$), 4.14 (s, 5H, Cp). ^{13}C: 307.75($\mathbf{C}_{carbene}$), 202.59($\mathbf{C}_{trans}$), 198.18($\mathbf{C}_{cis}$), 142.40(Th_{ipso}), 137.54($Th_{\alpha'}$), 96.18(Fc_{ipso3}),83.77 (Fc_{ipso2}), 80.07(Fc_{ipso}), 77.36($\mathbf{C}_{\alpha3}$), 76.92($\mathbf{C}_{ß3}$), 74.85($\mathbf{C}_{\alpha2}$), 71.20($\mathbf{C}_{ß2}$), 70.15($\mathbf{C}_\alpha$), 68.93($\mathbf{C}H_3$), 68.67($\mathbf{C}_ß$), 66.83(Cp). IR(dcm) ν(cm^{-1}): 2062 (m), 1971 (w), 1929 (vs, br). **Crystal data for 4.** Suitable single crystals of **4** were obtained by solution containing **4** at ambient temperature. $C_{31}H_{22}Fe_2O_6SW$, M_r = 818.10 g·mol^{-1}, crystal dimension 0.40 x 0.20 x 0.04 mm, monoclinic, $P2_1/n$, λ = 1.54184 Å, a = 14.3408(5) Å, b = 7.4003(2) Å, c = 26.4417(11) Å, β = 91.874(3) °, V = 2804.66(17) Å^3, Z = 4, ρ_{calcd} = 1.937 g·cm^{-3}, μ = 16.672 mm^{-1}, T = 105.00(10) K, Θ *range* = 3.34 – 66.00 °, reflections collected 13589, independent 4860 (R_{int} = 0.0387), R_1 = 0.0423, wR_2 = 0.1138 [$I \geq 2\sigma(I)$].

Compound **5**: Yield 0.99g (30%), dark brown crystals. Anal. Calcd. for $W_2Fe_2C_{36}H_{26}O_{12}$ (1101.94): C, 38.54; H, 2.05; found C, 38.57; H, 2.06. Mp: 248°C (decomp.). NMR ($CDCl_3$) ^{1}H: 6.85 (s, 2H, Th_α), 4.93 (m, 4H, $\mathbf{H}_{\alpha2}$), 4.72 (m, 4H, $\mathbf{H}_{ß2}$), 4.67 (m, 4H, $\mathbf{H}_\alpha$), 4.40 (m, 4H, $\mathbf{H}_ß$), 4.32 (s, 6H,C$\mathbf{H}_3$). ^{13}C: 308.47($\mathbf{C}_{carbene}$), 202.42($\mathbf{C}_{trans}$), 198.14($\mathbf{C}_{cis}$), 139.16 (Th_{ipso}), 123.97 (Th_α), 96.15 (Fc_{ipso2}), 82.99 (Fc_{ipso}), 77.34 ($C_{\alpha2}$), 76.86($C_{ß2}$), 74.78(C_α), 71.65($C_ß$), 68.68($\mathbf{C}H_3$).

IR(dcm) ν(cm^{-1}): 2060 (m), 1972 (w), 1929 (vs, br). **Crystal data for 5.** Suitable single crystals of **5** were obtained by solution containing **5** at ambient temperature. $C_{38}H_{24}Fe_2O_{12}SW_2$, M_r = 1184.03 g·mol^{-1}, crystal dimension 0.20 x 0.20 x 0.20 mm, triclinic, *P*–1, λ = 0.71073 Å, *a* = 6.9273(4) Å, *b* = 10.4607(8) Å, *c* = 13.1390(13) Å, α = 96.050(7) °, β = 105.079(7) °, γ = 99.971(6) °, *V* = 894.04(12) $Å^3$, *Z* = 1, ρ_{calcd} = 2.199 g·cm^{-3}, μ = 7.332 mm^{-1}, *T* = 103.3(2) K, Θ *range* = 3.08 – 25.49 °, reflections collected 10980, independent 3307 (R_{int} = 0.0418), R_1 = 0.0366, wR_2 = 0.1008 [$I \geq 2\sigma(I)$].

Electrochemistry. The electrochemical measurements were carried out under an argon atmosphere on 1.0 mmol·L^{-1} dichloromethane solutions containing 0.1 mol·L^{-1} of $[N^nBu_4][B(C_6F_5)_4]$ as supporting electrolyte utilizing a Voltalab 10 electrochemical laboratory from Radiometer analytical.[22] Furthermore, an OTTLE (= Optically Transparent Thin Layer Electrochemistry) cell placed in a Varian Cary 5000 UV-VIS/NIR absorption spectrometer or in a Thermo Nicolet 200 FT-IR spectrometer was used in spectroelectrochemical measurements.[14] For voltammetry, a three electrode cell with a platinum counter electrode, a glassy carbon working electrode and a Ag/Ag^+ reference electrode was used. The working electrode was prepared by polishing with a Buehler micro cloth using Buehler diamond pastes with decreasing sizes (1 to 0.25 µm). The Ag/Ag^+ reference electrode was constructed from a silver wire inserted into a luggin capillary with a vycor tip containing a solution of 0.01 mol·L^{-1} $AgNO_3$ as well as 0.1 mol·L^{-1} $[N^nBu_4][B(C_6F_5)_4]$ in acetonitrile. This luggin capillary was inserted into a second luggin capillary with vycor tip filled with a 0.1 mol·L^{-1} $[N^nBu_4][B(C_6F_5)_4]$ solution in dichloromethane. Successive experiments under the same experimental conditions showed that all formal reduction and oxidation potentials were reproducible within 5 mV. Experimentally potentials were referenced against a Ag/Ag^+ reference electrode but the results are presented referenced against the FcH/FcH^+ couple ($E_{1/2}$ = 0.0 V) as required by IUPAC.[23] When decamethylferrocene was used as an internal standard, the experimentally measured potential was converted in to *E vs* FcH/FcH^+ by addition of -0.61 V.[24] The cyclovoltammograms were taken after typical two scans and are considered to be steady state cyclovoltammograms, in which the signal pattern differs not from the initial sweep. Finally, the experimental data were processed on Microsoft Excel worksheets.

Single-Crystal X-ray Diffraction Analysis. Crystal data for **1, 4** and **5** were collected with an Oxford Gemini S diffractometer at 100 K using Mo-Kα (λ = 0.71073 Å) radiation. The structures were solved by direct methods using SHELXS-97 and refined by full matrix least-square procedures on F2 using SHELXL-97.[25] All non-hydrogen atoms were refined anisotropically and a riding model was employed in the refinement of the hydrogen atom positions.

Crystallographic data (excluding structure factors) for the structures in this paper have been deposited with the Cambridge Crystallographic Data Centre, CCDC, 12 Union Road, Cambridge CB21EZ, UK. Copies of the data can be obtained free of charge on quoting the depository numbers CCDC-969409 (**1**), 969408 (**4**) and 969407 (**5**) (Fax: +44-1223-336-033; e-mail: deposit@ccdc.cam.ac.uk, http://www.ccdc.cam.ac.uk).

7.5 ACKNOWLEDGMENT

D.I.B. and B.v.d.W. acknowledge the National Research foundation, South Africa for financial support (Grant number 76226). We are grateful to the Fonds der Chemischen Industrie for financial support J.M.S. and M.K. thank the FCI for Chemifonds Fellowships.

7.6 REFERENCES

(1) (a) Bezuidenhout, D. I.; Lotz, S.; Liles,D. C.; van der Westhuizen, B. *Coord. Chem. Rev.*, **2012**, *51*, 479; (b) Astruc, D. *Electron Transfer and Radical Processes in Transition Metal Chemistry*, VCH, New York, **1995**; (c) Astruc, D. *Acc. Chem. Res.*, **1997**, *30*, 383-391; (d) Long, N. J. *Angew. Chem.,* **1995**, *34*, 21; (e) Behrens, U.; Brussaard, H.; Hagenau, U.; Heck, J.; Hendrickx, E.; Kornich, J.; van der Linden, J. G. M.; Persoons, A.; Spek, A. L.; Veldman, N.; Voss, B.; Wong, H. *Chem. Eur. J.,***1996**, *2*, 98.

(2) (a) Watanuki, S.; Ochifuji, N.; Mori, M.; *Organometallics*, **1995**, *14*, 5062; (b) Fernández-Rodríguez, M. A.; García-García, P.; Aquilar, E. *Chem. Commun.*, **2010**, *46*, 7670.

(3) Bezuidenhout, D. I.; van der Watt, E.; Liles, D. C.; Landman, M.; Lotz, S. *Organometallics*, **2008**, *27(11),* 2447.

(4) (a) Lage, M. L.; Curiel, D.; Fernández, I.; Mancheño, M. J.; Gómez-Gallego, M.; Molina, P.; Sierra, M. A. *Organometallics,* **2011**, *30*, 1794; (b) Limberg, A.; Amélia, M.; Lemos, N. D. A.; Pombeiro, A. J. L. *Port. Electrochim. Acta.,* **1995**, *13*, 319; (c) Crause, C.; Görls, H.; Lotz, S.; *Dalton Trans.*, **2005**, 1649; (d) Terblans, Y. M.; Roos, H. M.; Lotz, S. *J. Organomet. Chem.*, **1998**, *566*, 133.

(5) (a) van der Westhuizen, B; Speck, J. M.; Korb, M.; Friedric, J.; Bezuidenhout, D. I.; Lang, H. *Inorg. Chem.* **2013**, in revision.; (b) Bezuidenhout, D. I.; Fernández, I.; van der Westhuizen, B.; Swarts, P. J.; Swarts, J. C. *Organometallics,* **2013**, in revision.

(6) Fischer, E. O.; Held, W.; Kreissl, F. R.; Frank, A.; Huttner, G. *Chem. Ber.* **1977**, *110(2)*, 656;

(7) Landman, M.; Pretorius, R.; Buitendach, B. E.; van Rooyen, P. H., Conradie, J. *Organometallics,* **2013**, *32*, 5491.

(8) Dong, T. Y.; Chang, C. K.; Lee, S. H.; Lai, L. L.; Chiang, M. Y. N.; Lin, K. L. *Organometallics*, **1997**, *16*, 5816.

(9) Negishi, E. L., King, A. O., Okukado, N. *J. Org. Chem.* **1977**, *42*, 1821.

(10) (a) Clark, H. C., Goel, A. B., Goel, R. G., Goel, S., Ogini, W. O., *Inorg. Chim. Acta*, **1978**, *31*, l441; (b) Goel, A. B. Goel, S., *Chim. Acta* **1985**, *98*, 67.

(11) Pickett, T. E., Richards, C. J., *Tetrahedron Lett.*, **1999**, *40*, 5251.

(12) (a) Braterman, P. S. *Metal Carbonyl Spectra;* Academic Press Inc.: London, U.K., **1975**, 68; (b) Adams, D. M. *Metal-Ligand and Related Vibrations;* Edward Arnold Publishers Ltd: London, U.K., **1967**, 98.

(13) McIver, J. W.; Komornicki, A. K. *J. Am. Chem. Soc.*, **1972**, *94*, 2625.

(14) Krejčik, M.; Daněk, M.; Hartl, F. *J. Electroanal. Chem.* **1991**, *317*, 179.

(15) Speck, J.M., Claus, R., Hildebrandt, A., Rüffer, T., Erasmus, E., van As, L., Swarts, J.C., Lang, H., *Organometallics*, **2012**, *31*, 6373.

(16) Baldoli, C.; Cerea, P.; Falciola, L.; Giannini, C.; Licandro, E.; Maiorana, S.; Mussini, P.; Perdicchia, D. *J. Organomet. Chem.* **2005**, *690*, 5777.

(17) (a) Connor, J. A.; Lloyd, J. P. *J. Chem. Soc., Dalton Trans.* **1972**, 1470; (b) Rosenblum, M.; Santer, J. O.; Howells, W. G. *J. Am. Chem. Soc.* **1957**, *85*, 1450; (c) Sohn, Y. S.; Hendrickson, D. N.; Gray, H. B. *J. Am. Chem. Soc.* **1971**, *93*, 3603.

(18) (a) Hildebrandt, A.; Rüffer, T.; Erasmus, E.; Swarts, J. C.; Lang, H. *Organometallics*, **2010**, *29*, 4900; (b) Hildebrandt, A.; Schaarschmidt, D.; Lang, H. *Organometallics*, **2011**, *30*, 556; (c) Speck, J. M.; Schaarschmidt, D.; Lang, H. *Organometallics* **2012**, *31*, 1975; (d) Hildebrandt, A.; Lehrich, S. W.; Schaarschmidt, D.; Jaeschke, R.; Schreiter, K.; Spange, S.; Lang, H. *Eur. J. Inorg. Chem.* **2012**, 1114; (e) Taher, D.; Awwadi, F. F.; Pfaff, U.; Speck, J. M.; Rüffer, T.; Lang, H. *J. Organomet. Chem.* **2013**, *736*, 9; (f) Hildebrandt, A.; Lang, H. *Dalton Trans.* **2011**, *40*, 11831; (g) Miesel, D.; Hildebrandt, A.; Korb, M.; Low, P. J.; Lang, H. *Organometallics* **2013**, *32*, 2993.

(19) Robin, M. B.; Day, P. *Adv. Inorg. Chem. Radiochem.* **1968**, *10*, 247.

(20) (a) Warratz, R.; Aboulfadl, H.; Bally, T.; Tuczek, F. *Chem. Eur. J.* **2009**, *15*, 1604; (b) Warratz, R.; Tuczek, F. *Inorg. Chem.* **2009**, *48*, 3591.

(21) (a) Atwood, C. G.; Geiger, W. E. *J. Am. Chem. Soc.* **1994**, *116*, 10849; (b) Lohan, M.; Ecorchard, P.; Rüffer, T.; Justaud, F.; Lapinte, C.; Lang, H. *Organometallics* **2009**, *28*, 1878; (c) Paul, F.; Toupet, L.; Thépot, J.-Y.; Costuas, K.; Halet, J.-F.; Lapinte, C. *Organometallics* **2005**, *24*, 5464.

(22) (a) LeSuer, R. J.; Buttolph, C.; Geiger, W. E. *Anal. Chem.* **2004**, *76*, 6395; (b) Barrière, F.; Camire, N.; Geiger, W. E.; Mueller-Westerhoff, U. T.; Sanders, R. *J. Am. Chem. Soc.* **2002**, *124*, 7262; (c) Barrière, F.; Geiger, W. E. *J. Am. Chem. Soc.* **2006**, *128*, 3980.

(23) Gritzner, G.; Kuta, J. *Pure Appl. Chem.* **1984**, *56*, 461.

(24) Nafady, A.; Geiger, W. E. *Organometallics* **2008**, *27*, 5624.

(25) (a) Sheldrick, G. M. *Acta Crystallogr., Sect. A* **1990**, *46*, 467; (b) Sheldrick, G. M. SHELXL-97, Program for Crystal Structure Refinement; Universität Göttingen, Göttingen, Germany, 1997.

CHAPTER 8

Redox behavior of cymantrene Fischer carbene complexes in designing organometallic multi-tags.

This chapter has been accepted for publication in Chemistry – A European Journal. The format reflects the style set by the journal.

Daniela I. Bezuidenhout,[a] Belinda van der Westhuizen,[a] Pieter J. Swarts,[b] Teshica Chatturgoon,[c] Orde Q. Munro,[c*] Israel Fernández,[d] Jannie C. Swarts,[b] *Chem. Eur. J.*, **2014**, DOI: 10.1002/chem.201304711.

Author contributors

Synthetic work: Belinda van der Westhuizen

Cyclic voltammetry and data analysis: Pieter J. Swarts, Jannie C. Swarts

Computational work: Irael Fernández

ESR analysis: Orde Q. Munro, Teshica Chattergoon

Article written: Belinda van der Westhuizen, Daniela I. Bezuidenhout, Jannie C. Swarts, Israel Fernández.

[a] *Chemistry Department, University of Pretoria, Private Bag X20, Hatfield, 0028, South Africa. Fax: +27-(0)12-420-4687; Tel: +27-(0)12- 420-2626; E-mail: daniela.bezuidenhout@up.ac.za*
[b] *Chemistry Department, University of the Free State, PO Box 339, Bloemfontein 9300, South Africa. Fax:+27-(0)51-444-6384; Tel: +27-(0)51-401-2781; E-mail: swartsjc@ufs.ac.za*

[c] *Departamento de Química Orgánica I, Facultad de Química, Universidad Complutense,28040-Madrid,Spain.*

Supporting Information. Supporting information for this article is available in **Appendix 7**.

ABSTRACT

A series of group 7 Fischer carbene complexes of the type $[Cp(CO)_2Mn^{I}=C(OEt)Ar]$ (Cp = cyclopentadienyl with Ar = Th = thienyl (**1a**), Fu = furyl (**2a**), or Fc = ferrocenyl (**3a**)) and biscarbene complexes $[Cp(CO)_2Mn=C(OEt)\text{-}Ar'\text{-}(OEt)C=Mn(CO)_2Cp]$with Ar' = Th' = 2,5-thienylene (**1b**), Fu' = 2,5-furylene (**2b**) or 1,1'-ferrocendiyl (Fc') (**3b**) were synthesized and characterized. Chemical oxidation of $[Cp(CO)_2Mn=C(OEt)Fc]$ (**3a**) and isolation of the oxidised species **[3a][PF$_6$]** possessing a Mn(II) centre proved possible below -30^{o}C in dichloromethane solution. The ESR spectrum of the transiently stable radical cation, **[3a][PF$_6$]**, confirmed the presence of a low-spin Mn(II) centre characterized by a rhombic g-tensor (g_x=1.975, g_y=2.007, g_z=2.130) in frozen dichloromethane at 77K with ^{55}Mn hyperfine coupling constants A_1, A_2 and A_3 of 115,33 and 43G, respectively. Electrochemical studies demonstrated the influence of the Ar substituent on the oxidation potential. All complexes showed redox potentials of carbene double bond reduction and Mn(I) oxidation were dependent on the type of Ar group, but only **3b** showed resolved oxidations for the two Mn(I) centres. Surprisingly, Mn(I) oxidation occurs at lower potentials than ferrocenyl oxidation. Density functional theory (DFT) calculations were carried out to delineate the nature of species involved in the oxidation and reduction processes and clearly confirm that oxidation of Mn(I) is favoured over that of ferrocene.

8.1 INTRODUCTION

Organometallic molecular tags or labels employed to manipulate chemical and analytical properties of chemical targets mostly contain an electron-donating ferrocenyl moiety which provides a neat reversible one-electron oxidation process.[1] The anodic electrochemistry of the ferrocenyl group leads to diverse applications including cancer therapy,[2] molecular sensors,[3] and energy transfer processes.[4] The electron-withdrawing properties and IR-active carbonyl

groups of a cymantrenyl moiety, Mn(η^5-C_5H_4)$(CO)_3$,[5] make this organometallic compound an interesting and significantly different alternative as a molecular tag, although its redox chemistry has been underutilized.[6] Despite the use of cymantrenyl cathodic chemistry for immunoassays,[7] applications of cymantrenyl anodic chemistry are hitherto lacking. This dearth can be attributed not only to the high oxidation potential of the cymantrene unit (*ca*. 0.9 V vs ferrocene) as a result of the effect of the π-accepting carbonyl groups[8] but also to the instability of the radical cation which is still poorly understood. This paper addresses the first of these points by substituting one carbonyl ligand with a less π-accepting ligand, namely a heteroatom-substituted carbene ligand. Studies of triphenylphosphine-substituted cymantrenyl complexes showed that the thermodynamic and kinetic stabilities of the cationic complexes are greatly enhanced.[9] The effect of employing Fischer carbenes as weaker π-acceptors than carbonyls is herein imposed by synthesizing a series of cymantrene Fischer alkoxycarbene complexes containing heteroaryl (thienyl (Th) or furyl (Fu)) substituents. Both the mono- and the biscarbene complexes with bridging 2,5-thienylene (Th') or 2,5-furylene (Fu') carbene substituents, were prepared. Fischer carbene complexes of the type $[(CO)_5M{=}C(X)R]$ (M = group 6 transition metal) are very well studied[10] and the electrochemical activity of these group 6 carbene complexes have recently been thoroughly investigated.[11] In contrast, examples of the group 7 type, $[Cp(CO)_2Mn{=}C(X)R]$,[12] are not as common, and reports on their redox behaviour are scarce.[13] Fine-tuning of the steric and electronic properties of the carbene moiety can be effected by modulation of the carbene substituents (X=heteroatom substituent, R=aryl substituent).[14] The introduction of a metal-containing substituent, such as ferrocenyl, opens the door for the design of organometallic multi-tag complexes. To this end, mono-and biscarbene ferrocenyl complexes were also synthesized. Electrochemical, ESR and molecular orbital investigations of these complexes as examples of possible anodic redox multi-tags are reported herein.

8.2 RESULTS AND DISCUSSION

Synthesis

A series of cyclopentadienyl dicarbonyl manganese carbene complexes was synthesised according to the classical procedure reported by E. O. Fischer and Maasböl.[15] Lithiation of the (hetero)arene precursors yielded a mixture of both the mono- and dilithiated (hetero)arene. The reaction mixture was reacted with 2 equivalents of $CpMn(CO)_3$ to produce the corresponding metal acylate and dimetal bisacylate complexes, which, after alkylation with Meerwein's reagent,[16] yielded both the neutral ethoxy-monocarbene and biscarbene complexes (Scheme 8.1).

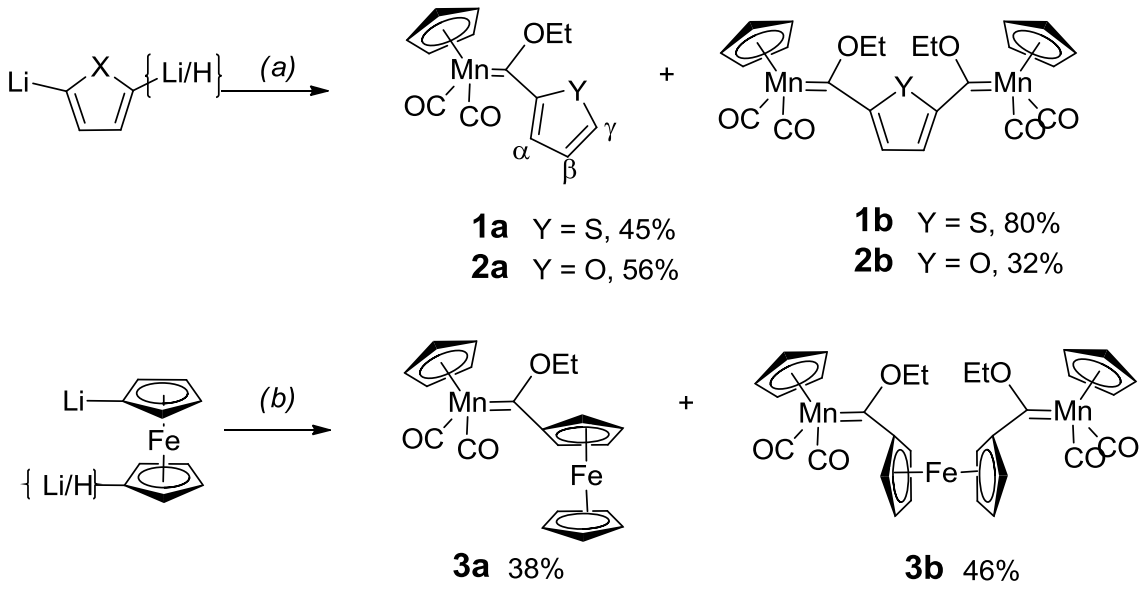

Scheme 8.1. Reagents and conditions: (a) (i) 2 eq $CpMn(CO)_3$, thf, -60°C; (ii) excess Et_3OBF_4, CH_2Cl_2, -40°C. (b) (i) 2 eq $CpMn(CO)_3$, thf, -50°C; (iii) excess Et_3OBF_4, CH_2Cl_2, -40°C.

Chemical oxidation of the Mn(I) centre of **3a** was achieved by the use of $AgPF_6$[17] (Scheme 8.2) to yield the radical Mn(II) species **[3a][PF$_6$]**. All neutral compounds were purified by column chromatography to give products as dark yellow to brown (Th, Fu) or dark red to maroon (Fc) solids. Complexes (except **2b**[18] and **[3a][PF$_6$]**) were stable in the absence of oxygen and could be stored for months under argon in the cold, however decomposition could be detected after 30 min in C_6D_6 and CH_2Cl_2 during electrochemical studies, but allowed enough time for electrochemical and spectroscopic studies to be completed.

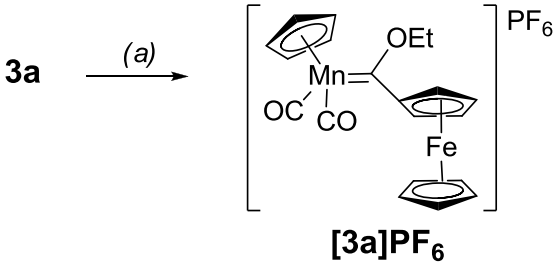

Scheme 8.2 Reagents and conditions: (a) 1 eq $AgPF_6$, CH_2Cl_2, -35^{o}C

Spectroscopy

By employing NMR and IR spectroscopy, electronic effects of the carbene substituents could be followed (Table 8.1). Both the α and ß protons in the ^{1}H NMR are deshielded as a result of π-resonance stabilization effects due to the coordination of the metal-carbene moiety. For the thienyl and ferrocenyl complexes (**1a, 1b, 3a** and **3b**) the H_α is used as a probe as it is most sensitive towards electronic ring substituent involvement. However, for furyl complexes (**2a** and **2b**) the H_γ resonances are used as a probe as these proton shifts show a more downfield shift compared to the H_α. The assignment of the thienyl and furyl ring proton chemical shifts is based on assignments following predicted shifts for ester derivatives.[19] No usable NMR spectra could be obtained for the paramagnetic **[3a][PF$_6$]**. The expected band pattern[20] associated with the carbonyl stretches of a $[CpMn(CO)_2L]$ system could be observed in the infrared spectra of all complexes, with very similar stretching frequencies (Table 8.1). The wavenumbers observed for complex **[3a][PF$_6$]** (Figure 8.1) show a significant shift of the carbonyl stretching mode bands to higher frequency, consistent with coordination to a Mn(II) ion and diminished metal-to-ligand π-backdonation due to the higher metal oxidation state and reduced d-electron density. Furthermore, the bands fall well within the expected range for the one-electron oxidation of a "piano-stool" complex. Thus, the average shift of 116 cm^{-1} from that of neutral **3a** compares favourably with that previously reported for cationic cymantrene complexes (~115 cm^{-1}).[6]

Table 8.1 Selected NMR and IR spectroscopic data

Complex	H_{probe} (^{1}H NMR, ppm)[a]	$C_{carbene}$ (^{13}C NMR, ppm)[a]	IR (cm^{-1})[b]
1a	6.93	319	1936, 1872
1b	7.52	319	1948, 1896
2a	6.71	309	1942, 1876
2b	6.84	306	1935, 1886
3a	4.83	328	1938, 1862
3b	4.92	336	1927, 1858
[3a][PF_6]	-	-	2024, 1978

[a] Spectra recorded in solvent C_6D_6. [b] Spectra recorded in solvent CH_2Cl_2.

The DFT-calculated IR spectra for **3a** and **3a**$^{\bullet+}$ (Figure 8.1) reproduced the key carbonyl band shifts upon oxidation of **3a** in the experimental spectrum to within 11 and 16 cm^{-1} for the antisymmetric and symmetric stretching modes, respectively. Moreover, the calculated peak separation between the two CO modes for the Mn(I) complex (68 cm^{-1}, **3a**) and Mn(II) complex (70 cm^{-1}, **3a**$^{\bullet+}$) fell within 6 wavenumbers of the experimental peak separation. Note that the absolute frequencies of the calculated peaks are not expected to correlate exactly with those measured experimentally due to intrinsic limitations in the calculation method.[21] That said, a scaling factor of 0.961 for the carbonyl frequencies calculated at the HSEH1PBE/6-311+g(d,p) level of theory (in CH_2Cl_2) would bring the theoretical spectra into the correct frequency range for direct comparisons with the experimental spectra to be made. The DFT-calculated Mn(I/II) coordination geometries (Figure 8.1) are in excellent agreement with the X-ray data reported for the neutral and oxidized forms of the cymantrene derivative Mn(η^5-$C_5H_4NH_2$)$(CO)_3$.[6] For example, the Mn–CO distances average 1.80(1) Å in the experimental structure (the data do not allow a distinction between Mn^I and Mn^{II} to be made). In the simulated structures of **3a** and **3a**$^{\bullet+}$, the Mn–CO bonds contract from 1.83(1) Å to 1.77(1) Å upon oxidation of the metal. The Mn=C

bond shows a similar contraction from 1.98 to 1.91 Å with the change in oxidation state of the manganese ion.

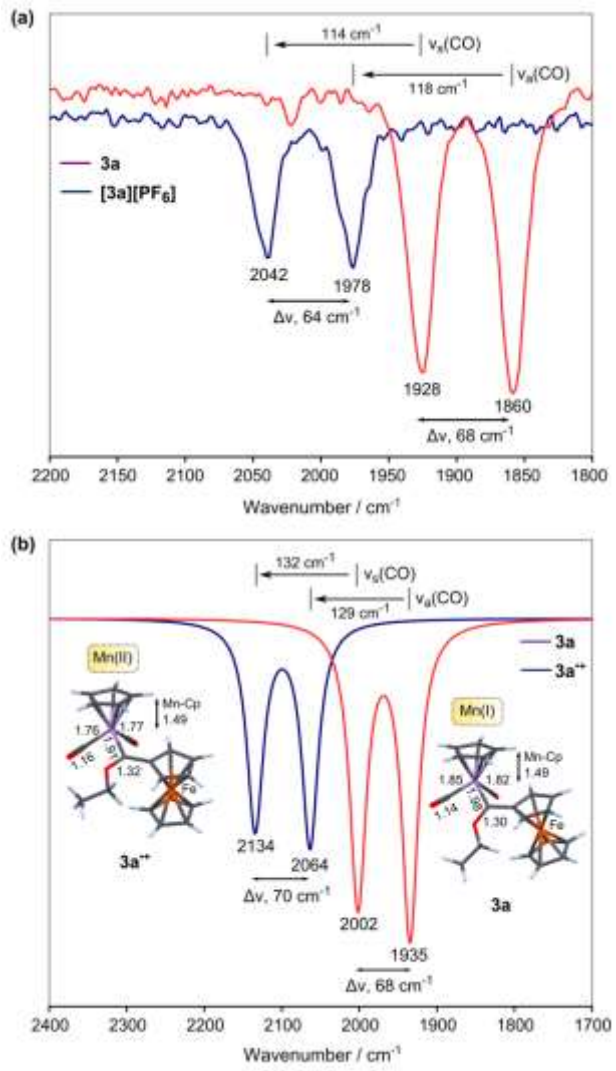

Figure 8.1 IR spectrum of the neutral and oxidized complex of **3a**

Electrochemistry

Cyclic voltammetry (CV), linear sweep voltammetry (LSV), and Osteryoung square wave voltammetry (SW) were conducted on **1** – **3**[18] in CH_2Cl_2 utilizing 0.1 mol·dm^{-3} [N(^{n}Bu)$_4$][PF_6] as supporting electrolyte in a glove box having oxygen and moisture levels less than 5 ppm.

CV's are shown in Figures 8.2 and 8.4 while data are summarized in Table 8.2.

As was the case with previously reported chromium[22] and tungsten[23] Fischer ethoxycarbene complexes, $[(CO)_5M=C(OEt)Ar]$ with M = Cr(0) or W(0), reduction of the $Cp(CO)_2\ Mn^{I}=C$ carbene double bond to a $^{-}Mn^{I}=C\bullet$ species is observed at low potentials (< -2.0 V vs FcH/FcH^{+}, wave I, Figure 8.2 and Table 8.2). However, in the Cr and W systems, the metals were in the zero oxidation state. In the present series of compounds, Mn is in the +1 oxidation state. Our computational results[24] are mutually consistent with the electrochemistry in showing that this reduction is not a Mn(I) reduction to Mn(0). Figure 8.3 shows the computed frontier molecular orbitals of complex **2a**, where the carbene ligand adopts a vertical coordination mode and the ethoxy-group is oriented towards the carbonyl ligands (in the so-called *anti*-conformation). This conformation is reported to be the most stable conformation in similar manganese(I)-alkoxycarbene complexes.[25] The LUMO is mainly centered in the p_z atomic orbital of the carbene carbon atom. Therefore, it should be expected that the one-electron reduction process should lead to the radical anion $\mathbf{2a}^{\bullet-}$ whose unpaired electron remains mainly located on the p_z orbital of the carbene carbon atom. Indeed, the computed spin density on $\mathbf{2a}^{\bullet-}$ indicates a value of 0.55e on the carbene carbon atom thus confirming the assignment of $^{-}Mn=C\bullet$ as reduction product (Figure 8.3). Similar LUMO's were observed for the rest of the mono- and biscarbene complexes considered in this study. The carbene double bond of **1** (Ar = Th) and **2** (Ar = Fu) is reduced at potentials at least 300 mV smaller (more negative) than the Cr(0) analogues.[22] This implies that compared to $Cr^{0}(CO)_5$, the $CpMn^{I}(CO)_2$ fragment is more electron-donating despite the metal being in the +1 oxidation state. As a consequence, the electrophilic nature of the carbene carbon atom is reduced in these group 7 Fischer carbene complexes as confirmed by the computed higher p_z occupation of the carbene carbon atom of **2a** (0.74 e) compared to its Cr(0)-carbene counterpart (0.63e), which is translated into a more difficult reduction. For Ar = Fc, reduction of the M=C double bond was only observed for the biscarbene complex **3b**. Repeated experiments with **3a** failed to show the carbene reduction within the allowed potential window of CH_2Cl_2. This finding correlates with the computed energy of the corresponding LUMO's (**3b**: -1.88 eV < **2a**: -1.83 eV < **3a**: -1.64 eV) which indicates that the reduction process should be much easier for complexes **3b** and **2a** than for **3a**, as experimentally observed (see Table 8.2). The spread of reduction potentials of wave I in the range $-2.334 < E^{o'} \leq -2.065$ V ($E^{o'}_{\mathbf{3a}}$ fell outside the lower limit of this range) is indicative of good electrochemical interaction between

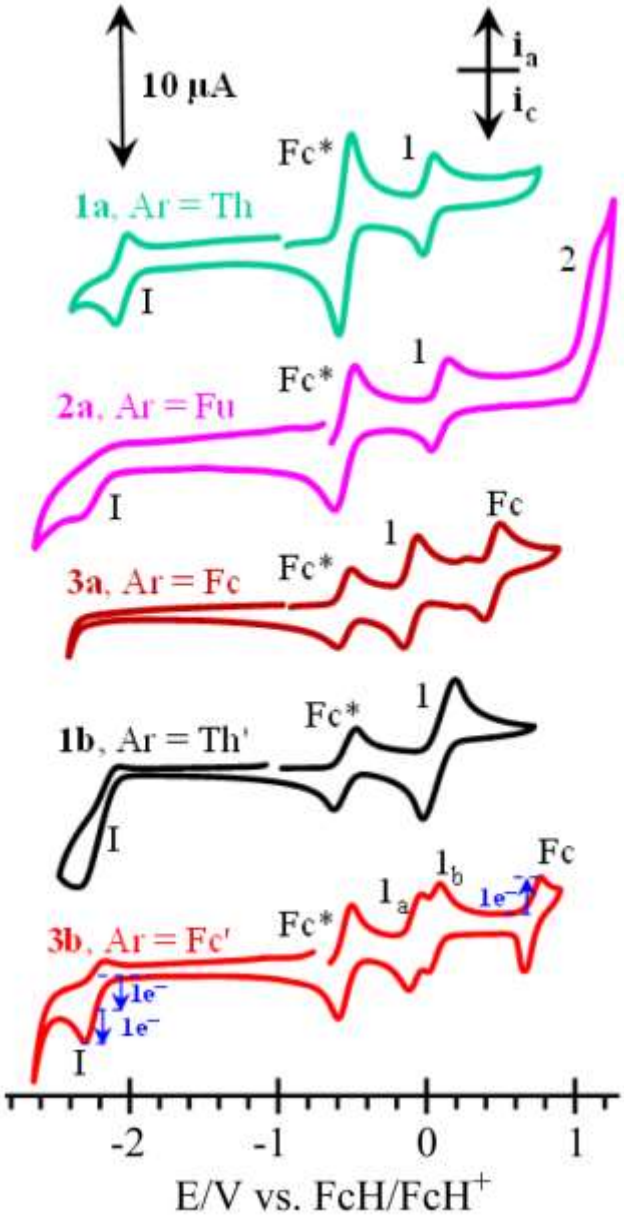

Figure 8.2. CV's of 0.5 mmol·dm^{-3} solutions of monocarbenes **1a** (green, top), **2a** (Mauve, 2nd from top) and **3a** (brown, third from the top) and biscarbene complexes [Cp(CO)$_2$Mn=C(OEt)-Ar'-(OEt)C=Mn(CO)$_2$Cp] **1b** (black 2nd from bottom) and **3b** (red, bottom) in CH_2Cl_2 containing 0.1 mol·dm^{-3} [N(^{n}Bu)$_4$][PF$_6$] as supporting electrolyte at a scan rate of 100 mV s^{-1} and 20 ^{o}C. Fc* = decamethylferrocene = internal standard. Under these conditions, each Mn center is involved in a one-electron transfer redox process.

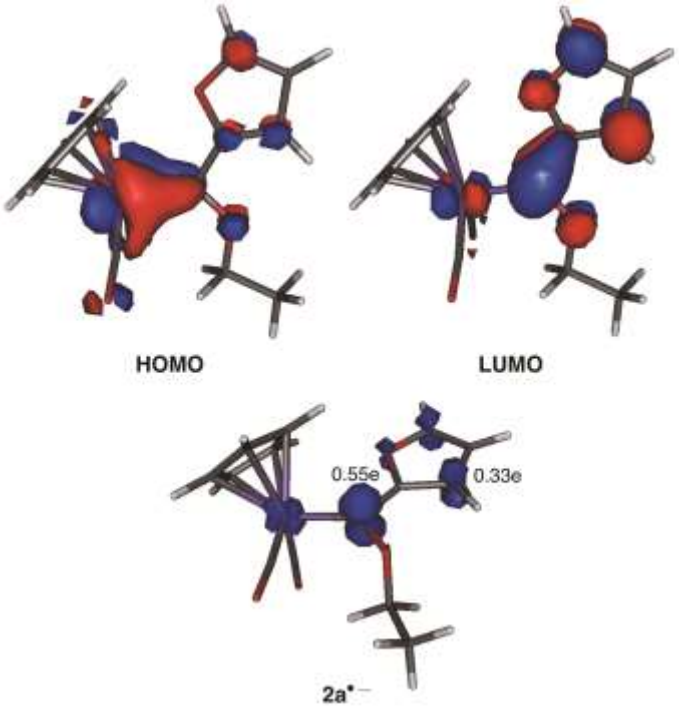

Figure 8.3. Computed frontiers orbitals of **2a** (top) and spin density of radical anion **2a**$^{\bullet-}$.

the Ar=Fu, Th or Fc group and the Mn^{I}=C moieties in **1**–**3**. Free ferrocene and cymantrene each display a one-electron oxidation with $E^{o'}$ = ½(E_{pa} + E_{pc}) of cymantrene 0.92 V vs. FcH/FcH^{+};[6] electrochemical and chemical reversibility of the cymantrenyl moiety is not as good as with the ferrocenyl fragment.[6,17,26,27] Electrochemical reversibility is associated with $\Delta E = E_{pa} - E_{pc}$ = 59 mV and i_{pc}/i_{pa} = 1.[27] Surprisingly, in the present carbene derivatised cymantrene series of compounds, Mn oxidation was found to occur at potentials comparable to free ferrocene. In particular, for **3a** and **3b**, results from the present electrochemical, computational and ESR study (see below) were mutually consistent in showing that Mn^{I} is oxidised *before* Ar = ferrocenyl at wave 1 in the potential range -0.106 < $E^{o'}$ < 0.086V. For the biscarbene complex $[Cp(CO)_2Mn=C(OEt)\text{-}Ar'\text{-}(OEt)C=Mn(CO)_2Cp]$, Ar'= Fc', relaying of the electrostatic effects of the mixed-valent intermediate $[Cp(CO)_2Mn^{II}=C(OEt)\text{-}Ar'\text{-}(OEt)C=Mn^{I}(CO)_2Cp]$ manifested in in the splitting of the oxidation peak in two components, waves 1a and 1b in Figure 8.2.

Table 8.2. Cyclic voltammetry data of 0.5 mmol·dm^{-3} solutions of [Cp(CO)$_2$Mn=C(OEt)]Ar and [Cp(CO)$_2$Mn=C(OEt)-Ar'-(OEt)C=Mn(CO)$_2$Cp] complexes **1** – **3** in CH_2Cl_2 containing 0.1 mol·dm^{-3} [N(^{n}Bu)$_4$][PF$_6$] as supporting electrolyte at a scan rate of 100 mV s^{-1} and 20 ^{o}C. Potentials are relative to the FcH/FcH$^+$ couple.

Complex	Peaks obs.	$E^{o'}$/V, ΔE/mV	$i_p/\mu A$, i_{pc}/i_{pa}
1a Ar=Th	I (carbene)	-2.065, 76	1.60, 0.73[a]
	1 (Mn)	0.015, 73	5.82, 0.87
1b Ar'=Th'	I (carbene)	-2.211, 246	18.7, 0.10 [a]
(bis derivative)	1a,b (Mn)	0.083, 214	5.82, 0.87
2a Ar=Fu	I (carbene)	-2.334, -[b]	1.44, -[b]
	1 (Mn)	0.086, 92	1.40, 0.91
	2 (OEt)	1.166, -	4.12, -
3a Ar=Fc	I (carbene)	-, -[c]	-, -[c]
	1 (Mn)	-0.106, 96	2.02, 0.91
	Fc	0.442, 92	1.91, 0.92
3b Ar'=Fc'	I (carbene)	-2.235, 116	7.85, 0.28 [a]
(bis derivative)	1a (Mn)	-0.074, 82	5.62, 0.92
	1b (Mn)	0.055, 86	5.42, 0.93
	Fc'	0.714, 113	5.23, 1.38[d]

[a] i_{pa}/i_{pa}. [b] No i_{pa} detected. [c] peak fell outside the solvent potential window. [d] i_{pc} larger than expected, probably due to product adsorption on the electrode surface.

The above described results show that the present cymantrene-carbene derivatives behave very different compared to the previously studied group 6 $Cr^0(CO)_5$ and $W^0(CO)_5$ Fischer carbene complexes. Differences in [L^1L^2M=C(OEt)-Ar] complexes (and by implication also the biscarbene analogues) may be summarised as follows:

a) For L^1L^2M = $(CO)_5Cr^0$, Cr(0) is first oxidised electrochemically reversibly to Cr(I) at $E^{o'}$ = 0.29 V, then Ar = Fc is oxidised electrochemically reversibly to Fc^+ at $E^{o'}$ = 0.70 V and finally Cr(I) is oxidised electrochemically irreversibly to Cr(II) at $E^{o'}$ > 1.15 V. For Ar = Fu or Th chromium carbene analogues, the irreversible $Cr^{I/II}$ couple is between 0.95 and 1.15 V (See

Figure S1).[20]

b) For $L^1L^2M = (CO)_5W^0$, Ar = Fc is first oxidised electrochemically reversibly (see Figure S1) to Fc^+ at $E^{o'}$ = 0.29 - 0.31 V depending on what electrolyte is used. W(0) is irreversibly oxidised to W(II) at E_{pa} = 1.11 V in two overlapping one-electron transfer steps in the presence of $[N(^nBu)_4][B(C_6F_5)_4]$ as supporting electrolyte, but to W(III) in three near-overlapping one-electron transfer steps at 0.81 V in the presence of $[N(^nBu)_4][PF_6]$ as supporting electrolyte.[23]

c) For $L^1L^2M = Cp(CO)_2Mn^I$, compound **3a**, Mn(I) is first oxidised electrochemically reversibly to Mn(II) at $E^{o'}$ = -0.106 V (ΔE = 96 mV), and then Ar = Fc is oxidised electrochemically reversibly to Fc^+ at $E^{o'}$ = 0.442 V (ΔE = 92 mV, Table 8.2). Although strictly speaking ΔE = 59 mV is diagnostic of electrochemical reversibility,[28] electrochemical reversible redox processes of the ferrocenyl group is universally accepted. Since ΔE for the Fc and Mn redox processes are for all practical purposes identical, we conclude that electrochemical reversibility of the cymantrenyl group is comparable with that of a ferrocenyl group in the present series of group 7 Fisher carbene complexes.

d) Only complex **2a** (Ar = Fu) showed an additional oxidative process at E_{pa} = 1.166 V. In analogy to the $Cr^{I/II}$ and $W^{0/III}$ couples, we believe that this may be an irreversible $Mn^{II/III}$ couple. However, all other complexes failed to show this redox process within the potential window of the solvent.

e) In terms of chemical reversibility, carbene reduction was almost irreversible with i_{pa}/i_{pc} very small (0 – 0.73; Table 8.2), but Mn(I) reductions was better than 85 % and in some cases approached 93 % (Table 8.2). Interestingly though, on LSV time scale, the ferrocenyl complexes showed the oxidised species $[Cp(OC)_2Mn^{II}=C(OEt)(Fc^+)]$, $\mathbf{3a^{2+}}$, began to decompose notably before the LSV experiment is completed (Figure 8.4).

f) Wave Fc for **3b**, $[Cp(CO)_2Mn^I=C(OEt)\text{-}Fc'\text{-}(OEt)C=Mn^I(CO)_2Cp]$, does not exhibit the usual ideal CV shape. The cathodic peak is much sharper than expected. A similar observation was made for $[(CO)_5Cr=C(OEt)\text{-}Fc'\text{-}(OEt)C=Cr(CO)_5]$[19] but i_{pc}/i_{pa} for the manganese derivative was better (1.38 versus >10). The unusually large i_{pc} value for wave Fc in **3b** is attributed to electrode deposition of $\mathbf{3b^{3+}}$, the fully oxidised product (Scheme 8.3) onto the active surface of the electrode.

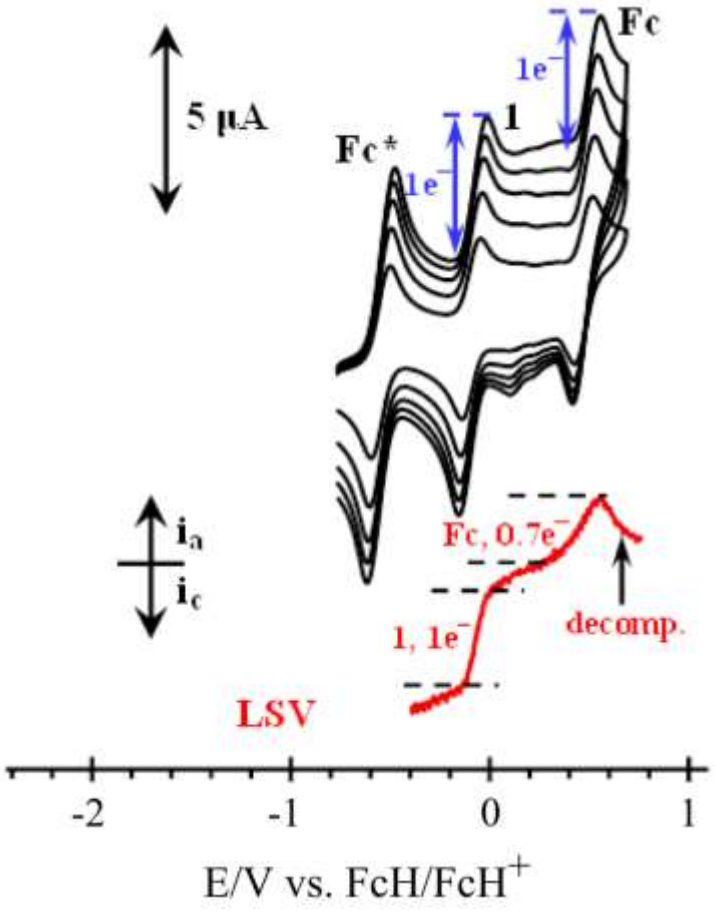

Figure 8.4 CV's of 0.5 mmol·dm^{-3} solutions of the [(Cp)(OC)$_2$Mn=C(Fc)(OEt)], **3a**, in CH_2Cl_2 containing 0.1 mol·dm^{-3} [N(^{n}Bu)$_4$][PF$_6$] as supporting electrolyte at a scan rate of 100 (smallest currents), 200, 300, 400 and 500 mV·s^{-1} and 20 ^{o}C. The blue arrows on the CV's shows the Mn center is involved in the same number of electrons being transferred as the ferrocenyl group, that is, it involves a one-electron transfer process. The LSV shows that the doubly oxidised **3a** is unstable on LSV time scale (1 mV·s^{-1}; currents were enlarged three fold for clarity): the compound begins to decompose notably after 0.7 electrons have flown during Fc oxidation. Fc* = decamethylferrocene.

Scheme 8.3 highlights the proposed electrochemical pathway of the observed redox processes of **3b**. The other ethoxybiscarbene complexes undergo essentially the same processes although wave 1 is not resolved into two separate one-electron transfer processes, and the ferrocenyl wave is absent.

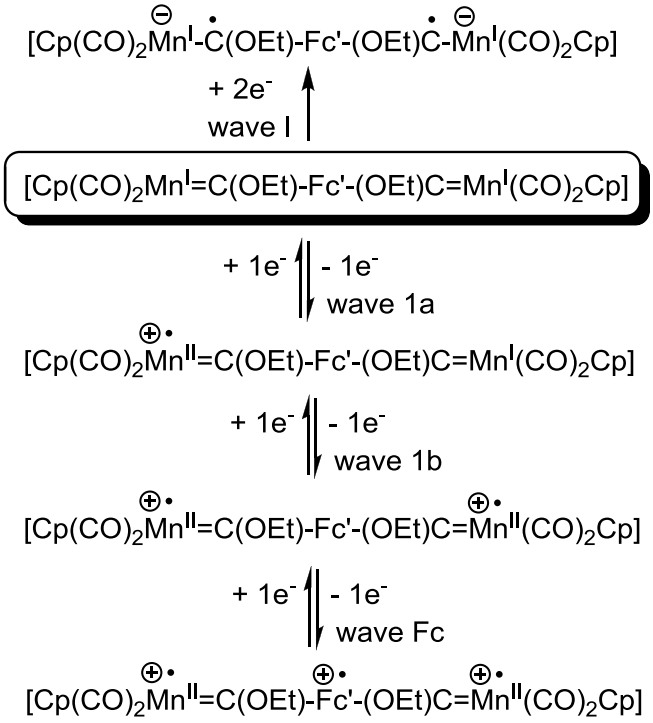

Scheme 8.3 Electrochemical reactions associated with **3b**.

DFT simulations-redox chemistry

In order to gain more insight into the oxidation processes and the nature of the species involved, a Density Functional Theory (DFT) study was carried out.[24] We first focused on the oxidation process of complex **2a**. As depicted in Figure 8.3, the HOMO of **2a** (i.e. the orbital from which the electron is released) is mainly located on a doubly occupied *d* atomic orbital of the manganese atom. This orbital nicely represents the π-backdonation of the transition metal to the vacant p_z atomic orbital of the carbene carbon atom. Therefore, the one-electron oxidation should lead to a radical cation where the unpaired electron is mainly located at the manganese. The computed spin density on **2a**$^{\bullet+}$ indicates a value of 1.21e on the transition metal atom thus confirming the assignment of $Cp(CO)_2Mn^{II\bullet}$=C(OEt)Fu as oxidation product (Figure 8.5a).

(a)

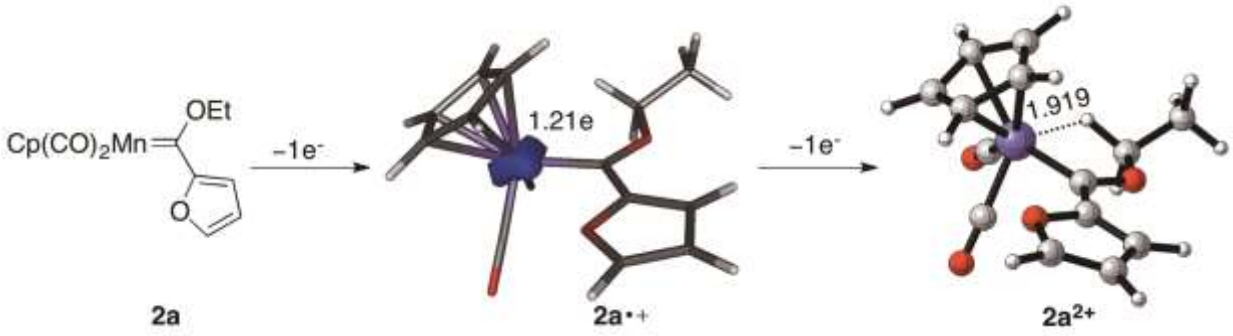

(b)

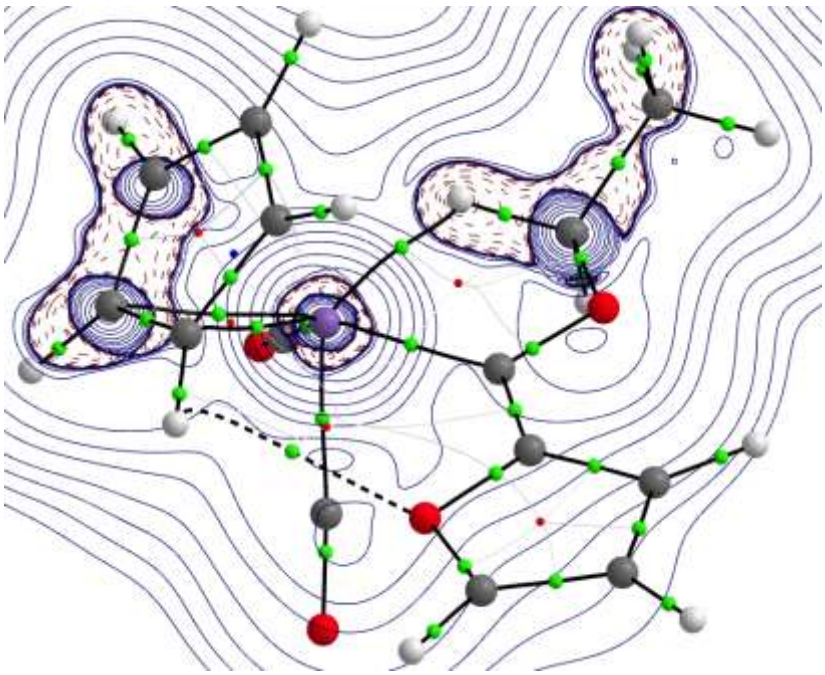

Figure 8.5 (a) Oxidation process of complex **2a**. (b) Contour line diagrams $\nabla^2\rho(r)$ for comple **2a**$^{2+}$ in the Mn−H−C plane. The solid lines connecting the atomic nuclei are the bond paths while the small red spheres indicate the corresponding bond critical points.

The second oxidation process was tentatively assigned to the formation of the corresponding Mn(III) dication **2a**$^{2+}$ (see above). Our calculations nicely agree with this assignment and reveals that the dication **2a**$^{2+}$ presents a peculiar bonding situation which is markedly different to the structures of **2a** and the radical cation **2a**$^{\bullet+}$. As a consequence of the oxidation process which eliminates the two electrons of the HOMO of **2a** (located at the manganese), the transition metal is prone to accept more electron density from the carbene ligand. Indeed, a clear C···H agnostic

interaction is present in $\mathbf{2a}^{2+}$ as confirmed by the computed short Mn···HC distance of 1.919 Å (Figure 8.5a). Additionally, the Atoms in Molecules (AIM) method further supports the existence of this agostic interaction. As seen in Figure 8.5b, the Laplacian distribution of $\mathbf{2a}^{2+}$ in the Mn-H-C plane clearly reveals the occurrence of a bond critical point located between the transition metal and the hydrogen atom, which is associated with a bond path running between these two atoms. Moreover, the computed value of 0.038 e.Å^{-3} for the electron density at the bond critical point, is in the range expected for CH agostic interactions.[28] The bonding situation of $\mathbf{2a}^{2+}$ resembles that found for related pentacarbonylchromium(0) and tungsten(0) carbene complexes formed upon 2-electron oxidation of the transition metal,[22,23] which indicates that this bonding situation seems to be general for oxidized Fischer carbene complexes regardless of the transition metal and associated ligands.

We then considered the oxidation processes of the ferrocenyl substituted carbene complexes **3a** and **3b**. Analogously to **2a**, the one-electron oxidation of **3a** leads to the formation of the radical cation $\mathbf{3a}^{\bullet+}$ whose unpaired electron is mainly located at the manganese (computed spin density of 1.21 e). This result confirms the above electrochemical conclusion that the manganese is oxidized before the iron atom and is consistent with the ESR spectrum of $\mathbf{3a}^{\bullet+}$. Subsequent one-electron oxidation may lead to two different species, namely the open-shell singlet complex formed upon oxidation of the Fe(II) to Fe(III) or, alternatively, the closed-shell singlet involving the oxidation of the Mn(II) to Mn(III). Our calculations reveal that the former species is 26.4 kcal/mol more stable than the latter, thus suggesting that the dication $\mathbf{3a}^{+2}$ presents two unpaired electrons (computed spin densities of -1.26 and 1.30 for Mn and Fe, respectively, see Figure 8.6a). A similar behaviour can be found in biscarbene complexes **3b**. As readily seen in Figure 8.6b, the first one-electron oxidation involves the Mn(I) to Mn(II) reaction to produce the radical cation $\mathbf{3b}^{\bullet+}$. This process is followed by the oxidation of the other manganese centre to produce the open-shell singlet $\mathbf{3b}^{+2}$. Finally, the Fe(II) to Fe(III) oxidation occurs to form complex $\mathbf{3b}^{\bullet+3}$ in which each metal bears an unpaired electron. Therefore, our calculations fully support the electrochemically pathway proposed in Scheme 8.3.

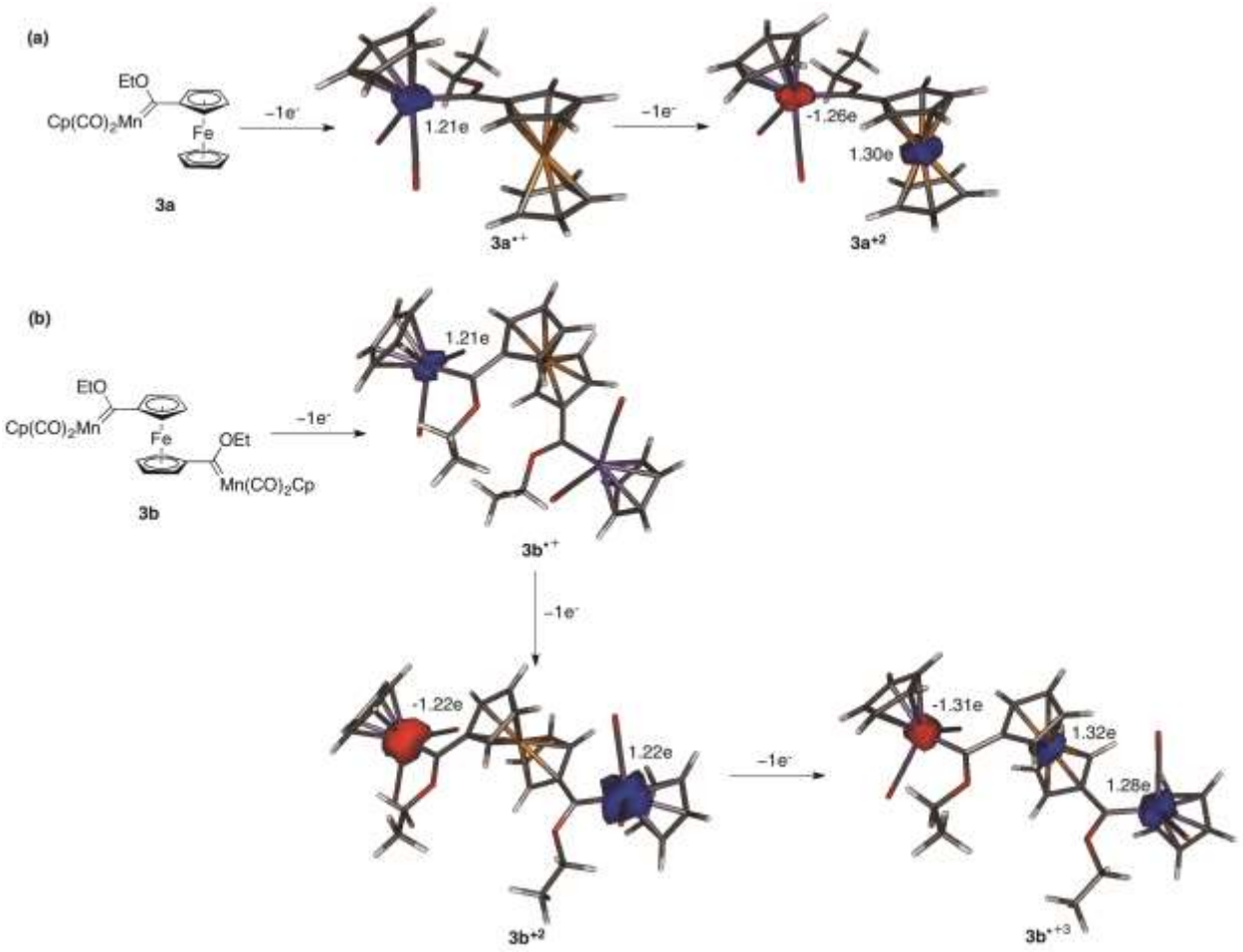

Figure 8.6 Oxidation processes of complexes **3a** (a) and **3b** (b). Spin densities were computed at the B3LYP/def2-SVP level.for Mn and Fe, respectively, see Figure 8.6a).

ESR spectroscopy

Lastly, we carried out an ESR analysis of the chemically oxidised product **[3a][PF$_6$]** to experimentally support the above computational assignment of the radical cation as a $Cp(CO)_2Mn^{II}$•–C species. Briefly, **[3a][PF$_6$]** was generated by $AgPF_6$-mediated oxidation of **3a** at –41 °C in CH_2Cl_2 (Scheme 8.2); transfer of the solution to a gas-tight ESR tube after 7 min followed by immediately recording the X-band ESR spectrum at 77 K permitted observation of a clean spectrum of the transiently stable radical cation (Figure 8.7). (Note that a sample removed from the reaction vessel after 35 min afforded only a low-resolution, low-intensity ESR spectrum indicative of time-dependent decay of **[3a][PF$_6$]** to one or more ESR-silent species in solution.)

The ESR spectrum of **3a**$^{\bullet+}$ is characterized by a rhombic *g*-tensor with the components g_z = 2.130, g_y = 2.007, and g_x = 1.975. Each *g*-component is, furthermore, split into six lines as a result of hyperfine coupling to the ^{55}Mn nucleus (I = 5/2, 100%). While the hyperfine coupling clearly confirms oxidation of Mn(I) (diamagnetic low-spin d^6) to Mn(II) (S = ½ d^5), the ensuing peak overlap significantly complicates interpretation of the derivative spectrum and creates difficulties not only when attempting to locate the *g*-tensor components, but also when attempting to delineate the hyperfine coupling constants (*A*-values). We found that deconvolution of the ESR absorption spectrum (Figure 8.7a) into a summation of Voigt functions[30] partly simplified the task of locating the *g*-tensor components and measuring the hyperfine coupling constants from the experimental spectrum. As is customary in spectroscopy,[30] we chose to fit the data with a summation of Voigt functions as these functions represent a convolution of Gaussian and Lorentzian line shapes, have a sound theoretical basis, and are well-suited to analysing spectroscopic absorption bands in which both lifetime broadening (e.g. due to spin-lattice relaxation) as well as Doppler, instrumental, and proximity line broadening are present to varying extents. This requires that the derivative ESR spectrum be fit in its integrated form (i.e. absorption spectrum, Figure 8.7a). In systems with rhombic *g*-tensors and no hyperfine coupling [e.g. low-spin Fe(III)] spectral deconvolution of the absorption trace is straightforward; the situation is, however, more complex in the case of low-spin Mn(II) due to each *g*-tensor component affording six absorption lines.

Given the above limitations expected for spectral deconvolution of the ESR absorption spectrum of a low-spin Mn(II) ion, precise location of g_y is nevertheless straightforward and simply achieved using H_{max} for the most intense component peak (3352 G) in the absorption spectrum (Figure 8.7a). Location of g_x and g_z is more difficult especially since the Voigt functions themselves are of variable band width and, in some cases, represent more than one overlapped peak. For g_z, the position of this tensor component is expected to be at the centre of gravity of the six independent equal-intensity lines into which the signal splits by virtue of hyperfine coupling to ^{55}Mn. Only the three low-field hyperfine lines are in fact easily discerned. That said, the experimental anisotropic hyperfine coupling constant A_1 (115 G) may be used to locate g_z since it is at precisely $2.5A_1$ to higher magnetic field from the lowest-field line in the spectrum. Unfortunately locating g_x is significantly more problematic. Our best estimate using an

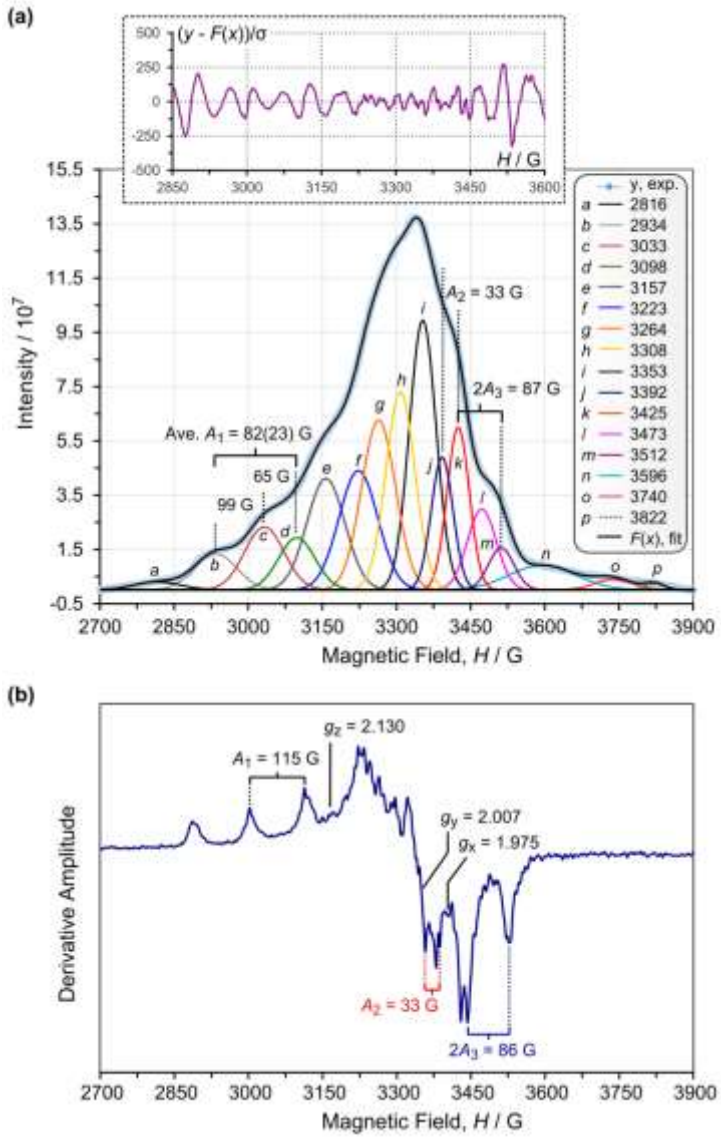

Figure 8.7. (a) ESR absorption spectrum of **[3a][PF_6]** recorded in CH_2Cl_2 at 77 K shortly after oxidation of **3a** with $AgPF_6$. The spectral envelope is deconvoluted into a series of Voigt functions; the sum of these, *F(x)*, fits the experimental spectrum with a correlation coefficient of 0.9999. The raw spectral data are shown without background subtraction; the first (2816 G) and last three (≥ 3596 G) bands simply mathc the background and may be ignored. The upper inset shows the weighted fit residueals for the spectral region containing useful spectroscopic information; the right inset lists the H_{max} values for the Voigt components. (b) Derivative mode ESR spectrum (12 scans) of **[3a][PF_6]** with assigned *g*-tensor components. Data acquisition: frequency, 9.421260 GHz; attenuation, 20.0 dB; power, 2.00 mW; modulation amplitude, 2.00 G (modulation frequency 100.00 kHz); time constant, 81.92 ms; conversion time, 38.00 ms; sweep width, 1200 G (centre field = 3300 G); data resolution, 2400 points.

analysis of the Voigt components in conjunction with the value of A_3 measured as indicated in Figure 8.7b places g_x at 3428 G (i.e., g_x = 1.975). From the Voigt functions in Figure 8.7a, the anisotropic hyperfine coupling constants A_2 and A_3 measure 33 and 43 G, respectively. Note that measurement of A_3 from either the absorption or derivative spectrum is complicated somewhat by the fact that the peak expected between the indicted pair of lines is unresolved (as a result of overlap). (The spacing $2A_3$ is, however, well-resolved and simple to measure.)

While useful, peak deconvolution of the ESR absorption spectrum is subject to significant uncertainty, particularly in the lower magnetic field range, contingent upon the lower intensity of the spectral envelope. The estimate of A_1 in Figure 8.7a [82(23) G] is therefore the least accurate of the three hyperefine coupling constants—in contrast to the situation when analyzing the first derivative of the spectral envelope. We therefore feel that for **[3a][PF$_6$]** it is not only practically sound, but indeed preferable, to use the value of A_1 determined from analysis of the derivative trace (i.e. A_1 = 115 G, Figure 8.7b).

A key question that emerged during analysis of the ESR spectrum of **[3a][PF$_6$]** concerned assignment of the *g*-tensor components as g_x, g_y, or g_z. Experimental assignment of the *g*-tensor components requires determination of the tensor axes relative to the molecular framework, which requires a large face-indexed crystal, the X-ray crystal structure, and analysis of the ESR spectrum as a function of the orientation of the crystal in the applied magnetic field. In the absence of a suitable single crystal, we resorted to calculating the *g*-tensor and anisotropic spin-dipole couplings for **3a**$^{\bullet+}$ using a suitable hybrid DFT functional and several basis sets both *in vacuo* and in a CH_2Cl_2 solvent continuum. The *g*-values calculated with the all-electron basis set 6- 311g(d,p)[31] (Table 8.3) are remarkably independent of the presence or absence of diffuse functions or solvent and are in excellent agreement with the experimental values. Furthermore, the calculated *g*-shifts relative to the free electron *g*-value allow unambiguous assignment of the experimental *g*-values as depicted in Figure 7b. The *g*-values calculated using the effective core potential (ECP) basis set SDD[32] are also in good agreement with the experimental values; only g_z deviates by more than 20,000 ppm from the experimental value. Because of the generally good precision in the simulation data we can determine the mean calculated *g*-values using all of the available data for **3a**$^{\bullet+}$: g_x = 1.998(1), g_y = 2.03(1), and g_z = 2.13(5).

Table 8.3. DFT-calculated parameters for **3a**$^{\bullet+}$ as a function of basis set type.[a]

	6-311+g(d,p) DCM PCM	6-311+g(d,p)	6-311g(d,p)	SDD
g-tensor x-shift	–4632.9	–5018	–4510.8	–2850
g-tensor y-shift	31090.6	31140	33090.8	9549.2
g-tensor z-shift	149600.2	151317.5	148546.9	57350
g_x calc.	1.998	1.997	1.998	1.999
g_y calc.	2.033	2.033	2.035	2.012
g_z calc.	2.152	2.154	2.151	2.060
g_{iso} calc.	2.061	2.061	2.061	2.024
Spin density	1.17	1.09	1.14	1.29
IFCC / G	–40.28	–41.33	–40.07	–0.01
A_1 / G	–71.104	–77.409	–76.83	–75.29
A_2 / G	22.278	36.133	30.636	35.728
A_3 / G	48.826	41.276	46.194	39.565
4s	0.357	0.353	0.346	0.318
4px	0.348	0.329	0.021	0.317
4py	0.356	0.342	0.024	0.324

[a] Units and abbreviations: DCM PCM, dichloromethane polarization continuum model; *g*-shifts relative to g_e for the free electron are in ppm; spin (Mulliken) and electron densities (NBO 3.0[33]) are given in electron charge units and are listed for the Mn(II) ion only; IFCC, isotropic Fermi contact coupling for Mn; A_n are the anisotropic spin-dipole coupling constants for Mn (where *n* is the principal axis system component).

The unpaired spin densities on the Mn(II) ion of **3a**$^{\bullet+}$ range from 1.09–1.29 e depending on the basis set used and are consistent with the value of 1.21 e calculated at the B3LYP/def2-SVP level of theory (*vide supra*). The calculated anisotropic spin-dipole couplings in Table 3 vary somewhat more with the basis set and/or the presence of solvent. The mean calculated anisotropic spin-dipole coupling constants are: A_1 = –75(3) G, A_2 = 31(6) G, and A_3 = 44(4) G. From the experimental ESR spectrum of **3a**$^{\bullet+}$, we were able to reliably measure A_2 (33 G) and A_3

(43 G), but not A_1. The value of A_1 determined from the derivative trace (115 G) clearly deviates significantly from the calculated value of A_1. That said, determination of A_1 from the Voigt functions below 3150 G in Figure 7a yields an estimated mean A_1 value of 82(23) G—somewhat closer to the DFT-calculated value, but subject to substantial uncertainty. Significantly, the relative absolute magnitudes of the experimental and DFT-calculated hyperfine coupling constants follow the same order ($A_2 < A_3 << |A_1|$), which affirms the approach we have used for assignment of the experimental ESR spectrum of **[3a][PF$_6$]**.

Importantly, replacement of one of the three CO ligands in cymantrene, Mn(Cp)(CO)$_3$, with a carbene ligand in the present case of **3a**$^{\bullet+}$ lowers the symmetry of the *g*-tensor from tetragonal to rhombic. A switch in the *g*-tensor anisotropy may thus be used to detect the substitution of a carbonyl ligand in Mn(II) cymantrene derivatives (at least for carbenes). With the exception of the rhombic *g*-tensor, the magnitudes of the key ESR spectral parameters for **3a**$^{\bullet+}$ are broadly in accord with the tetragonal *g*- and *A*-tensor components reported previously for Mn(Cp$^{\gamma}$)(CO)$_3$ derivatives, where γ is a substituent on the Cp ligand.[6] These latter tricarbonyl complexes have *g*- and *A*-values in the following ranges: $g_{\|} \sim 2.12–2.21$, $g_{\perp} \sim 2.01–2.08$, $A_{\|} \sim 65–79$ G, and $A_{\perp} \sim 30–50$ G.[6]

8.3 CONCLUSION

Mono- and biscarbene cymantrene derivatives [Cp(CO)$_2$Mn^{I}=C(OEt)Ar] **1a** (Ar = Th), **2a** (Ar = Fu), **3a** (Ar = Fc) and [Cp(CO)$_2$Mn^{I}=C(OEt)-Ar'-(OEt)C=Mn^{I}(CO)$_2$Cp] with Ar' = Th' (**1b)**, Ar' = Fu' (**2b)** and Ar' = Fc' (**1b)** were prepared via the classical Fischer route. Chemical oxidation of **3a** with $AgPF_6$ permitted isolation of transiently stable [Cp(CO)$_2$Mn^{II}=C(OEt)Fc][PF$_6$], [**3a][PF$_6$]**. From an FTIR study, the > 110 cm^{-1} shift of the carbonyl stretching frequencies for [**3a][PF$_6$]** relative to neutral **3a** indicates that the oxidation is that of the metal carbonyl moiety, as opposed to Fe^{II}/Fe^{III} oxidation of the ferrocenyl substituent. An electrochemical study on **1** – **3** confirmed that Mn(I) is oxidized before the ferrocenyl group, and that both these oxidations involve an one-electron transfer process. Complex **3b** showed clear splitting of the Mn(I) oxidation into "a" and "b" components but **1b** and **2b** did not. This is consistent with Ar' = Fc' being more effective in transmitting electrostatic interactions between cymantrenyl moieties than Ar' = Fu' or Th'. Poorly chemical reversible reduction of Mn=C to $^{-}$Mn^{I}-C• was observed at far

negative potentials (< -2.065 V vs FcH/FcH^+). DFT calculations showed that the mono- and biscarbene complexes containing one or two Mn(I) ions always undergo one-electron oxidation of manganese before the onset of ligand or ferrocene oxidation. This reflects localization of the HOMO on the Mn=C group of the cymantrene unit. Our interpretation of the electrochemical and DFT data was tested experimentally using ESR spectroscopy to probe $\mathbf{3a}^{\bullet+}$ produced by direct chemical oxidation of **3a**. The ESR spectrum revealed a rhombic *g*-tensor for an $S = ½$ Mn(II) ion with ^{55}Mn hyperfine coupling constants in accord with those observed for $[Mn(Cp^{\gamma})(CO)_3]^+$ derivatives. The rhombic *g*-tensor for $\mathbf{3a}^{\bullet+}$ evidently reflects reduced symmetry at the metal centre consistent with replacement of one cymantrene CO ligand by the Mn=C(OEt)Fc carbene moiety.

8.4 EXPERIMENTAL SECTION

General

All operations were carried out under an inert atmosphere of nitrogen or argon gas using standard Schlenk techniques. Solvents were dried by refluxing on sodium metal (hexane, tetrahydrofuran and diethylether) or over phosphorous pentoxide (CH_2Cl_2) and then distilled under nitrogen prior to use. Chemicals were used without further purification unless stated otherwise. Triethyloxonium tetrafluoroborate (Et_3OBF_4) was synthesized according to literature procedures.[15] Purification with column chromatography was done using silica gel 60 (0.0063–0.200 mm) as stationary phase. A Bruker AVANCE 500 spectrometer was used for NMR recordings. ^1H NMR spectra were recorded at 500.139 MHz and ^{13}C NMR spectra at 125.75 MHz. The signal of the solvent was used as reference: ^1H $CDCl_3$ at 7.24 ppm; C_6D_6 at 7.16 ppm and ^{13}C CDCl3 at 77.00 ppm; C_6D_6 at 128.06 ppm. IR spectra were recorded on a Perkin-Elmer Spectrum RXI FT-IR spectrophotometer in CH_2Cl_2 as solvent. Only the vibration bands in the carbonyl-stretching region (ca. 1600–2200 cm^{-1}) were recorded.

Synthesis

Synthesis and characterization of **1b**,[12c] **3a**[28, 12d] and **3b**[27, 12d] have been reported earlier. Novel complexes **1a**, **2a** and **2b** were prepared in an adapted version of previously reported method.[23]

*Synthesis of [Cp(CO)$_2$Mn=C(OEt)Th] (**1a**) and [Cp(CO)$_2$Mn=C(OEt)Th'(OEt)C=Mn(CO)$_2$Cp] (**1b**).*

2-Bromothiophene (2 mmol, 0.2 mL) was dissolved in 30 mL thf and cooled to -70^{o}C. One equivalent LDA (2 mmol) was added and the solution stirred for 15 minutes at low temperature. CpMn(CO)$_3$ (2 mmol, 0.40g) was added in one portion and stirred for 15 minutes after which the cold bath was removed and the mixture allowed to stir for an additional 1hr. The reaction mixture was then cooled to -60^{o}C and nBuLi (1.5M, 2 mmol, 1.3 mL) was slowly added. After 30 minutes another equivalent of CpMn(CO)$_3$ (2 mmol, 0.40g) was added and allowed to stir for 15 min in the cold. The bath was removed and the mixture stirred for 1 hr at room temperature. The solvent was changed to CH_2Cl_2 and the reaction cooled to -40^{o}C after which 2 equivalents of Et_3OBF_4 with 10% excess (4.4 mmol) dissolved in CH_2Cl_2 was added. After 15 min in the cold bath the mixture was allowed to reach RT over an hour. Purification with column chromatography on silica and gradient eluation starting with 1:4 CH_2Cl_2/Hexane solution afforded the ochre coloured monocarbene (**1a**) and the maroon coloured biscarbene (**1b**) complexes.

For **1a**: Yield 45% (0.28g), dark yellow crystals. Anal. calcd. for $MnC_{14}H_{13}O_3S$ (316.28), C:53.16, H:4.15; Found C:53.18, H:4.16. ^{1}H NMR (C_6D_6, δ/ppm): 7.80 (br, 1H, Th-H$_\alpha$), 6.93 (br, 1H, Th-H$_\gamma$), 6.96 (br, 1H, Th-H$_ß$), 4.75 (br, 2H, C**H$_2$**), 4.14 (br, 5H, **Cp**), 1.19 (br, 3H, C**H$_3$**); ^{13}C NMR (C_6D_6, δ/ppm): 319.46 ($C_{carbene}$), 231.19 (CO), 156.74 (Th$_{ipso}$), 136.60 (Th-C$_\gamma$), 136.30 (Th-C$_\alpha$), 130.78 (Th-C$_ß$), 83.97 (Cp), 73.99 (CH_2), 15.11 (CH_3). IR (CH_2Cl_2, ν(CO)/cm^{-1}): 1936, 1872.

*Synthesis of [Cp(CO)$_2$Mn=C(OEt)Fu] (**2a**) and [Cp(CO)$_2$Mn=C(OEt)Fu'(OEt)C=Mn(CO)$_2$Cp] (**2b**)*

Furan (2.7 mmol, 0.2 mL) was dissolved in 50 mL thf and cooled to -20^{o}C. nBuLi (1.5M, 1.8 mL) was added slowly to the stirring solution which was then left to react in the cold for 30 min. It was then cooled further to -40^{o}C and CpMn(CO)$_3$ (2.7 mmol, 0.55g) was added in one portion. The cold bath was removed after 15 min and the mixture left to stir at rt for 1 hr. The reaction was cooled again to -78^{o}C and LDA (0.18M, 15 mL) was added and the reaction stirred for 1 hr. It was warmed to -40^{o}C and CpMn(CO)$_3$ (2.7 mmol, 0.55g) was added. After stirring for 1 hr at rt the acylate was quenched with Et$_3$OBF$_4$ (0.54M, 12 mL) at -20^{o}C in CH$_2$Cl$_2$and stirred for another hour at rt. Purification was performed by column chromatography on silica and gradient eluation starting with 1:4 CH$_2$Cl$_2$/Hexane solution. The brown coloured monocarbene (**2a**) and the maroon coloured biscarbene (**2b**) complexes were collected.

For **2a**: Yield 56% (0.48g), dark yellow crystals. Anal. calcd. for MnC$_{14}$H$_{13}$O$_4$ (316.21), C:53.16, H:4.15; Found C:53.21, H:4.20. ^{1}H NMR (C$_6$D$_6$, δ/ppm): 6.71 (br, 2H, Fu-H$_\gamma$), 6.71 (br, 1H, Fu-H$_\alpha$), 5.97 (br, 1H, Fu-H$_ß$), 4.75 (br, 2H, C**H$_2$**), 4.38 (br, 5H, **Cp**), 1.21 (br, 3H, C**H$_3$**); ^{13}C NMR (C$_6$D$_6$, δ/ppm): 309.31 (C$_{carbene}$), 232.22 (CO), 164.49 (Fu$_{ipso}$), 145.20 (Th-C$_\gamma$), 112.03 (Fu-C$_\alpha$), 111.50 (Fu-C$_ß$), 84.27 (Cp), 73.20 (CH$_2$), 15.27 (CH$_3$). IR (CH$_2$Cl$_2$, ν(CO)/cm^{-1}): 1942, 1876.

For **2b**: Yield 32% (0.44g), maroon crystals. Anal. calcd. for Mn$_2$C$_{24}$H$_{22}$O$_8$ (548.38), C:52.56, H:4.05; Found C:52.59, H:4.07. ^{1}H NMR (C$_6$D$_6$, δ/ppm): 6.84 (br, 2H, Fu-H), 4.77 (br, 4H, C**H$_2$**), 4.41 (br, 10H, **Cp**), 1.25 (br, 6H, C**H$_3$**); ^{13}C NMR (C$_6$D$_6$, δ/ppm): 306.82 (C$_{carbene}$), 232.32 (CO), 161.57 (Fu$_{ipso}$), 116.57 (Fu), 85.84 (Cp), 73.35 (CH$_2$), 15.40 (CH$_3$). IR (CH$_2$Cl$_2$, ν(CO)/cm^{-1}): 1935, 1886.

*Synthesis of [Cp(CO)$_2$Mn=C(OEt)Fc][PF$_6$] (**[3a]PF6]**).*

Compound **3a** (0.006g, 0.01 mmol) was dissolved in CH_2Cl_2 and cooled to -35^{o}C. $AgPF_6$ (0.003g, 0.01 mmol) was added in one portion after which the colour changed rapidly from dark red to brown. The solution was filtered using canula filtration.

For **[3a]PF6]**: Yield 78% (0.006g), dark brown salt. IR (CH_2Cl_2, ν(CO)/cm^{-1}): 2042, 1978.

Electrochemistry

Cyclic voltammograms (CV's), square wave voltammograms (SW's) and linear sweep voltammograms (LSV's) were recorded on a Princeton Applied Research PARSTAT 2273 voltammograph running PowerSuite (Version 2.58). All experiments were performed in a dry three-electrode cell. A platinum wire was used as auxiliary electrode while a glassy carbon working electrode (surface area 3.14 mm^2) was utilized after polishing on a Buhler polishing mat first with 1 micron and then with 1/4 micron diamond paste. A silver wire was used as pseudo internal reference under an argon atmosphere inside an M Braun Lab Master SP glovebox filled with high purity argon (H_2O and O_2 < 5 ppm). All electrode potentials are reported using the potential of the ferrocene/ferrocenium redox couple [FcH/FcH$^+$] (FcH = (η^5-C_5H_5)$_2$Fe, E°′ = 0.00 V) as reference.[34] However, decamethyl ferrocene, Fc*, was used as internal standard to prevent signal overlap with the ferrocenyl of **3**. Decamethylferrocene has a potential of −550 mV versus free ferrocene with ΔE = 72 mV and i_{pc}/i_{pa} = 0.99 under the conditions employed.[26] Analyte solutions (0.5 mmol dm^{-3}) were prepared in dry CH_2Cl_2 in the presence of 0.1 mol dm^{-3} [(^{n}Bu$_4$)N][PF$_6$]. Analyses were performed at 20 °C. Data were exported to a spread sheet program for manipulation and diagram preparation.

ESR spectroscopy

The cation radical **[3a][PF$_6$]** was generated as follows for ESR spectroscopy. Solid compound **3a** (0.060 g, 0.10 mmol) and solid $AgPF_6$ (0.030 g, 0.10 mmol) were placed together in a dry Schlenk tube under nitrogen at –41 °C in an acetonitrile/liquid nitrogen slush bath. After thermal

equilibration, 10 mL of dry CH_2Cl_2 that had been pre-cooled to –41 °C was added to the solids via cannula transfer from a reservoir flask under nitrogen. The solution immediately changed from orange-brown to deep red and was mixed by swirling for *ca*. 6 min at –41 °C before transferring a *ca*. 600-µL aliquot of the reaction mixture by cannula filtration into a gas-tight ESR tube suspended in the slush bath at –41 °C. The sample aliquot was immediately flash-frozen in liquid nitrogen and then transferred to a liquid nitrogen-containing quartz finger dewar mounted in the sample slot of the microwave resonator of a Bruker EMX-plus X-band ESR spectrometer operating at a frequency of 9.421260 GHz. The final spectrum was obtained from 12 scans over the spectral range 2700–3900 G using the data acquisition parameters indicated in Figure 7. The spectral data in derivative mode were first filtered (boxcar averaging with a 7 point window and 9th order polynomial filter) and then resolution-enhanced (line-broadening function = 0.200 G) for the final plot. The ESR absorption spectrum (raw data) was deconvoluted into a series of constituent Voigt functions using FitYk 0.9.8[35] in order to facilitate *g*-value assignments. The fit parameters are given in the Supporting Information.

Molecular simulations

Geometry optimizations without symmetry constraints were carried out using the Gaussian09 suite of programs.[36] Electron correlation was partially taken into account using the hybrid functional denoted as B3LYP (and uB3LYP for radical cations and open-shell species)[37] in combination with double-ζ quality plus polarization def2-SVP[38] basis set for all atoms (this level is denoted B3LYP/def2-SVP). Calculation of the vibrational frequencies[39] at the optimized geometries showed that the compounds are minima on the potential energy surface.

The AIM[40] results described in this work correspond to calculations performed at the B3LYP/def2-SVP level on the optimized geometry of **2a**$^{+2}$. The topology of the electron density was studied using the AIMAll program package.[31]

DFT simulations for analysis of the ESR spectrum of **3a**$^{\bullet+}$, specifically determination of the *g*- and *A*-tensors, were performed with an unrestricted wave function using the full Heyd-Scuseria-Ernzerhof hybrid functional HSEH1PBE[42] and three basis sets: the effective core potential basis set SDD[32] and the all-electron basis sets 6-311g(d,p)[31] or 6-311+g(d,p). We also determined

the electronic structure of **3a**$^{\bullet+}$ in CH_2Cl_2 (polarization continuum model, PCM). The geometries of all structures were fully optimized; no negative eigenvalues were calculated in any of the post-optimization frequency jobs.

8.5 ACKNOWLEDGEMENTS

This work is supported by the National Research Foundation (NRF) of South Africa, (D.I.B., Grant number 76226; J.C.S., Grant number 81829). I. F. acknowledges the Spanish MICINN and CAM (Grants CTQ2010-20714-CO2-01/BQU, Consolider-Ingenio 2010, CSD2007-00006, S2009/PPQ-1634). O.Q.M. acknowledges financial support from the University of KwaZulu-Natal and the NRF.

8.6 REFERENCES

[1] a) L. Cuffe, R. D. A. Hudson, J. F. Gallagher, S. Jennings, C. J. McAdam, R. B. T. Connelly, A. R. Manning, B. H. Robinson, J. Simpson, *Organometallics*, **2005**, *24*, 2051-2060; b) S. Warren, T. McCormac, E. Dempsey, *Bioelectrochemistry*, **2005,** *67***,** 23-35; c) A. D. Ryabov, *Ad. Inorg. Chem.*, **2004**, 55, 201-269; d) K. C. Kemp, E. Fourie, J. Conradie, J. C. Swarts, J. C. *Organometallics*, **2008**, *27*, 353-362; e) P. D. Beer, E. Hayes, *J. Coord. Chem.*, **2003,** *240*, 167-189*;* (f) A. Chaubey, B. D. Malhotra, *Biosens. Bioelectron.*, **2002**, *17*, 441-456.

[2] a) R. F. Shago, J. C. Swarts, E. Kreft, C. E. J. Van Rensburg, *Anticancer Res.* **2007**, *27*, 3431-3433; b) C. E. J. Van Rensburg, E. Kreft, J. C. Swarts, S. R. Dalrymple, D. M. Macdonald, M. W. Cooke, M. A. S. Aquino, *Anticancer Res*. **2002**, *22*, 889-892; c) A. Gross, N. Hüsken, J. Schur, L. Raszeja, I. Ott, N. Metzler-Nolte, *Bioconjugate Chemistry*, **2012**, *23*, 1764-1774; d) J. C. Swarts, T. G. Vosloo, S. J. Cronje, W. C. Du Plessis, C. E. J. Van Rensburg, E. Kreft, J. E. Van Lier, *Anticancer Res.* **2008**, *28*, 2781-2784; e) I. Ott, K. Kowalski, R. Gust, J. Maurer, P. Mücke, R. F. Winter, *Bioorg. Med. Chem. Lett.* **2010**, *20*, 866-869.

[3] A. R. Pike, L. C. Ryder, B. R. Horrocks, W. Clegg, B.A. Connolly, A. Houlton, *Chem. Eur. J.* **2004**, *11*, 344-353.

[4] F. Spanig, C. Kolvacs, F. Hauke, K. Ohlubo, F. Fukuzumi, D. M. Guldi, A. Hirsch, *J. Am. Chem. Soc.* **2009**, *131*, 8180-8195.

[5] a) S. D. Lepore, A. Khoram, D. C. Bromfield, P. Cohn, V. Jairaj, M. A. Silvestri, *J. Org. Chem.*, **2005**, *70*, 7443-7446; b) Z. Zhang, S. D. Lepore, *Tetrahedr. Lett.*, **2002**, *43*, 7357-7360; c) H. Gradén, N. Kann, *Curr. Org. Chem.*, **2005**, *9*, 733-763; d) L. M. Dorozhkin, V. A. Nefedov, A. G. Sabelnikov, V. G. Sevastjanov, *Sens. Actuators B.*, **2004**, *B99*, 568-570.

[6] D. R. Laws, D. Chong, K. Nash, A. L. Rheingold, W. E. Geiger, *J. Am. Chem. Soc.*, **2008**, *130*, 9859-9870.

[7] a) M. Hromadova, M. Salmain, N. Fischer-Durand, L. Pospisil, G. Jaouen, *Langmuir*, **2006**, *22*, 506-511; b) M. Hromadoca, M. Salmain, R. Sokolova, L. Pospisil, G. Jaouen, *J. Organomet. Chem.*, **2003**, *668*, 17-24.

[8] a) C. N. Field, J. C. Green, A. G. J. Moody, M. R. F. Siggel, *Chem. Phys.*, **1996**, *206*, 211-223; b) D. C. Calabro, D. L. Lichtenberger, *J. Am. Chem. Soc.*, **1981**, *103*, 6846-6852; c) D. L. Lichtenberger, R. F. Fenske, *J. Am. Chem. Soc.*, **1976**, 98, 50-63.

[9] C. G. Atwood, W. E. Geiger, T. E. Bitterwolf, *J. Electroanal. Chem.*, **1995**, *397*, 279-285.

[10] Selected recent reviews on the chemistry of group 6 Fischer carbene complexes: a) M. A. Sierra, I. Fernández, F. P. Cossío, *Chem. Commun*. **2008**, 4671; b) K. H. Dötz, J. Stendel, *Chem. Rev*. **2009**, *109*, 3227; c) J. W. Herndon, *Coord. Chem. Rev*. **2010**, *254*, 103; d) M. A. Fernández-Rodríguez, P. García-García, E. Aguilar, *Chem. Commun*. **2010**, *46*, 7670; e) I. Fernández, F. P. Cossío, M. A. Sierra, *Acc. Chem. Res*. **2011**, *44*, 479; f) D. I. Bezuidenhout, S. Lotz, D.C. Liles, B. van der Westhuizen, *Coord. Chem. Rev.*, **2012**, *256*, 479-524.

[11] a) I. Hoskovcová, R. Světřinová, J. Roháčová, D. Dvořák, T. Tobrman, S. Záliš, J. Ludvík, *Electr. Chim. Acta,* **2011**, *56*, 6853-6859; b) I. Hoskovcová, J. Roháčová, D. Dvořák, T. Tobrman, S. Záliš, R. Světřinová, J. Ludvík,*Electr. Chim. Acta*, **2010**, *55*, 8341-8351.

[12] a) M. Landman, W. Barnard, P. H. van Rooyen, D. C. Liles, *J. Mol. Struct.*, **2012**, *1021*, 76-83; b) D. I. Bezuidenhout, S. Lotz, M. Landman, D. C. Liles, *Inorg. Chem.*, **2011**, *50(4)*, 1521-1533; c) Y. M. Terblans, M. H. Roos, S. Lotz, *J. Organomet. Chem.*, **1998**, *566(1-2)*, 133-142; d) E. O. Fischer, V. N. Postnov, F. R. Kreissl, *J. Organomet. Chem.*, **1982**, *231(4)*, C73-C77.

[13] A related electrochemical study on an Fe-NHC complex has been reported, see: L. Mercs, G. Labat, A. Neels, A. Ehlers, M. Albrecht, *Organometallics*, **2006**, *25*, 5648-5656.

[14] D. I. Bezuidenhout, W. Barnard, B. van der Westhuizen, E. van der Watt, D. C. Liles, *Dalton Trans.*, **2011**, *40*, 6711-6721.

[15] E. O. Fischer, A. Maasböl, *Angew. Chem.Int. Ed. Engl.***1964**, *3(8)*, 580-581.

[16] H. Meerwin, *Org. Synth.*, **1966**, *46*, 113-115.

[17] N. G. Connolley, W. E. Geiger, *Chem. Rev.*, **1996**, *96*, 877-910.

[18] Compound **2b** was prepared and spectroscopically characterized. However, the instability of **2b** with regards to atmospheric decomposition precluded it from the electrochemical studies, and no usable CV could be recorded.

[19] a) S. Lotz, C. Crause, A. J. Olivier, D. C. Liles, H. Gorls, M. Landman, D. I. Bezuidenhout, *Dalton Trans.* **2009**, 697−710; b) M. Landman, J. Ramontja, M van Staden, D. I. Bezuidenhout, P. H. van Rooyen, D. C. Liles, S. Lotz, *Inorg. Chim. Acta* **2010**, *363*, 705−717; c) G. M. Chu, I. Fernández, M. A. Sierra, *Chem. Eur. J.* **2013**, *19*, 5899−5908; d) E. Pretch, J. Seibl, T. Clerc, W. Simon, *Tables for Spectral Data for Structure Determination of Organic Compounds*, 2nd ed.; Springer-Verlag: Berlin, Germany, 1989.

[20] a) P. S. Braterman, Metal Carbonyl Spectra, Academic Press Inc., London, **1975**, p. 68; b) D. M. Adams, *Metal–Ligand and Related Vibrations*, Edward Arnold Publishers Ltd, London, 1967, p. 98.

[21] I. M. Alecu, J. Zheng, Y. Zhao, D. G. Truhlar, *J. Chem. Theory Comput.*, **2010,** *6*, 2872-2887.

[22] a) B. Van der Westhuizen, P. J. Swarts, I. Strydom, D. C. Liles, I. Fernández, J. C. Swarts, D. I. Bezuidenhout, *Dalton Trans.* **2013**, *42*, 5367-5378; b) B. Van der Westhuizen, P. J. Swarts, L. M. van Jaarsveld, D. C. Liles, U. Siegert, J. C. Swarts, I. Fernández, D. I. Bezuidenhout, *Inorg. Chem.* **2013**, *52*, 6674-6684.

[23] D. I. Bezuidenhout, I. Fernández, B. Van der Westhuizen,, P. J. Swarts, J. C. Swarts, *Organometallics*, **2013**, *32*, 7334-7344.

[24] See computational details.

[25] a) D. A. Valyaev, R. Nrousses, N. Lugan, I. Fernández, M. A. Sierra, *Chem. Eur. J.* **2011**, *17(24)*, 6602-6605; b) N. Lugan, I. Fernández, R. Brousses, D. A. Valyaev, G. Lavigne, N. A. Ustynyuk, *Dalton. Trans.*, **2013**, *42(4)*, 898-901.

[26] Leading references describing the electrochemical activity and behaviour of ferrocene and decamethylferrocene in a multitude of organic solvents are: a) I. Noviandri, K. N. Brown, D. S. Fleming, P. T. Gulyas, P. A. Lay, A. F. Masters and L. Phillips, *J. Phys. Chem. B*, **1999**, *103*, 6713-6722; b) N. G. Connelly and W. E. Geiger, *Chem. Rev.*, **1996**, *96*, 877-910; c) J.

Ruiz and D. Astruc, C. R. *Acad. Sci., Ser. IIc: Chim.*, **1998**, *1*, 21-27; d) R. J. Aranzaes, M. C. Daniel and D. Astruc, *Can. J. Chem.*, **2006**, 84, 288-299; e) E. Fourie, J. C. Swarts, I. Chambrier, M. J. Cook, *Dalton Trans.*, **2009**, 1145-1154.

[27] N. G. Connelly, W. E. Geiger, *Adv. Organomet. Chem.*, **1984**, *23*, 49.

[28] a) H. J. Gericke, N. I. Barnard, E. Erasmus, J. C. Swarts, M. J. Cook, M. A. S. Aquino, *Inorg. Chim. Acta*, **2010**, *363*, 2222-2232; b) D. H. Evans, K. M. O'Connell, R. A. Peterson, M. J. Kelly, *J. Chem. Educ.*, **1983**, *60*, 290-293; c) P. T. Kissinger, W. R. Heineman, *J. Chem. Educ.* **1983**, *60*, 702-706. d) J. J. Van Benschoten, J. Y. Lewis, W. R. Heineman, *J. Chem. Educ.*, **1983**, *60*, 772-776; e) G. A. Mobbott, *J. Chem. Educ.*, **1983**, *60*, 697-702; f) M. J. Cook, I. Chambrier, G. F. White, E. Fourie, J. C. Swarts, *Dalton Trans.* **2009**, 1136-1144.

[29] M. Lein, *Coord. Chem. Rev*. **2009**, *253*, 625-634.

[30] a) K. L. Letchworth, D. C. Benner, *J. Quant. Spectr. Radiative Transfer*, **2007**, *107*, 173-192; b) B. H. Armstrong, *J. Quant. Spectr. Radiative Transfer*, **1967**, *7*, 61-88.

[31] A. D. McLean, G. S. Chandler, *J. Chem. Phys.*, **1980**, *72*, 5639-5648.

[32] P. Fuentealba, H. Preuss, H. Stoll, L. Von Szentpály, *Chem. Phys. Lett.* **1982**, *89*, 418-422.

[33] A. E. Reed, R. B. Weinstock, F. Weinhold. *J. Chem. Phys.* **1985**, *83*, 735-746.

[34] a) G. Gritzner and J. Kuta, *Pure Appl. Chem.*, **1984**, *56*, 461-466; b) R. R. Gagne, C. A. Koval and G. C. Lisensky, *Inorg.Chem.*, **1980**, *19*, 2854-2855.

[35] Wojdyr, M. *J. Appl. Crystallogr.* **2010**, *43*, 1126-1128.

[36] M. J. Frisch, G. W. Trucks, H. B. Schlegel, G. E. Scuseria, M. A. Robb, J. R. Cheeseman, G. Scalmani, V. Barone, B. Mennucci, G. A. Petersson, H. Nakatsuji, M. Caricato, X. Li, H. P. Hratchian, A. F. Izmaylov, J. Bloino, G. Zheng, J. L. Sonnenberg, M. Hada, M. Ehara, K. Toyota, R. Fukuda, J. Hasegawa, M. Ishida, T. Nakajima, Y. Honda, O. Kitao, H. Nakai, T. Vreven, J. A. Montgomery Jr., J. E. Peralta, F. Ogliaro, M. Bearpark, J. J. Heyd, E. Brothers, K. N. Kudin, V. N. Staroverov, R. Kobayashi, J. Normand, K. Raghavachari, A. Rendell, J. C. Burant, S. S. Iyengar, J. Tomasi, M. Cossi, N. Rega, J. M. Millam, M. Klene, J. E. Knox, J. B. Cross, V. Bakken, C. Adamo, J. Jaramillo, R. Gomperts, R. E. Stratmann, O. Yazyev, A. J. Austin, R. Cammi, C. Pomelli, J. W. Ochterski, R. L. Martin, K. Morokuma, V. G. Zakrzewski, G. A. Voth, P. Salvador, J. J. Dannenberg, S. Dapprich, A. D. Daniels, Ö.

Farkas, J. B. Foresman, J. V. Ortiz, J. Cioslowski and D. J. Fox, Gaussian 09, Revision B.1, Gaussian, Inc., Wallingford, CT, 2009.

[37] a) A. D. Becke, *J. Chem. Phys.*, **1993**, *98*, 5648; b) C. Lee, W. Yang and R. G. Parr, *Phys. Rev. B: Condens. Matter*, **1988**, *37*, 785-789.

[38] F. Weigend, R. Ahlrichs, *Phys. Chem. Chem. Phys.*, **2005**, *7*, 3297-3305.

[39] J. W. McIver and A. K. Komornicki, *J. Am. Chem. Soc.*, **1972**, *94*, 2625-2633.

[40] R. F. W. Bader, *Atoms in Molecules - A Quatum Theory*, Oxford University Press, Oxford, 1990.

[41] T. A. Keith, AIMAll, 2010, http://tkgristmill.com]

[42] J. Heyd, G. Scuseria, *J. Chem. Phys.* **2004**, *121*, 1187-1192.

CHAPTER 9

Fischer-type gold(I) carbene complexes stabilized by aurophilic interactions

This chapter was published in Dalton Transactions. The format reflects the style set by the journal.

Daniela I. Bezuidenhout,[*a] Belinda van der Westhuizen,[a] Amos J. Rosenthal,[b] Michael Wörle,[b] David C. Liles, Israel Fernández, [*c] *Dalton Trans.*, **2014**, *43*, 389-401.
DOI:10.1039/C3DT52961D

Author contributors

Synthetic work: Belinda van der Westhuizen

Computational work: Israel Fernández

Crystallography: Amos J. Rosenthal, Michael Wörle, David C. Liles

Article written, submitted and response to reviewers: Belinda van der Westhuizen, Daniela I. Bezuidenhout, Israel Fernández, Amos J. Rosenthal, Michael Wörle, David C. Liles.

[a] *Chemistry Department, University of Pretoria, Private Bag X20, Hatfield, 0028, South Africa. Fax: +27-(0)12-420-4687; Tel: +27-(0)12- 420-2626; E-mail: daniela.bezuidenhout@up.ac.za*
[b] *Department of Chemistry and Applied Biosciences, ETH Zürich, Zürich 8093, Zwitzerland.*
[c] *Departamento de Química Orgánica I, Facultad de Química, Universidad Complutense,28040-Madrid,Spain.*

Electronic **Supplementary Information** (ESI) available: Synthetic procedures and analytical data; data tables for single crystal X-ray structural analysis; Computational details and Cartesian coordinates and energies for the optimised compounds **2** and **6**. CCDC numbers for complexes **1** – **6**: 962460, 962459, 962461, 963795, 962458 and 962457. See **Appendix 8**.

ABSTRACT

The synthesis and structure of rare acyclic alkoxy- and aminocarbene complexes of gold(I) are reported, including a novel ferrocenophane dinuclear biscarbene complex. X-Ray diffraction analyses and DFT calculations reveal that these complexes are stabilized by genuine aurophilic interactions.

9.1 COMMUNICATION

Interest in the structure of molecular gold complexes increased rapidly since 1970 due to the unexpected observation of intra- and intermolecular attractive forces between two linear gold(I) atoms.[1] Although the interaction between positively charged gold cations should result in a remarkable Coulomb repulsion, a good number of complexes with intra- and intermolecular equilibrium distances in the range from 2.50-3.50Å has been reported.[2] This phenomenon, referred to as aurophilicity, opened a new arena for the structural engineering of gold compounds.[3] Aurophilic bonding can be classified in three categories: unsupported, semi-supported and fully supported interactions.[2] Au···Au interactions can be separated by one (semi-supported) or two (fully supported) multi-atomic bridges. In the absence of such a bridge, interactions are unsupported. As stated by Gorin and Toste, the integration of theoretical and synthetic studies of Au(I) is required for deeper understanding of the fundamental properties of gold complexes in order to illuminate further avenues for study.[4] Due to the unprecedented success of Au-N-heterocyclic carbenes, as well as acyclic diaminocarbene complexes in the field of homogeneous catalysts for organic transformations, the structures of a variety of 'prototypes' have been determined.[5] However, examples of Fischer-type (i.e. mono-heteroatom substituted) acyclic gold(I) carbene complexes are not common.[6] Moreover, the presence of aurophilic interactions in these complexes remains scarcely explored so far. For these reasons, we report herein a series of novel acyclic Fischer-type Au(I) carbene complexes which exhibit genuine aurophilic interactions as clearly confirmed by X-Ray diffraction and computational studies.

Following the reaction conditions reported by Raubenheimer and co-workers,[6e] heteroaryl gold(I) chloro-monocarbene complexes **1-5** were synthesized by direct transmetallation[7] from their tungsten(0) analogues[8] in good to excellent yields using ClAu(tht) (tht = tetrahydrothiophene) in tetrahydrofuran (THF) at -5°C. Not unexpectedly, the ^{13}C NMR spectra of the gold(I) complexes generally displayed an upfield shift of the carbene carbon atom of *ca.* 50 ppm compared to the tungsten pentacarbonyl analogues (see Appendix 8). Interestingly, the carbon resonances for the rest of the atoms in the complexes, as well as the proton shifts, are shifted downfield, indicative of greater ring- and heteroatom involvement towards the stabilization of the electrophilic carbene carbon atom.

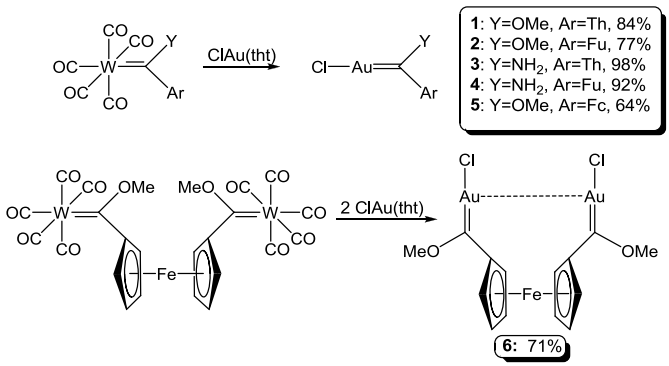

Scheme 9.1 Preparation of complexes **1-6**.

Crystals were obtained by layering a THF solution of the complex with hexane at 5°C. The Au-$C_{carbene}$ bond distances in the complexes **1-5** (Figure 9.1) fall within the typical range of an sp^2-hybridized carbon atom bonded to a gold centre *trans* to a chlorine atom (1.96-2.02Å).[6e,f,9] Similar to the M-$C_{carbene}$ bond lengths observed for their group 6 Fischer carbene counterparts,[10] the carbon-gold bond distances in the methoxycarbene complexes are slightly shorter as compared to the amine-stabilized carbenes. This is due to the well-known higher π-donor ability of the nitrogen atom compared to oxygen. In all the complexes, the gold atom is linearly coordinated with the C-Au-Cl bond angle varying between 173º and 179º. Moreover, the alkoxy group of complexes **1**, **2**, **5** and **6** adopts the so-called *anti*-conformation,[11] where the methyl group is oriented towards the transition metal analogously to group 6 Fischer alkoxycarbene complexes.

Apart from that, an important feature is exhibited by complexes **1-5** in the solid state, namely they present, with the adjacent molecule,[12] Au···Au distances in the range from 3.093 to 3.307 Å. This agrees with the classification of unsupported Au-Au interaction for these species.[2] In complexes **1** and **2** each gold centre participates in two such interactions (as indicated in Figure 9.1) thus infinite chains of linked molecules are formed. Taking into account this finding, we decided to prepare the novel ferrocenophane dinuclear biscarbene complex **6** (see Scheme 9.1), where the ferrocen-1,1'-diyl bridge should enforce a closer proximity between the gold atoms. Indeed, for complex **6**, a shorter Au···Au distance was found in the solid state (3.035 Å, Figure 9.1), thus confirming the semi-supported type of aurophilic interaction for this complex.

From the above structural study, it becomes clear that these novel gold(I) carbene complexes are stabilized by aurophilic interactions. To gain more insight into the nature of the Au···Au interaction in these species, Density Functional Theory (DFT) calculations were carried out using the dispersion-corrected M06 functional (M06/def2-TZVP level)[13] on the unsupported and semi-supported complexes **2** and **6**.[14] As shown in Figure 2, the computed Au···Au distance for complex **2** in the gas-phase (3.319 Å) concurs very well with the experimental distance in the solid state (3.307 Å). However, the agreement is not that good for complex **6**, very likely due to packing forces in the solid state. Despite this, the computed Au···Au distance in the latter compound is clearly shorter than in complex **2**, as a consequence of the semi-supported Au-Au interaction in this species.

The nature of the Au···Au bonding in complexes **2** and **6** was analysed with the help of the Atoms in Molecules (AIM) and Natural Bond Orbital (NBO) methods.[13] As depicted in Figure 9.3, the AIM method clearly reveals for both compounds the occurrence of a bond critical point (BCP) located at the midpoint between the two gold(I) atoms which is associated with a bond path running between these two atoms. These topological analyses therefore confirm the existence of an interaction between the Au(I) atoms. The computed electron density (ρ) and ellipticity (ε) values at the Au···Au BCP's are similar in both complexes (ρ = 0.014 e Å^{-3} , ε = 0.029 *vs* ρ = 0.013 e Å^{-3} , ε = 0.028 for **6** and **2**, respectively) thus indicating a similar type of interaction. In addition, the corresponding

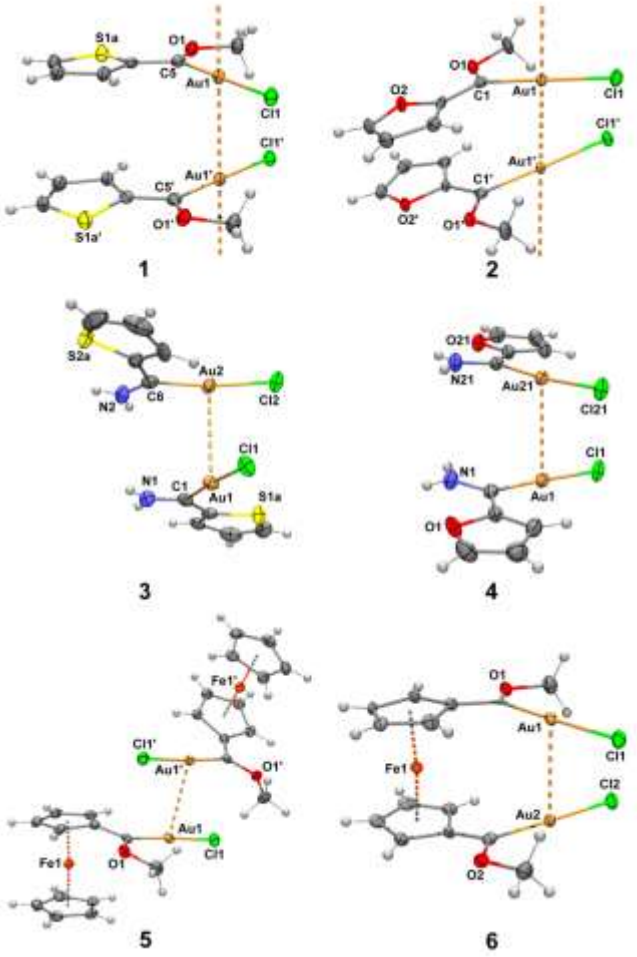

Fig. 9.1 Ortep/PovRay diagrams of **1-6** with adp ellipsoids shown at the 50% probability level. For **3**, a third molecule has been omitted. Au···Au interactions (Å): **1** 3.28083(11); **2** 3.3073(2); **3** 3.2179(7); **4** 3.0925(2); **5** 3.2885(2); **6** 3.0354(10). Au–$C_{carbene}$ bond distances (Å): **1** 1.970(4); **2** 1.974(3); **3** 1.985(6), 1.984(5); **4** 1.979(3), 1.977(3); **5** 1.977(3); **6** 1.970(7), 1.960(6).

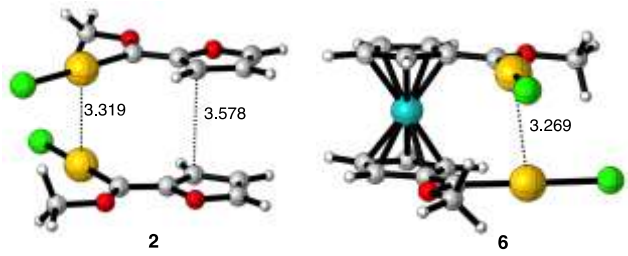

Fig. 9.2 Optimized (M06/def2-TZVP level) structures of complexes **2** and **6**. Bond distances are given in angstroms.

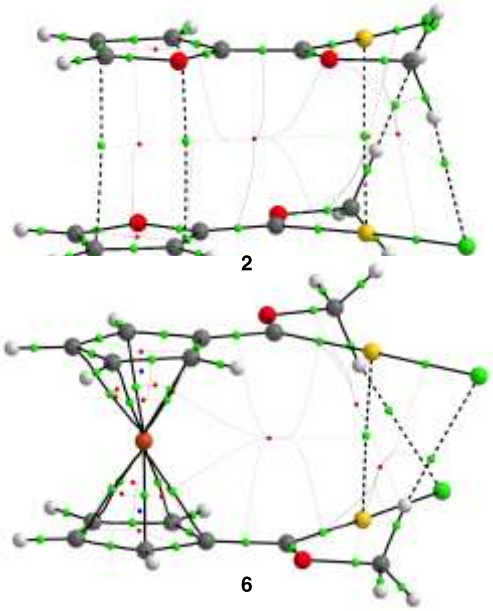

Fig. 9.3 AIM analyses of complexes **2** and **6**. BCP's are shown as green spheres.

Au-Au Wiberg Bond Index (0.14 and 0.15 for **2** and **6**, respectively) are also similar and comparable to the values found for related (NHC)AuCl dimers.[15]

Interestingly, the Second Order Perturbation Theory (SOPT) of the NBO method indicates that the aurophilic interaction is characterized by the donation of electron density from a doubly occupied *d* atomic orbital of one Au(I) to an empty *p* atomic orbital of the adjacent metal (see Figure 4). The associated SOPT energy computed for **2** and **6** is quite remarkable ($\Delta E^{(2)}$ = -9.4 and -9.3 kcal/mol, respectively), thus reflecting the importance of these aurophilic interactions in the global stabilization of the novel Fischer type Au(I)-carbene complexes described herein.

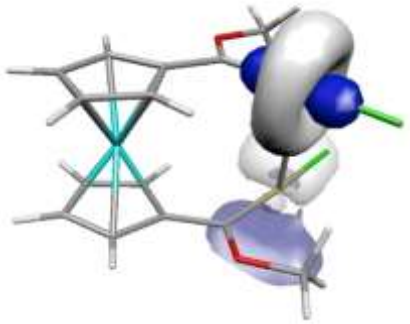

Fig. 9.4 NBO-molecular orbitals responsible for the Au···Au interaction in complex **6** (isosurface value of 0.035 au).

In summary, uncommen examples of Fischer-type gold(I) carbene complexes are prepared by direct transmetallation reaction from their correponding tungsten(0) carbene complexes and ClAu(thf). By means of X-ray diffraction analyses and DFT calculations, stabilizing aurophilic interactions in Fischer-type carbene complexes are characterized for the first time. Indeed, the Au···Au interaction allows the preparation of the first Fischer-type ferrocenophane biscarbene complex containing two Au(I) atoms. Futher work aimed at the preparation and reactivity of related (semi)supported carbene complexes exhibiting aurophilic interactions is in progress in our laboratories.

9.2 ACKNOWLEDGEMENTS

This work is supported by the National Research Foundation, South Africa (D.I.B., Grant number 76226), and the Spanish MICINN and CAM (I.F., Grants CTQ2010-20714-CO2-01/BQU, Consolider-Ingenio 2010, CSD2007-00006, S2009/PPQ-1634).

9.3 REFERENCES

1 (a) R. J. Puddephatt, *The Chemistry of Gold*, Elsevier, Amsterdam, 1978; (b) O. Crespo, *Modern Supramolecular Gold Chemistry*. Ed. A. Laguna, Chapter 2, Wiley-VCH, Weinheim, 2008; (c) S.-G. Wong and W. H. E. Schwarz, *J. Am. Chem. Soc.*, 2004, **126**, 1266; (d) P. Pyykkö, *Chem. Soc. Rev.*, 2008, **37**, 1967; (e) M. Andrejić and R. A. Mata, *Phys. Chem. Chem. Phys.*, 2013, **15**, 18115.

2 (a) H. Schmidbaur and A. Schier, *Chem. Soc. Rev.*, 2012, **41**, 370; (b) P. Schwerdtfeger and M. Lein, *Gold Chemistry. Current Trends and Future Directions.* Ed. F. Mohr, Wiley-VCH, Weinheim, 2009; (c) V. W.-W. Yam and E. C.-C. Cheng, *Chem. Soc. Rev.*, 2008, **37**, 1806.

3 (a) H. Schmidbaur, W. Graf and G. Müller, *Angew. Chem., Int. Ed. Engl.*, 1988, **27**, 417; (b) H. Schmidbaur, *Gold Bull.*, 2000, **33**, 3.

4 D. J. Gorin and F. D. Toste, *Nature*, 2007, **446**, 395-403.

5 (a) G. D. Frey, R. D. Dewhurst, S. Kousar, B. Donnadieu and G. Bertrand, *J. Organomet. Chem.*, 2008, **693,** 1674–1682; (b) H. G. Raubenheimer and S. Cronje, *Chem. Soc. Rev.*, 2008, **37**, 1998–2011; (c) H. G. Raubenheimer, *S.A.J.*, 2012, http://hdl.handle.net/10019.1/81278.

6 (a) R. Aumann and E. O. Fischer, *Chem. Ber.*, 1981, **114**, 1853; (b) E. O. Fischer, M. Böck and R. Aumann, *Chem. Ber.*, 1983, **116**, 3618; (c) E. O. Fischer and M. Böck, *Monatsh. Chem.*, 1984**, 115**, 1159; (d) M. Fañanás-Mastral and F. Azno, *Organometallics*, 2009, **28**, 666; (e) C. E. Strasser, S. Cronje and H. G. Raubenheimer, *New J. Chem.*, 2010, **34**, 458; (f) U. Schuber, K. Ackermann and R. Aumann, *Cryst. Struct. Commun.*, 1982, **11**, 519.

7 For a review on the transmetalation reaction from group 6 carbene complexes, see: (a) M. Gómez-Gallego, M. J. Mancheño and M. A. Sierra, *Acc. Chem. Res*. 2005, **38**, 44. For a computational study, see: (b) I. Fernández, M. J. Mancheño, R. Vicente, L. A. López, and M. A. Sierra, *Chem. Eur. J*. 2008, **14**, 11222.

8 (a) B. van der Westhuizen, J. M. Speck, M. Korb, J. Friedrich, D. I. Bezuidenhout and H. Lang, *Inorg. Chem.*, **2013**, *submitted*; (b) E. O. Fischer, W. Held, F. R. Kreißl, A. Frank

and G. Huttner, *Chem. Ber.*, **1977**, *111*, 656-666; (c) R. Streubel, S. Priemer, F. Ruthe, P. G. Jones and D. Gudat, *Eur. J. Inorg. Chem.*, **1998**, 575-578.

9 (a) G. Banditelli, F. Bonati, S. Calogero, G. Valle, F.E. Wagner and R. Wordel, *Organometallics*, 1986, **5**, 1346; (b) B. Bovio, A. Burini and B.R. Pietroni, *J. Organomet. Chem.*, 1993, **452**, 287; (c) S.-W. Zhang, R. Ishii and S. Takahashi, *Organometallics*, 1997, **16**, 20; (d) H.M.J. Wang, C.Y.L. Chen and I.J.B. Lin, *Organometallics*, 1999, **18**, 1216; (e) L. Weber, G. Dembeck, P. Lonneke, H.-G. Stammler and B. Neumann, *Organometallics*, 2001, **20**, 2288; (f) C.E. Strasser, E. Stander-Grobler, O. Schuster, S. Cronje and H.G. Raubenheimer, *Eur. J. Inorg. Chem.*, 2009, 1905; (g) H. Seo, B.P. Roberts, K.A. Abboud, K.M. Merz Jr. and S. Hong, *Org. Lett.*, 2010, **12**, 4860; (h) H. Seo, D.R. Snead, K.A. Abboud and S. Hong, *Organometallics*, 2011, **30**, 5725; (i) L.-A. Schaper, K. Öfele, R. Kadyrov, B. Bechlars, M. Drees, M. Cokoja, W.A. Herrmann and F.E. Kuhn, *Chem. Commun.*, 2012, **48**, 3857.

10 (a) B. van der Westhuizen, P. J. Swarts, I. Strydom, D. C. Liles, I. Fernández, J. C. Swarts and D. I. Bezuidenhout, *Dalton Trans.*, 2013, **42**, 5367; (b) B. van der Westhuizen, P. J. Swarts, L. M. van Jaarsveld, D. C. Liles, U. Siegert, J. C. Swarts, I. Fernández and D. I. Bezuidenhout, *Inorg. Chem*. 2013, **52**, 6674−6684.

11 (a) I. Fernández, F. P. Cossío, A. Arrieta, B. Lecea, M. J. Mancheño and M. A. Sierra, *Organometallics* 2004, **23**, 1065; (b) D. M. Andrada, M. E. ZoloffMichoff, I. Fernández, A. M. Granados and M. A. Sierra, *Organometallics* 2007, **26**, 5854; (c) D. A. Valyaev, R. Brousses, N. Lugan, I. Fernández and M. A. Sierra, *Chem. Eur. J*. 2011, **17**, 6602; (d) N. Lugan, I. Fernández, R. Brousses, D. A. Valyaev, G. Lavigne and N. A. Ustynyuk, *Dalton Trans*. 2013, **42**, 898.

12 In the asymmetric unit cell of the crystal structure of **3** there are 3 molecules of the complex of which just two have an aurophilic interaction. See SI.

13 See Computational Details in the Supplementary Material.

14 For a critical review on quantum chemical calculations to characterize aurophilic interactions, see reference 1d and references therein.

15 L. Ray, M. M. Shaikh and P. Ghosh, *Inorg. Chem*. 2008, **47**, 230.

CHAPTER 10

Conclusions

A series of Fischer mono- and biscarbene complexes of group 6 (Cr, W) and 7 (Mn) transition metals was synthesized and characterized spectroscopically. Both the carbene heteroatom substituent (alkoxy, amino) and the (hetero)aryl substituent (thienyl, furyl and ferrocenyl) were varied, and the redox behavior of the complexes was studied by electrochemical techniques.

The sequence of the successive electron transfer steps was established for both the chromium and tungsten complexes, and the influence of both the central metal and carbene substituents determined. Tungsten ferrocenyl complexes, in contrast to the chromium analogues, display ferrocenyl oxidation before the electrochemically irreversible oxidation process for W(0) involving a three electron-mediated process occurs. The experimental results were confirmed by computational data showing that the carbene double bond of all selected complexes is reduced pseudo-reversibly to form anion radicals. Crystal structure data obtained for the chromium thienyl ethoxy monocarbene showed mirror symmetry with the carbene ligand. Its biscarbene analogue crystallizes with two molecules in the asymmetric unit. Reactive cationic species, in certain examples, were shown by DFT molecular orbital calculations and NBO as well as AIM analyses, to be stabilized by agostic CH···M interactions for both chromium and tungsten complexes.

The ferrocenyl substituents were extended to form multi-metal carbene complexes, by utilizing the precursors biferrocene and the novel dibromobiferrocenyl thiophene. These precursors were lithiated, and according to the classical Fischer route, reacted with tungsten hexacarbonyl to yield novel tri- and tetrametallic mono- and biscarbene complexes. Crystal structure data was obtained for tungsten mono- and biferrocene complexes as well as for the ferrocenyl substituted thiophenes. All these structures include mono- and bis-carbenes. Metal-metal charge transfer between terminal tungsten carbene fragments was confirmed for the first time by infrared spectroelectrochemical studies.

Group 7 carbene complexes are not as common as their group 6 analogues, due to their limited application in organic synthesis and catalysis. However, the use of substituted cymantrene ($CpMn(CO)_2L$) as an organometallic molecular tag holds promise. The use of unfunctionalized cymantrene is impaired by the instability of its radical cation. Improved stability, monitored by electrochemical measurements, was accomplished by the introduction of a (hetero)aryl Fischer carbene moiety to yield the first organometallic *multi*-tags. Chemical oxidation of the ferrocenyl cymantrene monocarbene was performed, and the mono-cationic radical could be isolated and characterized with ESR analysis. Oxidation of Mn(I) to Mn(II) was confirmed by ESR, and an FTIR spectrum of the isolated salt was obtained.

Finally, transmetallation from various tungsten(0) Fischer carbene complexes yielded examples of rare acyclic alkoxy- and aminocarbene complexes of gold(I). Single crystal X-ray structures of all complexes, including a novel ferrocenophane dinuclear biscarbene Au(I) complex, displayed aurophilic interactions which were quantified by DFT calculations. Both unsupported and semi-supported Au–Au interactions were chartacterized.

FUTURE PERSPECTIVES

- The applications of Fischer carbene complexes in synthesis and catalysis have mostly focused on simple monocarbene monometal systems. Examples of assemblies of multi-carbene or multi-metal carbene systems are rare, but the inclusion of metal-carbene units into macromolecular assemblies or networks offer the opportunity of diverse properties and features. Especially important in such macromolecular organometallic assemblies (eg. metallomesogens and dendrimers) is the study of electron transfer for application in structured organised materials.
- Studies of neglected unstable organometallic tags should be rejuvenated in the attempt to stabilize them by employing new substituents (other than phosphine derivatives). The use of organometallic multi-tags provides the opportunity of fine-tuning the steric and electronic properties of said tags as per requirement.
- Gold complexes containing Fischer carbene carbene ligands represent in effect acyclic (oxy or amino) (alkoxy) carbene (AOAC or AAAC) complexes. Based on the success

of gold(I) carbene complexes in a variety of homogeneous catalytic processes, these less common type of gold(I) carbene complexes (mentioned above) should be tested for reactivity in the search for new and improved catalysts. Also, due to the increased reactivity sometimes seen for gold(III) complexes, an extension of this study should include electrochemical oxidation of gold(I) to gold(III), as well as the oxidative addition reaction of halides to yield gold(III) Fischer carbene complexes for further investigation.

APPENDIX 3a

Supporting Information: Chapter 4

Appendix. Supplementary Material

Synthesis and electrochemical investigation of ferrocenyl aminocarbene chromium(0) complexes.

Daniela I. Bezuidenhout,[a] Belinda van der Westhuizen,[a] Ian Strydom,[a] Pieter J. Swarts,[b] Jannie C. Swarts,[b*] Israel Fernández[c*]*

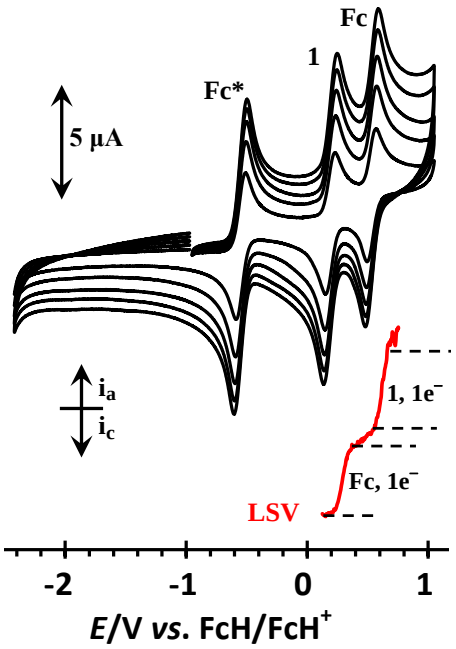

Fig. 1S. An LSV at 2 mV/s as well as CV's of 0.5 mmol dm^{-3} solutions of $[(OC)_5Cr{=}C(NHPr)\text{-}Fc]$, **2**, in CH_2Cl_2/0.1 mol dm^{-3} $[N(^nBu)_4][PF_6]$ on a glassy carbon-working electrode at scan rates of 100 (smallest currents), 200, 300, 400 and 500 mV/s. Decamethylferrocene, Fc*, was used as internal standard.

Cartesian coordinates (in Å) and total energies (in a. u., zero-point vibrational energy included) of all the stationary points discussed in the text. All calculations have been performed at the B3LYP/def2-SVP level. (**See Appendix 3b, CD**)

APPENDIX 5

Supporting Information: Chapter 6

Metal-Metal Interaction in Fischer Carbene Complexes – A Study on Ferrocenyl and Biferrocenyl Tungsten Alkylidene Complexes

Belinda van der Westhuizen,[a] J. Matthäus Speck,[b] Marcus Korb,[b] Joachim Friedrich,[c] Daniela I. Bezuidenhout[a]* and Heinrich Lang[b]*

[a]Chemistry Department, University of Pretoria, Private Bag X20, Hatfield 0028, South Africa.

[b]Technische Universität Chemnitz, Fakultät für Naturwissenschaften, Institut für Chemie, Anorganische Chemie, 09107 Chemnitz (Germany)

[c]Technische Universität Chemnitz, Fakultät für Naturwissenschaften, Institut für Chemie, Theoretische Chemie, 09107 Chemnitz (Germany)

Content.

References

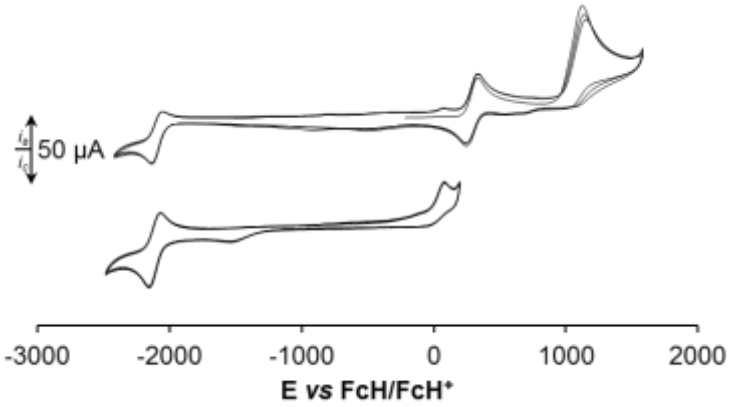

Figure SI-1. Cyclic voltammograms (multi scan) of **1**. Scan rates: 100 mVs^{-1} (top) and 500 mV^{-1} (bottom) in dichloromethane solutions (1.0 mmol.L-1) at 25 °C, supporting electrolyte $[N^nBu_4][B(C_6F_5)_4]$ (0.1 M).

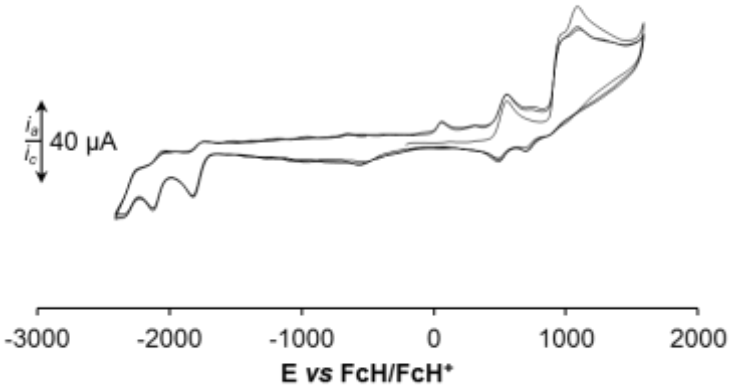

Figure SI-2. Cyclic voltammogram (multi scan) of **2**. Scan rate: 100 mVs^{-1} in dichloromethane solutions (1.0 mmol.L-1) at 25 °C, supporting electrolyte $[N^nBu_4][B(C_6F_5)_4]$ (0.1 M).

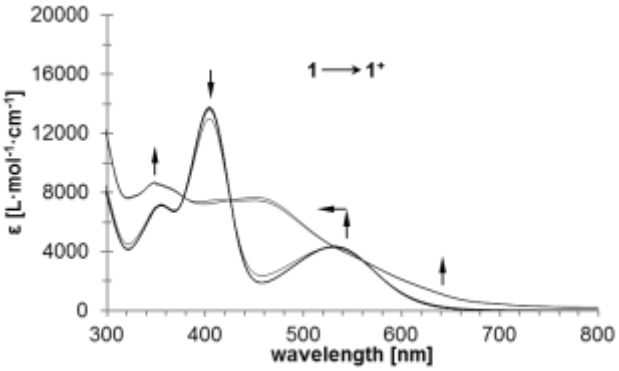

Figure SI-3. UV-Vis spectra of **1** at rising potentials (0 to 700 mV). All potentials *vs* Ag/AgCl at 25 °C in dichloromethane, supporting electrolyte $[N^nBu_4][B(C_6F_5)_4]$ (0.1 M). Arrows indicate increasing or decreasing as well as shifting absorptions.

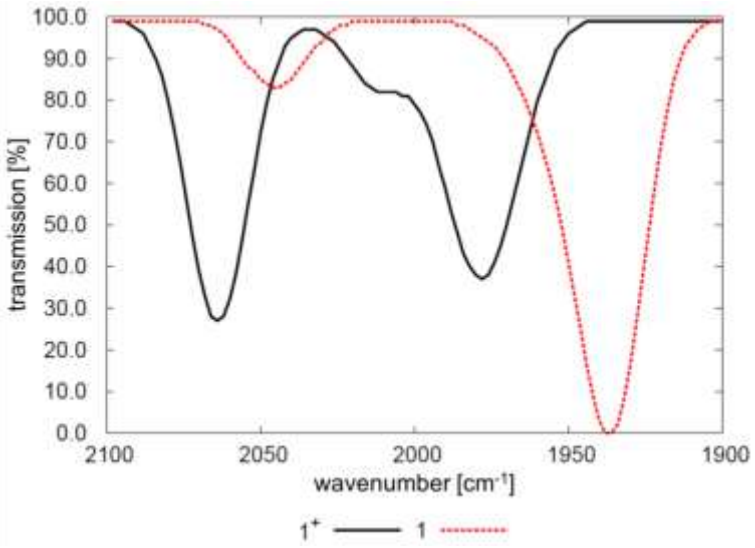

Figure SI-4. Calculated ν(CO) stretching frequencies of **1** and $\mathbf{1}^+$. Computational details are given in the Experimental Section.

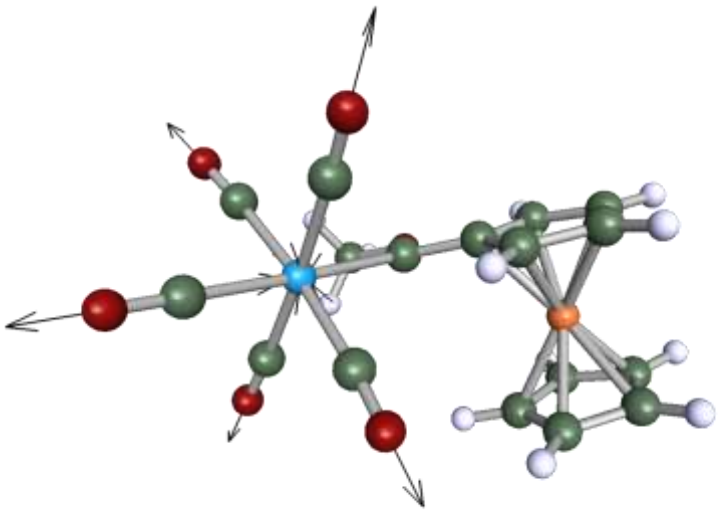

Figure SI-5. Visualization of calculated ν(CO) vibration mode for **1** at 2045 cm^{-1} (A_1'', Figure SI-2).

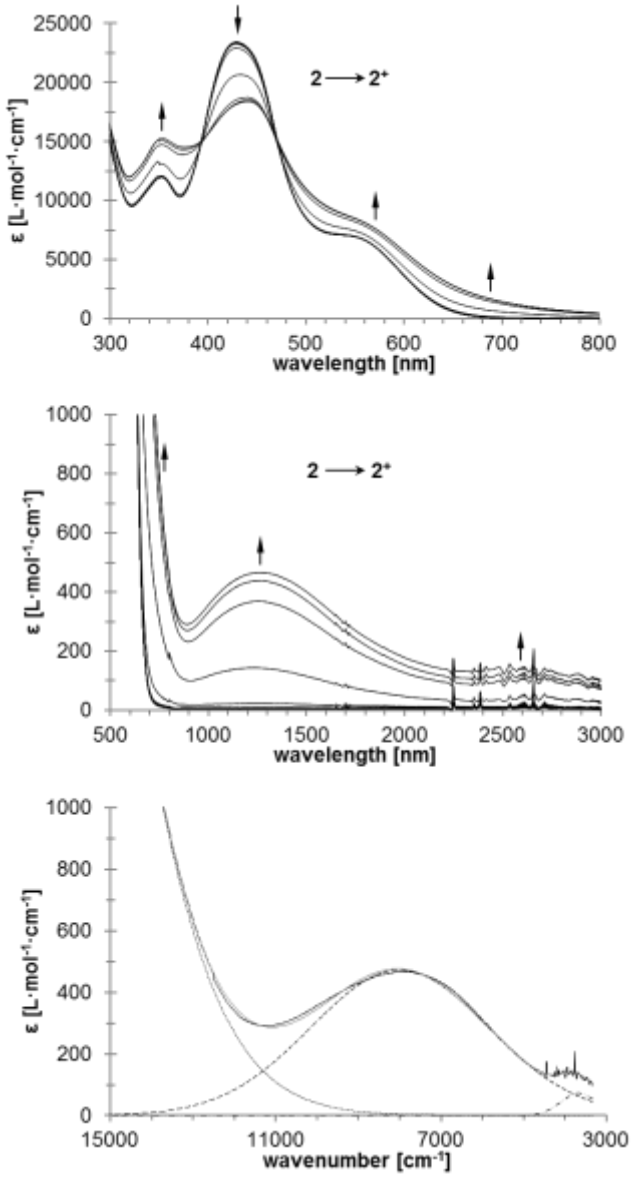

Figure SI-6. UV-Vis/NIR spectra of **2** at rising potentials (-100 to 1000 mV). Top: 300 – 800 nm. Middle: 500 – 3000 nm. Bottom: deconvolution of NIR absorptions at 1000 mV, using three distinct overlapping transitions with Gaussian shapes (dashed line indicates MMCT absorptions, dotted line corresponds to absorptions caused by interactions between ligand and metal, dotted dashed line represents ligand field transitions). All potentials *vs* Ag/AgCl at 25 °C in dichloromethane, supporting electrolyte $[N^{n}Bu_4][B(C_6F_5)_4]$ (0.1 M). Arrows indicate increasing or decreasing as well as shifting absorptions.

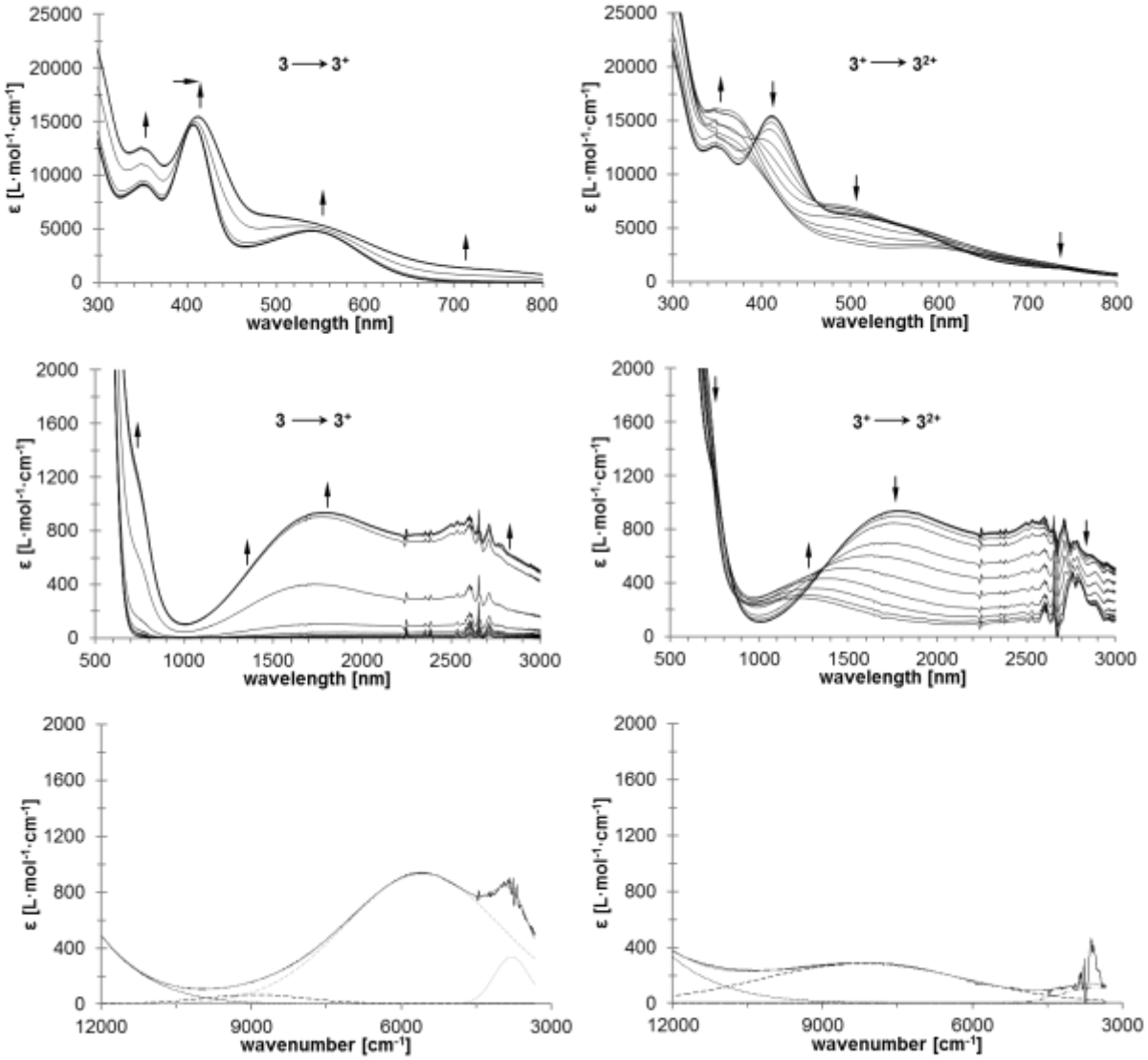

Figure SI-7. UV-Vis/NIR spectra of **3** at rising potentials (left: -100 to 400 mV; right: 400 to 1000 mV). Top: 300 – 800 nm. Middle: 500 – 3000 nm. Bottom (left): deconvolution of NIR absorptions at 400 mV, using three distinct overlapping transitions with Gaussian shapes. Bottom (right): deconvolution of NIR absorptions at 1000 mV, using three distinct overlapping transitions with Gaussian shapes (dashed line indicates IVCT (grey) or MMCT (black) absorptions, dotted line corresponds to absorptions caused by interactions between ligand and metal (black) as well as intrabiferrocenyl transitions (IBT, grey), dotted-dashed line represents ligand field transitions). All potentials *vs* Ag/AgCl at 25 °C in dichloromethane, supporting electrolyte $[N^nBu_4][B(C_6F_5)_4]$ (0.1 M). Arrows indicate increasing or decreasing as well as shifting absorptions.

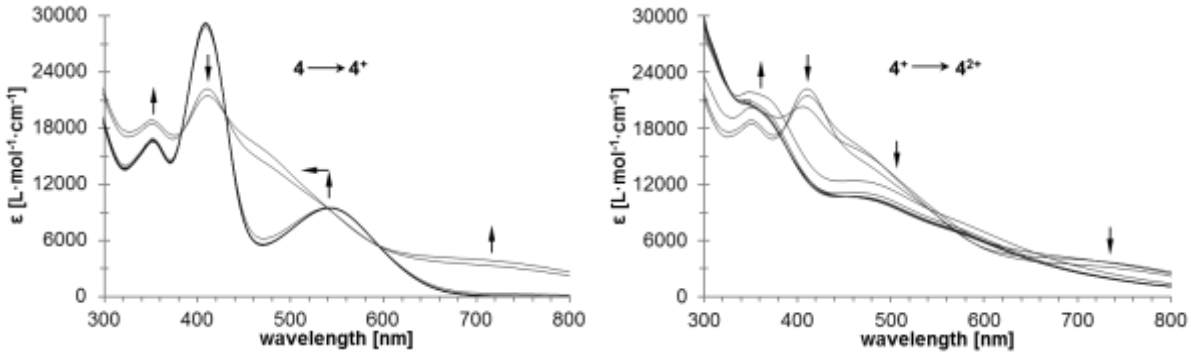

Figure SI-8. UV-Vis spectra of **4** at rising potentials (left: -100 to 600 mV; right: 600 to 1050 mV). All potentials *vs* Ag/AgCl at 25 °C in dichloromethane, supporting electrolyte $[N^nBu_4][B(C_6F_5)_4]$ (0.1 M). Arrows indicate increasing or decreasing as well as shifting absorptions.

Table SI-1. Data Collection and Crystal Structure Details for **1** – **4.**

	1	**2**	**3**	**4**
Chemical formula	$C_{17}H_{12}FeO_6W$	$C_{24}H_{14}FeO_{12}W_2$	$C_{27}H_{20}Fe_2O_6W$	$C_{34}H_{22}Fe_2O_{12}W_2$
Formula weight	551.97	917.90	735.98	1101.92
Crystal system, space group	orthorhombic, *Pca2*$_1$	orthorhombic, *Pbcn*	triclinic, *P–1*	monoclinic, *P2*$_1$*/n*
a [Å]	20.2216(14)	13.5817(8)	7.2565(3)	10.4968(3)
b [Å]	6.9527(5)	14.2798(8)	22.2626(7)	13.1509(3)
c [Å]	11.7231(9)	13.2044(6)	31.8703(10)	11.9019(3)
α, β, *γ* [°]			105.358(3), 95.673(3), 98.626(3)	97.546(2)
V [Å^3]	1648.2(2)	2560.9(2)	4856.5(3)	1628.74(7)
$\rho_{calc.}$ [g cm^{-3}]	2.224	2.381	2.013	2.247
F(000)	1048	1712	2848	0.71073 A
Crystal dimensions [mm]	0.4 x 0.2 x	0.4 x 0.4 x	0.40 x 0.28 x	0.40 x 0.40 x

	0.05	0.01	0.02	0.40
Z	4	4	8	2
Max., min. transmission	1.000, 0.592	1.000, 0.386	0.890, 0.200	0.1426, 0.1426
μ [mm^{-1}]	7.884	9.585	5.946	7.979
θ [°]	3.10–25.25	3.09–25.23	2.90–25.25	3.10–25.24
Index ranges	$-24 \le h \le 20$	$-10 \le h \le 16$	$-8 \le h \le 8$	$-12 \le h \le 12$
	$-5 \le k \le 8$	$-17 \le k \le 17$	$-26 \le k \le 26$	$-15 \le k \le 15$
	$-13 \le l \le 14$	$-15 \le l \le 15$	$-38 \le l \le 38$	$-11 \le l \le 14$
Total/unique reflections	6596/2749	8750/2302	45035/17555	11708/2938
Completeness to F^2	98.5 %	99.2 %	99.7 %	99.2 %
Data/restraints/parameters	2749/371/227	2302/308/182	17555/466/1297	2938/121/226
R_{int}	0.0510	0.0726	0.0405	0.0332
R_1, wR_2, $[I \ge 2\sigma(I)]$	0.0519, 0.1287	0.0564, 0.1372	0.0356, 0.0760	0.0184, 0.0414
R_1, wR_2 (all data)	0.0581, 0.1337	0.0673, 0.1457	0.0463, 0.0802	0.0204, 0.0422
Goodness-of-fit (S) on F^2	1.061	1.049	1.033	1.075
Largest diff. peak and hole [e Å^{-3}]	4.828, –1.400	2.760, –1.980	2.662, –1.273	0.562, –0.487

Absolute structure parameter[1]: 0.30(2) for **1**.

References

(1) Flack, H. D. *Acta Cryst., Sect. A*, **1983**, *39*, 876.

APPENDIX 6

Supporting Information: Chapter 7

Thiophenes modified by Tungsten Fischer Carbenes – Synthesis, Solid State Structure and Electrochemical Investigations.

Belinda van der Westhuizen,[a] J. Matthäus Speck,[b] Marcus Korb,[b] Daniela I. Bezuidenhout[a]* and Heinrich Lang[b]*

[a]Chemistry Department, University of Pretoria, Private Bag X20, Hatfield 0028, South Africa.

[b]Technische Universität Chemnitz, Fakultät für Naturwissenschaften, Institut für Chemie, Anorganische Chemie, 09107 Chemnitz (Germany)

Content.

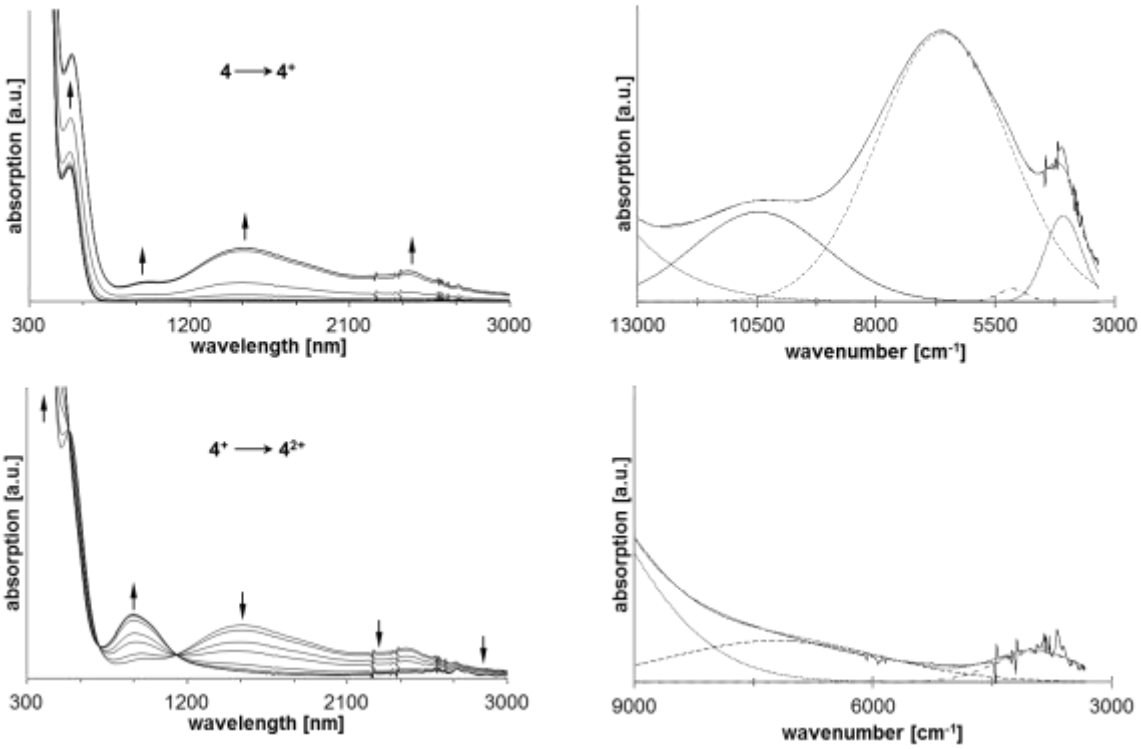

Figure SI-1. UV-Vis/NIR spectra of **4** at rising potentials. Left top: -100 to 390 mV. Left bottom: 390 to 525 mV. Right top: deconvolution of NIR absorptions at 390 mV, using five distinct overlapping transitions with Gaussian shapes (dashed line indicates IVCT absorptions, dotted line corresponds to absorptions caused by interactions between ligand and metal, dotted dashed line represents ligand field transitions).Right bottom: deconvolution of NIR absorptions at 525 mV, using three distinct overlapping transitions with Gaussian shapes (dashed line indicates MMCT absorptions, dotted line corresponds to absorptions caused by interactions between ligand and metal, dotted dashed line represents ligand field transitions). All potentials *vs* Ag/AgCl at 25 °C in dichloromethane, supporting electrolyte $[N^{n}Bu_4][B(C_6F_5)_4]$ (0.1 M). Arrows indicate increasing or decreasing as well as shifting absorptions.

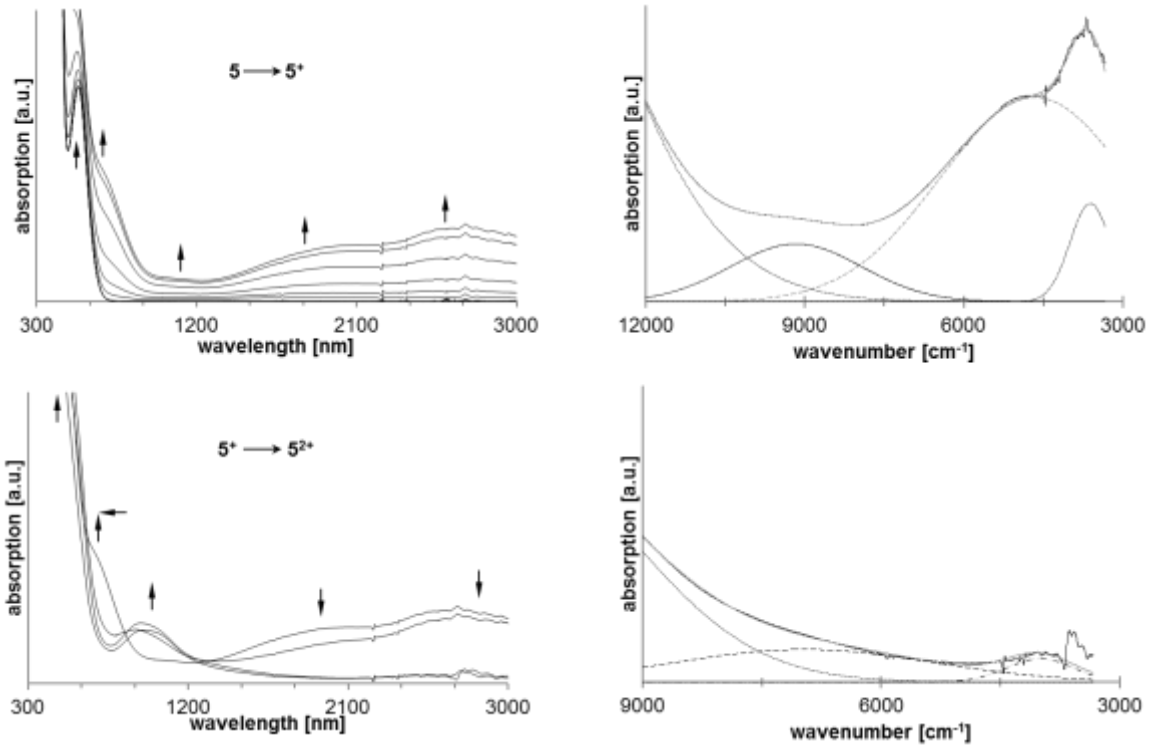

Figure SI-2. UV-Vis/NIR spectra of **5** at rising potentials. Left top: -100 to 670 mV. Left bottom: 670 to 710 mV. Right top: deconvolution of NIR absorptions at 670 mV, using four distinct overlapping transitions with Gaussian shapes (dashed line indicates IVCT absorptions, dotted line corresponds to absorptions caused by interactions between ligand and metal).Right bottom: deconvolution of NIR absorptions at 710 mV, using three distinct overlapping transitions with Gaussian shapes (dashed line indicates MMCT absorptions, dotted line corresponds to absorptions caused by interactions between ligand and metal, dotted dashed line represents ligand field transitions). All potentials *vs* Ag/AgCl at 25 °C in dichloromethane, supporting electrolyte $[N^{n}Bu_4][B(C_6F_5)_4]$ (0.1 M). Arrows indicate increasing or decreasing as well as shifting absorptions.

APPENDIX 8

Supplementary Information: Chapter 9

Fischer-type gold(I) carbene complexes stabilized by aurophilic interactions

Daniela I. Bezuidenhout[a*], Belinda van der Westhuizen[a], Amos J. Rosental[b], Michael Wörle[b], David C. Liles [a], Israel Fernández[c*]

[a] *Chemistry Department, University of Pretoria, Private Bag X20, Hatfield 0028, South Africa.*

E-mail: daniela.bezuidenhout@up.ac.za; Fax: +27-(0)12-420-4687; Tel: +27-(0)12-420-2626

[b]*Department of Chemistry and Applied Biosciences, ETH Zürich, Zürich 8093, Switzerland.*

[c]*Departamento de QuímicaOrgánica I, Facultad de Química, Universidad Complutense, 28040 Madrid, Spain.*

E-mail: israel@quim.ucm.es; Tel: +34-913944310.

Contents

1. General information

All operations were carried out under an inert atmosphere of nitrogen or argon gas using standard Schlenk techniques. Solvents were dried by refluxing on sodium metal (hexane, thf and diethylether) or over phosphorous pentoxide (CH_2Cl_2) and then distilled under nitrogen prior to use. Chemicals were used without further purification unless stated otherwise. Tetrahydrothiophenechloroaurate was synthesised according to literature procedures.[1] A Bruker AVANCE 500 spectrometer was used for NMR recordings. ^{1}H NMR spectra were recorded at 500.319 MHz and ^{13}C NMR spectra at 125.75 MHz. The signal of the solvent was used as reference: ^{1}H $CDCl_3$ at 7.26 ppm; CD_2Cl_2 at 5.32 ppm; ^{13}C $CDCl_3$ at 77.16 ppm; CD_2Cl_2 at 53.84 ppm. Mass spectrometry was done using a SYNAPT® G2 High Definition MS™ System from Waters. Crystal structure data collections for complexes **1**, **2**, **3**, **5** and **6** were performed using a Bruker diffractometer with a sealed tube Mo source, graphite monochromator and an APEX-II CCD detector and for complex **4** using a Bruker kappa geometry diffractometer with an IμS micro focus Mo source with focusing Montel optics and a Photon 100 CMOS detector. Data reduction was performed using Bruker SAINT and absorption corrections / scaling using Bruker SADABS (TWINABS for complex **1**). The structures were solved using Bruker SHELXTS and refined using SHELXTL (and Shelxl-2013 for complex **4**).

2. Synthesis of complexes

Precursor complexes for transmetallation were synthesized using the classical Fischer carbene route[2] and have previously been reported. [3,4,5]

General method for preparation of gold(I) Fischer carbene complexes via transmetallation from their tungsten(0)carbene analogues[6]*:* 2 mmol of the corresponding Fischer carbene complex was dissolved in thf and cooled to -5°C after which 2 mmol of ClAu(tht) was added in one portion (4 mmol for biscarbene complexes). After one hour, the reaction mixture was filtered using canula filtration and the target complex crystallized from this solution using thf and hexane at 5°C.

[ClAu=C(OMe)Th] (1)

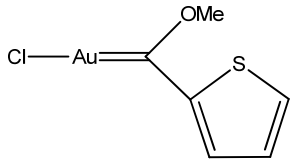

0.9g (2 mmol) of [$(CO)_5$W=C(OMe)Th] used as precursor complex. Yield: (84%, 0.6g), red crystals. ^{1}H NMR (CD_2Cl_2): δ 8.60 (br, 2H, H_α), 8.35 (d, J = 4.6 Hz, 2H, H_γ), 7.38 (dd, J = 4.8, 4.2 Hz, 2H, H_β), 4.78 (s, 3H, CH_3); ^{13}C NMR (CD_2Cl_2): 248.42(C_{carb}), 152.73 (C_α),n.o. (C_{ipso}), 145.56 (C_γ), 131.07 (C_β), 70.80 (CH_3). FAB-HRMS calcd for AuC_6H_6OSCl $[M\text{-}Cl]^+$: *m/z* 323.16; found, 322.98.

[ClAu=C(OMe)Fu] (2)

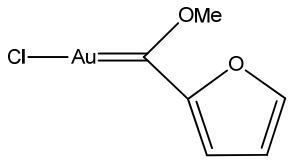

0.9g (2 mmol) of [$(CO)_5$W=C(OMe)Fu] employed as precursor complex. Yield: (77%, 0.53g), red crystals. ^{1}H NMR ($CDCl_3$): δ8.25 (d, J = 3.8 Hz, 2H, H_γ), 8.04 (br, 2H, H_α), 6.82 (dd, J = 3.9, 1.6 Hz, 2H, H_β), 4.79 (s, 3H, CH_3); ^{13}C NMR ($CDCl_3$): 237.46 (C_{carb}), 158.43 (C_γ), 154.09 (C_α), 142.17 (C_β), 116.42 (C_{ipso}), 70.99 (CH_3). FAB-HRMS calcd for $AuC_6H_6O_2Cl$ $[M\text{-}Cl]^+$: *m/z* 307.09; found, 307.03.

[ClAu=C(NH_2)Th] (3)

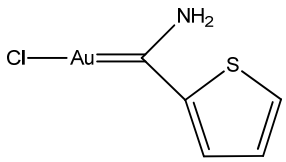

0.9g (2 mmol) of [$(CO)_5$W=C(NH_2)Th] used as starting material. Yield: (98%, 0.67g), light yellow crystals. ^{1}H NMR (CD_2Cl_2): δ9.12 (br, 1H, H_{syn}), 8.50 (br, 1H, H_{anti}), 8.09 (dd, J = 3.9, 1.2 Hz, 2H, H_α), 8.02 (dd, J = 5.0, 1.2 Hz, 2H, H_γ), 7.32 (dd, J = 5.0, 3.9 Hz, 2H, H_β); ^{13}C NMR (CD_2Cl_2): 197.93 (C_{carb}), 139.27 (C_α), 138.21 (C_γ), 130.15 (C_β). FAB-HRMS calcd for AuC_5H_5NSCl $[M\text{-}Cl]^+$: *m/z* 308.14; found, 307.98.

[ClAu=C(NH$_2$)Fu] (4)

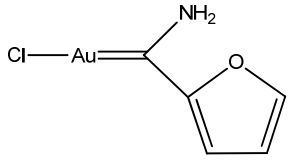

0.84g (2 mmol) of [(CO)$_5$W=C(NH$_2$)Fu] used as precursor complex. Yield: (92%, 0.60g), light yellow crystals. ^{1}H NMR (CD$_2$Cl$_2$): δ9.94 (br, 1H, H$_{syn}$), 9.19 (br, 1H, H$_{anti}$), 7.78 (br, 2H, H$_\gamma$), 7.59 (d, J = 3.6 Hz, 2H, H$_\alpha$), 6.64 (dd, J = 3.6, 1.7 Hz, 2H, H$_\beta$); ^{13}C NMR (CD$_2$Cl$_2$): n.o. (C$_{carb}$), 155.38 (C$_{ipso}$), 149.48 (C$_\gamma$), 131.64 (C$_\alpha$), 114.58 (C$_\beta$). FAB-HRMS calcd for AuC$_5$H$_5$NOCl [M-Cl]$^+$: *m/z*292.07; found, 292.00.

[ClAu=C(OMe)Fc] (5)

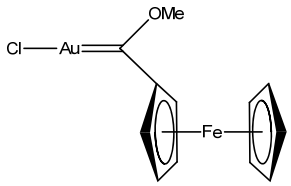

1.1g (2 mmol) of [(CO)$_5$W=C(OMe)Fc] employed as starting material. Yield: (64%, 0.59g), yellow crystals.^{1}H NMR (CD$_2$Cl$_2$): δ5.21 (br, 2H, H$_\alpha$), 5.07 (br, 2H, H$_\beta$), 4.51 (s, 3H, CH$_3$), 4.50 (s, 5H, Cp); ^{13}C NMR (CD$_2$Cl$_2$): n.o. (C$_{carb}$), 87.02 (C$_\alpha$), 79.82 (C$_\beta$), 72.10 (CH$_3$). FAB-HRMS calcd for AuFeC$_{12}$H$_{12}$OCl [M-Cl-CH$_3$+CH$_3$CN]$^+$: *m/z*451.06; found, 451.79.

[ClAu=C(OMe)Fc′(OMe)C=AuCl] (6)

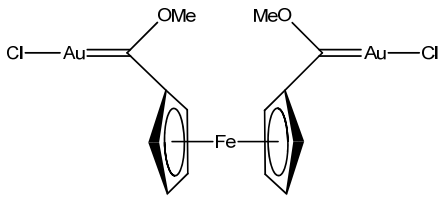

1.5g (2 mmol) of [(CO)$_5$W=C(OMe)-Fc'-(OMe)C=W(CO)$_5$], used as precursor complex. Yield: (71%, 1.04g), light brown crystals. ^{1}H NMR (CD$_2$Cl$_2$): δ5.29 (br, 2H, H$_\alpha$), 5.10 (br, 2H, H$_\beta$), 4.82 (s, 3H, CH$_3$); ^{13}C NMR (CD$_2$Cl$_2$): n.o. (C$_{carb}$), 97.79 (C$_{ipso}$),87.36 (C$_\alpha$), 80.68 (C$_\beta$)76.37 (CH$_3$). FAB-HRMS calcd for Au$_2$FeC$_{14}$H$_{14}$O$_2$Cl$_2$ [M+H-2Cl]$^+$: *m/z* 665.08; found, 664.98.

3. Crystallographic data

Table 1a. Crystal data and structure refinement for complexes **1** - **3**.

		1	**2**	**3**
Empirical formula		$C_6H_6AuClOS$	$C_6H_6AuClO_2$	$C_5H_5AuClNS$
Formula weight		358.60	342.53	343.59
Temperature (K)		100(2)	100(2)	100(2)
Wavelength (Å)		0.71073	0.71073	0.71073
Crystal system		Monoclinic	Orthorhombic	Triclinic
Space group		$P2_1/c$	$Pbca$	$P\bar{1}$
Unit cell dimensions	a(Å)	9.4467(3)	11.6474(6)	10.054(3)
	b(Å)	9.4467(3)	6.5160(3)	10.469(3)
	c(Å)	6.5606(2)	19.9970(10)	13.322(4)
	α (°)	90	90	73.798(5)
	β (°)	68.2817(13)	90	73.987(5)
	γ (°)	90	90	61.977(5)
Volume (Å^3)		833.04(4)	1517.66(13)	1171.2(5)
Z		4	8	6
Density (calculated) (g/cm^3)		2.859	2.998	2.923
Absorption coefficient (mm^{-1})		18.158	19.670	19.360
F(000)		648	1232	924
Crystal size (mm^3)		0.47 x 0.13 x 0.03	0.25 x 0.05 x 0.02	0.26 x 0.02 x 0.02
Θ range for data collection (°)		2.16 – 34.72	2.04 – 30.52	1.62 – 30.50
Index ranges	h	-14 – 13	-16 – 16	-14 – 14
	k	0 – 21	-9 – 9	-14 – 14
	l	0 – 10	-28–27	-18 – 18
Reflections collected		3023	21813	18555
Independent reflections		3023	2255	6883
R(int)		0.0000	0.0356	0.0352
Θ(full) (°)		30.50	30.52	30.50
Completeness to Θ(full) (%)		98.7	97.3	96.4
Absorption correction		multi-scan	multi-scan	multi-scan
Max. & min. transmission		0.1149 & 0.0362	0.9525 & 0.5785	0.2740 & 0.1598
Refinement method		Full-matrix least-squares on F^2		
Data / restraints / parameters		3023 / 72 / 109	2255 / 0 / 92	6883 / 0 / 286

Goodness-of-fit on F^2		1.073	1.051	1.028
R indices [$I>2\sigma(I)$]	*R*1	0.0231	0.0169	0.0276
	*wR*2	0.0611	0.0262	0.0533
R indices (all data)	*R*1	0.0365	0.0249	0.0414
	*wR*2	0.0649	0.0278	0.0569
Largest diff. peak & hole (e.Å^{-3})		1.323 & -1.268	0.745 & -0.868	1.433 & -0.926

Table 1b. Crystal data and structure refinement for complexes **4** - **6**.

		4	**5**	**6**
Empirical formula		$C_{10}H_{10}Au_2Cl_2N_2O_2$	$C_{12}H_{12}AuClFeO$	$C_{14}H_{14}Au_2Cl_2FeO_2$
Formula weight		655.03	460.49	734.94
Temperature (K)		150(2)	100(2)	100(2)
Wavelength (Å)		0.71073	0.71073	0.71073
Crystal system		Triclinic	Orthorhombic	Triclinic
Space group		$P\bar{1}$	*Pbcn*	$P\bar{1}$
Unit cell dimensions	*a*(Å)	8.7646(3)	18.3338(3)	6.867(3)
	b(Å)	9.3480(3)	9.7882(2)	9.991(4)
	c(Å)	9.5155(3)	13.3550(2)	12.498(5)
	α (°)	82.3723(14)	90	101.711(5)
	β (°)	68.2817(13)	90	91.574(5)
	γ (°)	85.2985(15)	90	108.988(5)
Volume (Å^3)		717.41(4)	2396.62(7)	789.9(5)
Z		2	8	2
Density (calculated) (g/cm^3)		3.032	2.552	3.090
Absorption coefficient (mm^{-1})		20.792	13.635	19.770
F(000)		584	1712	664
Crystal size (mm^3)		0.325 x 0.156 x 0.068	0.15 x 0.09 x 0.06	0.08 x 0.07 x 0.03
Θ range for data collection (°)		2.199 – 33.139	2.22 – 36.40	1.67 – 28.42
Index ranges	*h*	-13 – 13	-26 – 30	-9 – 9
	k	-14 – 14	-16 – 16	-13 – 13
	l	-14 – 14	-22 – 19	-16 – 16
Reflections collected		39322	43609	9970
Independent reflections		5472	5477	3926
R(int)		0.0506	0.0481	0.0273

Θ(full) (º)		33.139	30.499	28.42
Completeness to Θ(full) (%)		100.0	99.9	98.7
Absorption correction		multi-scan	multi-scan	multi-scan
Max. & min. transmission		0.7484 & 0.2550	0.3065 & 0.1987	0.2627 & 0.1660
Refinement method		Full-matrix least-squares on F^2		
Data / restraints / parameters		5472 / 0 / 175	5477 / 0 / 146	3926 / 0 / 192
Goodness-of-fit on F^2		1.087	1.007	1.105
R indices [$I>2\sigma(I)$]	*R*1	0.0246	0.0265	0.0260
	*wR*2	0.0622	0.0384	0.0542
R indices (all data)	*R*1	0.0279	0.0520	0.0391
	*wR*2	0.0637	0.0425	0.0575
Largest diff. peak & hole (e.Å^{-3})		3.377 & -1.602	0.933 & -1.141	2.226 & -1.138

The structure of complexes **1-6** were determined by single crystal x-ray diffraction analysis. The thiophene moieties in **1** and **3** were found to be disordered by a rotation of approximately 180º about the C_{ring}–$C_{carbene}$ bonds with ratios of the orientation with S approximately trans to X to that approximately cis to X about C_{ring}–$C_{carbene}$ bond of 0.909 : 0.091 for **1** (X = O) and 0.745 : 0.255 for **3** (X = N). In the asymmetric unit cell of the crystal structure of 3 there are 3 molecules of the complex of which just two have an aurophilic interaction.

4. Computational data

Computational Details

All the calculations reported in this paper were obtained with the GAUSSIAN 09 suite of programs.[7] The geometries of complexes **2** and **6** were optimized at the metahydrid M06 functional[8] using the triple-ξ valence plus polarization basis set def2-TZVP[9] for all atoms. This protocol is denoted M06/def2-TZVP. Both complexes were characterized by frequency calculations,[10] and have a positive defined Hessian matrix indicating that they are minima on the potential energy surface.

Donor-acceptor interactions have been computed using the natural bond orbital (NBO) method.[11] The energies associated with these two-electron interactions have been computed according to the following equation:

$$\Delta E^{(2)}_{\phi\phi^*} = -n_\phi \frac{\langle \phi^* | \hat{F} | \phi \rangle^2}{\varepsilon_{\phi^*} - \varepsilon_\phi}$$

where $\hat{F}$ is the DFT equivalent of the Fock operator and ϕ and ϕ^* are two filled and unfilled Natural Bond Orbitals having ε_ϕ and ε_{ϕ^*} energies, respectively; n_ϕ stands for the occupation number of the filled orbital.

All AIM results described in this work correspond to calculations performed at the M06/6-31G(d)/WTBS(for Au) level on the optimized geometries obtained at the M06/def2-TZVP level. The WTBS (well-tempered basis sets)[12] have been recommended for AIM calculations involving transition metals.[13] The topology of the ED was conducted using the AIMAll program package.[14]

Cartesian coordinates (in Å) and total energies (in a. u., non corrected zero-point vibrational energies included) of all the stationary points discussed in the text. All calculations have been performed at the M06/def2-TZVP + ΔZPVE level of theory.

2: E= -1956.921904

Cl	2.474597000	0.832710000	-2.376430000
O	0.039296000	2.200837000	2.034530000
C	1.404238000	2.112500000	2.476445000
H	1.699299000	1.061039000	2.529097000
H	1.428395000	2.569677000	3.462203000
H	2.047303000	2.653129000	1.781655000
O	-2.524378000	2.380258000	1.496808000
C	-2.291877000	1.948551000	-0.680940000
H	-1.823734000	1.712005000	-1.624851000
C	-3.722010000	2.452960000	0.918446000
C	-3.650045000	2.197994000	-0.417155000
H	-4.470745000	2.197473000	-1.115175000
Au	1.050951000	1.404200000	-0.652640000
C	-1.628645000	2.070525000	0.512162000
C	-0.238681000	1.950174000	0.800496000
H	-4.550217000	2.697795000	1.565670000
Cl	2.064525000	-1.432712000	2.415479000
C	0.778175000	-2.358419000	-2.476313000
H	1.266447000	-3.030042000	-1.769858000
H	0.695243000	-2.820553000	-3.456673000
H	1.322444000	-1.412531000	-2.538103000
C	-2.800955000	-1.331635000	0.653562000
H	-2.302449000	-1.235526000	1.606633000
C	-4.290659000	-1.453717000	-0.966221000
C	-4.176586000	-1.248800000	0.375018000
H	-4.982123000	-1.068908000	1.067480000
H	-5.145441000	-1.482493000	-1.624477000
Au	0.574125000	-1.605591000	0.662221000
C	-0.790493000	-1.803473000	-0.811239000

C	-2.171192000	-1.585564000	-0.536921000
O	-3.103038000	-1.656251000	-1.534364000
O	-0.569144000	-2.104565000	-2.045516000

6: E= -1969.885921

C	-0.426321000	1.499019000	-1.137117000
Au	1.110858000	-1.626058000	-0.159064000
Au	1.110660000	1.626157000	0.159059000
Fe	-2.854235000	-0.000074000	0.000066000
Cl	2.764642000	-1.791355000	-1.758722000
C	-3.585824000	1.785544000	0.741686000
H	-4.182768000	1.878252000	1.636154000
Cl	2.764373000	1.791499000	1.758785000
O	-0.351306000	-1.292862000	2.408929000
O	-0.351419000	1.292783000	-2.408957000
C	-2.181653000	1.811441000	0.681316000
H	-1.493181000	1.944490000	1.504267000
C	-1.793877000	1.605020000	-0.684253000
C	-2.992227000	-1.438297000	1.451100000
H	-3.034203000	-1.233669000	2.509646000
C	-0.426164000	-1.499048000	1.137077000
C	-1.793707000	-1.605158000	0.684200000
C	-4.086038000	-1.553463000	0.569466000
H	-5.126855000	-1.444924000	0.835888000
C	-2.992375000	1.437930000	-1.451140000
H	-3.034325000	1.233133000	-2.509655000
C	-2.181442000	-1.811451000	-0.681381000
H	-1.492949000	-1.944307000	-1.504346000
C	-3.585607000	-1.785711000	-0.741761000
H	-4.182526000	-1.878355000	-1.636253000
C	-4.086225000	1.553059000	-0.569538000
H	-5.127024000	1.444343000	-0.835959000
C	0.942645000	1.147531000	-3.021391000
H	1.595479000	1.953601000	-2.686282000
H	0.774105000	1.204721000	-4.093659000
H	1.374823000	0.181902000	-2.745844000
C	0.942736000	-1.147538000	3.021399000
H	1.595591000	-1.953634000	2.686395000
H	0.774142000	-1.204648000	4.093662000
H	1.374914000	-0.181922000	2.745811000

5. References

1. R. Uson, A. Laguna, M. Laguna, D. A. Briggs, H. H. Murray and J. P. Fackler, *Inorganic Syntheses, Volume 26*, 1989, 85-91.

2. E. O. Fischer and A. Maasböl, *Angew. Chem., Int. Ed. Engl.*,1964, **3**, 580–581.

3. B. van der Westhuizen, J. M. Speck, M. Korb, J. Friedrich, D. I. Bezuidenhout and H. Lang, *Inorg. Chem.*, 2013, *Submitted*.

4. E. O. Fischer, W. Held, F. R. Kreißl, A. Frank and G. Huttner, *Chem. Ber.*, 1977, **111**, 656-666.

5. R. Streubel, S. Priemer, F. Ruthe, P. G. Jones and D. Gudat, *Eur. J. Inorg. Chem.*, 1998, 575-578.

6. C. E. Strasser, S. Cronje and H. G. Raubenheimer, *New J. Chem.*, 2010, **34**, 458.

7. Gaussian 09, Revision B.01, M. J. Frisch, G. W. Trucks, H. B. Schlegel, G. E. Scuseria, M. A. Robb, J. R. Cheeseman, G. Scalmani, V. Barone, B. Mennucci, G. A. Petersson, H. Nakatsuji, M. Caricato, X. Li, H. P. Hratchian, A. F. Izmaylov, J. Bloino, G. Zheng, J. L. Sonnenberg, M. Hada, M. Ehara, K. Toyota, R. Fukuda, J. Hasegawa, M. Ishida, T. Nakajima, Y. Honda, O. Kitao, H. Nakai, T. Vreven, J. A. Montgomery, Jr., J. E. Peralta, F. Ogliaro, M. Bearpark, J. J. Heyd, E. Brothers, K. N. Kudin, V. N. Staroverov, R. Kobayashi, J. Normand, K. Raghavachari, A. Rendell, J. C. Burant, S. S. Iyengar, J. Tomasi, M. Cossi, N. Rega, J. M. Millam, M. Klene, J. E. Knox, J. B. Cross, V. Bakken, C. Adamo, J. Jaramillo, R. Gomperts, R. E. Stratmann, O. Yazyev, A. J. Austin, R. Cammi, C. Pomelli, J. W. Ochterski, R. L. Martin, K. Morokuma, V. G. Zakrzewski, G. A. Voth, P. Salvador, J. J. Dannenberg, S. Dapprich, A. D. Daniels, Ö. Farkas, J. B. Foresman, J. V. Ortiz, J. Cioslowski, and D. J. Fox, Gaussian, Inc., Wallingford CT, 2009.

8. Y. Zhao and D. G. Truhlar, *Theor. Chem. Acc.* 2008, **120**, 215-41.

9. F. Weigend and R. Ahlrichs, *Phys. Chem. Chem. Phys.*, 2005, **7**, 3297.

10. J. W. McIver and A. K. Komornicki, *J. Am. Chem. Soc.*, 1972, **94**, 2625.

11. (*a*) J. P. Foster and F. Weinhold, *J. Am. Chem. Soc.*, 1980, **102**, 7211; (*b*) A. E. Reed, F. Weinhold, *J. Chem. Phys*., 1985, **83**, 1736; (*c*) A. E. Reed, R. B. Weinstock and F.

Weinhold, *J. Chem. Phys*., 1985, **83**, 735; (*d*) A. E. Reed, L. A. Curtiss and F. Weinhold, *Chem. Rev*., 1988, **88**, 899.

12. (a) S. Huzinaga, B. Miguel, *Chem. Phys. Lett*. 1990, **175**, 289; (b) S. Huzinaga, M. Klobukowski, *Chem. Phys. Lett*. 1993, **212**, 260.

13. J. A. Cabeza, J. F. van der Maelen, S. García-Granda, *Organometallics* 2009, **28**, 3666 and references therein.

14. T. A. Keith, AIMAll, 2010, http://tkgristmill.com